

**Oligosaccharides based antibacterial drug
conjugates**

Von der Naturwissenschaftlichen Fakultät der
Gottfried Wilhelm Leibniz Universität Hannover
zur Erlangung des Grades

Doktorin der Naturwissenschaften (Dr. rer. nat.)

genehmigte Dissertation

von

Steffi Kruba Stephen, Master of Science,
(Indien)

2021

Referent: Prof. Dr. rer. nat. Mark Brönstrup

Korreferent: Prof. Dr. Russell Cox

Tag der Promotion: 18.08.2021

To my parents and brother
for their patience, unconditional love and encouragement that has led me to this point
and
Mr. Sanjay Mishra
my first Chemistry teacher who kindled the love for the subject at a very tender age.

Acknowledgements

This work would not have been possible without the support of a number of people in different capacities.

Firstly, I would like to express my sincere gratitude to my supervisor, Professor Mark Brönstrup, for giving me the opportunity to work on this exciting project. I am most grateful for his immense support, insights, encouragement and at times constructive criticism, which has been important in the fulfilment of this thesis. I also thank him for trusting me with teaching and supervising activities, which has been a great learning experience for me. Overall, it has been a pleasure to work under him and I believe his supervision has contributed significantly to my professional growth.

I am indebted to all the people from whom I have received technical and experimental support. Special thanks to Dr. Angie Jarrad for the stimulating discussions on the project and for performing the growth recovery assay. I would like to thank Dr. Christian Lentz for performing the fluorescence microscopy assay and FAP-MG assay and Heike Overwin for conducting the MIC assays. Big thanks to Dr. Arun Naini who has been part of this journey from day one. I would like to thank him for the many scientific discussions, his valuable suggestions in lab and for proofreading parts of my thesis. I appreciate all his assistance in making my transition to this foreign country effortless. I would also like to acknowledge all past and present members of chemistry department of CBIO-HZI for imparting their knowledge through the chemistry seminars. Special thanks to Dr. Stefan Saretz for his help with proofreading the thesis.

It has been a pleasure to work at the BMWZ. I am grateful to my lab-mates at different points: Dr. Christian Leitner, Haili Zhang, Dr. Steffen Friedrich for the nice working atmosphere. The cooperation from other working groups was helpful in solving many scientific hurdles. Special thanks to Katja Körner and her team for being quick to solve

any technical difficulties in the lab. I would also like to thank the members of the NMR and mass spectrometry department for the analytics.

Being a part of the Hannover School for Biomolecular Drug Research (HSBDR) has been a privilege. The seminars and workshops have contributed immensely to my professional development. I would like to mention Ayesha Dhillon-LaBrooy and Regina Weber for their pep-talks in moments when I felt lost. A special word of thanks to Mrs. Heike Lovelock for helping with the organizational work.

I am very fortunate to have had the company of my friends and their constant support though the ups and downs during this period. Special thanks to my constants Khushboo, Neha and Kavya for being there for me always. Thank you Amelie for giving me hope when I needed it the most. Amritha, Eri, Gretchen, Kata and Meta, thank you for your constant support and encouragement. To my family here in Hannover: Bhumika, Aparna and Prajna, thank you for always having my back. Ayan, special thanks for your company, help, advice, support and all the fun. Also, thank you for pushing me to do better. Finally, I would like to thank my parents for giving me the courage to pursue my dreams, believing in me and being patient with me. Also, to my little brother Shalom for being my biggest support.

Declaration

This thesis is composed of my original work, and contains no material previously published or written by another person except where due reference has been made in the text. I have clearly stated the contribution by others that I have included in my thesis. I furthermore declare that this thesis has not been submitted as a PhD thesis elsewhere.

I also declare that the growth recovery assay was performed by Dr. Angie Jarrad. Fluorescence microscopy and FAP assay were performed by Dr. Christian Lentz. MIC assay was conducted by Heike Overwin.

Steffi Kruba Stephen

Abstract

Gram negative bacteria are intrinsically resistant to antibiotics, as their outer membrane constitutes a permeability barrier that limits the number of antibiotics available for an effective treatment. There is also a lack of sensitive methods to diagnose infection in the early stages. The limited pipeline of new antibiotics demands novel ways to translocate antibiotics into gram negative bacteria. One possible strategy to improve bacterial penetration is to exploit the specific active transport machinery of bacteria to achieve facilitated transport of antibiotics, also referred to as Trojan horse strategy.

In recent years maltodextrins conjugates modified at the anomeric end have been used in the Trojan horse strategy to detect and treat bacterial infection. However, it is also reported that blocking the reducing end of maltodextrin by residues larger than methyl groups are not transported by the maltodextrin receptor. This thesis deals with the synthesis and investigation of conjugates with modification at the non-reducing end of maltodextrins. The conjugates can accommodate a fluorophore or an antibiotic for detection and treatment of infection, respectively. The critical structural requirements in the maltodextrin based conjugate design for an efficient uptake have been investigated. A systematic series of fluorescent conjugates with varying critical parameters including chain length of maltodextrins, linker types, site of modification and type of fluorophore have been synthesized. The uptake efficiencies of the conjugates have been studied using growth recovery assays, confocal microscopy and flow cytometry. The validation of intracellular uptake of conjugates was performed using a fluorogen activating protein (FAP)-based approach. Finally, maltodextrin-ampicillin conjugates were synthesized and tested for antibacterial activity in *E. coli* and *K. oxytoca*.

Keywords: Antibiotic resistance - maltodextrins - conjugates- bacterial imaging- drug transport

Zusammenfassung

Gramnegative Bakterien sind häufig intrinsisch resistent gegen Antibiotika, da ihre Außenmembranwenig durchlässig ist und dadurch die Zahl der Wirkstoffe für eine effektive Behandlung limitiert. Zudem gibt es nur wenige Methoden, die sensitiv genug sind, um eine frühe Infektion zu diagnostizieren. Aufgrund der begrenzten Auswahl an neuen Antibiotika ist es wichtig, neue Wege der Translokation in gramnegative Bakterien zu finden. Eine mögliche Strategie ist dabei die des Trojanischen Pferds. Dabei werden aktive Transporter von Bakterien für die Aufnahme von Antibiotika genutzt, um so deren Eindringen in die Bakterien zu verbessern. In den letzten Jahren wurde diese Strategie bereits angewandt, um bakterielle Infektionen zu diagnostizieren und zu behandeln. Dafür wurden Konjugate von Maltodextrin verwendet, die am anomeren Ende modifiziert werden. Es wurde festgestellt, dass der Transport über den Maltodextrinrezeptor nicht möglich ist, wenn das reduzierte Ende von Maltodextrin größere Reste als eine Methylgruppe trägt. Diese Doktorarbeit beschäftigt sich mit der Synthese und Untersuchung von Maltodextrin-Konjugaten mit Modifikationen am nicht reduzierenden Ende. Diese Konjugate können ein Fluorophor zur Erkennung einer Infektion oder ein Antibiotikum zur Behandlung tragen. Die strukturellen Voraussetzungen für eine effiziente Aufnahme der auf Maltodextrin basierten Konjugate zu erhalten, wurden im Rahmen dieser Arbeit untersucht. Dafür wurde eine Serie an Konjugaten synthetisiert, bei der verschiedene Parameter variiert wurden. Zu den Parametern zählen Kettenlänge, Linker-Typ, die Position der Modifikation und sowie die Art des Fluorophors. Um die Aufnahme der Konjugate zu untersuchen, wurden *Growth Recovery Assays* durchgeführt sowie Konfokalmikroskopie und Durchflusszytometrie verwendet. Für die Validierung der intrazellulären Aufnahme der Konjugate wurde eine Methode basierend auf dem *Fluorogen-Activating Proteins* (FAP) herangezogen. Abschließend erfolgte die Synthese von Maltodextrin-Ampicillin Konjugaten und die Testung auf ihre antibakterielle Aktivität in *E. coli* und *K. oxytoca*.

Schlüsselbegriffe: Antibiotische Resistenz – Maltodextrin – Konjugate – Bakterielle Verarbeitung – Medikamententransport

Table of Contents

Dedication	ii
Acknowledgements	iii
Declaration	v
Abstract	vi
Zusammenfassung	vii
Table of contents	viii
List of figures	xi
List of tables	xii
List of Abbreviations	xiv
1 Introduction	1
1.1 Developments in antibiotic research	1
1.2 Antimicrobial resistance	3
1.3 Pipeline of antibiotics	6
1.4 Bacterial imaging	7
1.5 Fluorogen Activating Protein-Malachite Green(FAP-MG) system	9
1.6 Permeability barrier in gram negative bacteria	11
1.7 Strategies to overcome permeability barrier	13
1.7.1 OM permeabilizers	13
1.7.2 Carriers of antibiotics	18
1.8 Trojan horse strategy	18

1.8.1	Siderophore transport systems	20
1.9	Maltodextrin transport system of <i>E. coli</i>	21
1.9.1	Components of the maltodextrin transport system	22
1.9.2	Mechanism of maltodextrin transport	24
1.9.3	Substrates of the maltodextrin transport system	25
1.9.4	Critical interactions governing specificity of the maltodextrin transport system	26
1.10	Previously reported maltodextrin conjugates	30
1.11	Aim of the thesis	35
1.12	Thesis Outline	37
2	Investigation of maltodextrin uptake	38
2.1	Design of modified maltodextrins	38
2.2	Synthesis of intermediates	40
2.3	Growth recovery assay	47
3	Maltodextrin based imaging probes	53
3.1	Design of fluorescent probes	53
3.2	Synthesis of fluorescent conjugates	57
3.3	Characterization of probe uptake	77
3.3.1	Growth recovery assay	78
3.3.2	Confocal microscopy assay	79
3.4	FACS analysis	84
4	Investigation of intracellular accumulation	90
4.1	Synthesis of maltodextrin-MG conjugates	90
4.2	FAP-MG assay	97
5	Antibiotic conjugates	101

5.1	Ampicillin conjugates	101
5.2	Design of antibiotic conjugates	102
5.3	Synthesis of antibiotic conjugates	103
5.4	The minimum inhibitory concentration (MIC) assay	107
6	Summary and outlook	108
7	Experimental	111

List of Figures

1.1	Mode of action of antibiotics	2
1.2	Timeline of development of antibiotic resistance	3
1.3	Resistance mechanism of antibiotics	5
1.4	Chemical structure of bacteria specific fluorescent imaging agents	9
1.5	Schematic representation of FAP-MG system	10
1.6	Structure of malachite green	11
1.7	Schematic representation FAP-MG system to demonstrate internalisation	11
1.8	Differences between gram positive and gram negative cell wall	12
1.9	Structures of polymyxin derivatives	15
1.10	Structures of representative CSAs	17
1.11	Trojan horse strategy	19
1.12	Chemical structure of Cefiderocol	20
1.13	Structure of maltodextrins.	21
1.14	Maltodextrin transport system	22
1.15	Crystal structure of maltoporin malB	23
1.16	Co-crystal structure of maltose binding protein malE	24
1.17	Substrates of maltodextrin transport system	26
1.18	Greasy slide of lamB	27
1.19	Hydrogen bonds between maltohexose and lamB	28
1.20	Schematic view showing critical interaction governing the selectivity	29
1.21	Schematic model of substrate recognition	30
1.22	Structure of MDP-1 and MDP-2	31
1.23	Structure of ¹⁸ F-labeled maltohexose probe	31
1.24	Structure of bimodal photoprobe	32
1.25	Maltohexose based SPECT tracer	33

1.26	Structure of maltotriose perylene conjugate	33
1.27	Structure of thiomaltose- perylene conjugate	34
1.28	Structure of thiomaltose- trimethoprim conjugate	34
1.29	Modifications at the non-reducing end	35
2.1	Structures of modified maltodextrins	39
2.2	Recovery of growth after 24 h measured by OD600.	49
2.3	Recovery of growth after 48 h measured by OD600.	49
2.4	Recovery of growth after 48 h measured by ATP-bioluminescence.	50
3.1	Structures of fluorescent conjugates	56
3.2	Recovery of growth after 48 h measured by ATP-bioluminescence.	78
3.3	Confocal microscopy images of labelling by perylene conjugates	80
3.4	Confocal microscopy images of labelling by coumarin conjugates	81
3.5	Confocal microscopy images of labelling by NBD conjugates	82
3.6	Confocal microscopy images of labelling by BODIPY conjugates	83
3.7	Quantification of uptake by FACS analysis: Small gate	84
3.8	Quantification of uptake by FACS analysis: Full gate	85
3.9	FACS analysis showing % of cells labelled by the probe	86
4.1	Structures of maltodextrin-MG conjugates	91
4.2	Fluorescence measurement FAP-MG assay.	98
4.3	Normalized probe uptake observed via FAP-MG assay	99
5.1	Crystal structure of PBP bound to ampicillin	102
5.2	Structures of maltodextrin ampicillin conjugates	103

List of Tables

1.1	Sequences of cationic peptide OM permeabilizers	16
2.1	Trials to oxidise the primary alcohol to carboxylic acid	42
3.1	Trials to oxidise the primary alcohol to aldehyde	58
3.2	Trials towards nucleophilic substitution	62
3.3	Trials towards oxidation of 17 to 36	63
3.4	Trials to prepare BOT_15 by deprotecting 35	65
3.5	Trials towards benzylidene acetal protection	74
3.6	Optimisation of microwave assisted benzylidene protection	75

Abbreviations

°C	degrees Celcius
Ac	acyl
AMR	antimicrobial resistance
ATP	Adenosine triphosphate
BAIB	bis(acetoxy)iodobenzene
[bmim]PF₆	1-butyl-3-methylimidazolium hexafluorophosphate
Bn	benzyl
Boc	di- <i>tert</i> -butyl dicarbonate
CAM	ceric ammonium molybdate
CSA	cationic steroid antibiotics
CDC	Center for Disease Control and Prevention
CT	computed tomography
CuAAC	Copper-catalyzed azide-alkyne cycloadditions
Da	dalton
DAPB	deacyl polymyxin B
DBU	1,8-Diazabicyclo[5.4.0]undec-7-ene
DCM	dichloromethane
DIPEA	N,N-Diisopropylethylamine
DMF	dimethylformamide

DMP	Dess-Martin periodinane
DMPU	N,N'-Dimethylpropyleneurea
DMSO	dimethyl sulfoxide
DNP	dinitrophenylhydrazine
<i>E. coli</i>	<i>Escherichia coli</i>
EDC	1-Ethyl-3-(3-dimethylaminopropyl)carbodiimide
eq.	equivalent
Et₃N	triethylamine
[¹⁸F	FDG] (2-fluoro-2-deoxy-d-glucose)
FACS	Fluorescence-activated cell sorting
FAP	fluorogen-activating protein
FDA	Food and Drug Administration
FIC	fractional inhibition concentration
FIAU	(1-(2'-deoxy-2'-fluoro-β-D-arabinofuranosyl)-5-iodouracil)
FSC	forward scattering
HPLC	high-performance liquid chromatography
<i>i.e.</i>	in other words
LB	lysogeny broth
LC-MS	liquid chromatography- mass spectrometry
LPS	lipopolysaccharide

MDP	maltodextrin based probes
Me	methyl
MeOH	methanol
MIC	minimum inhibition concentration
MRI	magnetic resonance imaging
MW	microwave
NaAsc	sodium ascorbate
NBD	nucleotide-binding domains
NMR	Nuclear Magnetic Resonance
OM	outer membrane
<i>P. aeruginosa</i> ..	<i>Pseudomonas aeruginosa</i>
PBP	Penicillin binding protein
PEG	polyethylene glycol
PET	positron emission tomography
PMB	1,2,3,4,5-pentamethylbenzene
PMBH	polymyxin B heptapeptide
PMBN	polymyxin B nonapeptide
PMBO	polymyxin B octapeptide
RM	reaction mixture
RT	room temperature

ROS	reactive oxygen species
s	second
SPECT	single-photon emission CT
SSC	side scattering
<i>S. typhimurium</i>	<i>Salmonella typhimurium</i>
T₃P	1-Propanephosphonic anhydride
TBAI	tetra- <i>n</i> -butylammoniumfluoride
TBTA	tris((1-benzyl-4-triazolyl)methyl)amine
THF	tetrahydrofuran
TLC	Thin layer chromatography
TMD	transmembrane domains
Ts	<i>p</i> -toluenesulfonyl
WHO	World Health Organisation

1 | Introduction

1.1 Developments in antibiotic research

Pathogenic bacteria are causative agents of a number of infectious diseases including infections such as tetanus, typhoid fever, diphtheria, syphilis, and leprosy; food-borne illnesses such as salmonella, and other life threatening diseases such as pneumonia and tuberculosis. The health burden caused by these diseases can be understood from the fact that globally infectious diseases cause more than 8 million deaths per year.¹ Pneumonia and other lower respiratory infections alone claimed 2.6 million lives in 2019, ranking as the fourth leading cause of death.² The development of antibiotics however, has not only brought the deaths caused by these infections under control, but also revolutionised modern medicine by aiding advancements in surgery, chemotherapy and organ transplantation.

The modern era of antimicrobial chemotherapy can be said to have begun when Paul Ehrlich started working on the antibacterial effects of dyes. He observed that some stains were toxic for bacteria and started his search for the 'magic bullet'.³ Following his lead, Gerhard Domagk developed Prontosil, a sulfonamide that became the first commercially available antibacterial drug in 1930.⁴ The major breakthrough however occurred with the serendipitous discovery of Penicillin in 1928 by Alexander Fleming.⁵ Later, Florey and Chain successfully purified the antibiotic and scaled-up the production. It was not until 1945 that Penicillin was introduced on a large scale as a treatment for bacterial infections. The contributions of Fleming, Florey and Chain were recognized by the scientific community when they were awarded the Nobel Prize in Physiology or Medicine in 1945.⁶ The introduction of Penicillin marked the beginning of the Golden Era of antibiotics. The period between 1940-1960 saw the rapid increase in the discovery of antibiotics. Most of the antibiotic classes known today, for exam-

ple, the aminoglycosides (streptomycin),⁷ tetracyclines (chlorotetracyclin),⁸ macrolides (erythromycin),⁹ rifamycins (rifampicin),¹⁰ glycopeptides (vancomycin)¹¹ were discovered and introduced to the market during this time. The following years saw a decrease in the development of new antibiotics. On the brighter side this period saw an advancement on the medicinal chemistry front. Chemical optimisation of the existing antibiotic classes resulted in the development of successive generations of cephalosporins,¹² macrolides and tetracyclines etc.. Two new antibiotic classes of synthetic origin, fluoroquinolones¹³ and oxazolidinones,¹⁴ were also discovered.

The common modes of action of the above-mentioned antibiotic classes include (Figure 1.1):

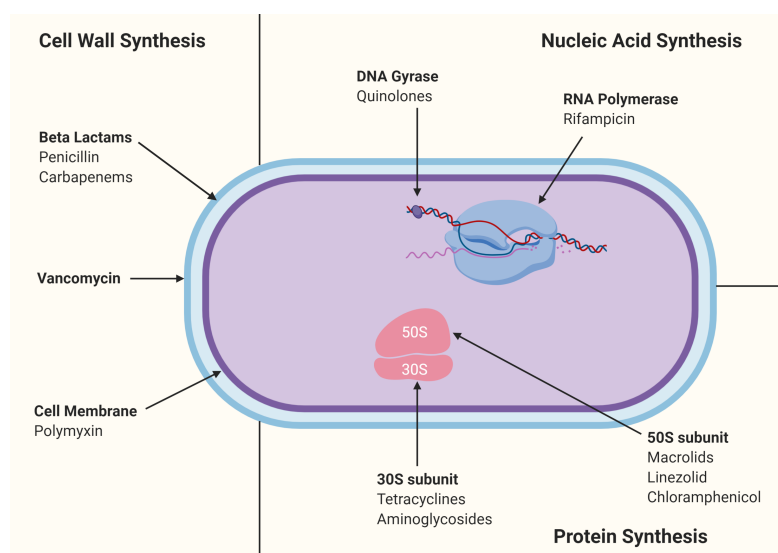


Figure 1.1: Mechanism of action of antibiotics. Adapted from^{15,16}

- Inhibition of cell-wall biosynthesis at the stage of crosslinking of peptidoglycan peptide strands by trans-peptidases and trans-glycosylases. eg. β -lactams.
- Inhibiting one or more steps involved in protein biosynthesis at the ribosome. eg. macrolides, tetracyclines, aminoglycosides and oxazolidinones
- Interruption of DNA replication. eg. fluoroquinolone, rifampicin.

1.2 Antimicrobial resistance

Parallel to the discovery of antibiotics, as described aptly by Nobel laureate Ada Yonath: "bacteria want to live, and they are cleverer than us". Bacteria were able to develop resistance against these drugs in a short time period, with the reports of resistance against most drugs within 10 years of their introduction to the market. The time-line of development of antibiotics resistance is depicted in Figure 1.2.

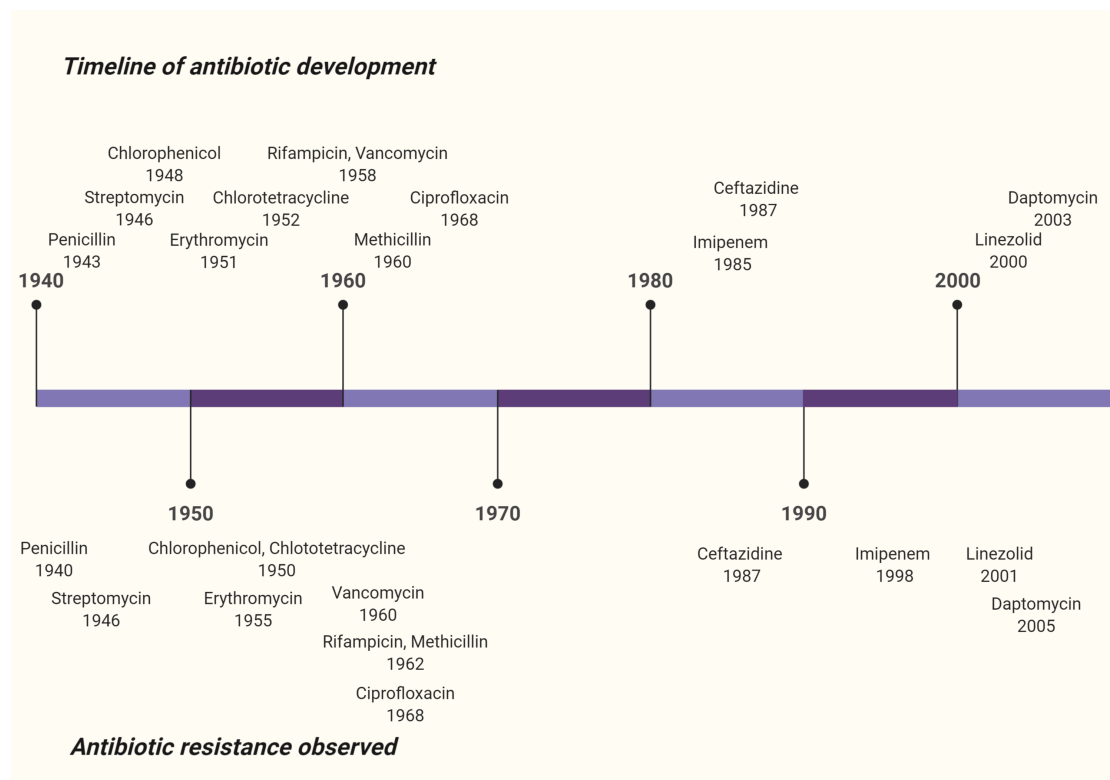


Figure 1.2: Timeline of development of antibiotic resistance. The development of antibiotics is shown on the top and the emergence of resistance is shown at the bottom.¹⁶

Antimicrobial resistance (AMR) is the ability of micro-organisms to survive the exposure to antimicrobial agents, thereby rendering standard treatments ineffective. Although it is a natural phenomenon, overuse and inappropriate use of antibiotics has

accelerated the process. The recent reports from World Economic Forum on Global Risks have listed antibiotic resistance as one of the greatest threats to human health.^{1,17} According to the estimation by the Center for Disease Control and Prevention (CDC), in the US, more than 2.8 million people are infected by antibiotic-resistant bacteria every year, causing at least 35000 deaths.¹⁸ In Europe according to a study in 2019, antibiotic resistance is responsible for approximately 33000 deaths per year.¹⁹ In the agriculture sector, antibiotics are extensively used as supplements for livestock.²⁰ The rise of AMR challenges the effectiveness of veterinary medicines, causing major impacts on food production and food security. In addition, AMR has huge ramifications on the economy. The rise of resistance leads to increase in costs associated with specialised equipments, longer hospital stays and isolation procedures for the patients. In Europe, the overall economic burden of antibiotic resistance is estimated to be at least €1.5 billion per year, with more than €900 million corresponding to hospital costs.¹⁹ In the US, the approximate costs incurred due to AMR was \$ 55 billion per year as estimated by CDC.¹⁸

Antibiotic resistance can broadly be classified as acquired resistance and intrinsic resistance. The common mechanisms of antibiotic resistance are summarized in Figure 1.3

Acquired resistance is the ability of bacteria to develop resistance against an antibiotic that was previously an effective treatment. Acquired resistance is usually found in a sub-populations of a bacterial species. Bacterial mechanisms to acquire resistance include chemical or enzymatic inactivation of the active molecule, modification of the target and reduced drug concentration at the target without modification of the compound itself.

The innate ability of certain bacterial types to resist the action of antibiotics due to the bacteria's structural or functional characteristic is called intrinsic resistance. It is typically shown by all strains of a given bacterial species. The most common bacterial mechanisms involved in intrinsic resistance are reduced permeability of the outer

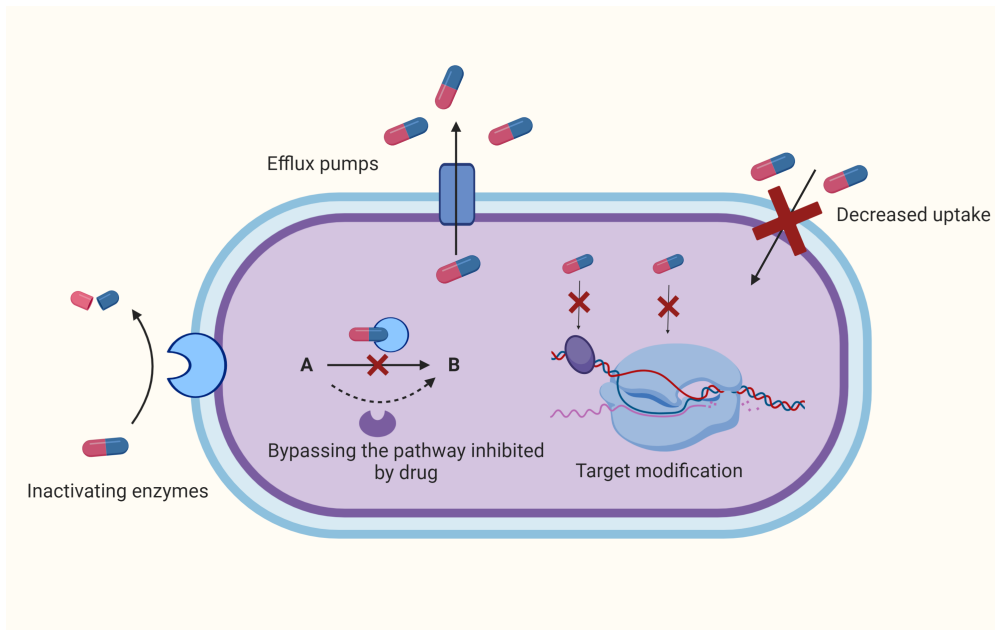


Figure 1.3: Resistance mechanism of antibiotics. Adapted from ^{16,21}

membrane and the removal of antibiotics by efflux pumps.

Infectious diseases caused by gram-negative *Enterobacteriaceae*, *Acinetobacter*, and *Pseudomonas* species are becoming increasingly difficult to treat.²² A few examples of the pertaining to the severity of the problem are detailed below. Infections caused by *P. aeruginosa* can be treated by only a few specific fluoroquinolones, β -lactams, or aminoglycosides. However, even these few antibiotics fail against antibiotic-resistant *P. aeruginosa* isolates. Infections caused by carbapenem-resistant *Klebsiella* species, have a mortality rate of up to 50%.²³ In the absence of a robust pipeline to treat these multi-drug resistant infections, there is an urgent need to explore novel therapeutic options against gram negative infections.

1.3 Pipeline of antibiotics

The rise of antibiotic resistance and increasing awareness campaigns by international organisations (WHO, UN, CDC etc.) has once again piqued interest in antibiotic research. Some noteworthy findings regarding the pipeline of antibiotics in clinical development are^{24,25} :

- The period between 2014-2018 saw an approval of 13 new antibiotics. 6 of these antibiotics were active against gram negative bacteria. Only two of the approved antibiotics belonged to a novel class.
- As of December 2019, the current clinical pipeline contains 40 antibiotics, with 15 antibiotics in Phase 1 clinical trials, 12 in Phase 2, 13 in Phase 3. Of the 13 antibiotics in Phase 3 trial, three are based on novel classes.
- 32 of these antibiotics are active against the WHO priority pathogens. At least 17 of the 42 antibiotics in development have the potential to treat infections caused by Gram-negative bacteria. But, only 1 of these 17 represents a novel class (and Phase 3 studies have since been terminated).
- The clinical development of antibiotics is primarily driven by small- or medium-sized enterprises, with only one company ranking among the top 50 pharmaceutical companies by sales. Nearly 75 percent of these companies have no products on the market.

To summarize, although the pipeline seems to be robust, statistically, only 1 out of 5 infectious disease drugs that reach the initial phase of testing in humans is approved by the Food and Drug Administration (FDA). Following this trend 8 new drugs can be expected to be approved in the near future. While the activity of 32 antibiotics against the priority pathogens listed by WHO is encouraging,²⁶ in the absence of novel

antibiotic classes, they provide little advantage over already existing drugs. Also, the pipeline of antibiotics that are effective against Gram-negative bacteria compared with the number and type of compounds that inhibit growth of Gram-positive organisms is limited.

1.4 Bacterial imaging

The conventional methods in microbiology used to diagnose bacterial infection require clinical samples (blood, urine, etc.). Deep seated infections require biopsy for a definitive diagnosis. The removal of cells or sample from their natural environment give little information about the precise site of infection. Additionally, these methods can detect only late-stage infections.²⁷

A combination of traditional methods with molecular imaging has helped in bridging these gaps in diagnosis. Molecular imaging allows the visualisation of living systems in their natural environment, without perturbing the system. Clinically available imaging techniques such as radiography, ultrasonography, computed tomography (CT), and magnetic resonance imaging (MRI) are based on changes in anatomy or tissue morphology and cannot differentiate between infection and inflammation.²⁸ Nuclear imaging techniques such as positron emission tomography (PET) and single-photon emission computed tomography (SPECT) have significantly improved the diagnosis of infections due to their high sensitivity. The detection of infection has predominantly been carried out with ¹⁸F-FDG (2-fluoro-2-deoxy-D-glucose)²⁹ or radiolabelled leukocytes.³⁰ Since these probes rely on imaging the physiological changes in response to infection rather than targeting bacteria directly, their specificity for bacterial infections is low. To overcome this limitation several bacteria specific radionuclide probes have been reported. Some examples of these tracers include radiolabelled sugars (MH¹⁸F),³¹ nucleosides (FIAU (1-(2'-deoxy-2'-fluoro-β-D-arabinofuranosyl)-5-

iodouracil)),³² siderophores, antimicrobial peptides (^{99m}Tc-ubiquicidin),³³ antibiotics (^{99m}Tc-Ciprofloxacin)³⁴ etc. However, nuclear imaging is relatively expensive due to the cost associated with the labelling and synthesis of these probes. Also, the probes have short shelf-life due to decay of the radionuclide and therefore need special infrastructure.

Recent advancements in fluorophore design (fluorescent proteins, synthetic fluorescent dyes etc.), microscopy and imaging equipments have led to the development of optical molecular imaging tools. Optical molecular imaging relies on the detection of fluorescence or bioluminescence at a target site. Bioorthogonal labeling³⁵ and enzymatic methods (SNAP-tag, CLIP-tag, HALO-tag, and TMP-tag)³⁶ have made it possible to attach synthetic fluorophores to small molecules that bind to biological targets in bacteria. A number of bacteria specific targeting moieties have been attached to fluorescent dyes to image infections. A fragment of the antimicrobial peptide UBI, labelled with NIR dye ICG02 (UBI-ICG02) was used to image infections caused by gram positive and gram negative bacteria with high selectivity.³⁷ Vancomycin conjugated to IRDye800 (Vancomycin-IR800) has been used to image *S. aureus* infection in mice.³⁸ A siderophore-BODIPY conjugate was shown to label all the tested Gram-negative bacteria of the ESKAPE panel³⁹ (Figure 1.4). Maltodextrin based imaging probes will be discussed towards the end of this chapter (section 1.9). However, due to poor signal to noise of fluorophores within the body and the inherent issue of light scattering and absorbance within tissues, these tools are yet to be used in the clinical setting.³⁶

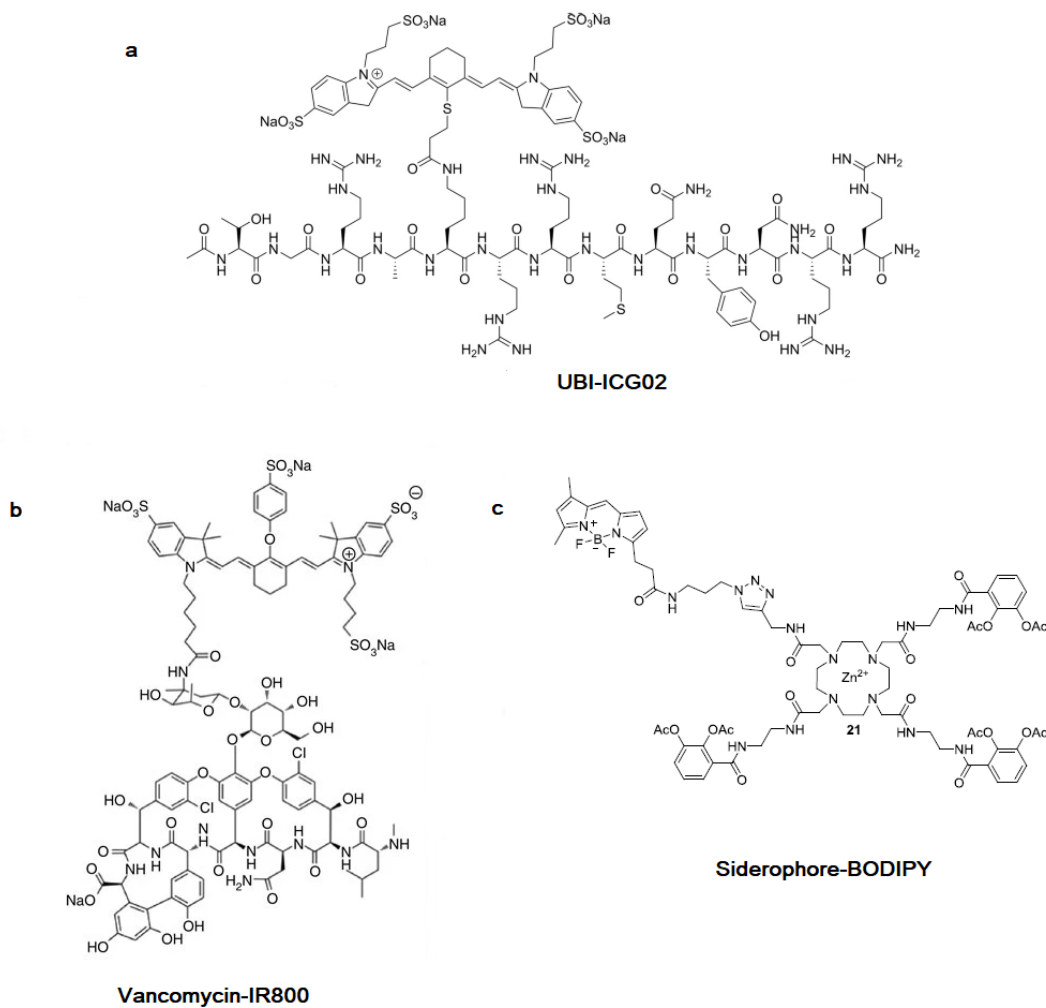


Figure 1.4: Chemical structure of bacteria specific fluorescent imaging agents. **a.** UBI-ICG02³⁷, **b.** Vancomycin-IR800,³⁸ **c.** siderophore-BODIPY.³⁹

1.5 Fluorogen Activating Protein-Malachite Green(FAP-MG) system

The FAP system involves the utilization of specific proteins to activate the fluorescence of otherwise non-fluorescent (i.e. fluorogenic) dyes⁴⁰ (Figure 1.5).

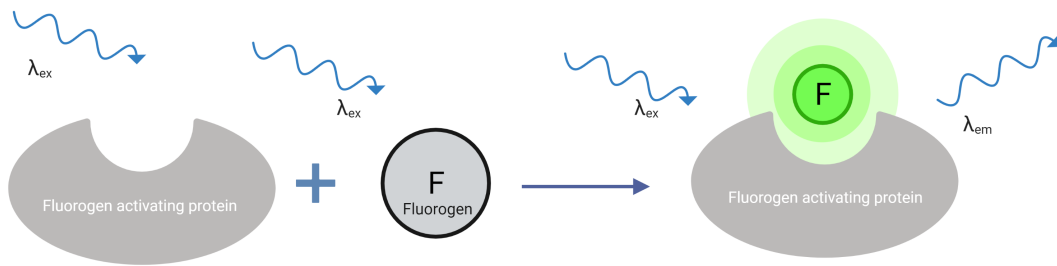
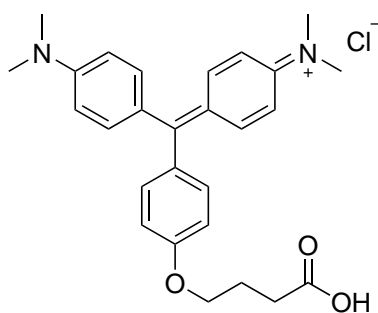


Figure 1.5: Schematic representation of FAP-MG system¹⁶

The FAP system offers numerous advantages over conventional fluorescence labelling techniques. Some of them include:

- Since the unbound dye remains non-fluorescent in solution, fixation and washing of the fluorophore is not required. This property makes the approach appealing for live-cell imaging.
- The FAP proteins have affinities towards fluorogens in the nanomolar range. This results in multiple-fold increase in fluorescence of the fluorogens.
- The genetic engineering of FAPs is easy owing to their small size (<30 kDa).
- The spatial (periplasm or cytoplasm) accumulation of the fluorogens can be tracked by controlling the expression of the protein as well as by using permeable and non-permeable fluorogens.

MG (Figure 1.6) acts as a fluorogen for the FAP system. It is a non fluorescent dye which when bound to FAP exhibits red fluorescence. The excitation wavelength of bound MG is 610 nm and its emission wavelength is 665 nm. MG shows nanomolar affinity to certain FAP proteins. The increase in red fluorescence of MG is thought to be because of the restricted rotation across the single bond of MG.



Malachite green

Figure 1.6: Structure of malachite green

The FAP-MG system can be used as an efficient tool to prove the internalisation of maltodextrin-conjugates. FAPs can be overexpressed in the periplasm or cytoplasm of the bacteria.³⁹ On treatment with the maltodextrin-MG conjugates, an increase in fluorescence would be observed only if the probes are internalized, as the complexation with FAP can take place only inside the bacteria (Figure 1.7).

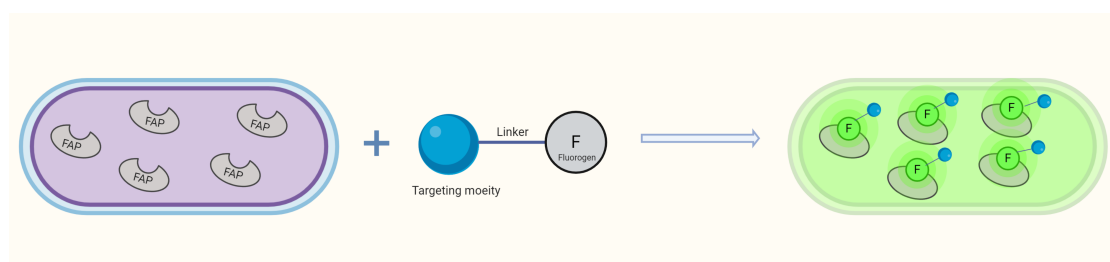


Figure 1.7: Schematic representation FAP-MG system to demonstrate internalisation¹⁶

1.6 Permeability barrier in gram negative bacteria

The development of antibiotics against gram negative bacteria is a major challenge because they are intrinsically resistant to many antibiotics.⁴¹ The cause of this inherent resistance can be understood by having a closer look at the differences in the cell wall structure of the gram negative bacteria compared to gram positive bacteria (Figure 1.8).

The presence of an additional outer membrane (OM) in gram negative bacteria significantly hampers the uptake of antibiotics. The OM is made up of an asymmetric bilayer, with the outer monolayer consisting predominantly of lipopolysaccharides (LPS) and the inner membrane of phospholipids. The membrane also contains non-specific porins and specific uptake channels that regulate the movement of substances in and out of the cell.

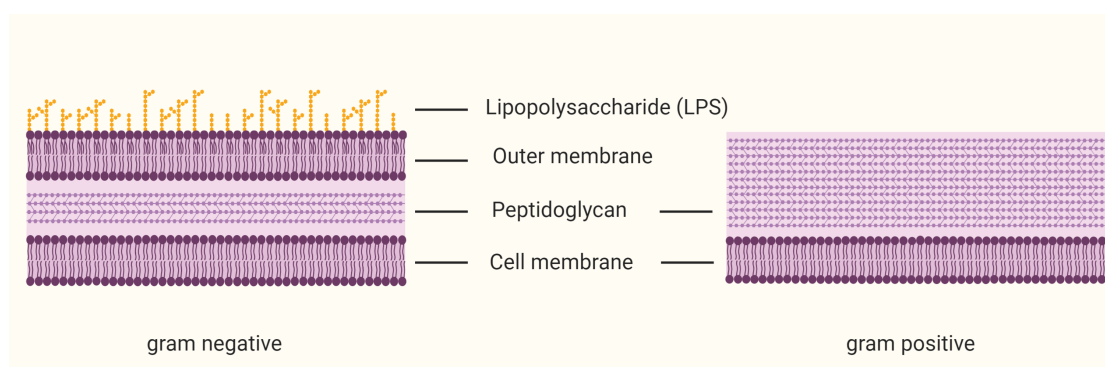


Figure 1.8: Differences between gram positive and gram negative cell wall¹⁶

LPS is an amphiphilic molecule containing a hydrophobic region (lipid A, also known as endotoxin) that has 5 or 6 fatty acids linked to diglucosamine phosphate. The LPS carries a net negative charge, resulting in the strong negative surface charge of gram-negative cells. The lipid A portion of the LPS contributes directly to the bilayer formation. The phosphate groups on neighbouring lipid A molecules attach non-covalently through interactions with divalent cations (Mg^{2+} and Ca^{2+}). This cross-bridging provides extra rigidity compared to normal bilayers, hence slowing the passive diffusion of hydrophobic compounds. Porins are bacterial β -strand proteins that form a water-filled β -barrel pore within the OM that allows passive transport of molecules across the membrane.⁴² The porin size in gram negative cell wall limits the penetration of larger hydrophilic drugs (> 600 Da). The slow uptake of drugs across the OM is further opposed by active efflux mediated by pumps which decreases the amount of required drug

at the target.⁴³

1.7 Strategies to overcome permeability barrier

As mentioned above, the permeability barrier provided by the outer membrane and efflux of antibiotics are the primary cause of intrinsic resistance in gram negative bacteria. The most important methods to overcome the permeability barrier will be discussed in this section.

1.7.1 OM permeabilizers

Permeabilizers of the OM make gram-negative bacteria susceptible to hydrophobic antibiotics which are otherwise an ineffective treatment. These are generally cationic, amphiphilic molecules that act by destabilizing the LPS layer. The mechanism of action is thought to involve interaction of the cationic molecules with the negatively charged outer leaflet of the OM and subsequent displacement of the divalent cations bound on the lipid A. This disrupts the LPS layer and renders liquidity to the OM, thereby allowing penetration of the hydrophobic molecules.

The permeabilizing ability of the molecules is quantified by the formula for synergism, in terms of fractional inhibition concentrations (FICs), which are calculated as follows:

$$FIC = \frac{[A]}{MIC_A} + \frac{[B]}{MIC_B}$$

where, MIC_A and MIC_B , are the minimum inhibition concentrations (MICs) of compounds A and B, respectively, and [A] and [B] are MIC of compounds A and B, in combination with each other. FIC values ≤ 0.5 indicate synergistic effects.

Another commonly used method to monitor permeability is based on the uptake of hy-

dophobic molecules like *N*-phenyl-naphthalen-1-amine (NPN). Permeabilization of the OM allows NPN to diffuse into the hydrophobic environment of the OM and cytoplasmic membrane, which results in an increase in fluorescence intensity of NPN.⁴⁴

Some of the outer membrane permeabilizers include:

Polymyxins

Polymyxins are membranotropic compounds that increase the susceptibility of bacteria to a variety of hydrophobic compounds by disrupting the OM. These are pentacationic amphipathic lipodecapeptide characterized by a cyclic heptapeptide core, linked to a linear tripeptide with an N-terminal fatty acyl moiety. Their bactericidal activity involves a dual mode of action. Initially polymyxins bind to the anionic LPS layer in the OM and permeabilize it (this accounts for the sublethal action). Then they enter the cytoplasmic membrane where the final and lethal damage is caused by the leakage of the cytoplasmic components.⁴⁵⁻⁴⁷ Due to the nephrotoxicity of polymyxins their clinical use was abandoned in the 1960s. However, continued research in the field has led to the development of derivatives that are more efficacious and less toxic. Vaara and co-workers reported that derivatives of polymyxins lacking the fatty acid tail showed less or no bactericidal activity but retained the OM-permeabilizing action.⁴⁸⁻⁵² The directly antibacterial polymyxins also exhibit permeabilizing action at sub-inhibitory concentrations. Polymyxin B nonapeptide (PMBN) is one of the best characterised permeabilizer of the OM and remains the standard by which other OM permeabilizers are measured. PMBN lacks the fatty acyl tail as well as the N-terminal diaminobutyryl residue. Its MICs against *E. coli* and *S. typhimurium* are 300 µg/ml, but concentration as low as 0.3 to 1 µg/ml are sufficient to permeabilize the OM to otherwise inactive antibiotics like rifampicins (100 fold decrease in MIC), erythromycin and fusidic acid (100 fold decrease in MIC).^{49,50,53} Other derivatives of polymyxin B, deacyl polymyxin B (DAPB), the octapeptide (PMBO) and heptapeptide (PMBH), are also effective permeabilizers, with

FIC values <0.3 for various antibiotics.^{53,54} Polymyxin E (colistin) was shown to display potent synergism with rifampicin against multidrug-resistant *A. baumannii* (FICs as low as 0.07).⁵⁵ The chemical structures of some important polymyxin derivatives is shown in Figure 1.9

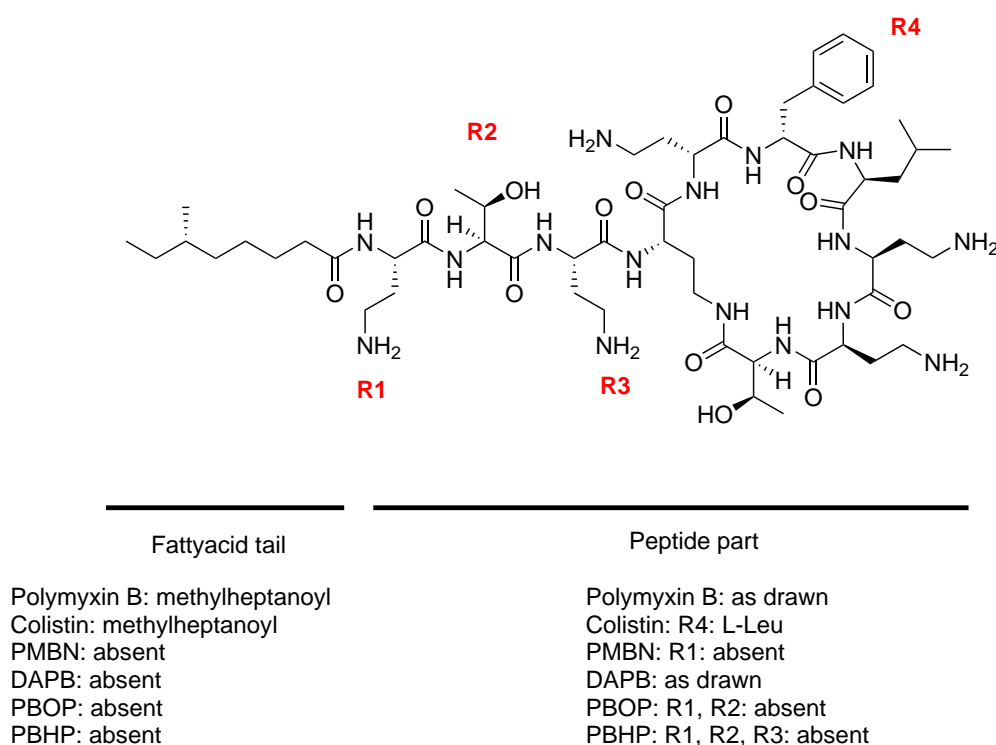


Figure 1.9: Structures of polymyxin derivatives

Cationic peptides

Cationic peptides are endogenous to a wide range of organisms ranging from bacteria to mammals. Their antimicrobial properties have attracted significant research interest. Antimicrobial peptides are rich in lysine and arginine and comprise 12 to 45 amino acid residues. Structurally, these peptides form alpha-helices and beta-sheet motifs in the presence of bacterial membranes. The common conformation adopted by the peptides is such that the cationic groups orient towards one face of the molecule and hydropho-

bic side chains towards the other face. This conformation facilitates the interaction of the cationic peptide with the LPS layer. Peptides such as buforin II, cecropin P1 and magainin II resulted in FIC values in the range of 0.250-0.375 when used in combination with a variety of hydrophobic antibiotics against drug-resistant *P. aeruginosa*⁵⁶ and *S. maltophilia*.⁵⁷ Vaara and Porro reported a series of synthetic peptides that exhibited synergism when used in combination with rifampin, erythromycin, fusidic acid, and novobiocin, with FIC values comparable to PBNP. Peptide P1 (entry 4 Table 1.1), consisting of cationic lysine residues and hydrophobic phenylalanine residues, resulted in a 300 fold decrease in the MIC of rifampicin at the concentration of 3 $\mu\text{g/ml}$, in *E. coli*.⁵⁸ Sawyer et al. demonstrated that defensins, which exists as β -sheets, could permeabilize the outer membrane of *P. aeruginosa*.⁵⁹ Structural variants of polyphemusin I, another peptide known to adopt β -sheet structure, was shown to facilitate the internalization of the hydrophobic molecule NPN in *E. coli*. Recently, conjugation of magainin to an arginine-rich cell penetrating peptide R9 was shown to increase the the antimicrobial activity (4-16 fold) in gram negative bacteria.⁶⁰ The sequences and the source of the peptides is summarized below (Table 1.1).

Table 1.1: Sequences of cationic peptide OM permeabilizers

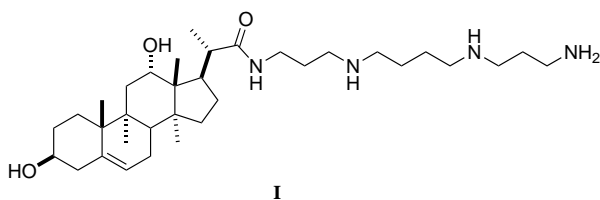
S. No.	Peptide	Sequence	Source	FIC
1	Buforin II	TRSSRAGLQFPVGRVHRLLRK	Toad	0.3-0.5
2	Magainin II	SWLSKTAKKLENSAKKRISGIAIAIQGGPR	Frog	0.25-0.5
3	Cecropin P1	GIGKFLHSAKKFGKAWGEIMNS	Insects	0.25-0.5
4	P1	KFFKFFKFF	Synthetic	0.03-0.1
6	Polyphemusins	RRWCFRVCYRGFCYRKCR	Crab	-
7	R9-magainin	RRRRRRRRRGGGGIGKWLHSAKKFGKAFVGEIMNS	Synthetic	-

Cationic steroids

Similar to polymyxins, cationic steroid antibiotics (CSAs) exhibit dual antibacterial action: the bactericidal activity and OM permeabilizing activity. CSAs can be classified into two categories: polymyxin mimics and squalamine mimics (a CSA isolated from the dogfish shark). Polymyxin mimics are characterized by the attachment of three

amino groups, via tethers, to a steroid nucleus (Figure 1.10). Kikuchi et al. synthesized an extensive series of squalamine mimics containing 24 compounds.⁶¹

Squalamine mimic



Polymyxin mimics

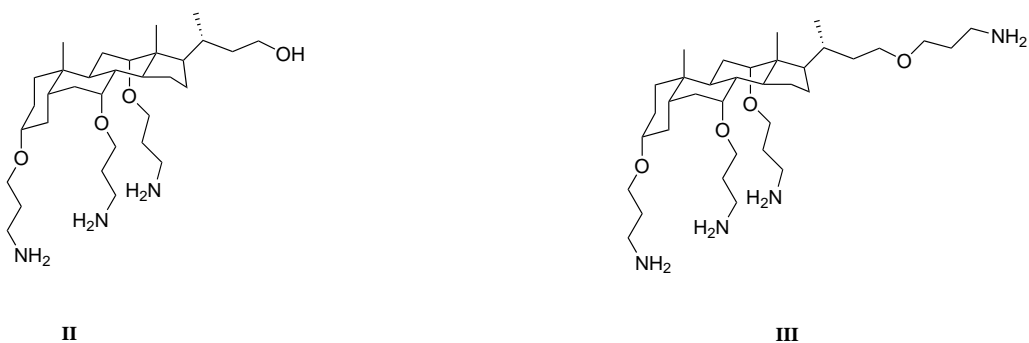


Figure 1.10: Structures of representative CSAs

CSAs have been reported to sensitize gram negative bacteria to a number of inactive antibiotics like erythromycin, fusidic acid, novobiocin and rifampicin. Polymyxin mimics compounds **II** and **III** (Figure 1.10), at concentrations of 0.7 and 0.5 $\mu\text{g}/\text{mL}$, respectively, lowered the MIC of erythromycin to 1 $\mu\text{g}/\text{mL}$ (FIC values of < 0.057 and < 0.093, respectively). In *K. pneumoniae* at a concentration of 0.73 $\mu\text{g}/\text{mL}$, **II** lowered the MIC of novobiocin from 75 to 1 $\mu\text{g}/\text{mL}$ (an FIC of 0.029).^{62,63} Squalamine mimic **I** resulted in enhancement of the activity of rifampin by subinhibitory concentrations of **II** with *E. cloacae*, *K. pneumoniae*, and *S. marcescens* (FIC values 0.046-0.156).^{61,62}

Drawbacks of cationic permeabilizers

The main concerns relating to the use of cationic permeabilizers include their selectivity and toxicity. In addition to destabilizing the bacterial OM, the permeabilizers also affect the eukaryotic membranes.⁵⁸ Many of these CPA and CSAs are haemolytic. As mentioned earlier, the use of polymyxins has been limited due to their nephrotoxicity.

1.7.2 Carriers of antibiotics

Carrier-mediated intracellular delivery of antibiotics is another approach to overcome the permeability barrier. Several nanotechnology-derived carriers including liposomes,⁶⁴ micelles,⁶⁵ dendrimers,^{66,67} nanoparticles,⁶⁸ and hydrogels⁶⁹ have been employed for this purpose. Liposomes are one of the most investigated drug carriers due to their good bio-compatibility and ability to encapsulate both hydrophilic and hydrophobic molecules. Liposomes encapsulating fusidic acid (an antibiotic with activity limited to gram-positive bacteria) interacted with cell membranes and release the enclosed drug into the cytoplasm.⁷⁰ In another study, vancomycin-gold nanoparticles were shown to destabilize the LPS membrane in *E. coli*, thereby increasing the permeability of vancomycin into the cell and resulting in the lysis of the cell wall.⁶⁸

1.8 Trojan horse strategy

The narrow pipeline of antibiotics and lack of novel antibiotic classes to treat gram negative bacterial infections calls for innovative solutions to overcome the OM permeability barrier in gram negative bacteria. The trojan horse strategy, by conjugating drugs and other compounds of interest to siderophores, has proved to be an elegant method to achieve intracellular delivery of antibiotics in gram negative bacteria. A schematic representation of the trojan horse strategy is shown in Figure 1.11.

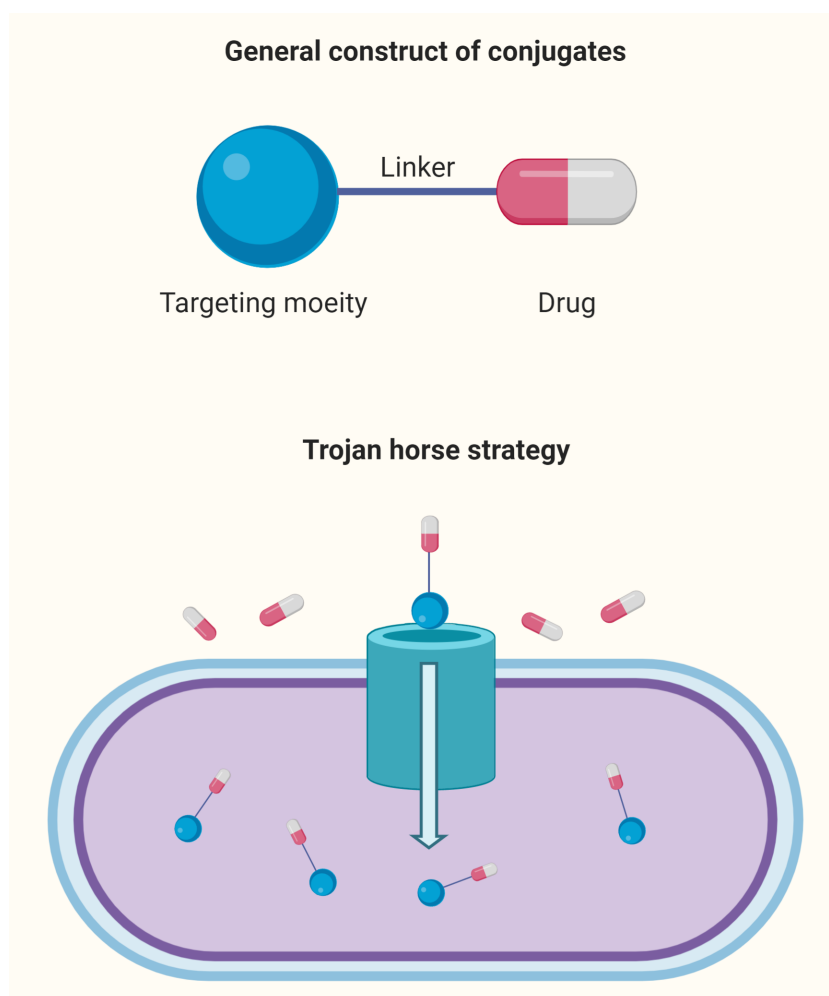


Figure 1.11: Trojan horse strategy: Drugs which are excluded due to the OM permeability barrier can be intra-cellularly transported by conjugating drugs to nutrients essential to bacterial growth and metabolism into the cell.¹⁶

This strategy involves smuggling of drugs into gram negative bacteria, similar to the entry of Greek army into the city of Troy disguised in a wooden trojan horse. The concept behind this strategy is to hijack the active transport machinery of the bacteria to obtain facilitated transport of the antibiotics. Essential nutrients, that are actively transported into the bacteria via specific pathway are conjugated with the antibiotics of interest, such that the nutrient uptake pathways serve as gates for the antibiotics.

1.8.1 Siderophore transport systems

Exploiting the iron uptake system has been highly efficient in overcoming the permeability barrier in gram negative bacteria. Iron uptake by bacteria is carried out by small molecule iron chelators called siderophores, that are secreted by bacteria into the extra-cellular environment.⁷¹ Due to their high affinity for iron, siderophores solubilize and bind iron in the bacterial environment and transport it to the bacterial periplasm via specific ferri-siderophore TonB-dependent transporters present in the OM.⁷² Inspired from natural sideromycins, a number of synthetic siderophore conjugates with antibiotics such as β -lactams,⁷³ ciprofloxacin,⁷⁴ daptomycin,⁷⁵ linezolid⁷⁶ etc. have been widely researched. Some of the major advantages of this strategy include decrease in MIC values up to 1000-fold,⁷⁷ transforming gram-positive antibiotics into potent gram-negative antibiotics,⁷⁸ and enhancing potencies against MDR bacteria.⁷⁹ Recently, Cefiderocol (Figure 1.12), a siderophore–cephalosporin conjugate, has been approved by US FDA for the treatment of complicated urinary tract infection.²⁴

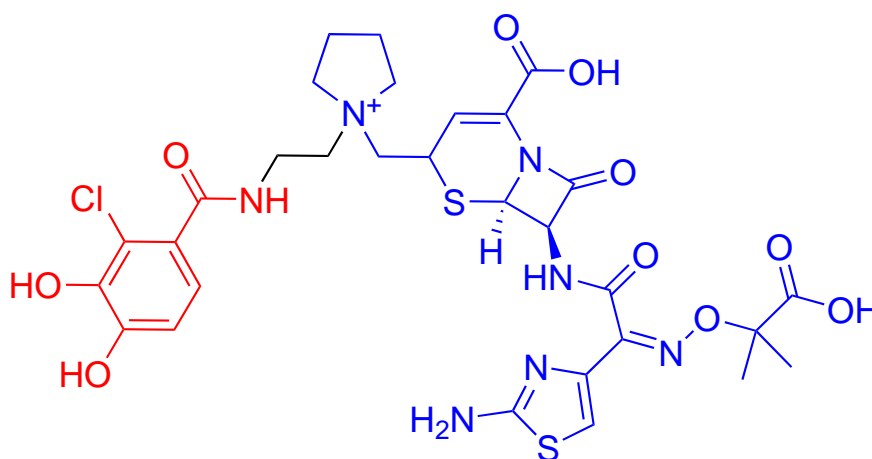


Figure 1.12: Chemical structure of FDA approved Cefiderocol. Catechol part is represented in red, and the antibiotic cephalosporin in blue.

However, over-dependence on just a few transporters poses the threat of acquired resistance against these conjugates. For example acquired resistance has been observed for

siderophore conjugated monobactam MB-1⁸⁰ and monocarbam SMC-3176 in *P. aeruginosa*.⁸¹ Bacteria avoid uptake of these conjugates by switching to other favourable iron uptake pathways. Therefore, it is desirable to identify additional pathways to be used to transport antibiotics in gram negative bacteria.

1.9 Maltodextrin transport system of *E. coli*

Maltodextrins are oligomers of D-glucose, linked together via $\alpha(1-4)$ linkage (Figure 1.13). They occur in nature as breakdown products of starch and amylose degradation. In solution, maltodextrins exist predominantly in a left handed helical conformation.⁸²

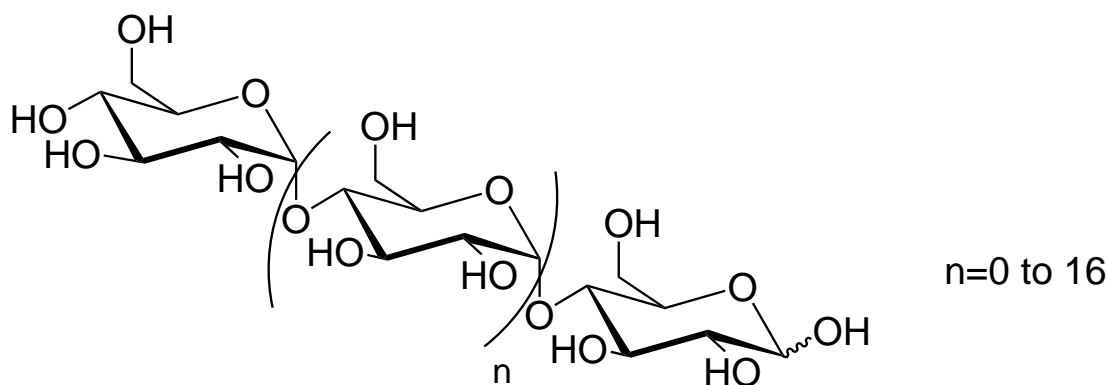


Figure 1.13: Structure of maltodextrins.

The maltodextrin transport system is an attractive targeting moiety to be used in the trojan horse strategy because of the following reasons:

- The transport of maltodextrins by the maltodextrin transport system is well understood due to the availability of numerous crystal structures, genetic and biochemical data.
- Maltodextrins are the major source of glucose in bacteria, and are actively transported into the bacteria via the maltodextrin transport pathway.

- Maltodextrin transporters are not expressed in mammalian cells, making it a highly selective and sensitive system to target bacteria.

1.9.1 Components of the maltodextrin transport system

The maltodextrin transport is mediated by a system responsible for the uptake and catabolism of maltodextrins containing upto 7 glucose units. It consists of three components: maltoporin (also called LamB) a porin embedded in the OM; a periplasmic substrate-binding protein, MBP (MalE); and an inner membrane ABC transporter, MalFGK₂ (Figure 1.14).

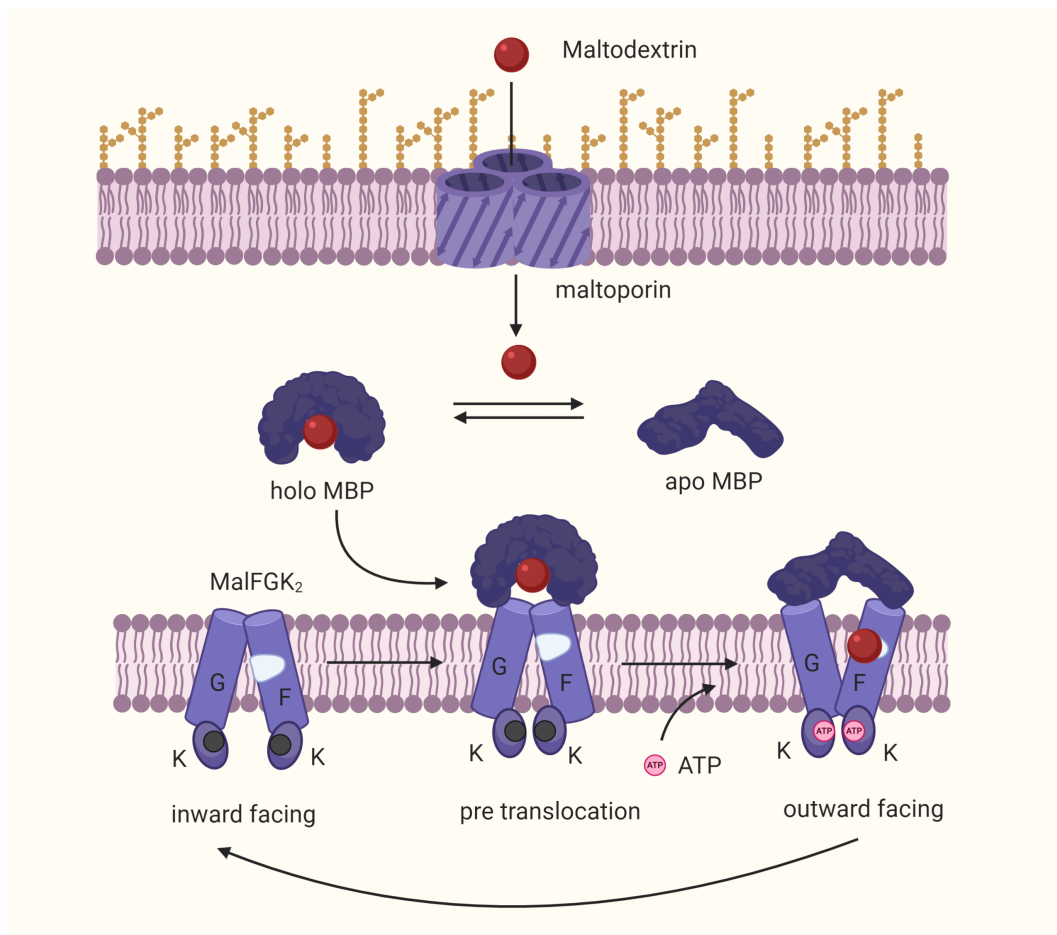


Figure 1.14: Maltodextrin transport system¹⁶

Maltoporin is a homotrimer of β -barrels, each subunit has a wide channel formed by an 18-stranded antiparallel β -barrel (Figure 1.15). Each channel is capable of allowing the passage of substrates across the OM.⁸³ About halfway through the channel there is a constriction due to three inwardly folded loops, rendering it an hourglass shape.⁸⁴

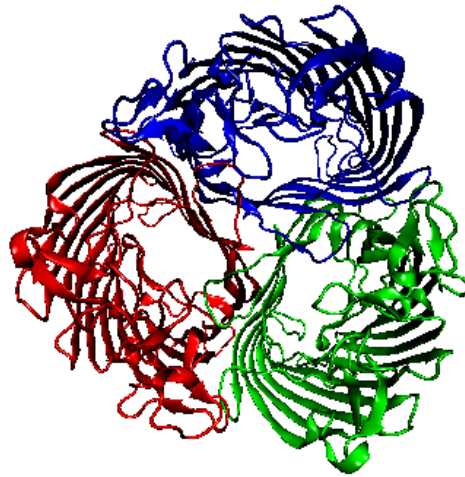


Figure 1.15: Crystal structure of maltoporin malB depicting the homotrimer of β -barrels⁸⁴

The MBP is a water soluble protein present in the periplasm. It consists of two nearly symmetrical lobes, each formed by parallel β sheets flanked by α helices on both sides (Figure 1.16). The two lobes are connected to each other by two anti-parallel β sheets and an alpha helix. The binding site is in between the two lobes.^{85,86}

MBP exists in two conformational forms: Substrate-bound and substrate-free. In the substrate bound form the lobes exist in a closed conformation, thereby excluding interactions between bulk solvent and bound substrate.^{88,89} On the other hand, when in substrate free form the lobes are open and the the bulk solvent can access the substrate-

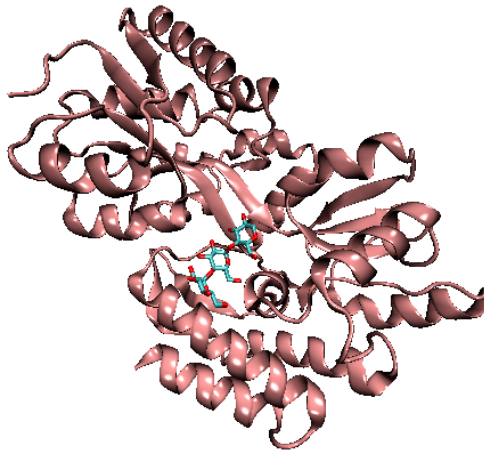


Figure 1.16: Co-crystal structure of maltose binding protein malE from *E. coli*, complexed with maltotriose.⁸⁷

binding site.⁸⁹ The inner membrane MalFGK2 is made up of the construct characteristic of the ABC transporter: two transmembrane domains (TMDs) that are embedded in the membrane bilayer (Mal F and Mal G), and nucleotide-binding domains (NBDs) that are located in the cytoplasm (MalK).⁹⁰ The hydrophobic MalF protein consisting of eight membrane-spanning α -helical segments with both the C- and N-terminals of the polypeptide chain extending into the cytoplasm.⁹¹⁻⁹³ Between the MSS 3 and 4, MalF contains a large periplasmic loop (scoop loop), that plays an important role in the specificity of the system. Similarly, MalG consists of six membrane-spanning α -helical segments with both terminals protruding into the cytoplasm.^{94,95} The Mal K consists of two subsites, the A and B domains for the binding of ATP.⁹⁶

1.9.2 Mechanism of maltodextrin transport

Maltoporin LamB facilitates the passive diffusion of the substrate through the OM to the periplasmic MBP. The substrates can enter the periplasmic space also through other porins, eg. OmpC and OmpF porins. At substrate concentrations less than 10^{-4} M,

transport predominantly operates via the LamB route. Also, lower maltodextrins (maltose and maltotriose), when present in higher concentrations can be transported via the OmpC/F porins. In the absence of the substrate, the MBP in the periplasm is bound to the LamB. This interaction facilitates the substrate to gain easy access to the binding site of the MBP. Substrate binding to the MBP disrupts the interaction between LamB and MBP, and substrate bound MBP is released in the periplasm. A conformational change is induced when the maltodextrins bind to MBP, from an substrate unbound open form to a bound closed form.⁸⁵ The MalFGK2 exists two conformations, depending on its interaction with the MBP. The first conformation corresponds to an inward facing conformation, such that the two NBDs are well separated and the substrate recognition site is exposed to the cytoplasm.⁹⁰ Binding of substrate-loaded MBP triggers a conformational change of the transporter, such that the NBDs are in closer proximity to one another. This movement of NBDs permits intracellular ATP to bind to the NBD of MalK, which in turn brings about a concerted motion that opens the substrate binding site to the periplasmic side (outward-facing conformation).⁹⁰ Subsequently, MBP releases the substrate into the cell. The hydrolysis of ATP results in the reversal of the transporter to its inward-facing conformation, releasing the substrate to the intracellular side.

1.9.3 Substrates of the maltodextrin transport system

The maltose transport system is highly selective towards maltodextrins. Glucose units linked via α -1, 4 glycosidic bonds are accepted as substrate by the maltodextrin transport system. The smallest substrate maltose contains two glucose units, while the largest substrate maltoheptaose contains seven glucose units.⁹⁷ The transport of closely related oligosaccharides through LamB is hampered, eg. for sucrose (40 times slower), cellobiose (8 times slower), isomaltose (2 times slower), lactose (11 times slower)⁹⁸ (Figure 1.17). Moreover, modification of the anomeric hydroxyl group at the reducing end of the maltodextrins by residues larger than methyl group results in maltodextrin analogs

are no longer transported into the cell.^{97,99-101}

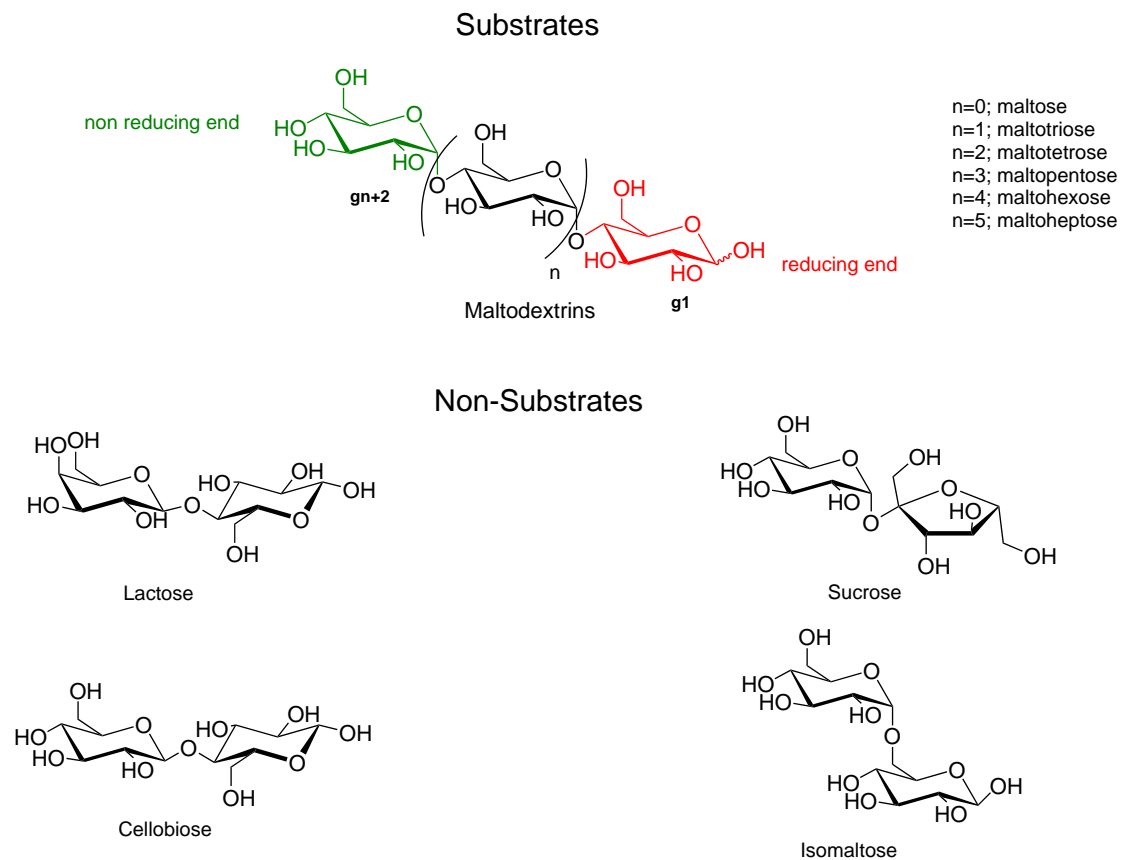


Figure 1.17: Substrates of maltodextrin transport system. Maltodextrins ranging up to maltohexose serve as the substrates for the maltodextrin transport system. The critical reducing end of the substrate is shown in red and the non reducing end in green. The glucose units are numbered from the reducing end as g_1, g_2, \dots, g_n .

1.9.4 Critical interactions governing specificity of the maltodextrin transport system

Maltoporin has a millimolar affinity for maltodextrins. The constriction in the middle of the beta barrel acts as a binding site and is favourable for the binding of the left-handed helical conformation of the maltodextrins. Its channel lining compliments the amphipathic nature of saccharides. In the binding site, the hydrophobic regions of the

pyranose ring of the maltodextrins exerts apolar van der Waals interaction to the “greasy slide” (a hydrophobic path that is composed of aromatic residues). The greasy slide can accommodate three consecutive glucosyl units. For example as observed in the crystal structure of LamB bound to maltohexose, the pyranose rings of the g2, g3, and g4 units interact with the greasy slide¹⁰² (Figure 1.18).

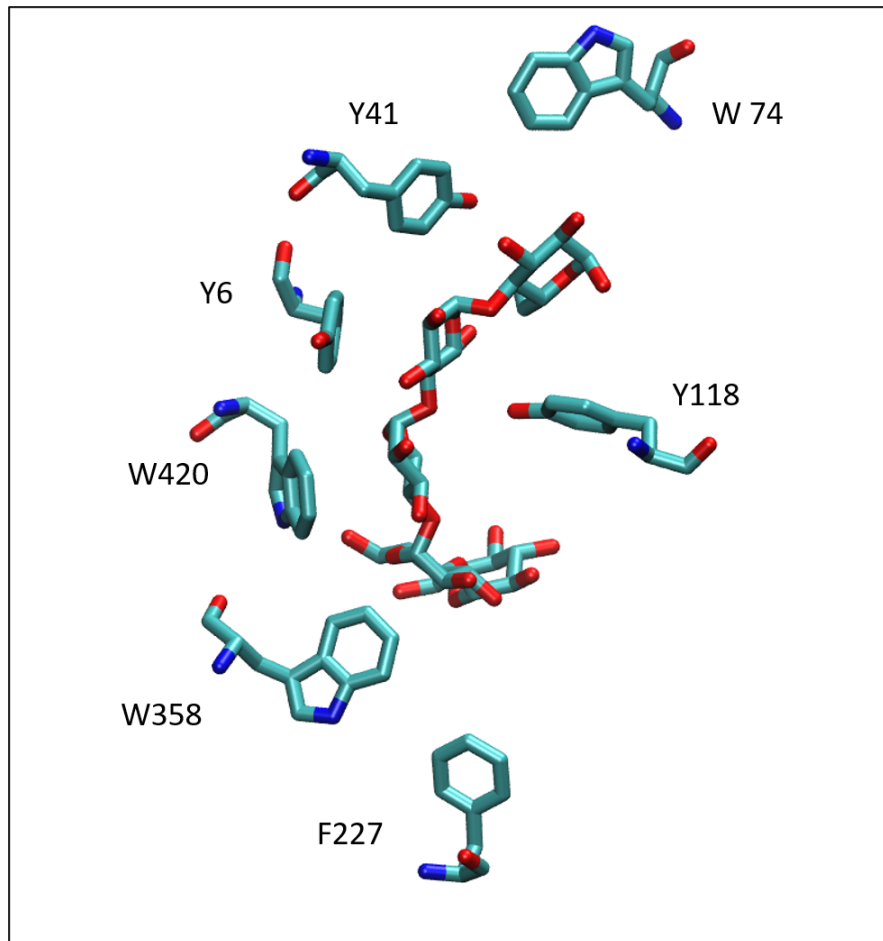


Figure 1.18: Schematic view of maltohexose bound to maltoporin depicting the amino acids involved in the greasy slide.¹⁰²

Also, all the equatorial hydroxyl groups of these units form hydrogen bonds with polar residues inside the channel.¹⁰² The remaining glucosyl units do not interact with the LamB (Figure 1.19).

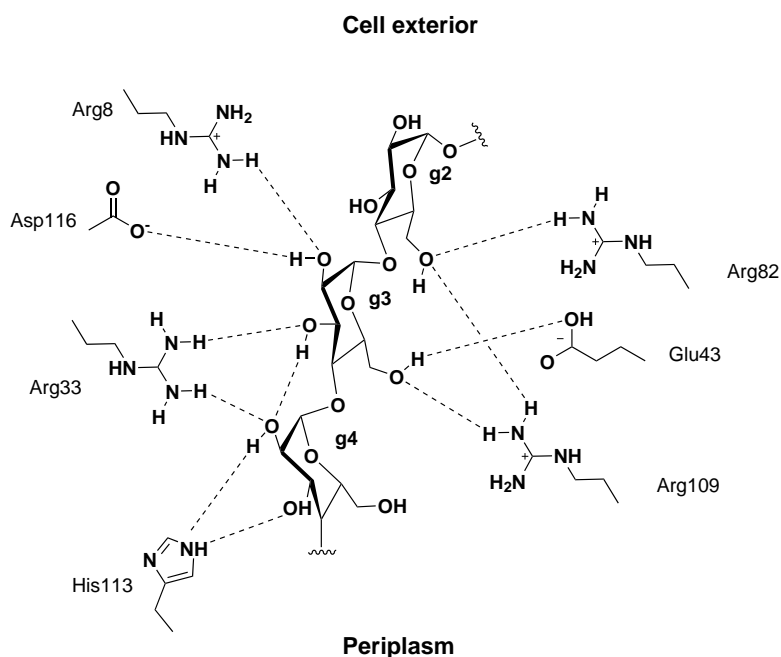


Figure 1.19: Schematic view of the hydrogen bonds between maltohexose and malto-porin. Adopted from ¹⁰²

Coming to the MBP, the shape-complementarity, extensive hydrogen-bonding, and amphiphilic nature of binding site of MBP results in the binding of variety of sugar substrates, ranging from maltodextrins, cyclodextrins to amyloses.⁸⁶ However, not all of these sugars are transported inside the cell. The maltodextrins bind in a groove between the two lobes of MBP. The substrates are recognized from their reducing end. Crystal structure obtained with the maltoheptose bound to the pre-translocation showed interaction between the four glycosyl units of maltoheptose from the reducing end (g1,g2,g3 and g4) with MBP.¹⁰³ The substrate specificity is primarily governed by the inner membrane transporter, MalFGK2. In the pre-translocation state, a conserved glutamine residue (Q256) in the scoop loop of MalG forms hydrogen bonds with the primary hydroxyl group and the ring oxygen of the g1 unit (Figure 1.20).¹⁰³ This interaction restricts the modifications at the reducing end of the sugar.

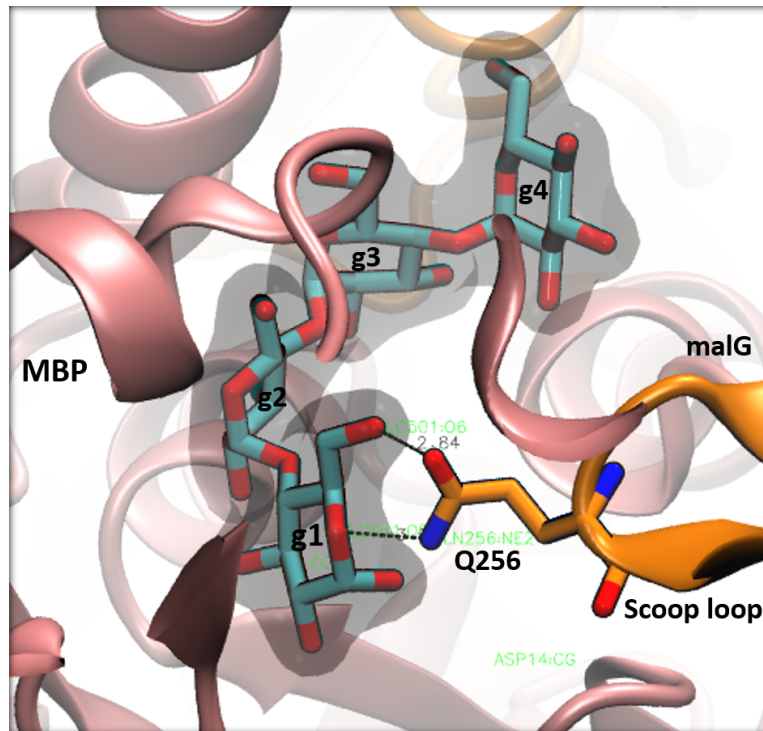


Figure 1.20: Schematic view of the critical interaction between the glutamine residue (Q256) of MalG and reducing end of maltoheptose. ^{16,103}

In the outward-facing state, MalG recognizes four units (g1, g2, g3 and g4) from the reducing end of the sugar, similar to MBP. MalF recognizes three glucosyl units from the non-reducing end (Figure 1.21). As the MBP and MalG recognize the sugars from the reducing end of the sugar and MalF interacts with the opposite end, the maltodextrin transport system is specific to linear malto-oligosaccharides with the α -1, 4 linkage.

The size limitation for the substrates can be explained by the space constraint in the binding site of the pretranslocation state. The cavity measuring 2400 \AA^3 can only accommodate dextrans containing up to 7 glucosyl units. ¹⁰² Although larger maltodextrins bind to MPB, they disrupt the interaction between MBP and MalFGK2, thereby preventing ATP hydrolysis and the transport across the inner membrane.

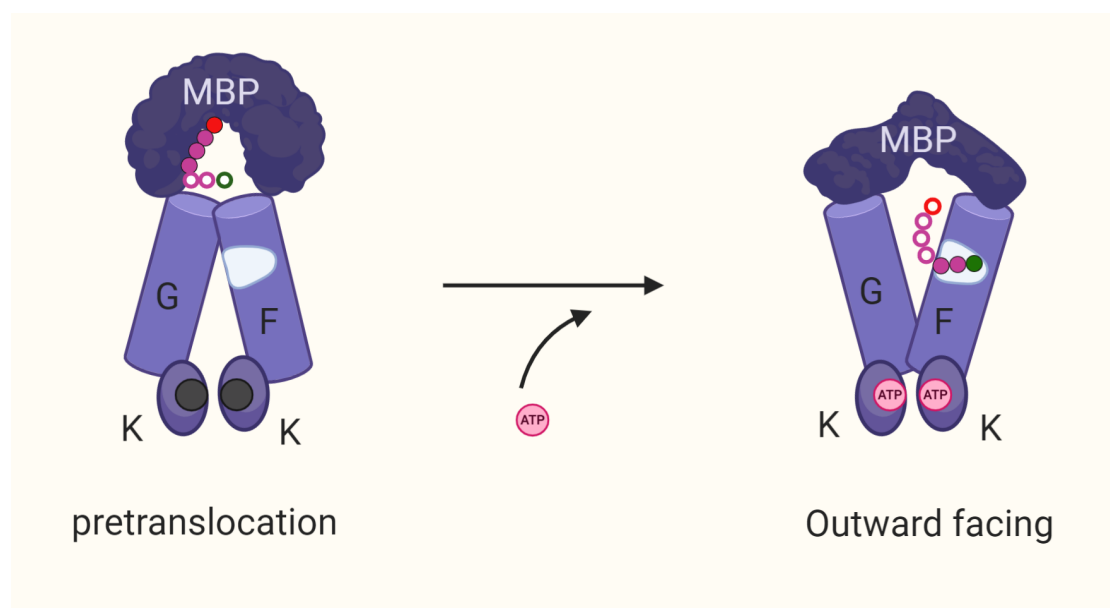


Figure 1.21: Representation of substrate recognition in the outward-facing state and the pre-translocation state. The MBP recognizes the sugar from the reducing end (shown in red) and malF from the non-reducing end (green). The solid and dashed circles represent the glucosyl units bound and unbound to protein, respectively. Adapted from [16,102](#)

1.10 Previously reported maltodextrin conjugates

The first maltodextrin conjugates used in the Trojan horse approach was reported in 2011 by Murthy et al.. Two probes, MDP-1 (BOT_10) and MDP-2 (Figure 1.22) bearing imaging moieties perylene dye and IR786 NIR-dye, respectively, at the reducing end of maltohexose were synthesized. These probes were shown to be internalized through the maltodextrin transport system in both gram positive (*B. subtilis* and *S. aureus*) and gram negative (*E. coli* and *P. aeruginosa*) bacteria in millimolar concentration. MDP-1 was also shown to penetrate biofilms of bacteria. *In vivo* imaging in mice showed that MDP-1 could image *E. coli* infection in mice muscle. Additionally, the probes could distinguish between bacterial infections and other sterile inflammation caused by injection of LPS. [104](#)

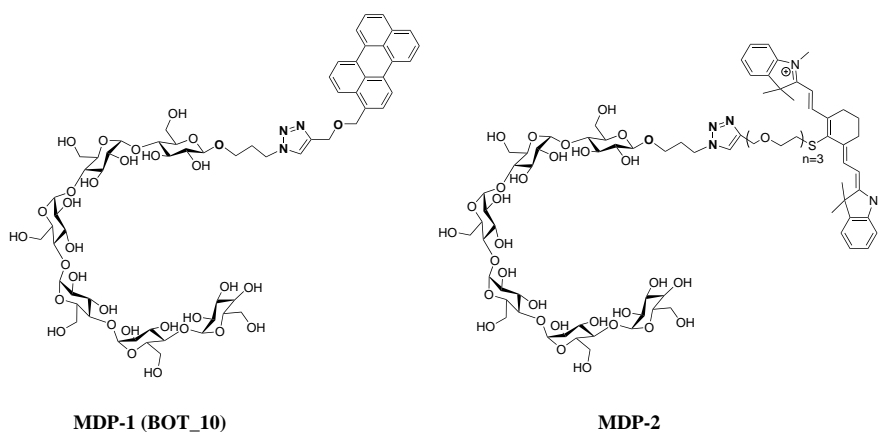


Figure 1.22: Structure of MDP-1 and MDP-2¹⁰⁴

In a subsequent study, Murthy and co-workers synthesized a positron emission tomography (PET) tracer containing a ^{18}F -labeled maltohexose MH^{18}F (Figure 1.23). In *E. coli*, the probe was shown to detect infections with better sensitivity and selectivity as compared to the current standard tracer, fluorodeoxyglucose (^{18}F FDG). *In vivo* imaging in rats demonstrated that MH^{18}F could measure drug resistance and also monitor the therapeutic effect of antibiotics.³¹

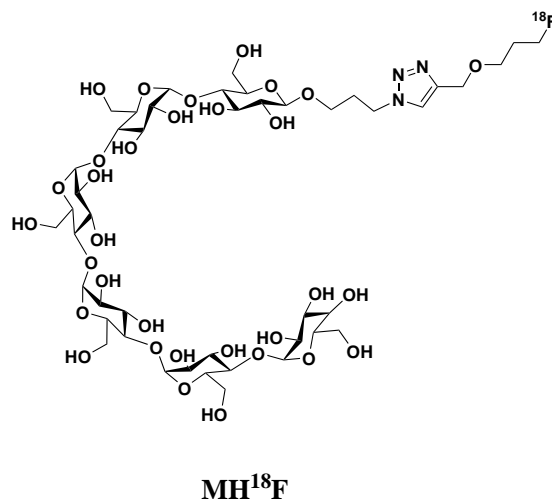


Figure 1.23: Structure of ^{18}F -labeled maltohexose probe³¹

Galstyan et al. synthesized a maltohexose-functionalized Si^{IV} phthalocyanine (Figure 1.24) which has a dual functionality, comprising the fluorescent labeling of bacteria due to its intrinsic fluorescence and induced killing of bacterial infection by producing reactive oxygen species (ROS).¹⁰⁵ Internalization studies conducted on gram-positive methicillin-resistant *S. aureus* (MRSA) and the antibiotic resistant gram-negative *E. coli* demonstrated that the probes label both bacterial types, but selectively inactivate only the gram-positive strain. This result indicates that the probes result in superficial labelling of bacterial cell wall as opposed to intracellular uptake.¹⁰⁶ The failure in internalization of this probe is speculated to be due to the modification of the anomeric center at the reducing end of the sugar.¹⁰⁶

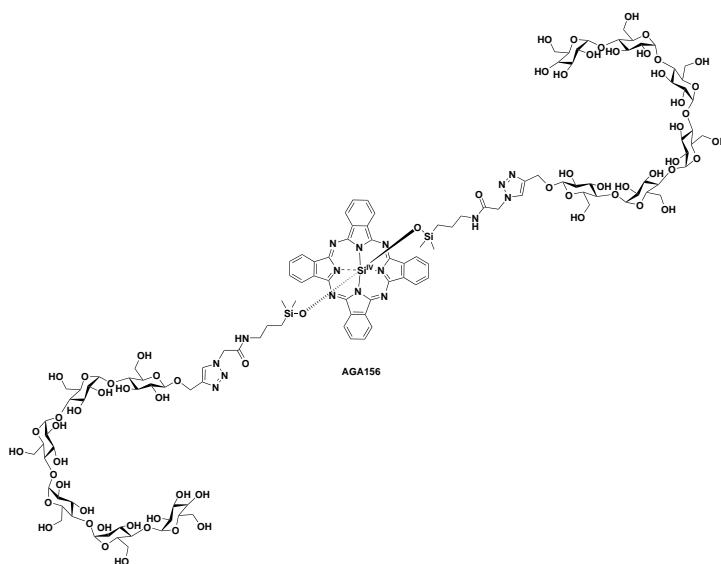


Figure 1.24: Structure of bimodal photoprobe¹⁰⁶

In a following study by Axer et al., a ^{99m}Tc -labeled maltohexose (Figure 1.25) mimicking MDP-1 was synthesized as a tracer to be used in single-photon emission computed tomography (SPECT) imaging. In vivo imaging studies of *S. aureus* infection in mice revealed specific uptake only in the infected area. However, the sensitivity of the probe was poor when compared to the ones currently available. The low sensitivity is specu-

lated to be due to blockage of the anomeric end of the sugar.¹⁰⁷

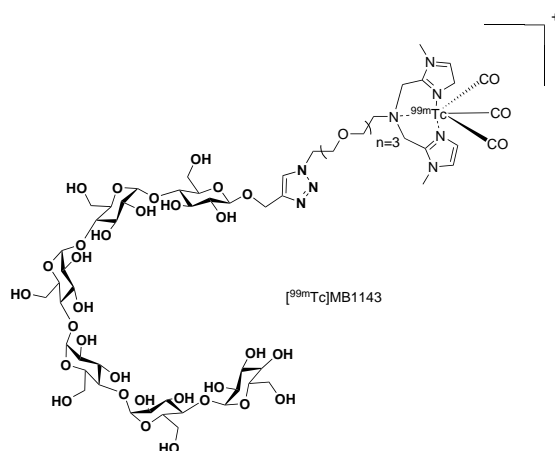
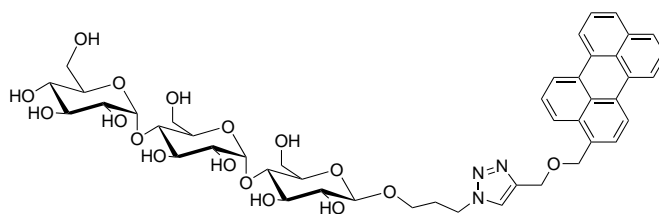


Figure 1.25: Maltohexose based SPECT tracer.¹⁰⁷

Dumont et al. reported the synthesis of BOT_14, the maltotriose analogue of MDP-1 (Figure 1.26). Intracellular accumulation studies, supported by electrophysiology experiments showed that cpd-2 is transported better than MDP-1. BOT_14 was shown to auto-induce its own entry into the bacteria by inducing the expression of *malE*, which produces the MBP in the periplasm.¹⁰⁸

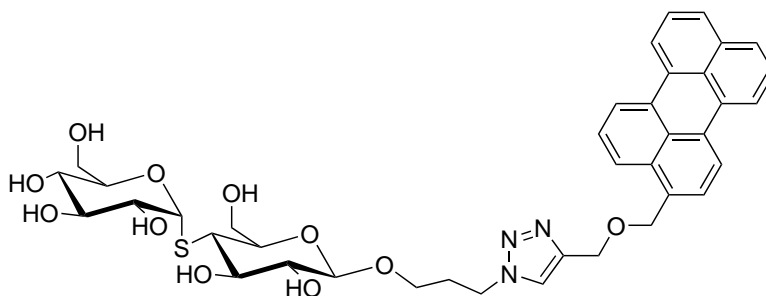


BOT_14

Figure 1.26: Structure of maltotriose perylene conjugate¹⁰⁸

Recently Murthy et al. synthesized a thiomaltose perylene conjugate, TM-P (Figure 1.27), to improve the stability of maltodextrin based probes, by preventing the in vivo degradation by enzymes like amylases and maltases. Uptake of TM-P in wild-type

E. coli was 2.5-fold higher than that in a lamB knockout mutant, indicating a lamB dependent transport of the probe. Uptake of TM-P in bacteria was 6-fold higher than that of MDP-1, indicating smaller maltodextrins penetrate better inside the bacteria.,^{107 109}

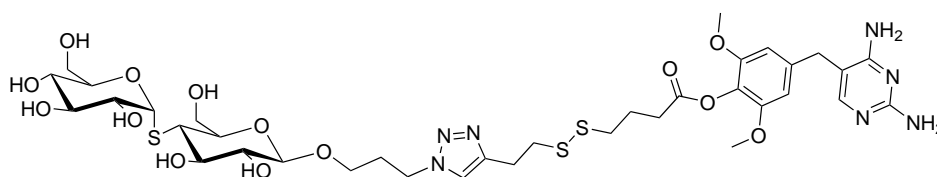


TM-P

Figure 1.27: Structure of thiomaltose-perylene conjugate¹⁰⁹

The synthesis of a thiomaltose-trimethoprim conjugate, TM-TMP (Figure 1.27) was also reported.¹⁰⁹ Thiomaltose and TMP were linked via a self immolative disulfide linkage. The application of trimethoprim in treatment of bacterial infection is limited owing to poor solubility and toxicity.

The conjugate TM-TMP showed significantly improved solubility compared to trimethoprim and decreased the toxicity. In mice models, it was also used to treat urinary tract infection.



TM-TMP

Figure 1.28: Structure of thiomaltose- trimethoprim conjugate¹⁰⁹

1.11 Aim of the thesis

The principal theme of this thesis is to explore the possibility of exploiting the maltodextrin transport system as a transporter to be utilized in a Trojan horse strategy.

As explained in the previous section, there are conflicting reports in the literature regarding the uptake of maltodextrin conjugates. While the reports from Murthy et al. suggest the internalization of probes with modification at reducing end,^{31,104} reports from Faust et al. argue that modification at the reducing end of the sugar is detrimental to uptake.^{106,107} In addition, previous studies in this regard also emphasize the importance of the free anomeric end of the sugar for their recognition through the maltodextrin transport pathway.^{97,100}

Within this thesis, the possibility of attaching imaging agents and antibiotics at the non-reducing end of the sugar was explored, such that the reducing end of the maltodextrins is available for recognition by the maltodextrin transport system (Figure 1.29).

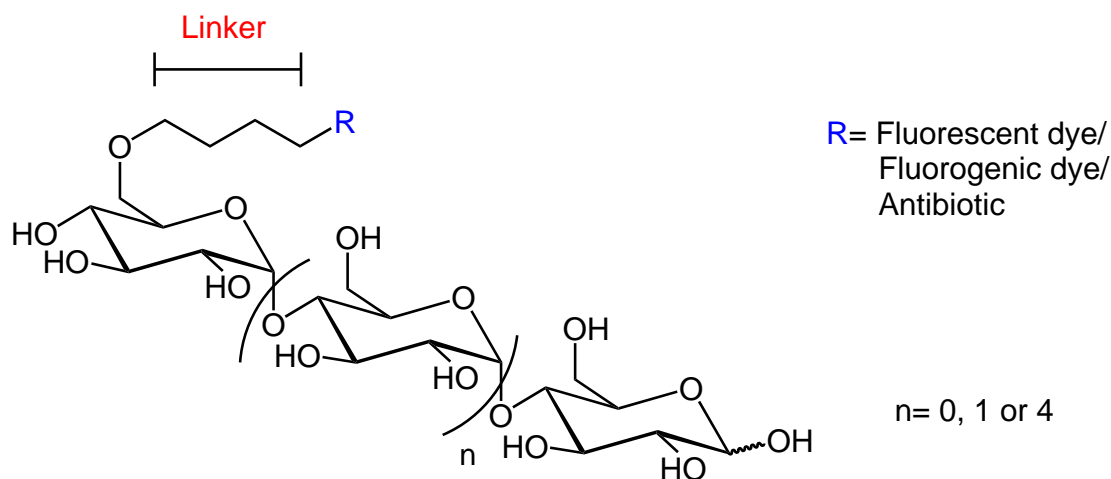


Figure 1.29: Modifications at the non-reducing end

A first aim of the thesis was to systematically investigate the preferred site of modifica-

tion for an efficient uptake of conjugates.

To this end, the synthesis of several maltodextrin derivatives containing small modifications at the reducing and non reducing end was envisioned. Internalization studies of these maltodextrin analogues should shed better light on the importance of the free anomeric end of the maltodextrins. It would also give insights on the modifications tolerated at the non-reducing end of the maltodextrins, which would be instrumental in the design of the conjugates for treatment and diagnosis.

The thesis also aimed to perform a detailed structure activity relationship study on the uptake of conjugates.

In this direction, synthesis of a comprehensive series of maltodextrin-fluorescent conjugates at the non-reducing end was planned. The compounds should differ by the linker, the effector moiety and the size of maltodextrin. The uptake efficiency of the probes should be investigated by subsequent biological assays.

The final aim of this thesis was to translate the knowledge gained from the structure activity relationship with maltodextrin-fluorophore conjugates to synthesize maltodextrin-antibiotic conjugates, which can overcome the permeability barrier in gram negative pathogens and perform intracellular delivery of antibiotics.

1.12 Thesis Outline

The remainder of this report is organised as follows:

Chapter 2 — describes the proof of concept that the modification at the non-reducing end is tolerated by the maltodextrin transport system. The design and synthesis of maltodextrin analogues containing small modifications is reported in this chapter. The uptake of the analogues in *E. coli* and *K. oxytoca* was shown by a growth recovery assay.

Chapter 3 — details the design and synthesis of a systematic series of fluorescent maltodextrin conjugates. Critical parameters essential for uptake were varied to perform detailed structure activity relationships. The uptake of these molecules in *E. coli* was studied using confocal microscopy and growth recovery assays.

Chapter 4 — evaluates the intracellular accumulation of the conjugates by using a fluorogen activation protein (FAP) system. The synthesis of maltodextrins conjugated to a fluorogenic malachite green (MG) dye is described. Translocation across the membrane in *E. coli* was monitored by measuring fluorescence over time in a plate reader.

Chapter 5 — describes the synthesis of maltodextrin-ampicillin conjugates. Antibacterial activity of the synthesized conjugates was assessed against *E. coli* and *K. oxytoca*.

2 | Investigation of maltodextrin uptake

As described in the introduction, the maltose transport system is highly substrate selective. Maltodextrin analogues with modification of the glucosyl unit at the reducing end of the sugar are not transported by the maltose transport system.⁹⁷ To overcome this transportation barrier, in this study the modifications were carried out at the primary hydroxy group at the non-reducing end. To determine whether the malto-oligosaccharides modified at the non-reducing end are transported by the maltose system, small modifications were carried out at the non-reducing end of the sugar. The uptake of these modified sugars by bacteria was verified by a growth recovery assay. The design and synthesis of the modified maltodextrins is discussed in detail in the following sections. The results of the uptake of the modified analogues in the growth recovery assay and the inferences derived are discussed towards the end of the chapter.

2.1 Design of modified maltodextrins

To investigate the effect of small structural modifications on the uptake pathway, five maltodextrin analogues with minor modifications (hereafter referred to as intermediates) were designed (Figure 2.1) that carry a small linker attached to the maltodextrin. BOT_46 is the intermediate containing modifications at the reducing end of the maltohexose. The anomeric hydroxy group of the maltohexose is extended by 3-azidopropane via a glycosidic linkage. This intermediate would help us verify the existing literature regarding effect of modification at the reducing end of the sugar on the uptake. The modification at the non-reducing end involves multi-step reactions requiring optimisations. Also considering the cost of the higher maltodextrins, the modifications were carried out on the simplest maltodextrin, maltose. First, propyl azide was attached to the primary hydroxy group at the non reducing end using an amide coupling to yield

BOT_41, and an ether formation to yield BOT_42 respectively. BOT_43, a side product formed during the synthesis of BOT_42, is a useful tool to investigate the effect of a non polar propyl group on the uptake. BOT_49, containing a long polyethylene glycol (PEG) linker, was synthesized to study the effect of linker length on the uptake.

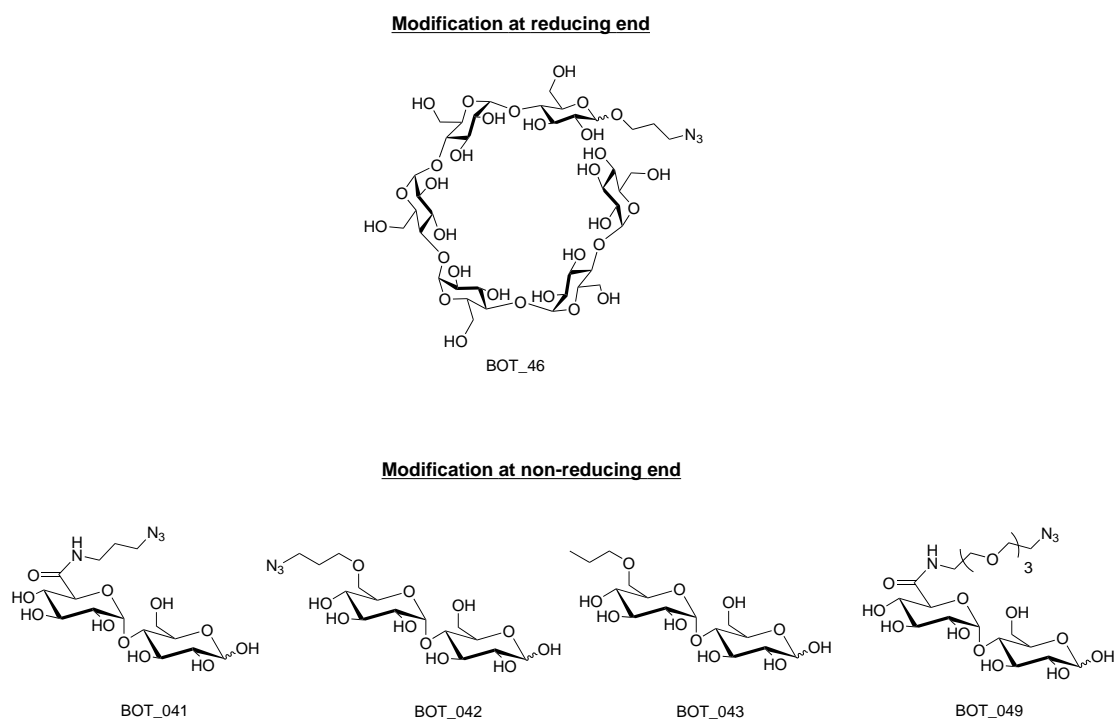
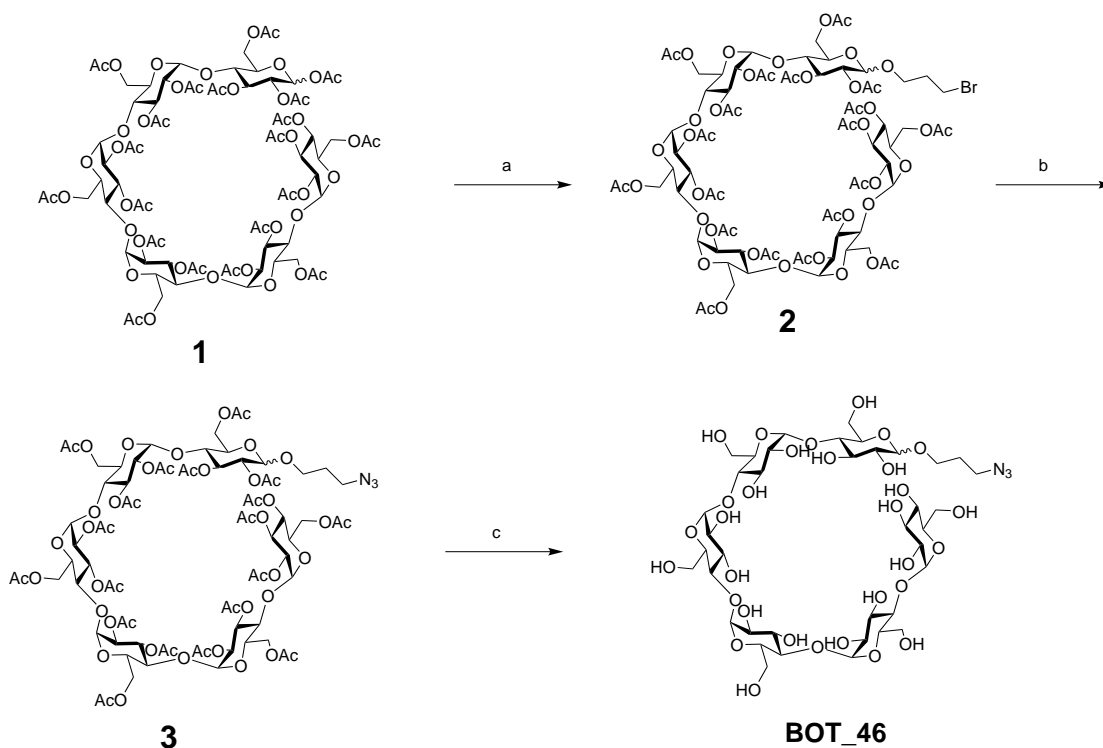


Figure 2.1: Structures of modified maltodextrins

2.2 Synthesis of intermediates

Synthesis of intermediates with modification at the reducing end

BOT_46 was synthesised in three steps starting from the peracetylated maltohexose as shown in Scheme 2.1. A Lewis acid promoted glycosylation of peracetylate maltohexose at the anomeric carbon was performed with 3-bromopropanol to yield the bromopropyl compound **2**.¹⁰⁴ The bromide was converted into an azide by a nucleophilic substitution. In the last step, Zemplén deacetylation was carried out to yield the desired intermediate BOT_46.

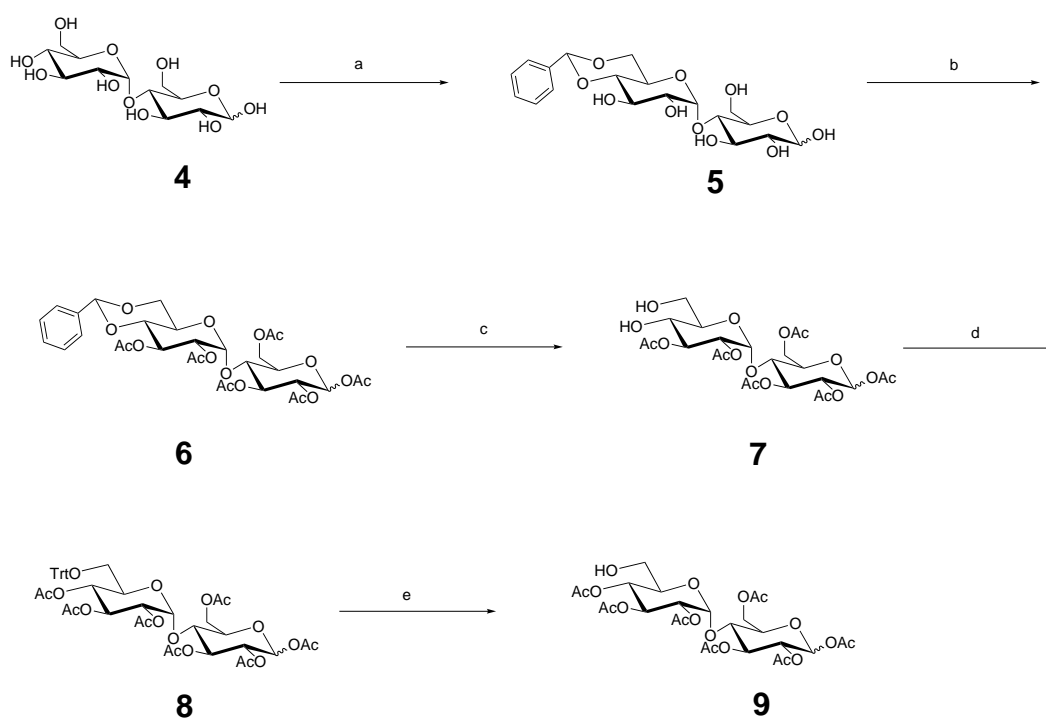


Scheme 2.1: **a.** 3-bromopropanol, $\text{BF}_3 \cdot \text{Et}_2\text{O}$, 0 °C, CH_2Cl_2 , 24%. **b.** NaN_3 , DMF, 60 °C, 92%. **c.** NaOMe, MeOH, rt, 72%.

Synthesis of intermediates with modification at the non reducing end

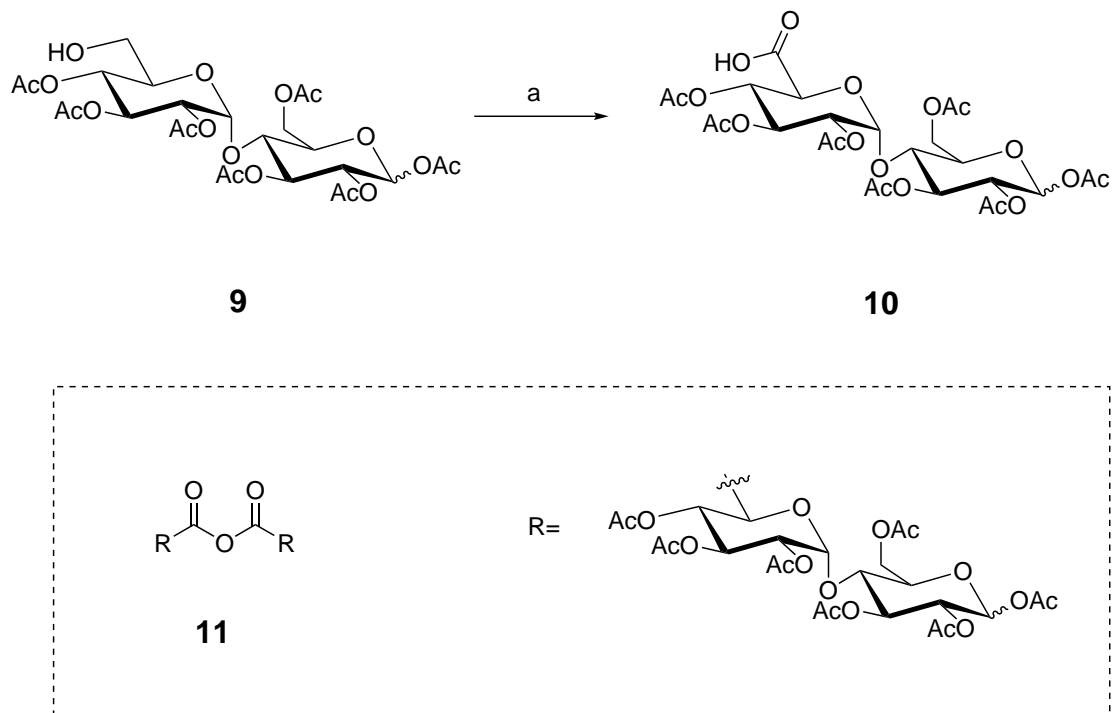
Synthesis of BOT_41 and BOT_49

In order to carry out the modifications at the primary hydroxyl group at the non reducing end compound **9** was targeted, which was synthesized from commercially available maltose **4** in five steps (Scheme 2.2). The free 4' and 6' hydroxy groups were protected with benzylidene acetal under mildly acidic condition, followed by acetylation to yield **6**. In the next step the benzylidene acetal was cleaved by acid hydrolysis to yield **7**. The primary hydroxy group was selectively protected with a bulky trityl group, followed by acetylation of the secondary hydroxy group. Finally, the trityl group was removed by acid hydrolysis to yield the desired compound **9**.



Scheme 2.2: **a.** PTSA · H₂O, DMF, 50 °C, 39 mbar, 64%. **b.** Ac₂O, pyridine, 81%. **c.** AcOH/H₂O, 95 °C, 67%. **d.** i. TrCl, pyridine, 95 °C; ii. Ac₂O, pyridine, 86%. **e.** AcOH/H₂O, 95 °C, 76%.

In the next step, the primary hydroxy group in **9** should be oxidised to the corresponding carboxylic acid **10** (Scheme 2.3).



Scheme 2.3: Trials to oxidise the primary alcohol to carboxylic acid

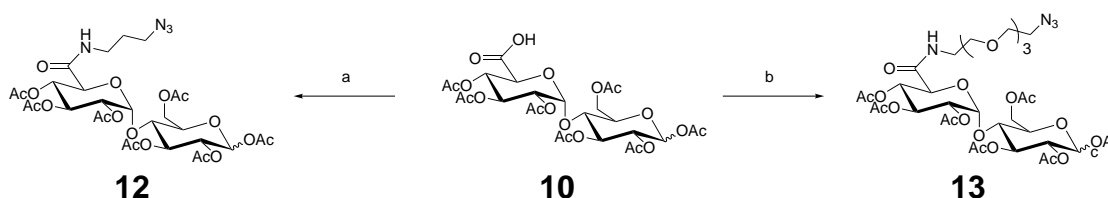
Table 2.1: Trials to oxidise the primary alcohol to carboxylic acid

S. No	Condition	Comments
1	Jones oxidation	Poor conversion
2	IBX (1-15 eq.), DMSO	25%
3	TEMPO/ BAIB, DCM/H ₂ O(1:1), rt	65%
4	TEMPO/ BAIB, DCM/H ₂ O(1:1), 40	11

The reaction was attempted using various chromium and periodinane based reagents. However, the reactions suffered from low yields (Table 2.1). The best yield of 65% was achieved by TEMPO mediated oxidation in the presence of Bis(acetoxy)iodobenzene (BAIB) as a secondary oxidant in dichloromethane (DCM) / water as solvent. Further

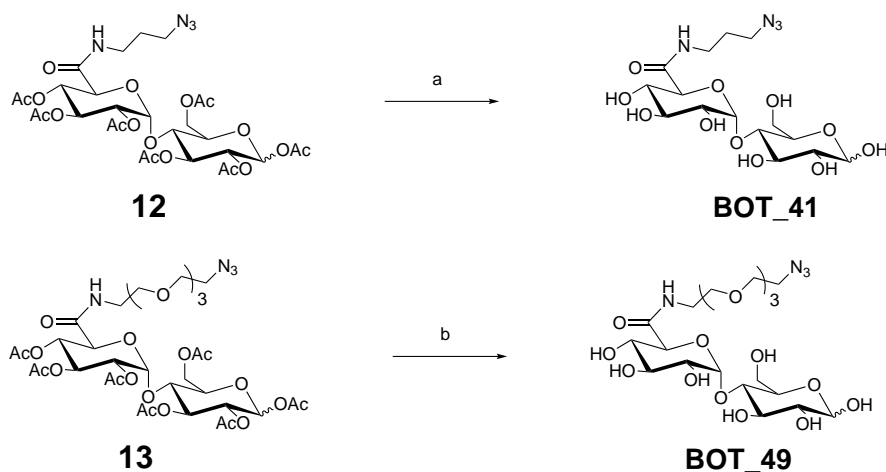
attempts to increase the yield were unsuccessful, elevation in temperature yielded the anhydride **11** as a major product.

The carboxylic acid **10** was treated with the respective amines under standard conditions using T3P as a coupling reagent to obtain the products **12** and **13** (Scheme 2.4).



Scheme 2.4: **a.** 3-azidopropylamine, T3P, Et₃N, CH₂Cl₂, 37%. **b.** Azide-PEG₃-Amine, T3P, Et₃N, CH₂Cl₂, 62%.

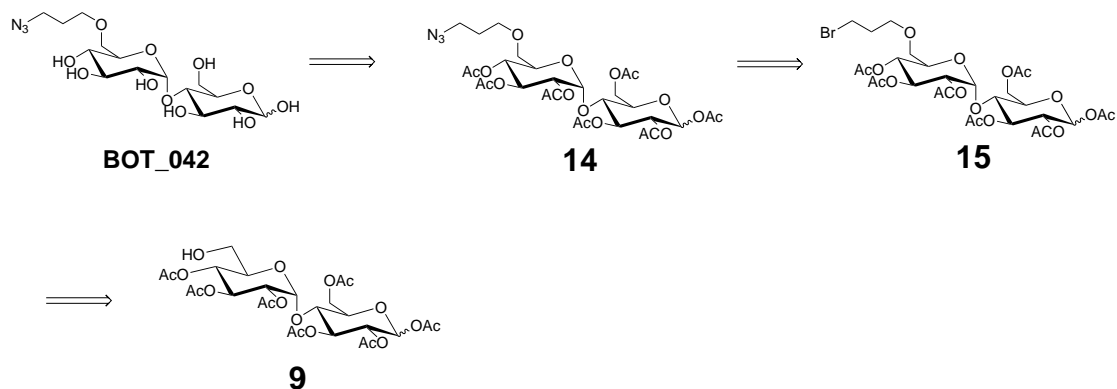
Finally, Zemplén deacetylation was performed on **12** and **13** to deprotect the acetyl groups. The reactions showed clean conversions to yield BOT_41 and BOT_49 when monitored by LC-MS, but the isolation of the highly polar compounds was difficult and resulted in low yields. The compounds were purified by reverse phase flash chromatography using an ion exchange amino cartridge.



Scheme 2.5: **a.** NaOMe, MeOH, 36%. **b.** NaOMe, MeOH, 64%.

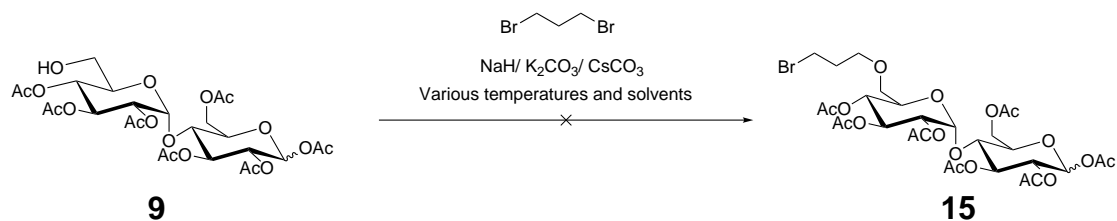
Synthesis of BOT_42 and BOT_43

The synthesis of BOT_42 was attempted by the following strategy (Scheme 2.6). The azide should be obtained from the corresponding bromide. The bromide was intended to be introduced on compound **9** via a nucleophilic substitution reaction.



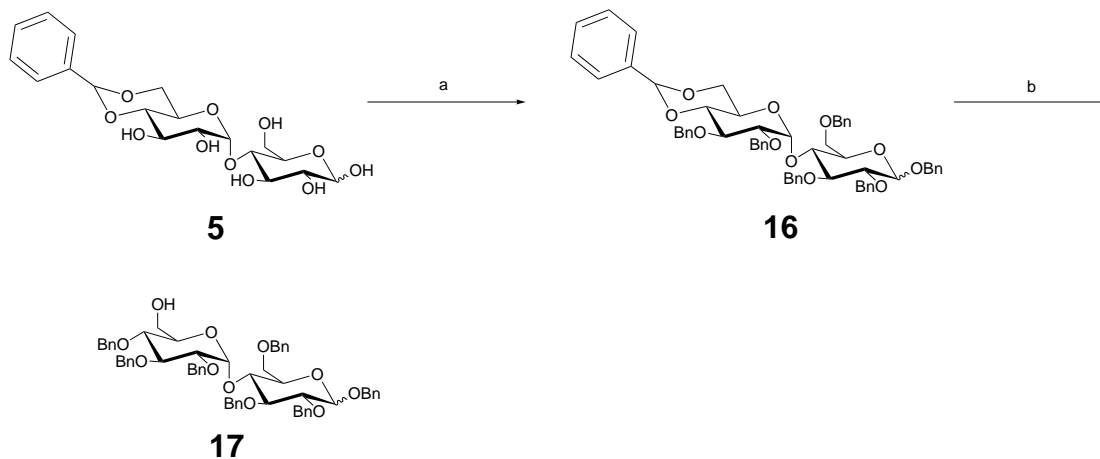
Scheme 2.6: Retrosynthetic analysis of synthesis of BOT_42

In the forward direction, the synthesis of **15** was attempted by performing a nucleophilic substitution on compound **9** with 1,3 dibromopropane. However, this reaction failed to yield the desired product. Using a strong base like NaH resulted in deacetylation of **9**, whereas using a mild base like K_2CO_3 or Cs_2CO_3 resulted in retention of starting material.



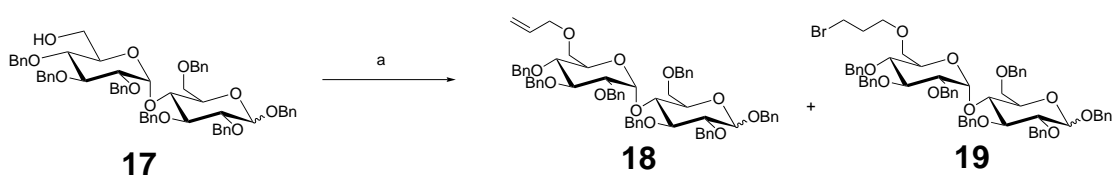
Due to the limitation of acetate groups as protecting groups to carry out nucleophilic

substitution, a synthetic route based on benzyl protecting group was proposed. The benzyl analogue of compound **9** was synthesized as described in Scheme 2.7.



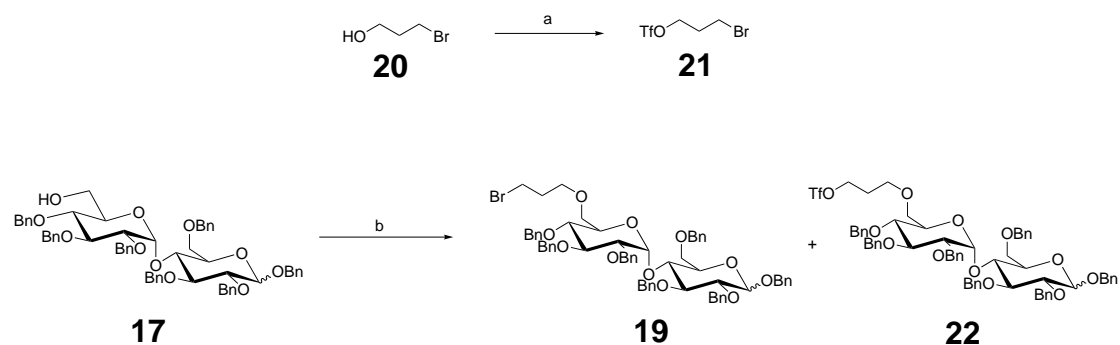
Scheme 2.7: **a.** BnBr, NaH, DMF, 0 °C, 67%. **b.** DIBAL-H, Toluene, -10 °C, 72%.

The introduction of bromopropyl group was a bottleneck even after changing to the benzyl protecting group. Initial trials to introduce the bromopropyl group via nucleophilic substitution with 1,3 dibromopropane yielded the elimination product **18** as the major compound.



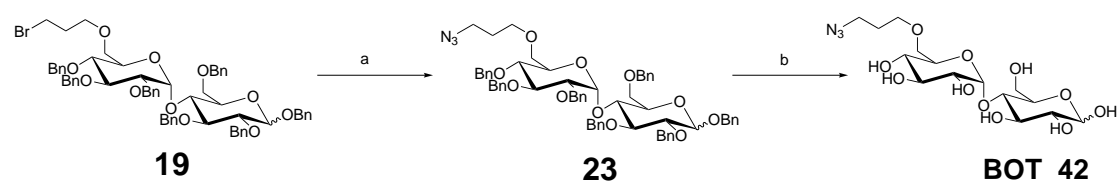
Scheme 2.8: **a.** 1,3 dibromopropane, BnBr, NaH, DMF, 0 °C, 72% (**18**), 12% (**19**).

To overcome the elimination reaction, one bromine atom was replaced by a better leaving group. As shown in Scheme 2.9, 3-bromopropanol was converted into the triflate **21**, which was then used to perform a nucleophilic substitution on **17**, to yield the desired product **19** as a major product and **22** as a minor product.



Scheme 2.9: **a.** Tf₂O, Pyridine, CH₂Cl₂, -78 °C, 89%. **b.** **21**, DIPEA, CH₂Cl₂, 17.5%.

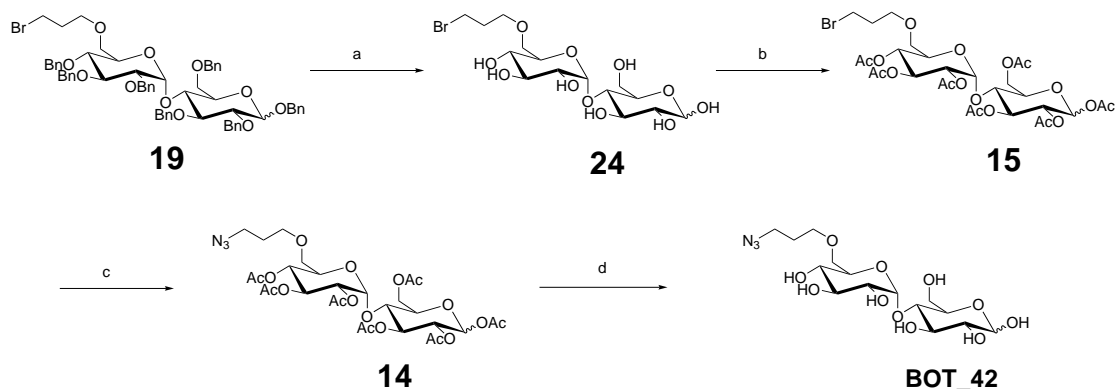
As shown in Scheme 2.10 the next step was to convert the bromide to an azide through a nucleophilic substitution to yield **23**. Finally, the deprotection of the benzyl groups was attempted by BCl₃ in the presence of pentamethyl benzene as a cation scavenger. Although the formation of the product could be observed by LC-MS, the efforts to purify it were unsuccessful.



Scheme 2.10: **a.** NaN₃, DMF, 60 °C, quant. **b.** BCl₃, PMB, DCM, -78 °C.

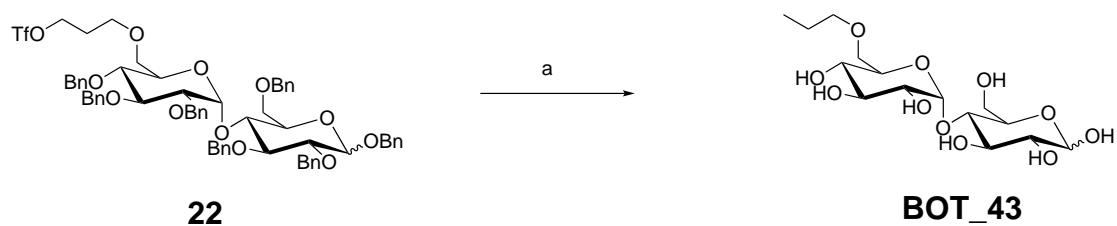
Therefore, the route was modified as shown in Scheme 2.11. After extensive optimisation, the ideal condition for debenzylation was found to be palladium catalyzed hydrogenation at 10 bar for 12 h to yield **24**. Efforts to substitute the bromo group in **24** to azide to directly yield BOT_42 resulted in an undesired product which could not be characterized. Therefore, acetate group as protecting group was reintroduced, as the de-protection could be obtained without effecting the azide functionality. Subsequently, the bromo group was converted into the azide. Finally, the acetate groups were removed

by Zemplén deacetylation.



Scheme 2.11: **a.** H₂, Pd/C, EtOAc/EtOH (2:1), 84% **b.** Ac₂O, pyridine, 78%. **c.** NaN₃, DMF, 60 °C, 95%. **d.** NaOMe, MeOH, 37.2%.

A palladium catalysed hydrogenation was carried out on **22** to yield BOT_43.



Scheme 2.12: **a.** H₂, Pd/C, EtOAc/EtOH (2:1), 90%.

2.3 Growth recovery assay

To study the uptake of the synthesized intermediates by bacteria, a growth recovery assay was devised. Bacteria were grown in a carbon-free minimal media to hamper growth. Carbon source in the form of native substrates or intermediates were added, and growth recovery was measured as an increase in OD600 at two intervals 24 h and 48 h. The assay was performed on four bacterial strains *E. coli* WT, *E. coli* ΔlamB,

E. coli Δ TolC (NCTC8960) and *K. oxytoca*. The *E. coli* Δ lamB is a knockout strain lacking *LamB*, the gene encoding for maltoporin, hence cannot transport higher maltodextrins. The absence of growth recovery in the mutant Δ lamB strain would prove that the uptake of the intermediates is dependent on the maltodextrin transport system. On the Δ TolC *E. coli* strain, a major efflux pump is deleted. The strain was included as a control to monitor the efflux of the intermediates. *K. oxytoca* contains an additional cyclodextrin transporter. On the substrate front, a LB medium (50% LB medium and 50% minimal medium with no carbon source) was used as a positive control to compare relative growths. The native substrates of the maltodextrin transport system maltose (G2), maltotriose (G3) and maltohexose (G6) were used to optimise the assay. Acarbose is transported by the maltodextrin transport system, but it does not support growth because it is a poor substrate for maltodextrin metabolic enzymes.¹¹⁰ It was included as a negative control to demonstrate that compounds that do not restore growth may still be transported. A limitation of this assay was that high concentrations of even the native substrates were required to elicit a response detected by the OD600 measurements. To increase the sensitivity of this assay, an ATP-bioluminescence readout was multiplexed to the OD600 measurements. This assay involves the addition a BacTiter-Glo™ reagent to bacterial cells. The reagent results in cell lysis and generation of a luminescent signal. The measured luminescence is proportional to the ATP content, which is proportional to the number of cells. This assay allows the measurement of ATP from as few as 10 bacterial cells. This helps in detection of molecules that are capable of maintaining metabolism, but cannot induce significant growth to elicit an increase in OD600.¹¹¹ The results of the growth recovery assay are summarized in the Figure 2.2 (OD measurement after 24h), Figure 2.3 (OD measurement after 48h) and Figure 2.4 (ATP-bioluminescence measurement after 48h).

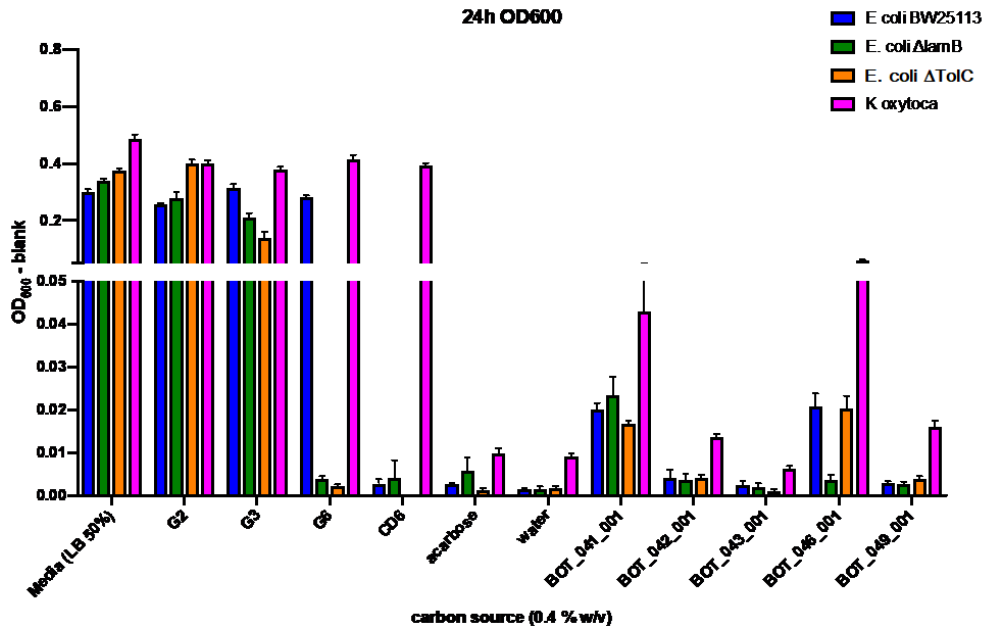


Figure 2.2: Bacteria were grown in a carbon free medium and treated with 0.4% w/v of the carbon source. The recovery of growth after 24 h measured by OD600. G2, G3, G6 and CD6 represent maltose, maltotriose, maltohexose and cyclodextrin, respectively. $n \geq 6$, except $n=3$ for CD6 in *K. oxytoca*

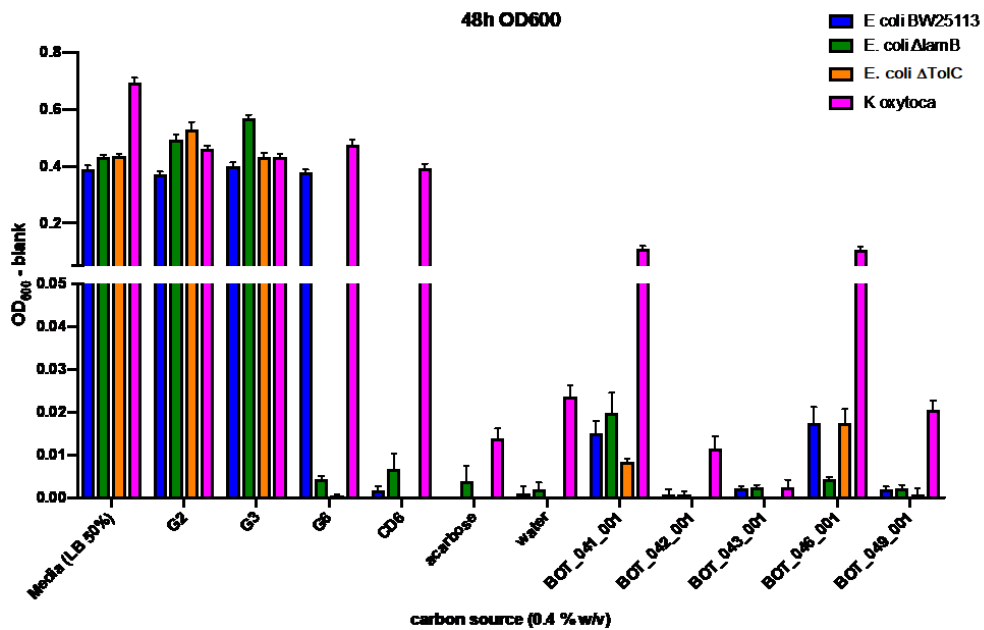


Figure 2.3: Recovery of growth after 48 h measured by OD600. $n \geq 6$, except $n=3$ for CD6 in *K. oxytoca*

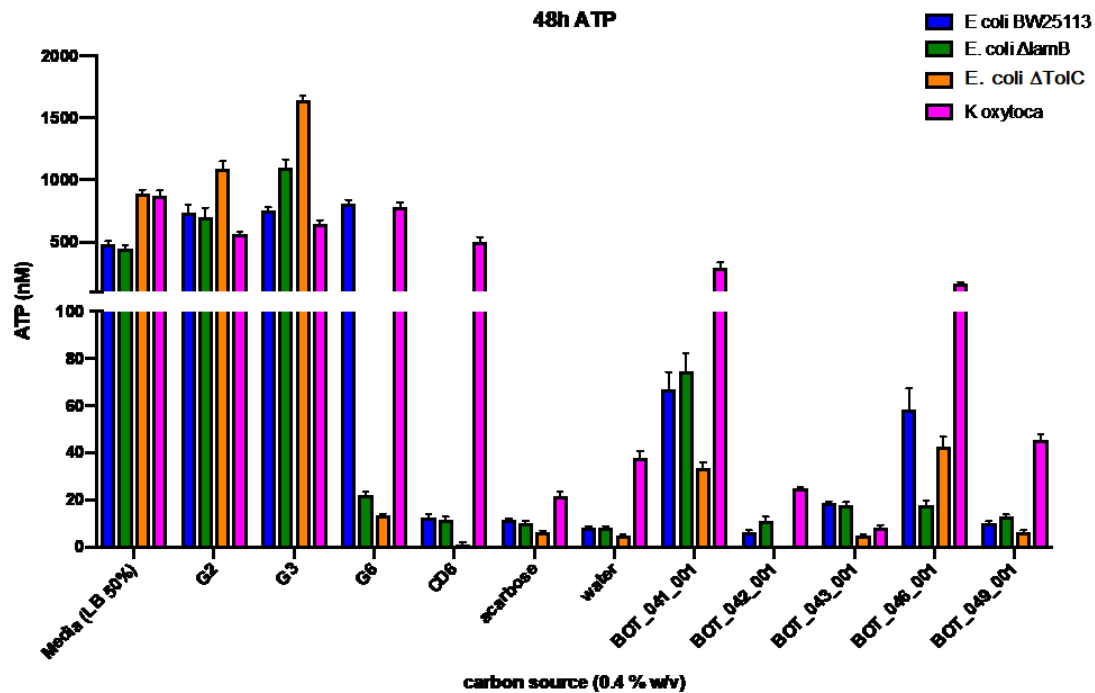


Figure 2.4: Recovery of growth after 48 h measured by ATP-bioluminescence. $n \geq 6$, except $n=3$ for CD6 in *K. oxytoca*

As seen in Figure 2.2, the native substrates maltose(G2), maltotriose(G3) and maltohexose(G6) recovered growth as effectively as the positive control (LB medium). Maltohexose recovered growth only in *E. coli* WT indicating uptake dependent on the maltodextrin transport system. Cyclodextrin (CD), which is not a substrate for the system, did not recover growth in *E. coli*. In *K. oxytoca* which has an additional cyclodextrin transporter, cyclodextrin recovered growth effectively. No recovery in growth was observed for acarbose which was used as a negative control.

The most notable observations here can be summarized as follows:

- A minor restoration in growth is observed by BOT_41 in *E. coli* as well as in $\Delta lamB$ *E. coli*. In *K. oxytoca* the recovery of growth by BOT_41 is comparable to that by the native substrates.

-
- BOT_46 restores growth in *E. coli* and *K. oxytoca* in a lamB dependent manner.

The restoration of growth by BOT_41 but not by BOT_42 and BOT_43 in *E. coli* suggests that the amide functionality at the non reducing end is better tolerated by the transport system as well as the metabolic enzymes compared to the ether linkage. The comparable recovery of growth in *E. coli* Δ lamB is not surprising, as specificity is introduced only in the higher maltodextrins, as evident in recovery of growth by maltose(G2) and maltotriose(G3). The absence of growth recovery by BOT_49 indicates that the long PEG linker is detrimental to the uptake or metabolism. The recovery of growth by BOT_46 only in *E. coli* WT, indicates specific transport by the maltodextrin transport system. This result is inconsistent with literature reports that blocking the reducing end results in no uptake.⁹⁷ However, it supports the reports that maltodextrin–perylene conjugates are transported in the bacteria in millimolar concentration.^{104,108}

The comparable recovery of growth by BOT_41 and BOT_46 as compared to the native substrates in *K. oxytoca* indicates a possible uptake of these intermediates also through the cyclodextrin transport in addition to the maltodextrin transport. The results also indicate that no significant efflux of the intermediates take place, as the restoration of growth in *E. coli* Δ TolC is comparable to that of the *E. coli* WT and remains unvaried over the course of time (comparing recovery between 24 h and 48 h).

It should be emphasized here that the growth restoration by the synthesized intermediates in the growth recovery assay was not be as efficient as that of native substrates. This could be due to two reasons: a) The modified maltodextrins may not be as efficiently transported by the transport system, b) the modified intermediates may not serve as substrates for the metabolic enzymes, as evident from acarbose.

In conclusion, the positive growth recovery by BOT_41 is an encouraging sign that maltodextrins modified at the non reducing end can be exploited in the trojan horse strategy. Recovery of growth exclusively by BOT_41 illustrates that an amide functionalized in-

intermediate with a short linker is a better substrate both for the transport and metabolism of maltodextrins. While the growth recovery assay is a robust method to prove the uptake of the intermediates by the bacteria, the absence of recovery does not prove lack of uptake. To overcome this limitation, the uptake is studied by imaging of fluorescence probes, as discussed in the next chapter.

3 | Maltodextrin based imaging probes

Fluorescence probes serve as powerful tools in chemical biology, due to the simplicity, low detection limit and most importantly their utility in bioimaging of cells.¹¹² In this Chapter, fluorescent probes have been employed to conduct a detailed structure activity relationship study, to assess the tolerated modifications on the substrate by the maltodextrin transport system. A series of fluorescent conjugates with maltodextrins has been synthesized by systematically varying important parameters, which will be discussed in detail in the following sections. The probes have been investigated for uptake using a growth recovery assay and confocal microscopy. The results have been further validated using a FACS analysis.

3.1 Design of fluorescent probes

A systematic series of fluorescent probes was designed by varying critical parameters that could effect the uptake of the conjugates. These parameters include:

- **Choice of maltodextrins**

Three different maltodextrins *i.e* maltose, maltotriose and maltohexose, were used as base sugars to understand the effect of the number a glucose units on the transport of the conjugates.

- **Choice of linker**

The choice of linker can also be critical in the uptake of the conjugates. Linking groups are used to attach the maltodextrins to the fluorescent dye and also to reduce the impact of the fluorescent group on the maltodextrin by acting as a spacer. In this study, in the most basic form, a three carbon alkyl linker has been used. In general, the hydrophobic alkyl linker may exhibit non specific binding to

proteins through hydrophobic interactions. As an alternative, a long PEG linker has been used. In addition to minimizing the non-specific uptake, it helps to improve the solubility of the probes.

- **Choice of fluorescent dyes**

It is important that the optical properties of the fluorescent dyes are tailored towards use in biological environments. These properties include photostability, extinction coefficients and quantum yields in aqueous media, visible or near-IR excitation and emission profiles to reduce or eliminate sample damage and autofluorescence from endogenous chromophores. Considering these properties, BODIPY FL, NBD and perylene were selected.

- **Attachment site**

As previously explained, the attachment site of the linker plays a crucial role in the transport of the maltodextrins. To further investigate the results obtained from the growth recovery assay, a series of conjugates were synthesized with modifications at the non reducing end. In addition, literature-known compounds with modification at the reducing end were synthesized.

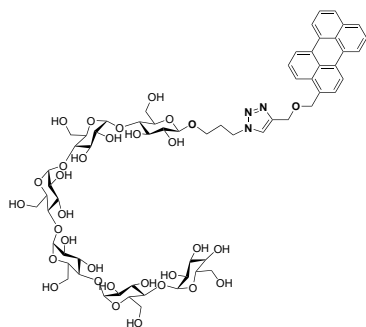
- **Mode of attachment**

Three main reactions have been employed to conjugate the fluorescent dyes to the maltodextrins, which include classical methods like reductive amination and amide coupling and more recently developed azide-alkyne cyclo-addition.

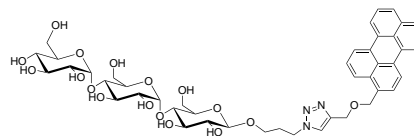
A list of novel fluorescent conjugates with modifications at the non reducing end is shown in Figure 3.1. BOT_10 and BOT_14, the two perylene containing probes conjugated at the reducing end of the sugar and reported to be specifically internalized through the maltodextrin transport system are also shown in Figure 3.1.

The rationale behind the design of these molecules was to obtain a direct comparison between a set of probes to understand the effect of critical parameters on the uptake. A comparison between BOT_10, BOT_14 and BOT_47 will help to understand the effect of attachment site. BOT_16 and BOT_51 could be compared to show the effect of the number of sugar units. BOT_15, BOT_16, BOT_18 could be used to explain the effect of mode of attachment. The effect of linker length can be understood by comparing BOT_45 with BOT_50, BOT_44 with BOT_48 and BOT_16 with BOT_18. Finally, comparison between BOT_44, BOT_45 and BOT_47; and BOT_48 and BOT_50 will give an understanding about the effect of dye on uptake.

Literature reported probes with modification at the reducing end

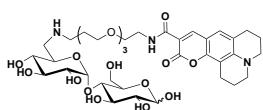


BOT_10

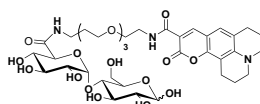


BOT_14

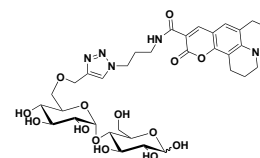
Novel probes with modification at the non-reducing end



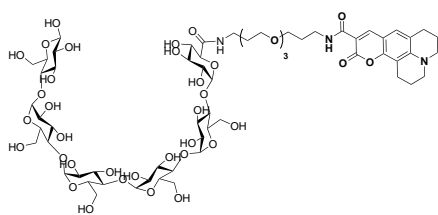
BOT_15



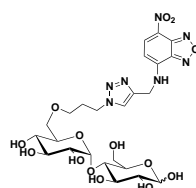
BOT_16



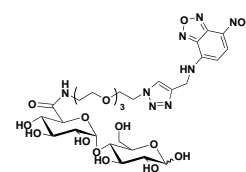
BOT_18



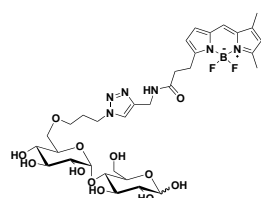
BOT_51



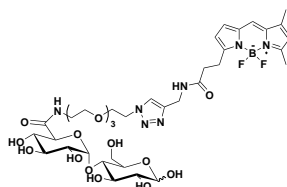
BOT_45



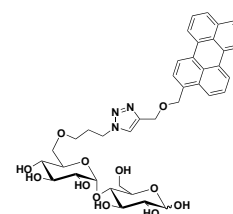
BOT_50



BOT_44



BOT_48



BOT_47

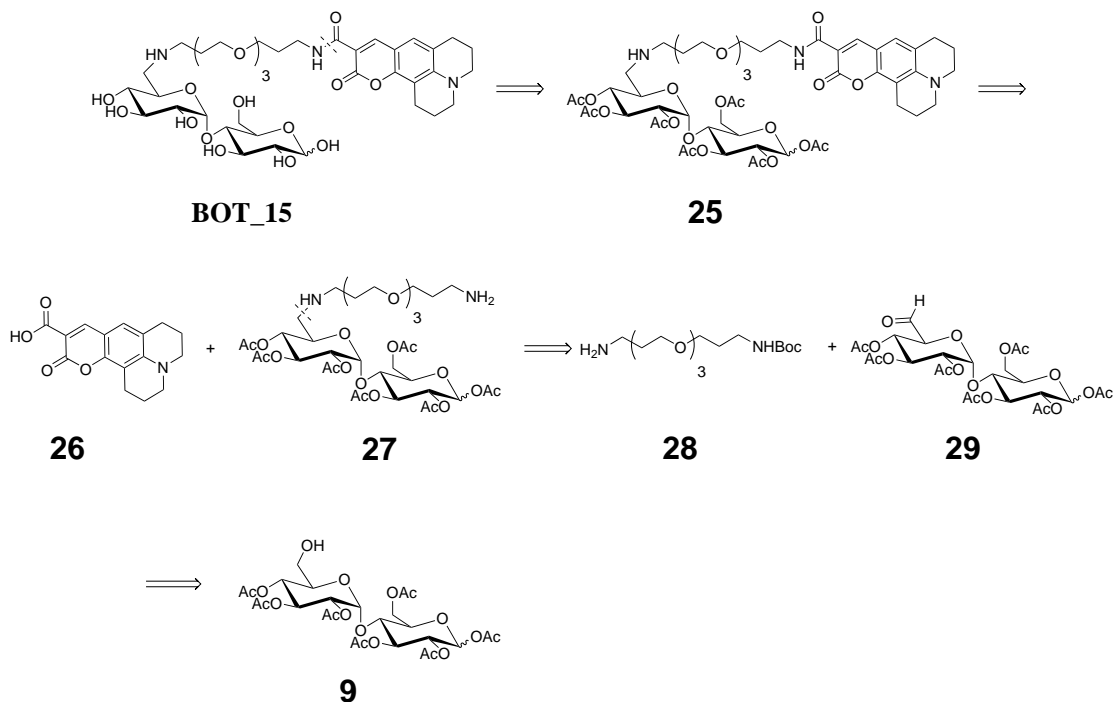
Figure 3.1: Structures of fluorescent conjugates

3.2 Synthesis of fluorescent conjugates

Synthesis of coumarin based probes

Synthesis of BOT_15

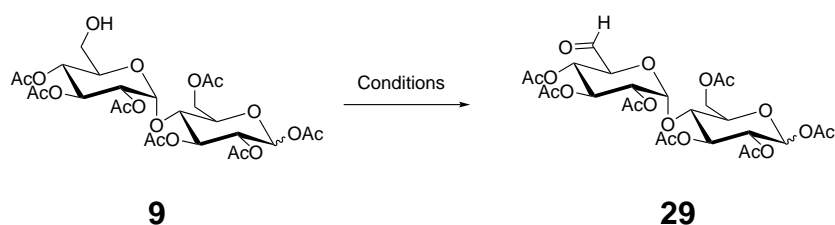
In the first approach, the synthesis of BOT_15 was planned as depicted in Scheme 3.1. BOT_15 could be obtained from the de-protection of acetylated conjugate **25**. Coumarin 343 (**26**) was planned to be added at a late stage of the synthesis using an amide coupling. A reductive amination of amine **28** and aldehyde **29** could yield the maltose-linker conjugate **27**. The aldehyde **29** could be obtained from the oxidation of **9**.



Scheme 3.1: Retrosynthetic analysis of synthesis of BOT_15

The controlled oxidation of the primary hydroxy group in compound **9** to aldehyde was attempted by using various oxidising agents. The conditions are summarized in

Table 3.1. As evident from the table, multiple attempts using standard oxidising agents resulted either in no or very poor conversion (< 30%). The poor conversion could be due to the tendency of the acyl groups to undergo intra-molecular migration to the free hydroxy group.¹¹³

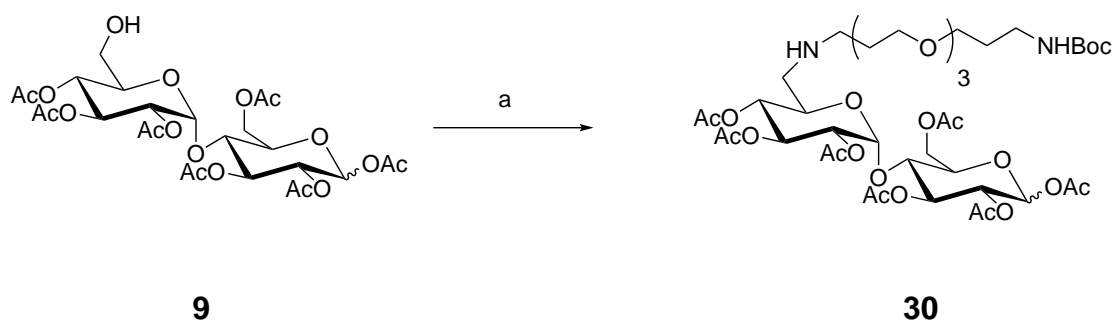


Scheme 3.2: Trials to oxidise the primary alcohol to aldehyde

Table 3.1: Trials to oxidise the primary alcohol to aldehyde

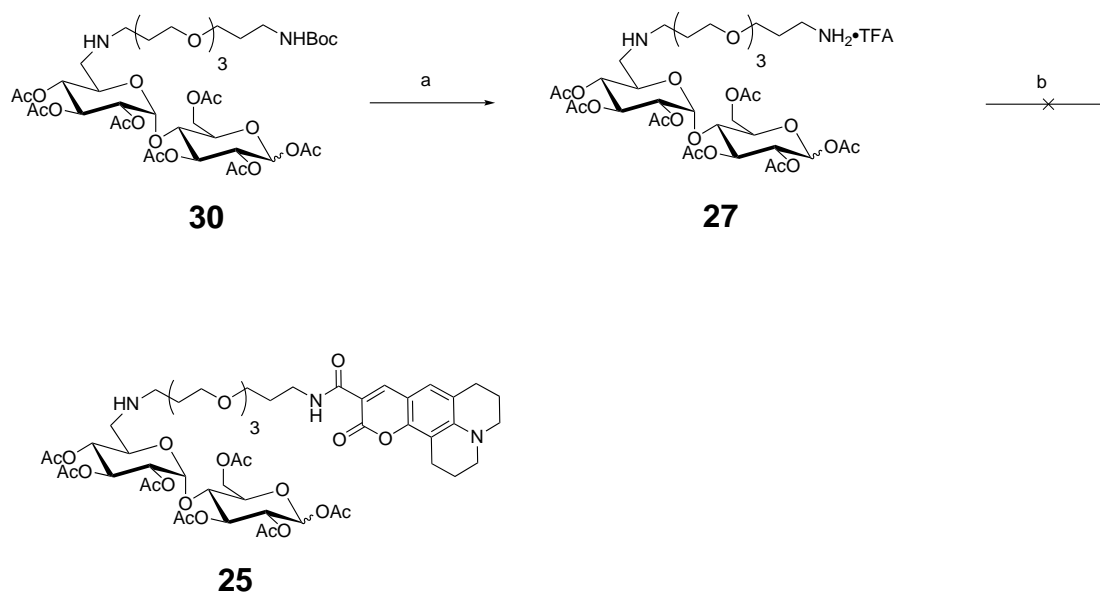
S. No	Condition	Comments
1	PCC, DCM, rt	Poor conversion
2	DMP, DCM, rt	Poor conversion
3	Swern oxidation	No reaction
4	Parikh Doering oxidation	No reaction
5	IBX (1-15 eq.), EtOAc, 80 °C	Poor conversion
6	IBX (1-15 eq.), DMSO, rt	Poor conversion
7	TEMPO, NaOCl, <i>t</i> -BuOH/ H ₂ O, rt	No conversion
8	TEMPO, NaBr, TBAF, <i>t</i> -BuOH/ H ₂ O, rt	No conversion
9	TEMPO, 5,5-dimethylhydantoin, <i>t</i> -BuOH/ H ₂ O, rt	Carboxylic acid
10	TEMPO/ BAIB, DCM, rt	Poor conversion

In addition to the poor conversions, the isolation of the aldehyde was unsuccessful. Therefore, using a one-pot two-step sequence with the reactants **28** and **9** involving an oxidation with TEMPO and BAIB, imine formation and reduction was performed (Scheme 3.3) to give the desired product **30** in 15% yield .



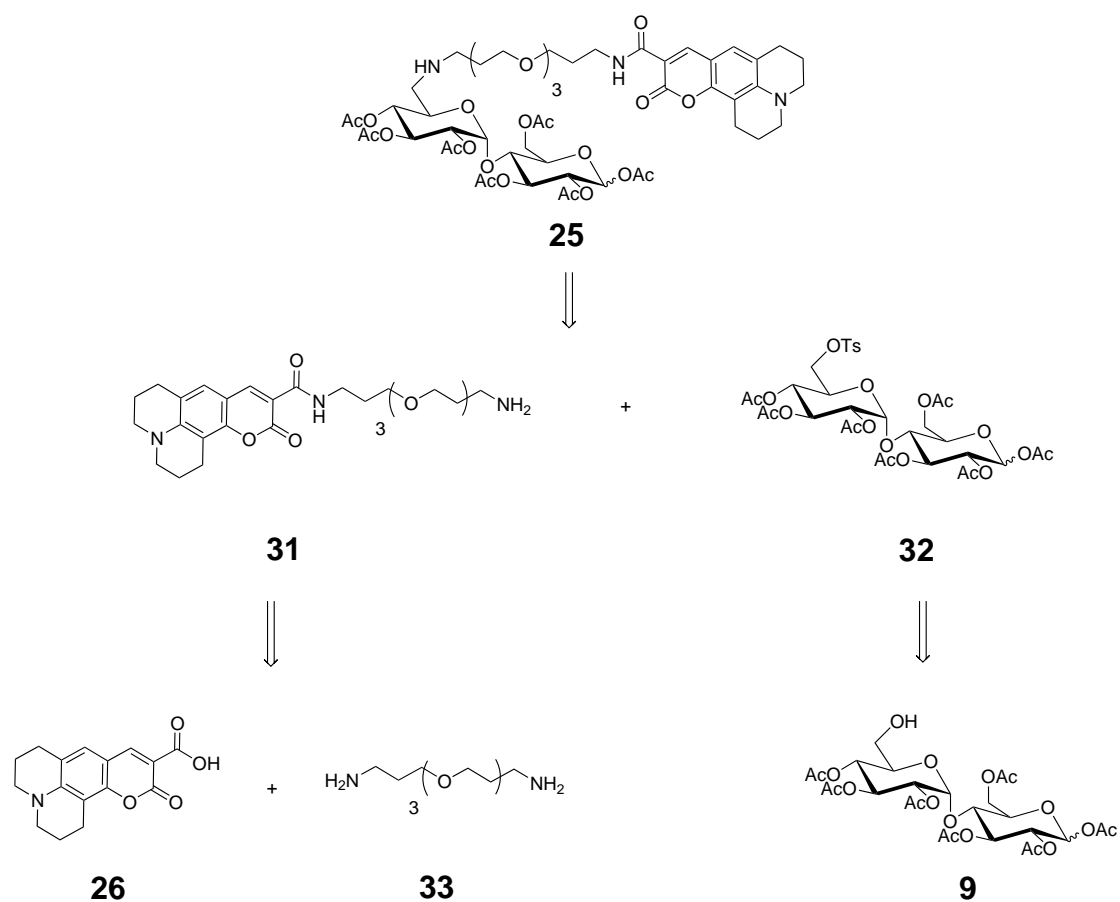
Scheme 3.3: **a.** i. **28**, TEMPO/ BAIB, DCM, ii. Na(OAc)₃BH, 15%.

In the next step, the Boc protecting group was removed to yield the amine **27**. The amide formation between compound **27** and coumarin 343 was unsuccessful using standard EDC coupling, due to solubility issues (Scheme 3.4).



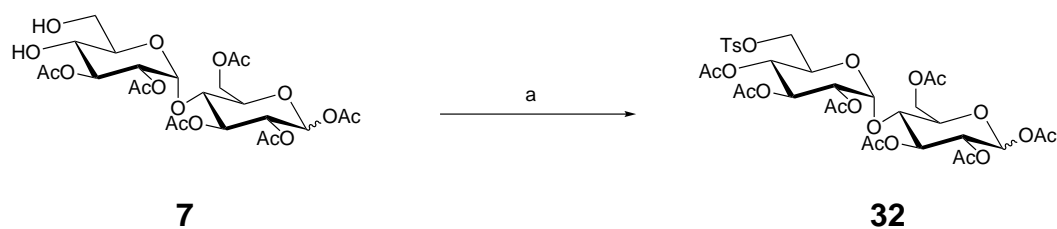
Scheme 3.4: **a.** TFA/CH₂Cl₂(1:1), quant. **b.** EDC/ HOBt, DMF, rt.

Therefore, an alternate synthetic route was envisioned (Scheme 3.5). This strategy involved the initial conjugation of coumarin 343 with the linker, which could then be used to perform a nucleophilic substitution on compound **32** to yield the acetylated conjugate **25**.



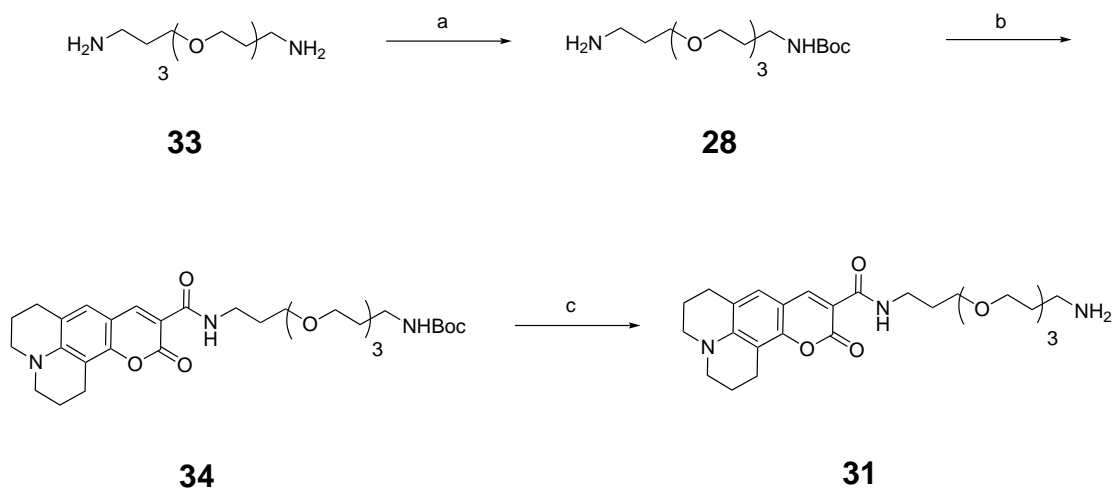
Scheme 3.5: Retrosynthetic analysis of compound **25**

As a first step, **32** was synthesized by converting the hydroxy group in **7** into a better leaving tosyl group to facilitate the substitution reaction (Scheme 3.6). Selective tosylation is achieved at the primary hydroxy group due to the steric hindrance at the secondary hydroxy group.



Scheme 3.6: **a.** i. TsCl (1.1 eq.), pyridine; ii. Ac₂O, pyridine, 72%.

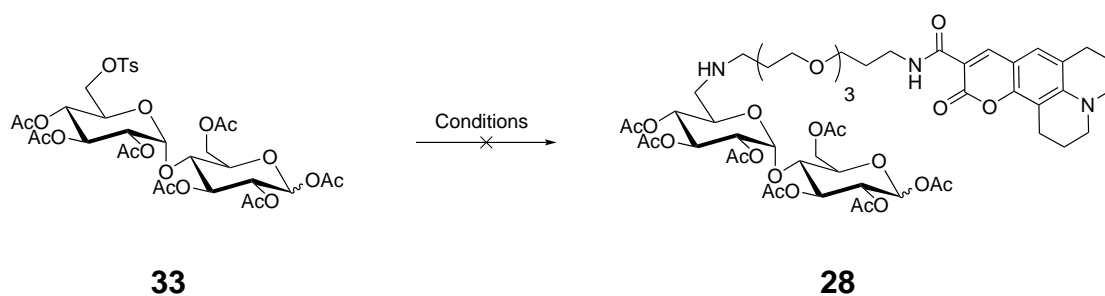
The coumarin-PEG conjugate **31** for substitution was synthesized starting from **33** in three steps in good yield. Initially, selective Boc protection of one of the amine group of compound **33** was performed to give **28**. An amide coupling between **28** and coumarin 343 was performed by employing T3P to yield **34**. Finally, the Boc protecting group was removed under acidic condition to yield the desired amine **31**.



Scheme 3.7: **a.** Boc₂O, DCM, rt, 48%. **b.** T3P, DCM, rt, 82%. **c.** TFA:DCM(1:1), rt, 56%.

The nucleophilic substitution of tosylate **32** by amine **31** was unsuccessful under various conditions (Scheme 3.8). In the absence of a base, increasing the temperature had no effect on the reaction (Table 3.2 Entry 1,2). Owing to the base-labile nature of the acetate groups, only a weak base such as Et₃N and a non-nucleophilic base such as DBU

could be employed to facilitate the reaction. However, adding the base had no effect on the reaction (Table 3.2 Entry 3-7). Ionic liquids are known to significantly enhance the reactivity of nucleophilic substitution reactions.¹¹⁴ However the reaction performed in [bmim]PF₆ as opposed to conventional solvents resulted in no reaction (Table 3.2 Entry 8,9). Attempts to obtain microwave (MW) assisted substitution to accelerate the reaction as reported in¹¹⁵ also remained unsuccessful (Table 3.2 Entry 10-12). A brief summary of the attempted conditions is provided in table Table 3.2.



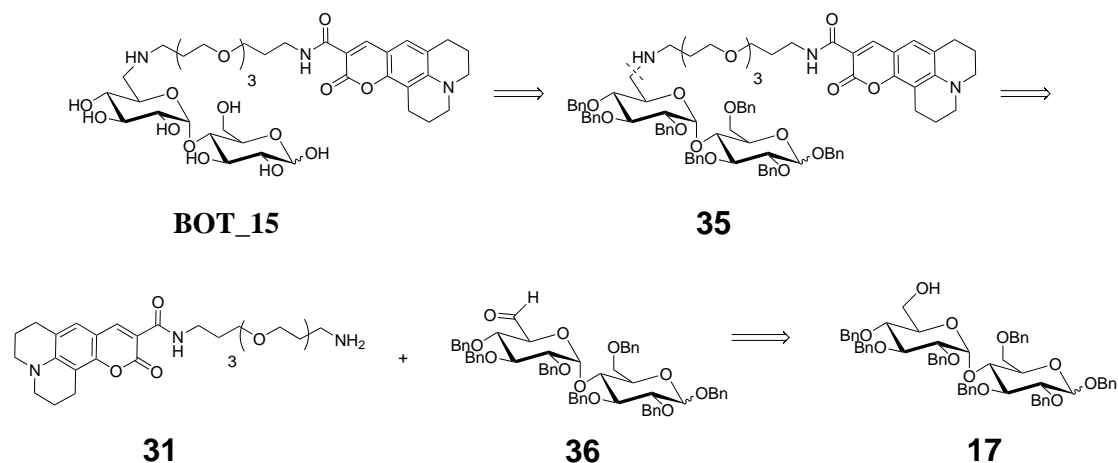
Scheme 3.8: Trials towards nucleophilic substitution

Table 3.2: Trials towards nucleophilic substitution

S No	Conditions
1	31 , DMF, rt, 24 h
2	31 , DMF, 100 °C, 24 h
3	31 , DMF, Et ₃ N, rt, 24 h
4	31 , DMF, Et ₃ N, 60 °C, 12 h
5	31 , THF, Et ₃ N, 60 °C, 12 h
6	31 , DMSO, DBU, rt, 12 h
7	31 , DMSO, DBU, 100 °C, 12 h
8	31 , [bmim]PF ₆ , rt, 24h
9	31 , [bmim]PF ₆ , CsOH, rt, 24h
10	31 , DMF, 100 °C, MW
11	31 , DMF, DBU, 100 °C, MW
12	31 , DMF, TBAI, DBU, 100 °C, MW

To overcome the difficulties in oxidation and substitution reaction owing to the labile

nature of the acetate protecting group, a synthesis based on permanent benzyl protecting group was envisioned (Scheme 3.9). BOT_15 could be obtained by palladium catalysed hydrogenation of the benzyl protection groups in conjugate **35**, which could be obtained by coupling the coumarin-linker conjugate **31** with the benzylated aldehyde **36** by means of a reductive amination. The aldehyde **36** should be prepared from **17**.



Scheme 3.9: Retrosynthetic analysis based on benzyl protecting group

The oxidation of the primary hydroxy group in benzylated compound **17** under different oxidising conditions gave the aldehyde **36** in markedly better yields as compared to the acetylated analogue (Table 3.3).

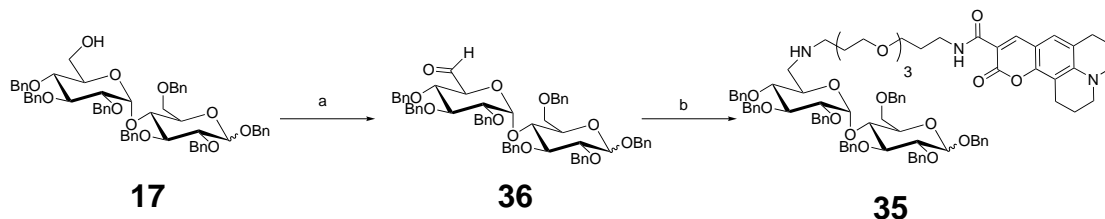
Table 3.3: Trials towards oxidation of **17** to **36**

S. No.	Conditions	Yields (%)
1	DMP, DCM, rt	45
2	PCC, DCM, rt	30
3	TEMPO, BAIB, DCM, rt	36
4	IBX, EtOAc, rt	42
5	Swern oxidation	No reaction
6	EDC.HCl, Pyr, DMSO, CF ₃ CO ₂ H	48

Yield were determined by LC-MS.

However, the isolation of the aldehyde was not successful. Therefore, reductive amina-

tion was carried out using the crude mixture of **17** and **36**, and the coumarin containing linker **31** to yield **35** in 20% yield.



Scheme 3.10: **a.** EDC.HCl, pyridine, DMSO, CF₃CO₂H, 48%, **b.** **31**, Na(OAc)₃BH, MeOH, rt, 20%.

The final step in the synthesis was the deprotection of benzyl groups in **35**. Table 3.4 depicts all the conditions screened for this transformation. Anhydrous FeCl₃ has been reported to efficiently cleave benzyl ether at room temperature in very good yields.¹¹⁶ Employing FeCl₃ to for deprotection of **35** however resulted in no reaction (Entry 1). A similar result was observed on attempting Pd/C-induced catalytic transfer hydrogenation with triethylsilane¹¹⁷ (Entry 2). Palladium catalysed hydrogenation using 5% Pd/C as catalyst resulted in no reaction. Increasing the catalyst load to 10% had no effect on the reactivity (Entry 3). Using Pearlman's catalyst and increasing the catalyst load up to 20 % in methanol and ethanol failed to facilitate the reaction (Entry 4 and 5). When performed in acetic acid, the reaction resulted in de-colouration of solution, indicating degradation of the fluorophore (Entry 6). When catalytic amount of acetic acid was used the reaction was extremely slow, with only partially debenzylated products observed even after 3 days (Entry 7). To accelerate the reaction a pressure of 10 bar was applied. This did not significantly improve the results of the reaction, however, on increasing the catalyst load to 20% at 10 bar, degradation of fluorophore was observed (Entry 9). The reason for the inefficient removal of benzyl group by palladium catalysed hydrogenation could be because of the poisoning of catalyst by the amine group generated by the reductive amination. Therefore, the debenzylation was attempted under mildly acidic

condition with PMB as a cation scavenger.⁷⁷ Monitoring the reaction by LC-MS showed clean conversion to BOT_15 in 4 h. However, the isolation of the product was inefficient due to solubility issues, accounting for the moderate yield of 40% (Entry 10).

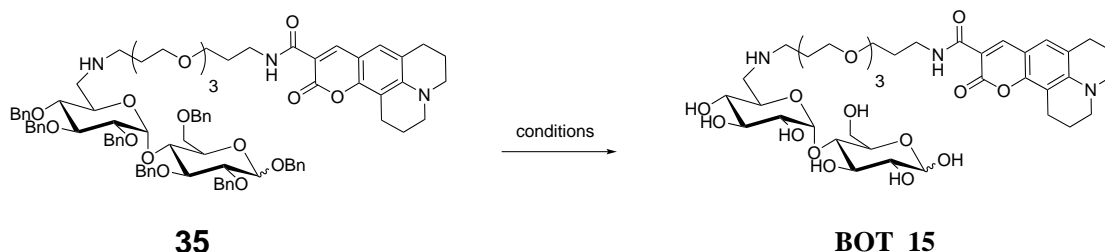
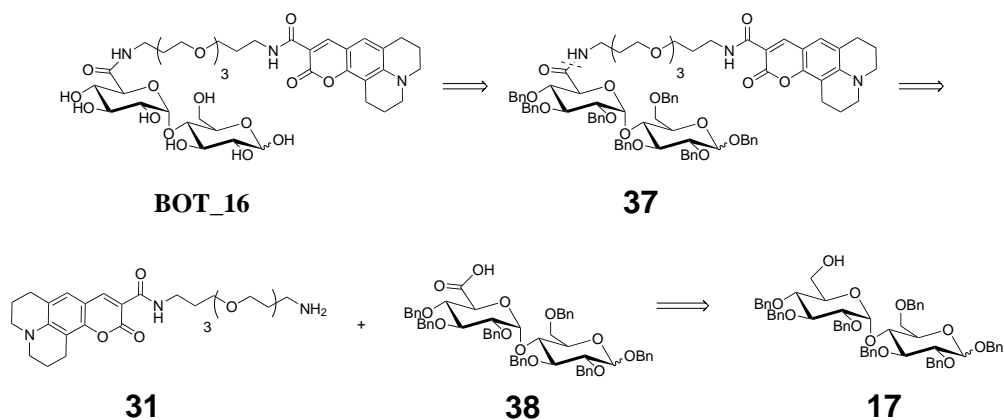


Table 3.4: Trials to prepare BOT_15 by deprotecting **35**

S. No.	Conditions	Comments/ Yields (%)
1	35 , FeCl ₃ , DCM, rt, 24h	No reaction
2	35 , Pd/C (10-20 %), Et ₃ SiH, MeOH, 48 h	No reaction
3	35 , Pd/C (5-10 %), H ₂ , MeOH, 24 h	No reaction
4	35 , Pd(OH)/C (10-20 %), H ₂ , EtOH, 24 h	No reaction
5	35 , Pd(OH)/C (10 %), H ₂ , MeOH, 24 h	No reaction
6	35 , Pd(OH)/C (10 %), H ₂ , CH ₃ COOH, 24 h	Fluorophore decomposed
7	35 , Pd(OH)/C (10-20 %), H ₂ , MeOH, CH ₃ COOH (cat.), 3 days	Partial debenylation
8	35 , Pd(OH)/C (5 %), H ₂ , MeOH, CH ₃ COOH (cat.), 10 bar, 12 h	Partial debenylation
9	35 , Pd(OH)/C (20 %), H ₂ , MeOH, CH ₃ COOH (cat.), 10 bar, 12 h	Fluorophore decomposed
10	35 , BCl ₃ , PMB, DCM, -78 °C	36%

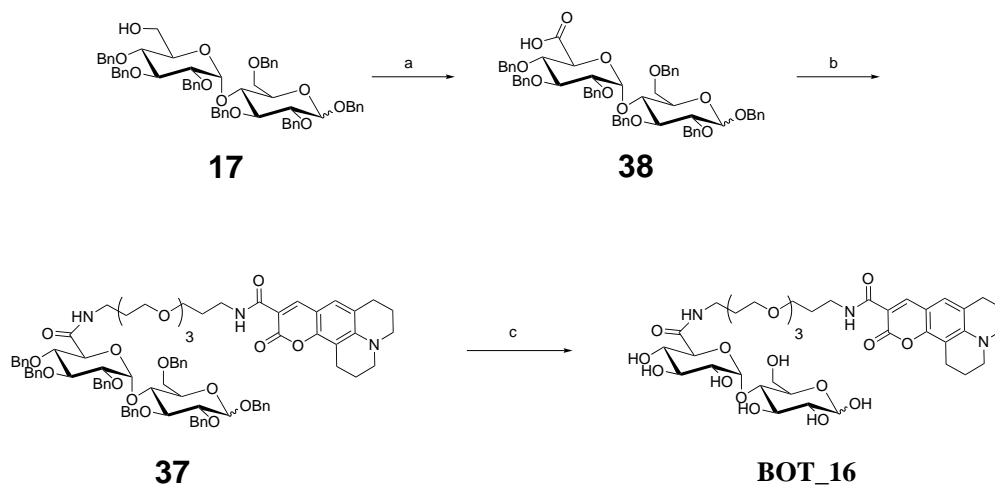
Synthesis of BOT_16

The retrosynthetic approach to BOT_16 is shown in Scheme 3.11. The benzylated precursor **37** should be obtained by an amide coupling between the amine **31** and benzylated carboxylic acid **38**. A TEMPO mediated oxidation of the primary hydroxy group in **17** was planned to obtain **38**.



Scheme 3.11: Retrosynthesis of BOT_16

The synthesis of BOT_16 was straightforward (Scheme 3.12). TEMPO mediated oxidation of **17** gave **38** in very good yields. Compound **38** was attached to the coumarin-linker conjugate **31** using T3P as a coupling reagent to obtain **37** which was subsequently debenzylated using BCl_3 to yield BOT_16 in a yield of 60%.

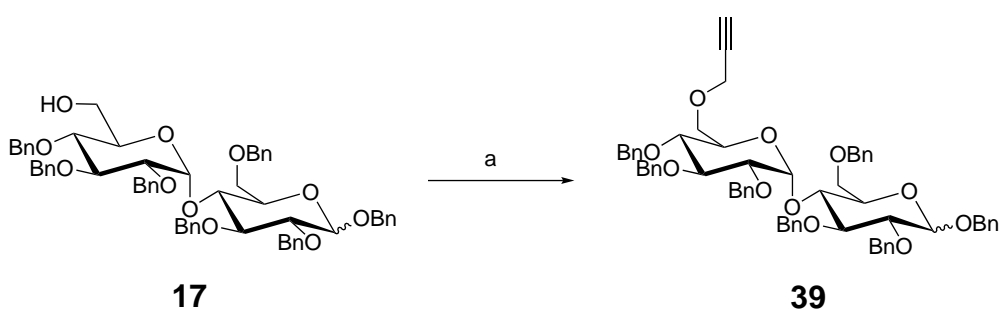


Scheme 3.12: **a.** TEMPO/BAIB, $\text{CH}_2\text{Cl}_2/\text{H}_2\text{O}$ (1:1), 85% **b.** **31**, T3P, Et_3N , CH_2Cl_2 , 65% **c.** BCl_3 , PMB, DCM, -78°C , 45%.

Synthesis of BOT_18

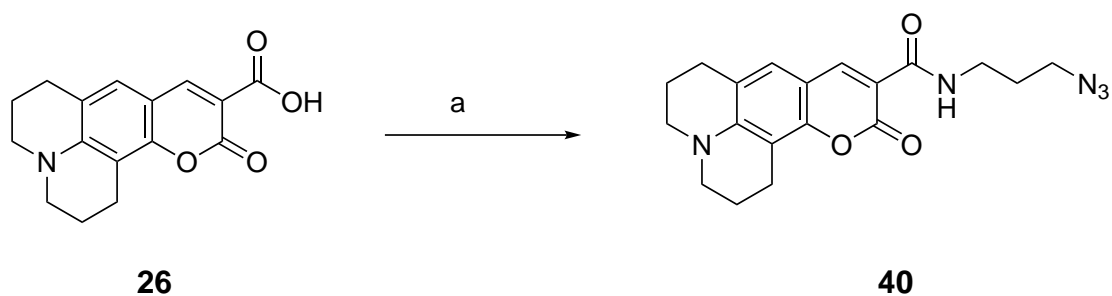
The synthesis of the 1,2,3-triazole ring in BOT_18 was planned via a copper catalyzed click reaction, which required introduction of alkyne and azide functional groups on the sugar and coumarin 343, respectively.

A Williamson ether synthesis¹¹⁸ was carried by using propargyl bromide as alkylation agent and sodium hydride as a base to introduce the alkyne handle on the primary hydroxy group in **17** (Scheme 3.13).



Scheme 3.13: **a.** propargyl bromide, NaH, THF-DMPU, rt, 95%.

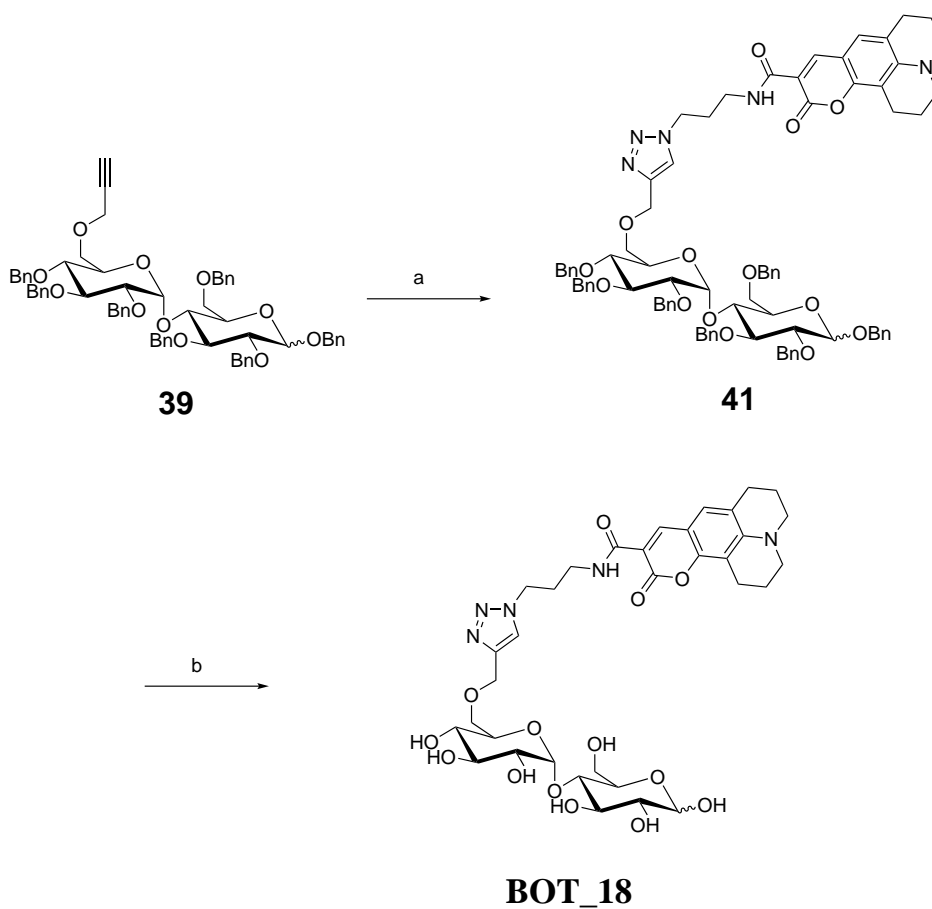
The azide moiety was introduced on the coumarin by means of an amide coupling with 3-azidopropylamine using T3P as a coupling agent.



Scheme 3.14: **a.** 3-azidopropylamine, T3P, Et₃N, CH₂Cl₂, 74%.

The two building blocks for the triazole **39** and **40** were added to undergo a copper-catalyzed azide-alkyne cycloadditions (CuAAC). CuSO₄ · 5 H₂O (Cu(II)) was treated

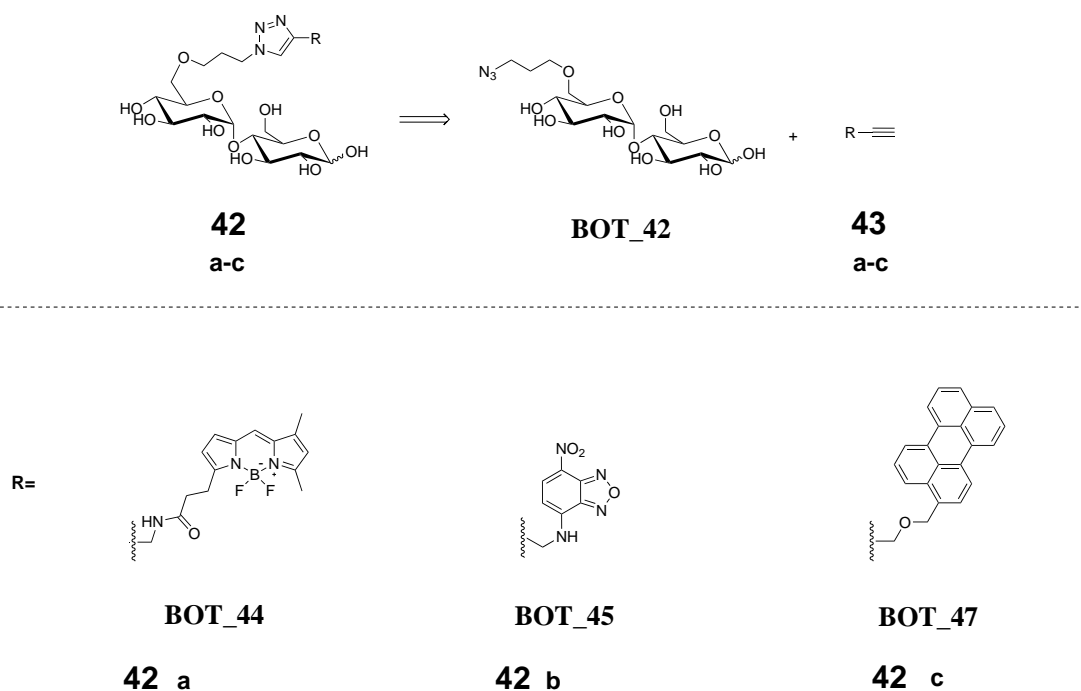
with sodium ascorbate to generate the Cu(I) as an active catalyst in situ. To account for the solubility of **39** a DCM/H₂O biphasic solvent was used in the reaction. Tris(benzyltriazolylmethyl)amine (TBTA) was added as a Cu chelator to stabilize the Cu(I) species. Under the above-mentioned conditions the reaction resulted in the formation of the desired product **41** (Scheme 3.15). **41** was subsequently debenzylated using BCl₃ to yield BOT_18 in a yield of 28%.



Scheme 3.15: **a.** **40**, CuSO₄, NaAsc, TBTA, CH₂Cl₂/H₂O (1:1), rt, 73.5% **b.** BCl₃, PMB, DCM, -78 °C, 28%.

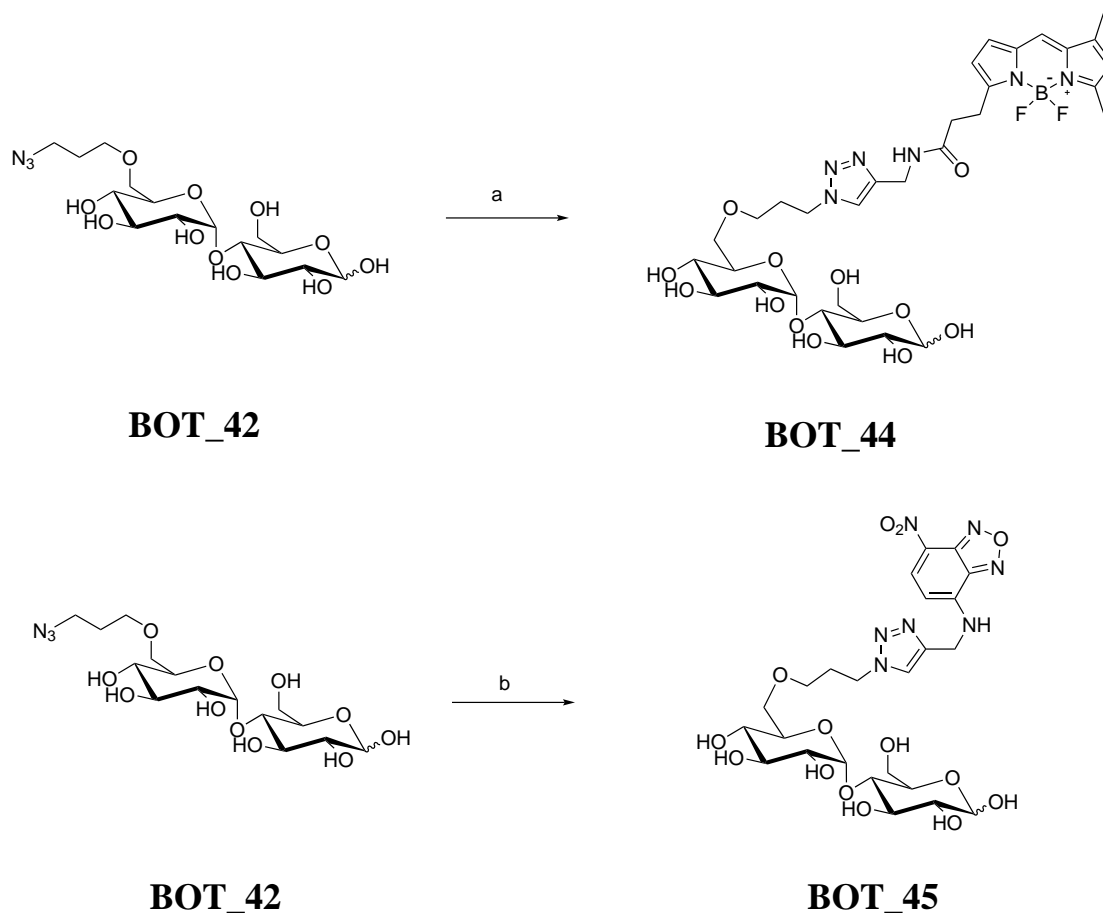
Synthesis of BOT_44, BOT_45 and BOT_47

BOT_44 (BODIPY conjugate), BOT_45 (NBD conjugate) and BOT_47 (Perylene conjugate) could be obtained from a CuAAC between common azide intermediate BOT_42 and the respective fluorophore modified alkynes (Scheme 3.16).



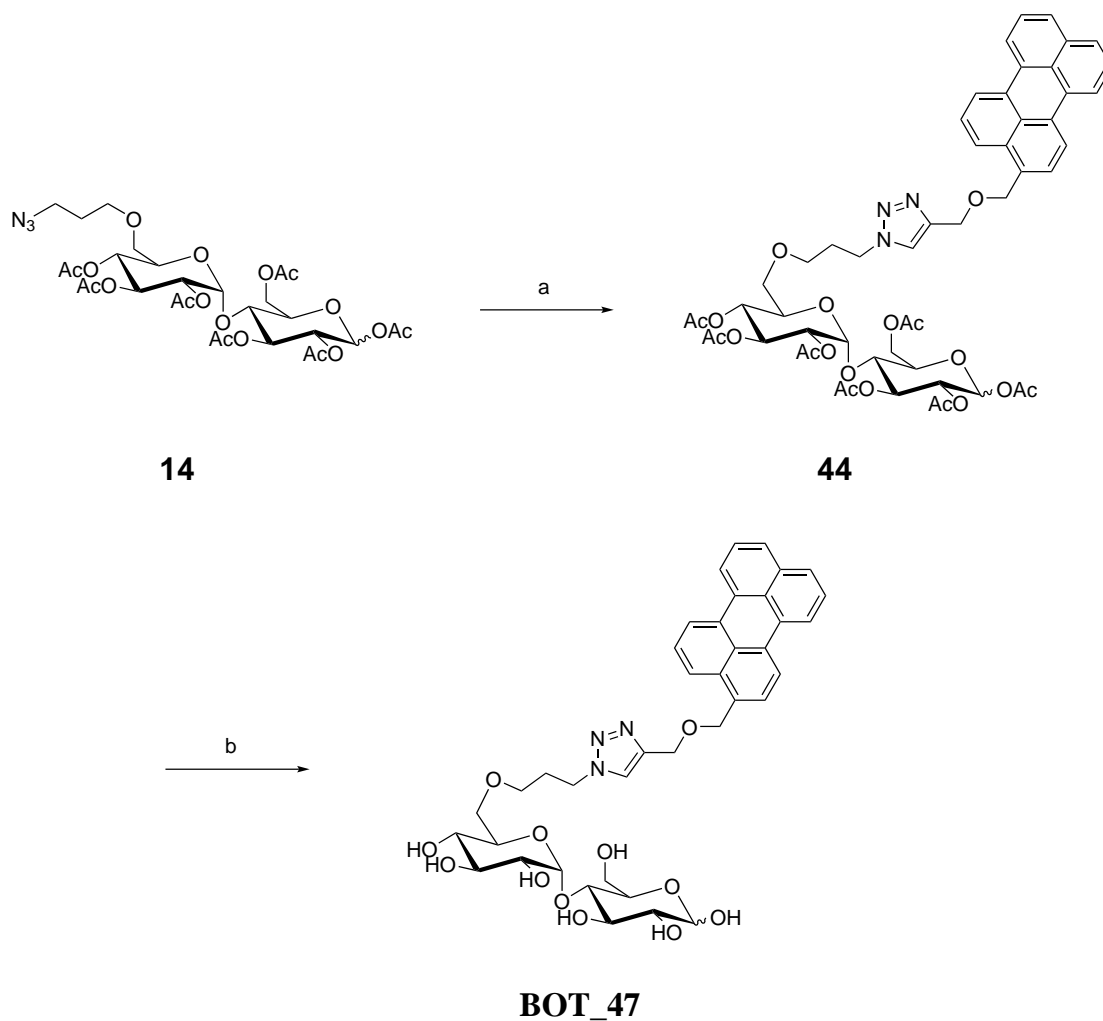
Scheme 3.16: Retrosynthetic analysis of BOT_44, BOT_45 and BOT_47

Standard CuAAC conditions with *in situ* generation of Cu(I) from CuSO₄ was employed for the synthesis of BOT_44 and BOT_45. Since the intermediate BOT_42 is water soluble, the reactions were performed in a homogeneous DMF/H₂O (1:4) mixture as solvent. The choice of solvent was also made to simplify the purification process, as the reaction mixture could be directly injected in the HPLC for purification. BOT_42 was treated with BODIPY FL-alkyne **43a** and NBD alkyne **43b** to yield BOT_44 and BOT_45, respectively, in good yields (Scheme 3.17).



Scheme 3.17: **a.** **43a**, CuSO₄, NaAsc, TBTA, DMF/H₂O (1:4), rt, 85% **b.** **43b**, CuSO₄, NaAsc, TBTA, DMF/H₂O (1:4), rt, 73%.

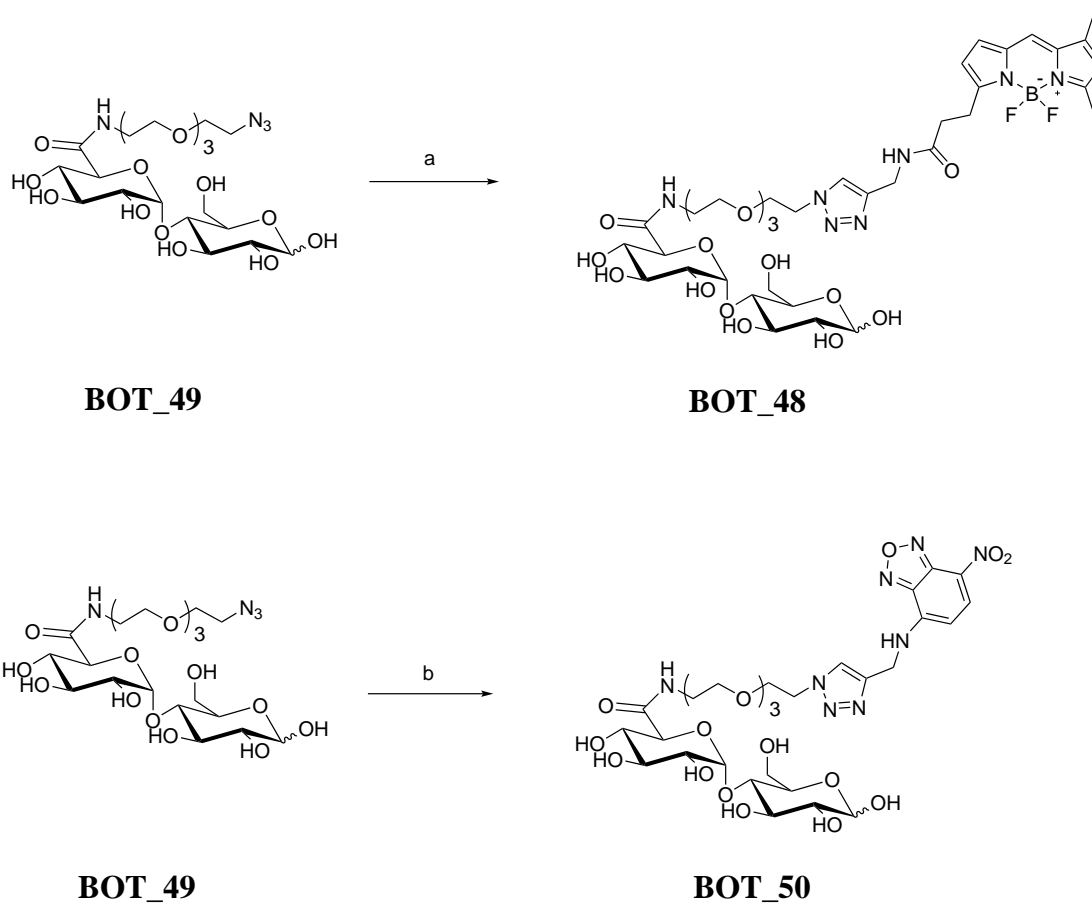
The synthesis of BOT_47 by treating BOT_42 with the perylene alkyne **43c** under the above mentioned conditions, resulted in poor yields due to the insolubility of the perylene alkyne in water. Therefore, the reaction was performed using the acetylated azide **14** in DMF/H₂O. The acetylated conjugate **44** was then deprotected using the Zemplén deacetylation (Scheme 3.18). However due to solubility issues, purification by HPLC resulted in low yields.



Scheme 3.18: **a.** **43c**, CuI, DMF, DIPEA, rt, 49% **b.** NaOMe, MeOH, 15%.

Synthesis of BOT_48 and BOT_50

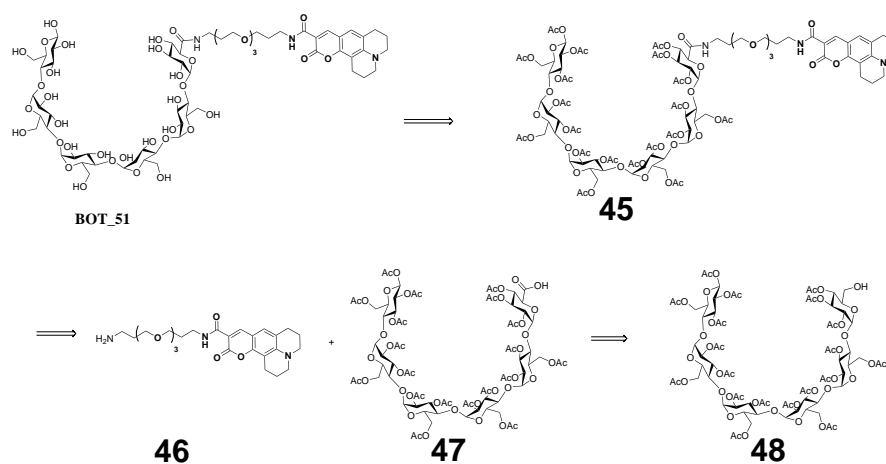
Similar to the synthesis of BOT_44, a CuAAC between BOT_49 and **43a** and **43b** using CuSO₄ and sodium ascorbate yielded BOT_48 and BOT_50, respectively (Scheme 3.19).



Scheme 3.19: **a.** **43a**, CuSO₄, NaAsc, TBTA, DMF/H₂O (1:4), rt, 17% **b.** **43b**, CuSO₄, NaAsc, TBTA, DMF/H₂O (1:4), rt, 15%.

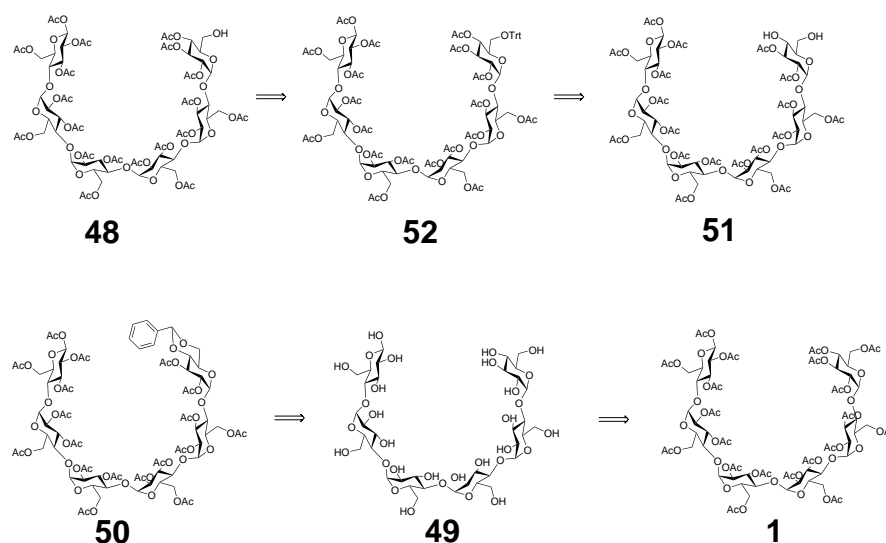
Synthesis of BOT_51

The synthesis of the maltohexose-coumarin conjugate BOT_51 was planned according to the synthesis of its maltose analogue BOT_16 as described in Scheme 3.20.



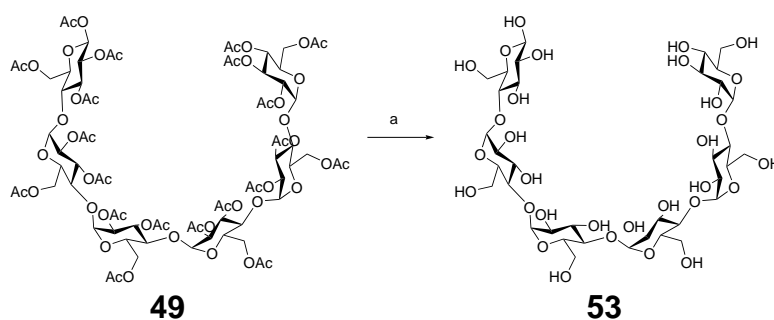
Scheme 3.20: Retrosynthesis of BOT_51

The retrosynthesis of the acetylated maltohexose containing a free primary hydroxy group at the non-reducing end **48** is depicted in Scheme 3.21, similar to the maltose analogue.



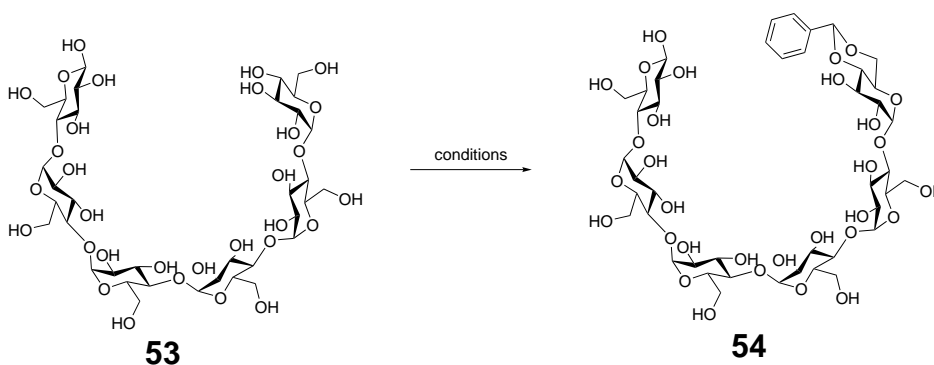
Scheme 3.21: Retrosynthetic route for the synthesis of **48**

As the maltohexose eicosacetate **49** is an inexpensive starting material as compared to the commercially available maltohexose, maltohexose was synthesized by performing a Zemplén deacetylation **49** (Scheme 3.22).



Scheme 3.22: a. NaOMe, MeOH, 87%.

The protection of the free C-4' and C-6' hydroxyl groups of maltohexose using benzylidene dimethyl acetal under mild acidic conditions was attempted to yield **54** (Scheme 3.23).



Scheme 3.23: Trials towards benzylidene acetal protection

Table 3.5: Trials towards benzylidene acetal protection

S. No	Conditions	Yield (%)
1	Benzaldehyde dimethyl acetal (5-10 eq.), PTSA, DMF, 50-80 °C, 40mbar	10-12
2	Benzaldehyde dimethyl acetal (5-10 eq.), Amberlyst IR-120, DMF, 50 °C, 150 mbar	7
3	Benzaldehyde dimethyl acetal, PTSA, MW, conditions (Table 3.4)	12-40

Under the conditions optimised for the maltose analogue, the yields of the reaction were poor (10-15%). We assume that the yield of this reaction was low, because the formation of the benzylidene acetal is a reversible reaction. Attempts to increase the yield of the reaction by increasing the temperature and increasing the equivalents of benzaldehyde

acetal were unsuccessful (Table 3.5 Entry 1). Literature reports involving the use of Amberlyst[®] 15H⁺ as an acid in the reaction to obtain the product in fair yields¹⁰⁷ could not be reproduced (Table 3.5 Entry 2).

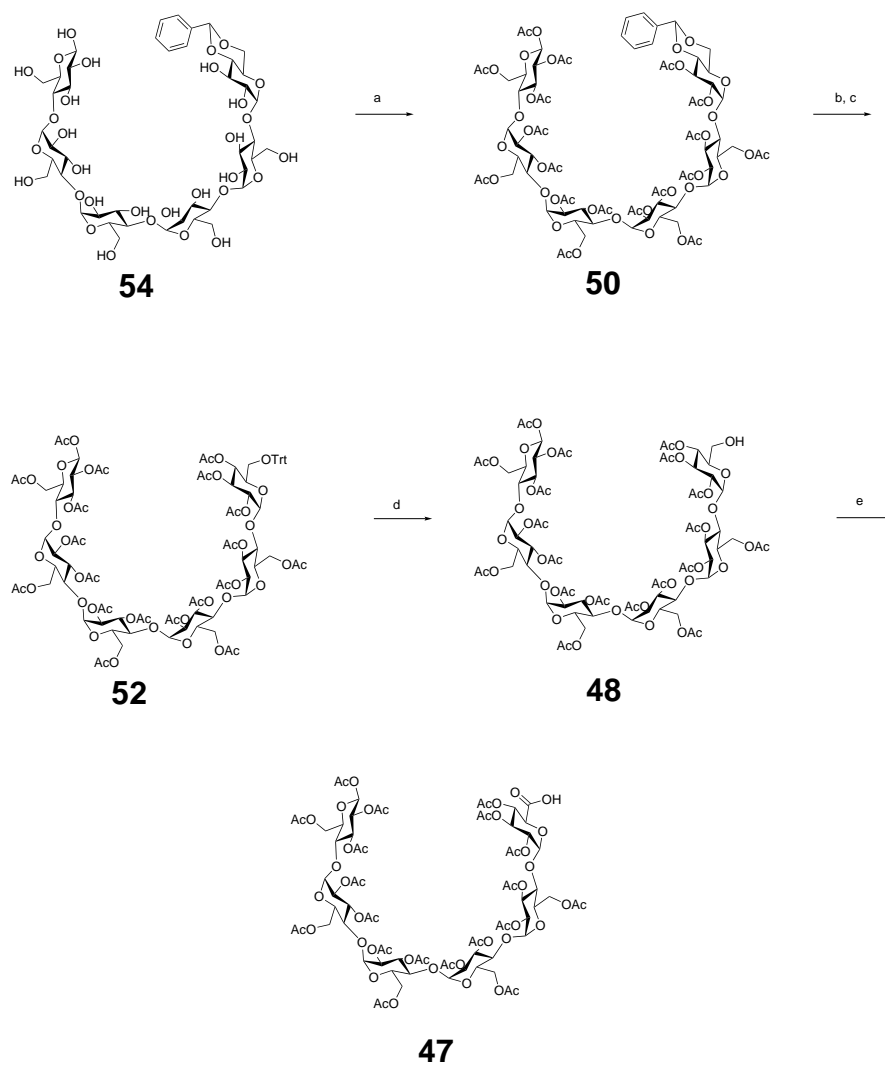
Table 3.6: Optimisation of microwave assisted benzylidene protection

S. No.	Scale (mg)	Source of 53	Temperature (°C)	Eq. of acetal	Time (h)	Yield (%)
1	10	Commercial	60	5	1-5	12-15
2	10	Commercial	60	5-10	1-5	12-15
3	10	Commercial	60	10	1	35
4	10	Commercial	60	20	1	Mixture of products
5	100	Commercial	60	10	1	38
6	100	Commercial	60	10	1	26
7	100	Commercial	80	10	1	40
8	500	deacetylation of 1	80	10	1	40
9	1g	deacetylation of 1	80	10	1	10

Finally, attempts were made to improve the yield by performing the reaction in microwave. At 60 °C with 5 eq. of the acetal, the reaction did not show any improvement (Table 3.6; Entry 1). Increasing the concentration of the acetal in the same reaction mixture did not have any positive impact on the reaction (Entry 2). On performing the reaction with 10 eq. of acetal resulted in improvement of the yield to 35%. Increasing the acetal concentration to 20 eq. resulted in a mixture of products corresponding to multiple acetal containing product (Entry 4). Therefore the concentration of the acetal was optimised to 10 eq. The reaction was scalable up to 500 mg (Entry 5-8). On a 1 g scale the reaction suffered from poor yields. The reaction temperature could be increased to 80 °C to achieve slightly better yields. Also, the reactivity of commercially available maltohexose and deacetylated maltohexose synthesized according to (Scheme 3.22) remained consistent.

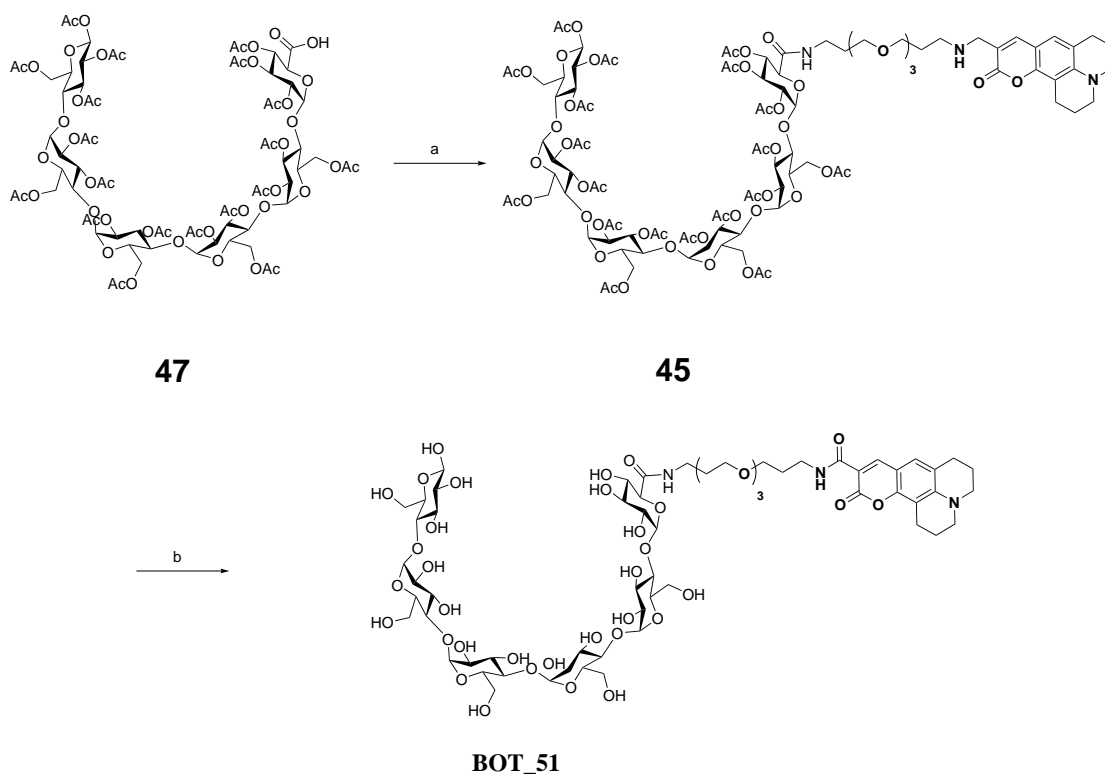
The next steps were similar to the synthesis of the maltose analogue. The free hydroxy groups in compound **54** were acetylated to yield **50**. In the next step the benzylidene acetal was cleaved by acid hydrolysis to yield **51**. The primary hydroxy group was selectively protected with a bulky trityl group, followed by acetylation of the secondary

hydroxy group to yield compound **52**. The desired alcohol **48** was synthesized by acidic removal of the trityl group. Finally, the synthesis of the acid **47** was achieved via a TEMPO mediated oxidation of the primary hydroxy group in **48** (Scheme 3.24).



Scheme 3.24: **a.** Ac_2O , pyridine, 22%. **b.** $\text{AcOH}/\text{H}_2\text{O}$, 95°C . **c.** i. TrCl , pyridine, ii. Ac_2O , pyridine, 37%. **d.** $\text{AcOH}/\text{H}_2\text{O}$, 95°C , 45%. **e.** TEMPO/BAIB, $\text{CH}_2\text{Cl}_2/\text{H}_2\text{O}$, 50%.

Compound **47** was coupled to the coumarin-linker conjugate **31** using T3P to obtain the acetylated conjugate **45** in good yields. In the final step, the acetyl protecting groups were cleaved via a Zemplén deacetylation to yield the desired conjugate BOT_51 (Scheme 3.25).



Scheme 3.25: **a.** **31**, T3P, Et₃N, CH₂Cl₂, 56%, **b.** NaOMe, MeOH, 10.7%.

3.3 Characterization of probe uptake

The uptake of the fluorescent probes in bacteria was studied using a growth recovery assay and imaging by confocal microscopy. To get quantitative information on the number of labelled cells a fluorescence-activated cell sorting (FACS) analysis was performed.

3.3.1 Growth recovery assay

Fluorescent probes BOT_10, BOT_14, BOT_44, BOT_45 and BOT_48 were tested for uptake in a growth recovery assay using the same conditions discussed in section 2.3. Since the ATP- bioluminescence assay is more sensitive than the OD600 measurements, only the ATP measurements were performed. The results of the growth recovery assay as observed by the ATP measurement after 48 h are summarized in Figure 3.2.

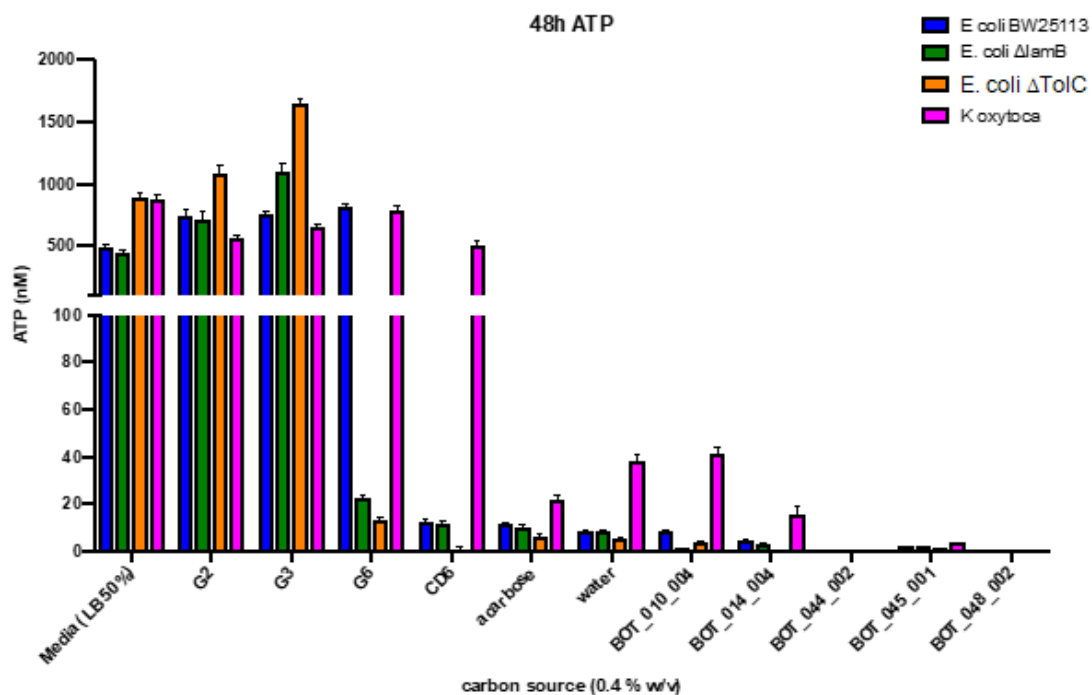


Figure 3.2: Recovery of growth after 48 h measured by ATP-bioluminescence. g1, g2, g6 and CD6 represent maltose, maltotriose, maltohexose and cyclodextrin, respectively. Acarbose is used as a negative control. $n \geq 6$, except $n=3$ for CD6, BOT_44 and BOT_44 in *K. oxytoca*

It can be seen from Figure 3.2 that no restoration in growth was observed for any of the conjugates. The small amount of growth observed for BOT_10 was about the same as that of the negative control acarbose. As discussed earlier, absence of growth recovery does not rule out the possibility of uptake.

Also, no ATP content was recorded for the BODIPY conjugates BOT_44 and BOT_48, indicating decrease in the initial bacterial count. One possible reason could be that the BODIPY conjugates BOT_44 and BOT_48 are toxic to bacteria.

3.3.2 Confocal microscopy assay

Internalisation of the fluorescent probes in *E. coli* was further studied by imaging using confocal microscopy. To determine if the uptake is dependent on the maltodextrin pathway, the probes were tested on Δ lamB *E. coli*.

E. coli WT and Δ lamB *E. coli* were incubated at a concentration of 0.2 μ M of the probes. Confocal microscopy was performed after 30 min of incubation with the probes. Cells were washed twice with PBS to remove any background fluorescence. A 488 nm laser was used as an excitation wavelength for the BODIPY conjugates and a 405 nm laser was used for the coumarin, perylene and NBD conjugates.

The results of the experiments are discussed according to the type of dyes used.

Perylene conjugates

The confocal microscopy images of *E. coli* WT and Δ lamB *E. coli* incubated with perylene conjugates BOT_10, BOT_14 and BOT_47 are summarized in Figure 3.3.

From the overlay of fluorescence microscopy and bright field images, all three conjugates could label a sub-population of *E. coli* WT. This could be because of the differential staining of cells in different stages of their growth cycle. Also, very few cells of Δ lamB *E. coli* were labelled by these conjugates. This result indicates that all three probes are transported in a lamB dependent manner.

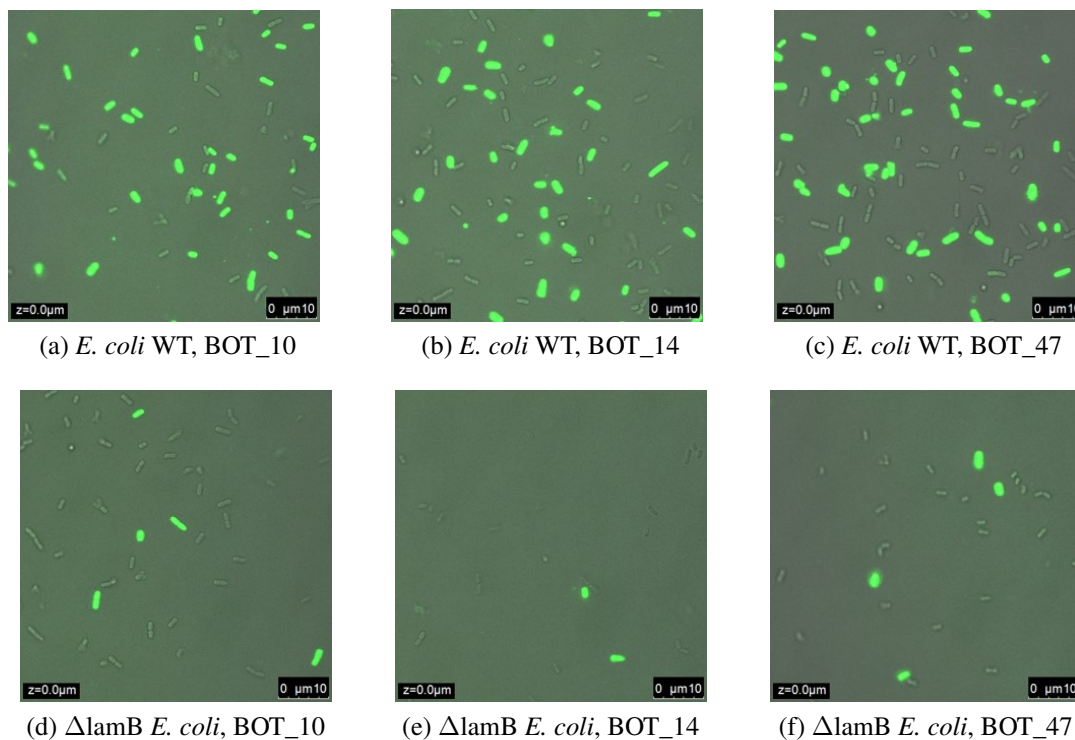


Figure 3.3: Confocal microscopy images of labelling by perylene conjugates. 200 μL cellular suspension was incubated with 2 μL of the probes. Excitation wavelength: 405 nm, emission wavelength: 435 nm.

Coumarin conjugates

The confocal microscopy images of *E. coli* and ΔlamB *E. coli* incubated with coumarin conjugates BOT_15, BOT_16, BOT_18 and BOT_51 are summarized in Figure 3.4.

Of the three maltose based probes BOT_15, BOT_16, BOT_18, only BOT_18 labelled *E. coli* WT. ΔlamB *E. coli* was labelled to a much lesser extent by BOT_18. The images obtained for the maltohexose probe BOT_51 indicate equal labelling in both *E. coli* WT and ΔlamB *E. coli*. This could mean that a) the probes are transported in a manner independent of lamB, or b) the probes show non specific binding to the bacterial surface.

It should be noted that the intensity of fluorescence of the coumarin conjugates is much lower compared to the perylene conjugate. It could mean that the concentration of these conjugates is less inside the cells. The difference in fluorescent intensities could also be due to the lower quantum yield of coumarin 343 (0.63) as compared to perylene (0.99).

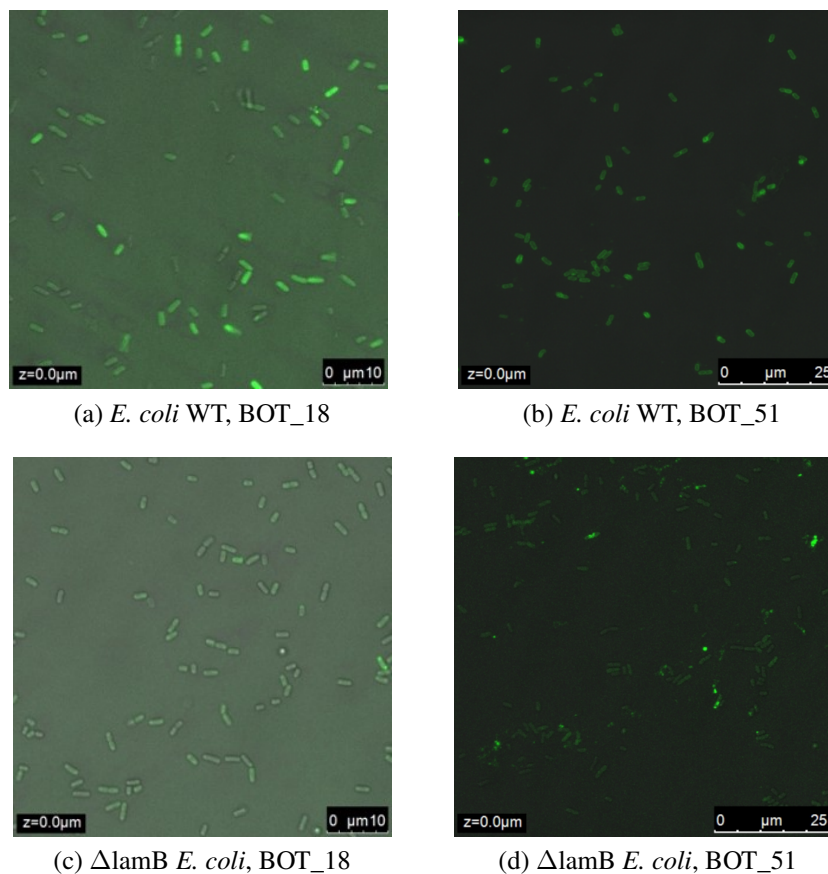


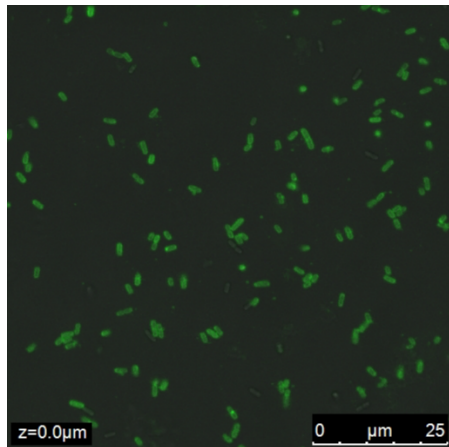
Figure 3.4: Confocal microscopy images of labelling by coumarin conjugates. 200 μ L cellular suspension was incubated with 2 μ M of the probes. Excitation wavelength: 405 nm, emission wavelength: 477 nm.

NBD conjugates

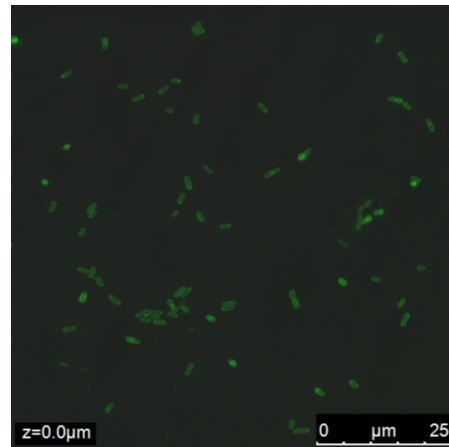
BOT_45, the maltose-NBD conjugate bearing a short linker was able to label both *E. coli* and Δ lamB *E. coli* (Figure 3.5). A closer look at the image shows that the la-

bellings is localized at the surface *E. coli* (Fig. 3.5c), indicating that the probes bind non-specifically to the surface.

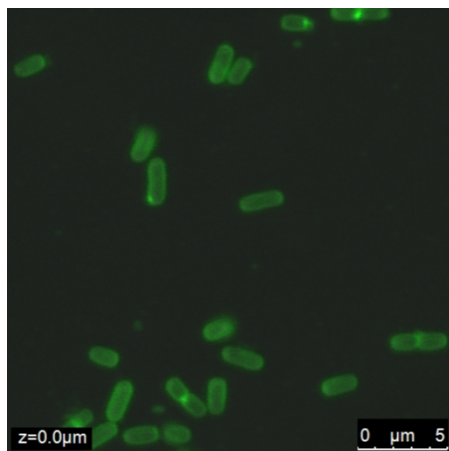
No imaging was observed for BOT_50, the maltose-NBD conjugate with the longer PEG linker.



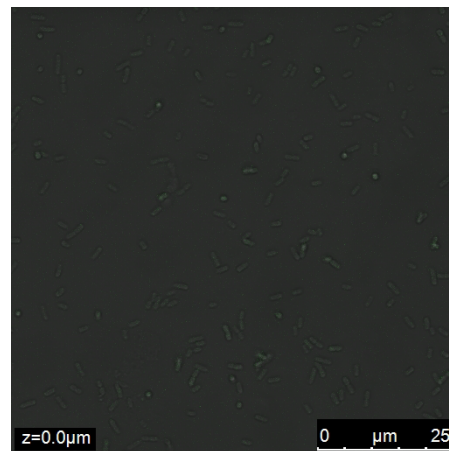
(a) *E. coli* WT, BOT_45



(b) Δ lamB *E. coli*, BOT_45



(c) *E. coli* WT, BOT_45



(d) *E. coli* WT, BOT_50

Figure 3.5: Confocal microscopy images of *E. coli* and Δ lamB *E. coli* upon incubation with NBD conjugates at a concentration of $0.2 \mu\text{M}$. Excitation wavelength: 405 nm, Emission: 440 nm.

BODIPY conjugates

No labelling of either *E. coli* WT or Δ lamB *E. coli* was observed for the BODIPY conjugates BOT_44 and BOT_48 (Figure 3.6). This result supports the speculation made from the growth recovery assay concerning the toxicity of the BODIPY conjugates.

The confocal microscopy experiment gives only a qualitative understanding of imaging by these probes. To get a quantitative picture a FACS analysis was performed.

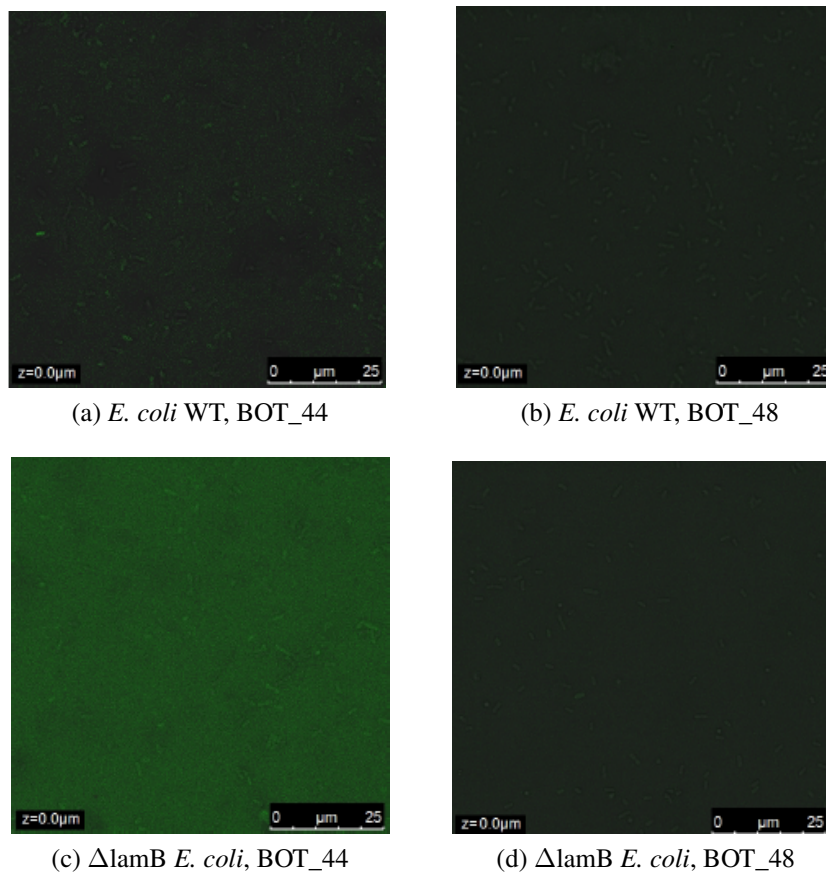


Figure 3.6: Confocal microscopy images of *E. coli* upon incubation with BODIPY conjugates at a concentration of $0.2 \mu\text{M}$. Excitation wavelength: 405 nm, emission wavelength: 513 nm.

3.4 FACS analysis

Selected probes that could label bacteria in the microscopy assay, which include the perylene conjugates BOT_10, BOT_14, BOT_47 and coumarin conjugate BOT_18 were also analyzed by FACS. FACS analysis of *E. coli* WT or Δ lamB *E. coli* was performed after incubating the bacteria with 2 μ M of the probes for 30 mins. A 405 nm laser was used as the excitation wavelength. To understand the effect of bacterial morphology on the labelling, analysis was performed using two different cell gates, a full cell gate and a small cell gate. The small cell gate contained bacterial population of small cells. The full gate contains large cells in addition to the small cells. The result of the FACS analysis is shown in Figure 3.7 and Figure 3.8.

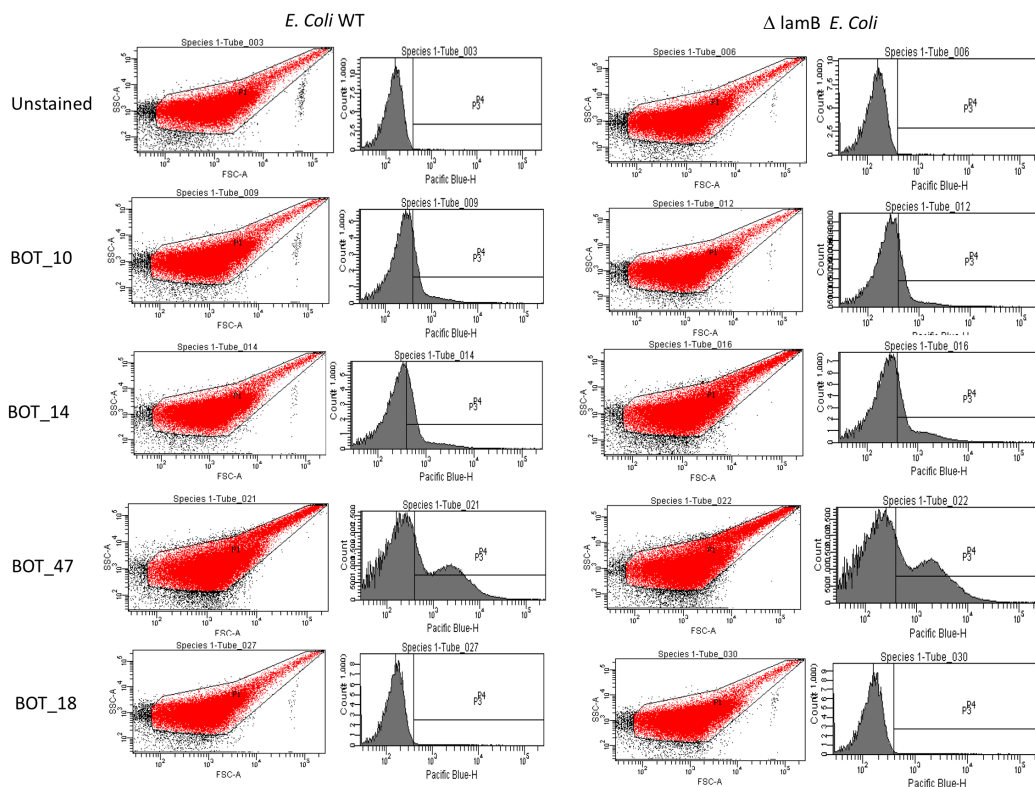


Figure 3.7: Quantification of uptake by FACS analysis: Small gate

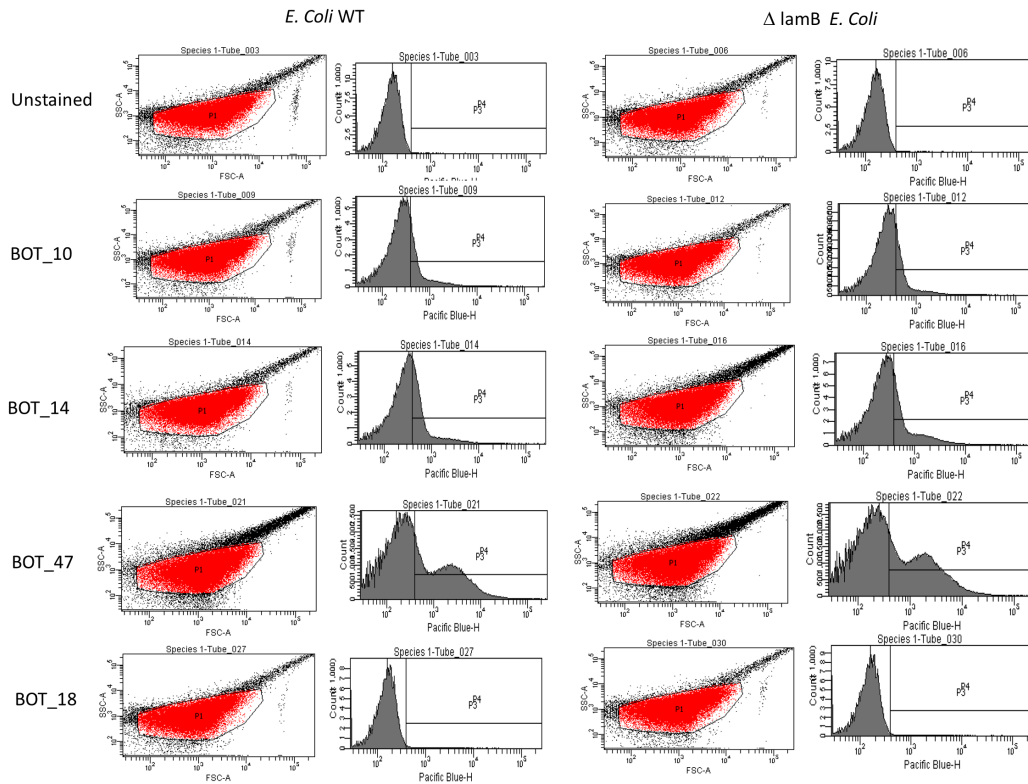
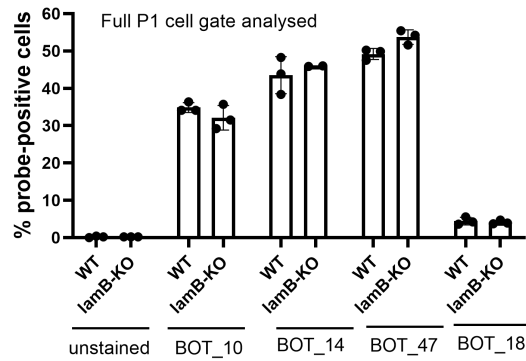


Figure 3.8: Quantification of uptake by FACS analysis: Full gate. Flow cytometric analysis of *E. coli* and Δ lamB *E. coli* upon incubation with BOT_10, BOT_14, BOT_47 and BOT_47 at a concentration of $2 \mu\text{M}$ for 16 h. FSC-forward scatter, SSC-side scatter.

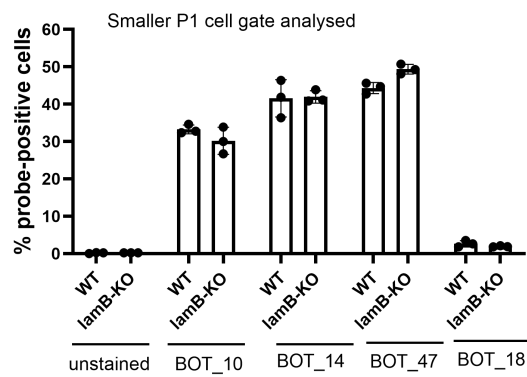
The results of the % of cells labelled by the probes is summarized in Figure 3.9.

Some important observations are listed below:

- 30-50% of the *E. coli* WT are labelled by the perylene probes BOT_10, BOT_14 and BOT_47. The results are similar both in both the full cell gate and the small cell gate.
- Similarly, 30-50% of the Δ lamB *E. coli* are labelled by the perylene probes BOT_10, BOT_14 and BOT_47.
- Only 3-5% of the *E. coli* WT and Δ lamB *E. coli* were labelled by the the coumarin-probe BOT_18.



(a) Full cell gate

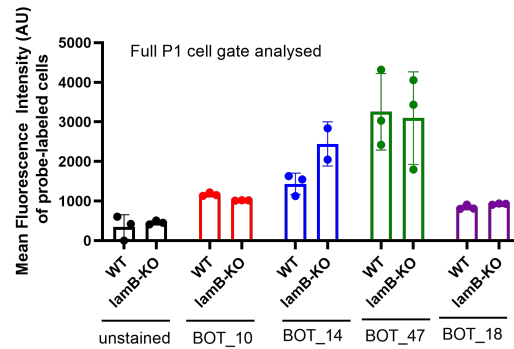


(b) Small cell gate

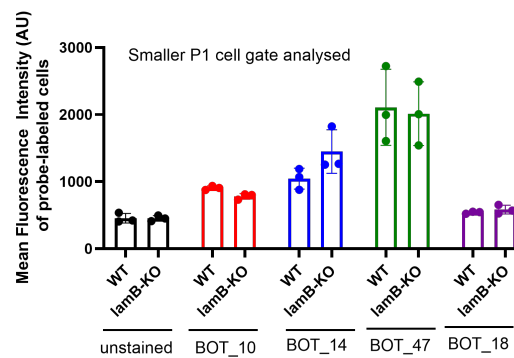
Figure 3.9: FACS analysis showing % of cells labelled by the probe

The FACS analysis confirmed that only a sub-population of the bacteria are labelled by the probes, as observed by microscopy. However, 30-50% labelling of the Δ lamB *E. coli* is a huge deviation from the cell count as seen from the microscopy. This result indicates that the uptake of these probes is independent of lamB. The coumarin-probe BOT_18 showed much lower fluorescence at the detection limit resulting in only 3-5% of probe-positive cells according to flow cytometry. This is in agreement with the microscopy images.

The mean fluorescent intensities were calculated and summarized in Figure 3.10. Some important observations include:



(a) Full cell gate



(b) Small cell gate

Figure 3.10: FACS analysis showing mean fluorescence intensity of the labelled cells.

- Significant difference in the fluorescent intensities compared to the unstained control can only be observed for the perylene probes BOT_10, BOT_14 and BOT_47. The staining in BOT_18 is almost equal to the unstained control.
- Comparing the mean fluorescence intensities of the probes it can be seen that the cells of the full cell gate are stained more intensely by most probes. It is hypothesized that they may represent clusters of cells or elongated dividing cells which are also observed microscopically.
- As these populations seem to be morphologically distinct, a separate analysis of only the smaller cell population was performed, which gave qualitatively similar

results to the full cell gate analysis (3.10b).

Discrepancies in the results of imaging and FACS

- A difference in background and probe signal is observed between imaging and FACS. The unstained control in FACS analysis shows a fluorescence signal, which is not observed in the imaging studies. Also, clear labelling of *E. coli* is observed by BOT_18 by imaging (Figure 3.4) but no significant staining is observed by FACS (Figure 3.9).

FACS is the more sensitive assay compared to microscopy. *E. coli* exhibits autofluorescence at shorter light wavelengths under standard conditions in flow cytometric analysis, with most endogenous fluorophores absorbing at 350-500 nm¹¹⁹ (Figure 3.10). As discussed earlier, fluorescence intensity of the coumarin probe BOT_18 is lower as compared to the perylene probes. Due to the lower intensity of BOT_18 the signal overlaps with the autofluorescence, resulting in poor signal to noise ratio according to flow cytometry.

- There is also a significant difference in labelling of the Δ lamB *E. coli* by both the methods. While there was a clear preference in the labelling of *E. coli* by the probes in fluorescence microscopy, 30-50% of both the *E. coli* and Δ lamB *E. coli* was observed in FACS assay.

This difference could be attributed to non-specific binding of the probes to the cells. In the microscopy assay, during sample preparation the cells were incubated with the probes and washed three times with PBS to reduce non-specific binding. This washing step was not followed in the FACS sample preparation and hence may result in non-specific binding.

Insights into the structure activity relationship

Effect of number of sugar units

Qualitatively labelling by maltohexose probe BOT_51 is significantly weak when compared to the maltose probe BOT_18. However, as observed in the microscopy assay, since BOT_51 is transported in lamB independent manner, it is difficult to comment on the role of number of sugar units.

Effect of dye

The fluorescence intensity of the perylene and NBD conjugates is higher as compared to the coumarin conjugates, making them better suited for probe development. However, the NBD conjugates appear to stick non-specifically to the surface of the bacteria. From the FACS analysis it can be seen that the cells were labelled with the perylene probes a in a manner independent of lamB. The BODIPY conjugates show no labelling, possibly due to their toxicity to the cells .

Effect of linker

On comparing labelling by BOT_45 with BOT_50, BOT_44 with BOT_48 and BOT_16 with BOT_18, it is evident there is no uptake of probes containing the long PEG linker. Therefore, shorter alkyl liker is favourable for the design of the probes.

Effect of the attachment site

The perylene conjugates modified at reducing end, BOT_10, BOT_14 and the conjugate modified at the non-reducing end BOT_47 result in similar labelling in the imaging studies indicating no preference for the non-reducing end probes.

4 | Investigation of intracellular accumulation

This chapter deals with investigating the intracellular translocation of the conjugates. The fluorogen activating protein (FAP)-malachite green (MG) system is described at the beginning of the chapter. The next section deals with the design and synthesis of the maltodextrin-MG conjugates. The internalisation of the maltodextrin-MG conjugates has been studied by monitoring the fluorescent in a plate reader assay.

4.1 Synthesis of maltodextrin-MG conjugates

Design of MG conjugates

Three maltodextrin-MG conjugates were designed to study the uptake of the conjugates (Figure 4.1). BOT_17 contains a maltose attached to MG via a small alkyl linker using a click reaction. BOT_52 contains maltose conjugated to MG through a longer PEG linker via an amide coupling. BOT_53 is the maltohexose analogue of BOT_52.

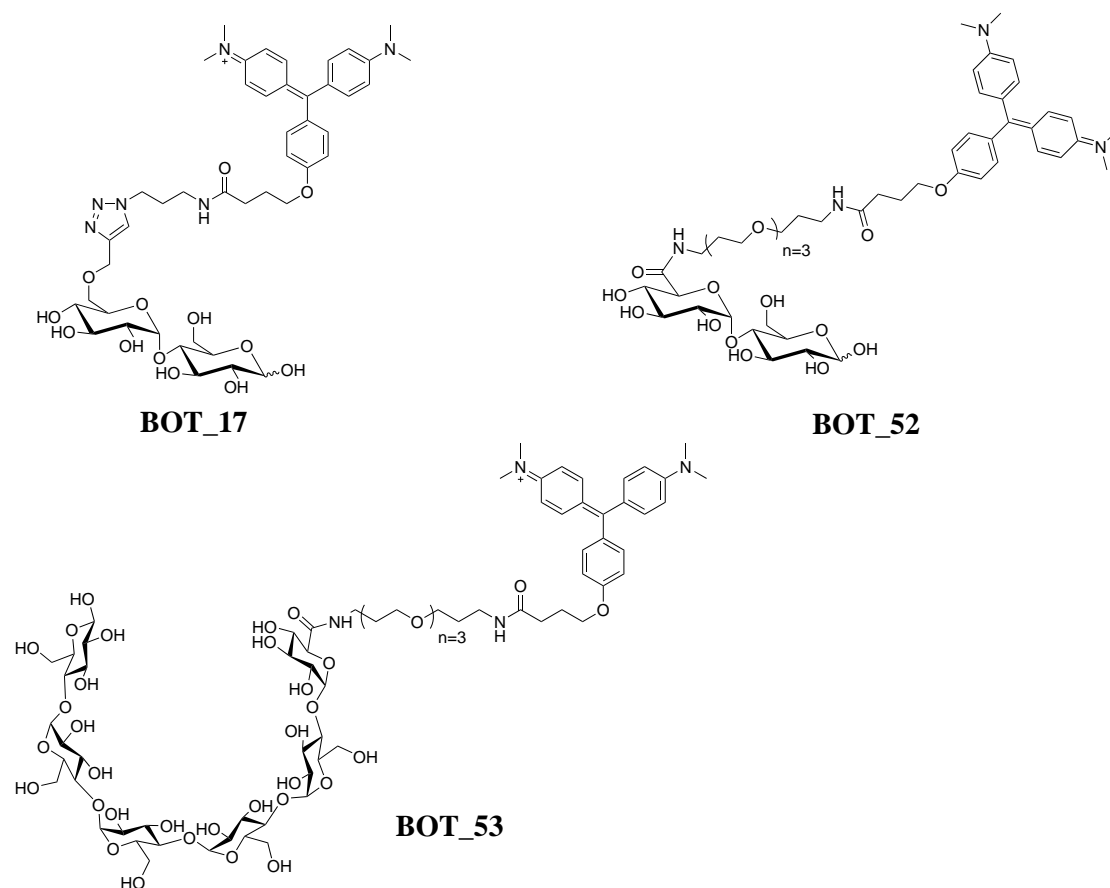
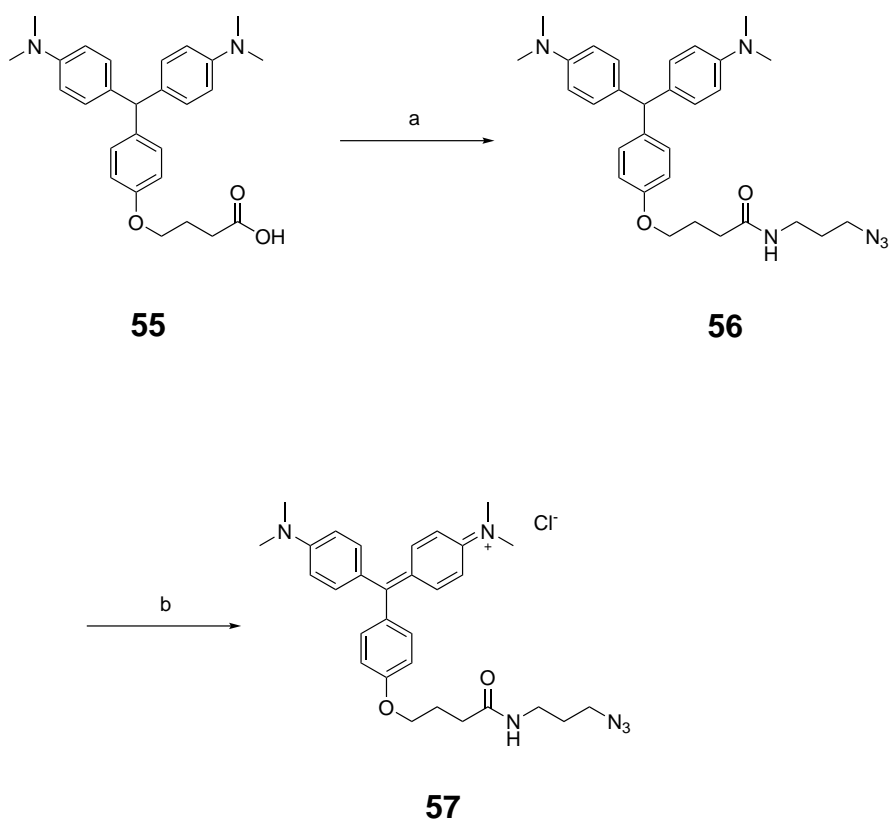


Figure 4.1: Structures of maltodextrin-MG conjugates

Synthesis of MG precursors

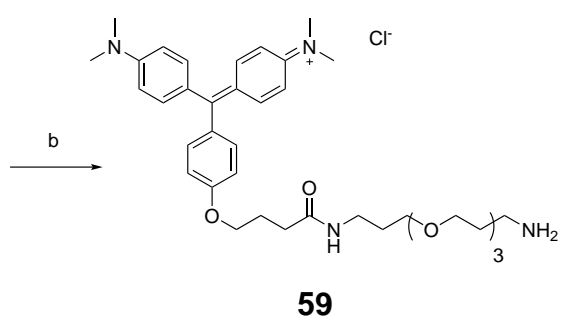
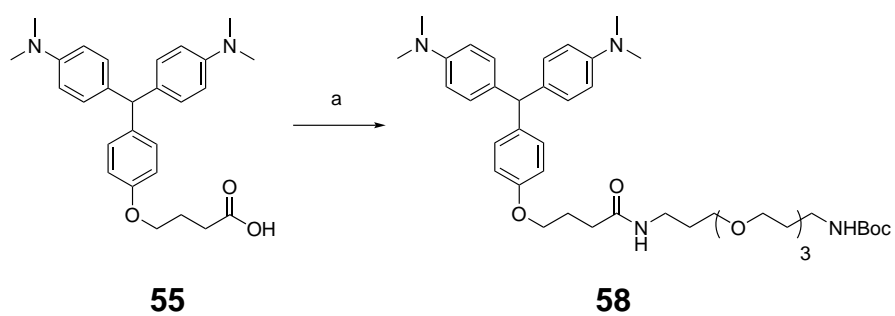
Two malachite green precursors were synthesized: The azide containing MG **57** to synthesize BOT_17 and the amine functionality containing MG **59** to synthesize BOT_52 and BOT_53.

Compound **55** was synthesized as reported in the literature.⁴⁰ The azide moiety was introduced in **55** by an amide coupling with 3-azidopropylamine using T3P. Compound **56** was then oxidized with *p*-chloranil to give the desired MG-azide **57** (Scheme 4.1) in 30% yield.



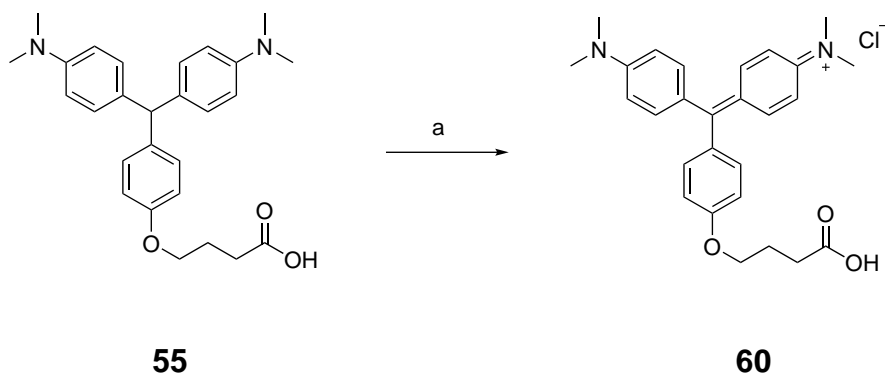
Scheme 4.1: **a.** 3-azidopropylamine, T3P, Et₃N, CH₂Cl₂, 37%, **b.** *p*-chloranil, CH₂Cl₂, rt, 30%.

Similarly, the amine functionality was introduced on **55** by an amide coupling with PEG linker **28** using T3P. Oxidation followed by removal of boc protecting group gave the desired MG-PEG precursor **59** (Scheme 4.2) in 43% yield.



Scheme 4.2: **a.** **28**, T3P, Et₃N, CH₂Cl₂, 51%, **b.** i. *p*-chloranil, CH₂Cl₂, rt. ii. HCl, EtOH, rt, 43%.

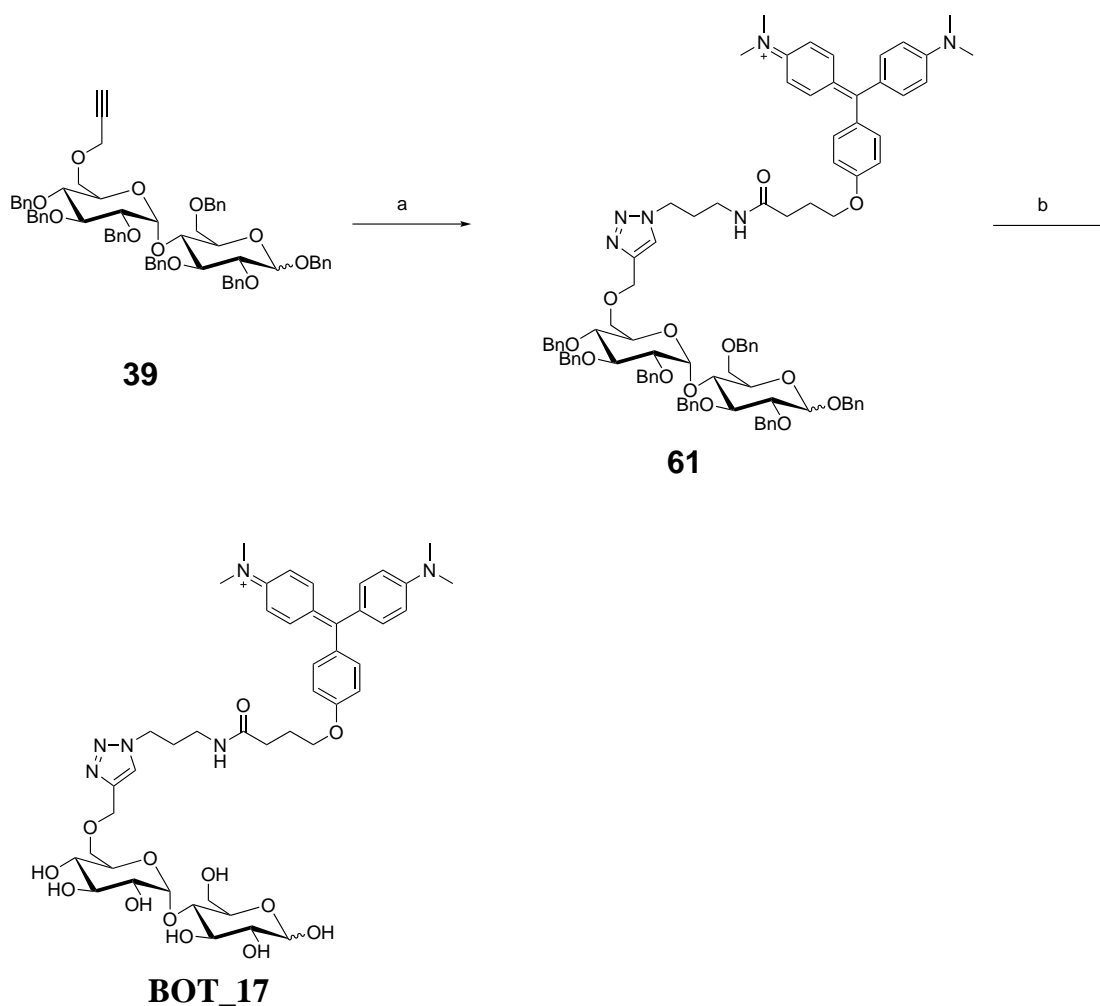
Compound **60** was synthesized by oxidation of **55** in good yields, to be used as a positive control in the FAP-MG assay.



Scheme 4.3: **a.** *p*-chloranil, CH₂Cl₂, rt, 43%.

Synthesis of maltodextrin MG conjugates

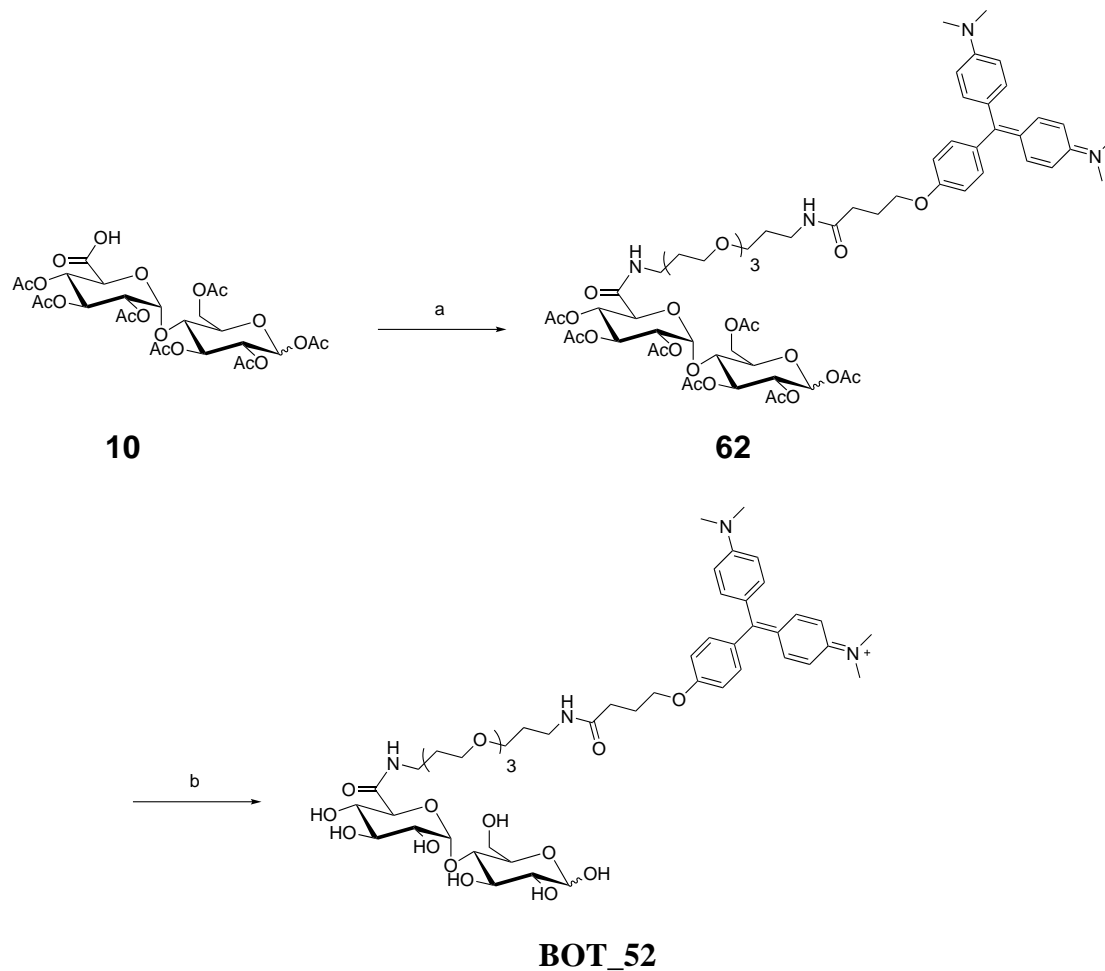
A CuAAC between azide **57** and alkyne **39** using CuSO_4 and sodium ascorbate gave the benzylated conjugate **61**. The benzyl protection groups were cleaved by BCl_3 to yield BOT_17 (Scheme 4.4).



Scheme 4.4: **a.** **57**, CuSO_4 , NaAsc, TBTA, DMF/ H_2O (1:4), rt, 95% **b.** BCl_3 , PMB, DCM, -78°C , 28%.

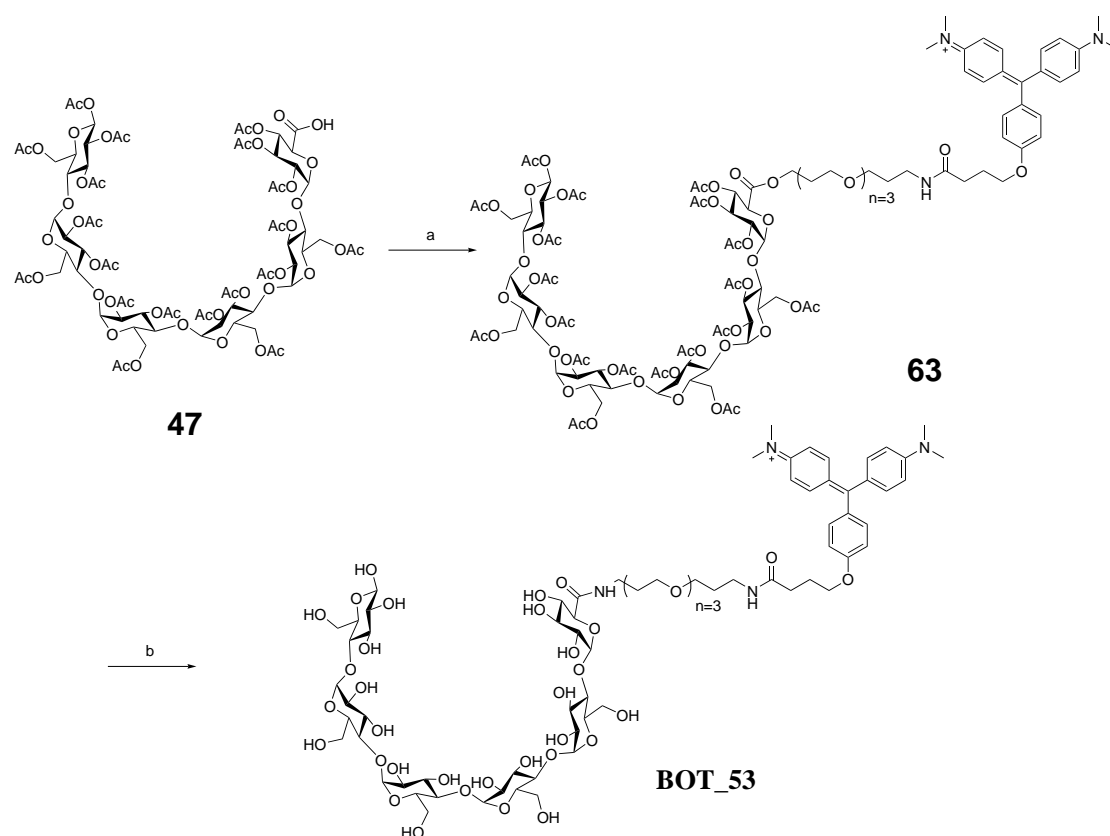
The carboxylic acid **10** was treated with the amine **59** under standard conditions using T3P to give the acetylated conjugate **62** in 40% yields. Finally, Zemplén deacetyla-

tion was performed on **62** to deprotect the acetyl groups to yield BOT_52 in 9% yield (Scheme 4.5).



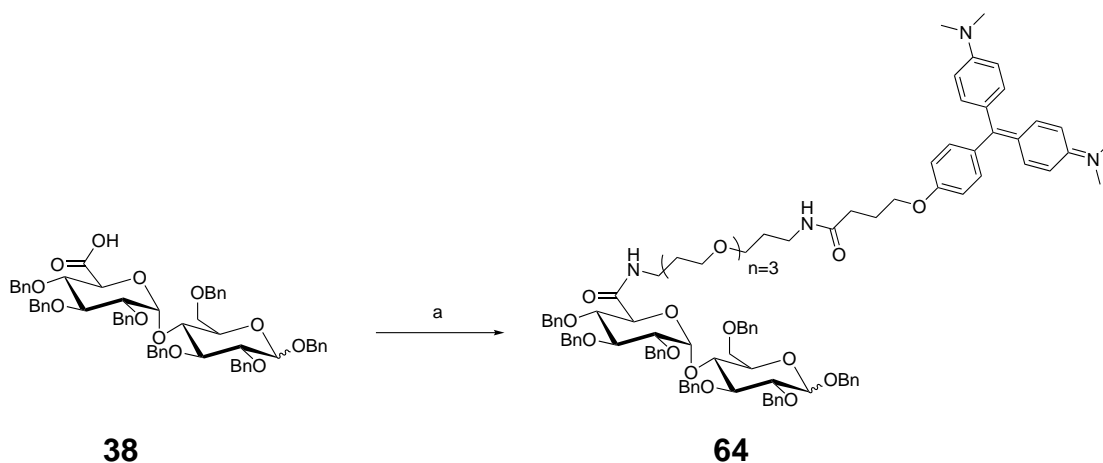
Scheme 4.5: **a.** **57**, T3P, Et₃N, CH₂Cl₂, 40%, **b.** NaOMe, MeOH, 9%.

Similarly, the maltohexose analogue BOT_53 was synthesized by performing an amide coupling between acetylated carboxylic acid **47** and amine **59**, followed by Zemplén deacetylation (Scheme 4.6).



Scheme 4.6: **a.** **59**, T3P, Et₃N, CH₂Cl₂, 70%, **b.** NaOMe, MeOH, 15%.

The benzylated conjugate **64** was synthesized to verify that the probes are taken up by the maltodextrin transport system. **64** was synthesized by performing a T3P mediated amide coupling between **38** and amine **59** (Scheme 4.5).



Scheme 4.7: a. **57**, T3P, Et₃N, CH₂Cl₂, 40%.

4.2 FAP-MG assay

The uptake of the conjugates was studied *in vitro* in a *E. coli* FAP-knock-In strain (*E. coli*_FAP6.2). The FAP expression was induced by addition of IPTG. As a negative control, bacteria were grown in the absence of IPTG. The assay was performed in a 96 well plate and the fluorescence measured over 16 h with the excitation wavelength at 625 nm and emission wavelength at 665 nm. Compound **60** is a known substrate for the FAP-MG assay,¹²⁰ therefore it is used as a positive control in the assay. Compound **59** was tested to determine whether the PEG bearing MG acts as a substrate. To determine whether the conjugates are transported inside the cell, BOT_17, BOT_52 and BOT_53 were tested in the assay. The benzylated version of BOT_52 compound **64** was tested to determine whether the uptake is mediated by the maltodextrin transport system. The compounds were tested at two concentrations, 1 μ M and 10 μ M.

The results of the fluorescence measurements have been summarized in Figure 4.2.

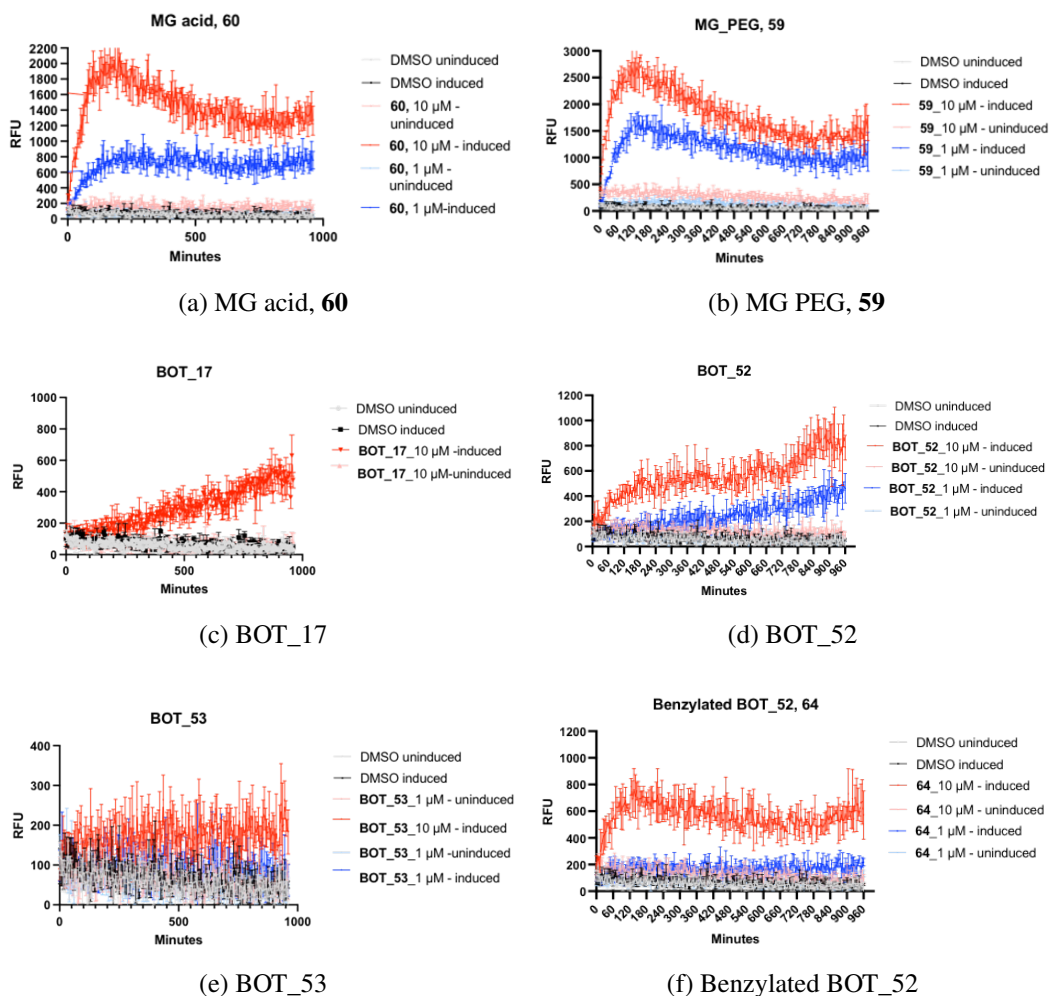


Figure 4.2: Kinetic studies on fluorescence emission of MG conjugates with *E. coli_FAP6.2*. The compounds were tested at two concentrations, 1 μM and 10 μM . Excitation wavelength=625 nm, Emission=665 nm.

The notable observations are as following:

- The control compound **60** induces fluorescence emission at 665 nm, in accordance with the literature. The fluorescence intensity induced by **59** is higher than that of **60**, implying that it is taken up more efficiently.
- The fluorescence induction at 10 μM works better than 1 μM . Also, the fluores-

cence was dependent on IPTG induction.

- Of the three test compounds, BOT_52 shows the highest fluorescent intensity. At 10 μM concentration BOT_17 shows a small increase in fluorescence over time. However the intensities of fluorescence are lower when compared to the control compounds.
- The benzylated BOT_52 **64** also induces fluorescence similar to that of **60** but with lower intensity.

The normalised uptake of the probes has been shown in Figure 4.3.

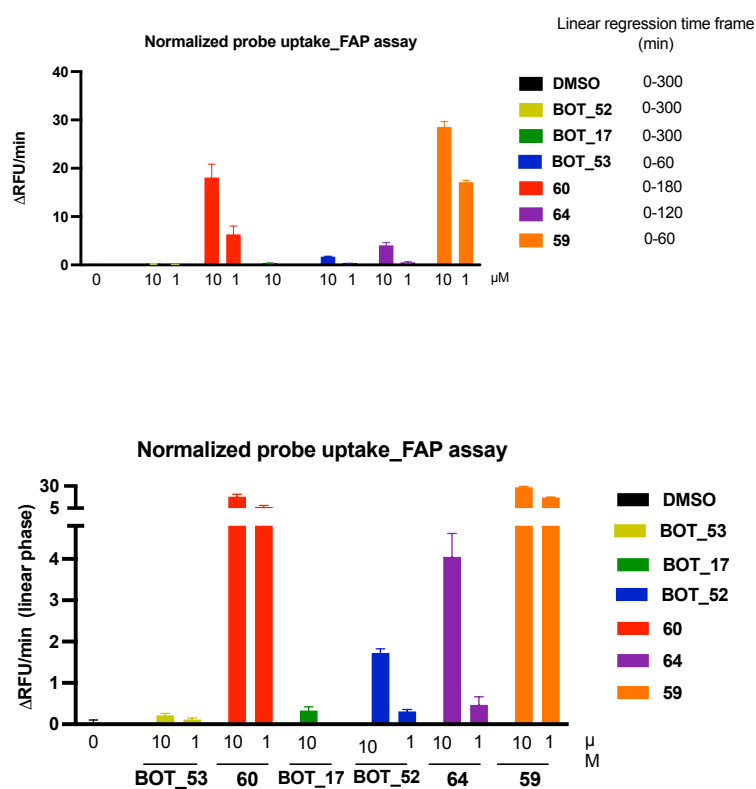


Figure 4.3: Normalized probe uptake observed via FAP-MG assay

All samples tested in the kinetic study were analyzed individually by non-linear regres-

sion during the linear phase of the curve using Graph Pad Prism 5.0. The time frame for linear regression was adjusted according to the uptake kinetics (0-60 min for probes **60** and **58** which were taken up fast, 0-120 min for compound **64**, 0-180 min for BOT_52 and 0-300 min for DMSO control, BOT_53 and BOT_17).

From Figure 4.3 it can be concluded that BOT_52 shows most efficient uptake. BOT_17 is taken up slowly over time. The uptake of benzylated control compound **64** suggests that the uptake is not driven by the maltodextrin transport system. However, it should be noted that there is a late increase in the RFU value for BOT_52 (480 – 960 min), which is not observed for the control compound **64**. This hints the possibility of a maltodextrin pathway specific uptake during this time window in the growth curve. The uptake of the BOT_52 provides further evidence that the amide linked conjugates are preferentially transported compared to the ether linked conjugates, as observed earlier in the growth recovery assays.

5 | Antibiotic conjugates

This chapter deals with the final aim of the thesis, which involves the synthesis of maltodextrin-antibiotic conjugates to achieve intracellular delivery of antibiotics. The choice of antibiotics, the design and synthesis of antibiotic conjugates will be discussed in detail in the following sections. Initial results of MIC assay performed in *E. coli* and *K. oxytoca* are discussed towards the end of the chapter.

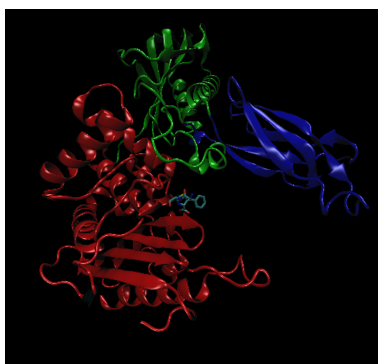
5.1 Ampicillin conjugates

Ampicillin, a β -lactam antibiotic was chosen to synthesize the antibiotic conjugates. Ampicillin is an ideal candidate for drug conjugation due to the following reasons:

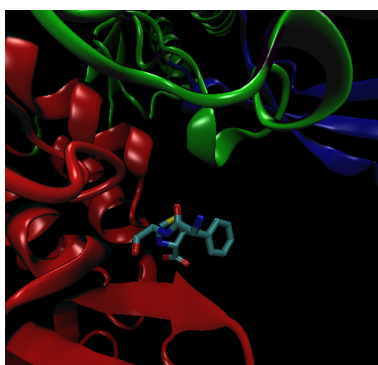
- It is a clinically validated low molecular weight antibiotic, which is used to treat a number of bacterial infections.¹²¹
- The target for ampicillin, penicillin binding protein (PBP) is located in the periplasmic space. The advantage of an ampicillin conjugate is that it only needs to cross through the outer bacterial membrane to access the target, as opposed to accessing cytoplasmic targets.¹²²
- Cleavable linkers are not required in synthetic β -lactam antibiotic conjugates for their active transport and enhanced MIC potencies.¹²³
- A number of β -lactam conjugates have been successfully synthesized, therefore, the chemistry is well understood.^{39,124}

5.2 Design of antibiotic conjugates

The active site of PBP is located in the cleft formed between domain I (shown in red) and domain III (shown in blue) (Figure 5.1). On binding to PBP, the secondary amine in the ampicillin is pointing away from the active site. Therefore, there is scope for modification at this position, without impairing the anti-bacterial activity. In this study, following the report from Zheng and Nolan, an alkyne handle was introduced at the secondary amine to be used in click reaction.⁷⁷



(a) Amp PBP



(b) Amp PBP

Figure 5.1: Co-crystal structure of penicillin binding protein 4 (dacB) from *E. coli*, complexed with ampicillin. a. Global view b. zoom of global view with ampicillin.¹²⁵

Translating the information gained from the previous assays, ampicillin was attached to intermediates that were shown to be internalised by bacteria (Figure 5.2). BOT_55 con-

taining maltohexose conjugated to ampicillin at the reducing end was designed as the maltohexose intermediate BOT_46 was internalised in the growth recovery assay. Maltotriose has the best serum stability amongst the maltodextrins.¹⁰⁷ Therefore, BOT_55, the maltotriose analogue of BOT_54 was envisioned. Maltose-ampicillin conjugate BOT_56 was synthesized because the fluorescent probes containing shorter alkyl linker were internalised better.

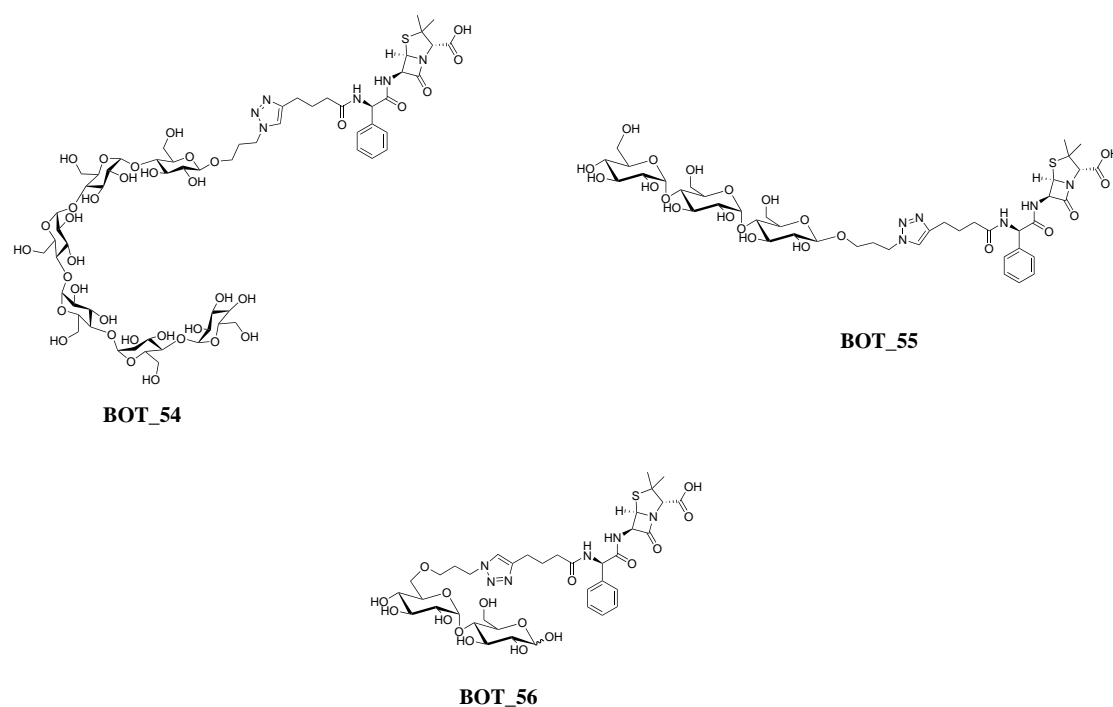


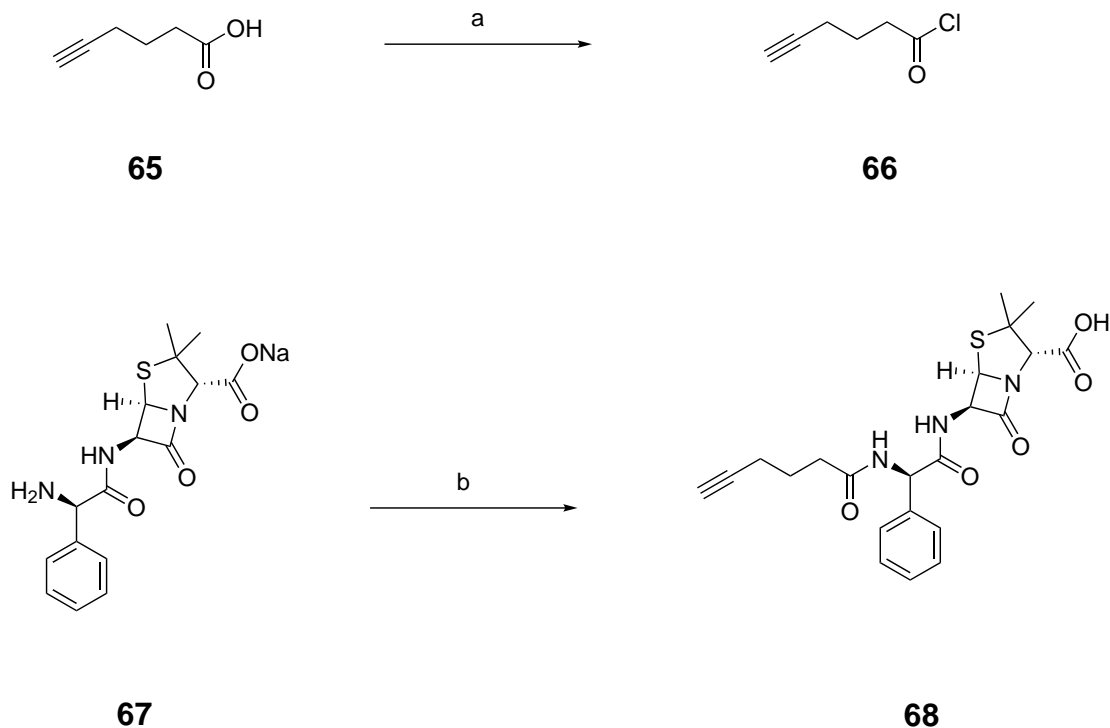
Figure 5.2: Structures of maltodextrin ampicillin conjugates

5.3 Synthesis of antibiotic conjugates

Synthesis of ampicillin alkyne

As explained earlier, an alkyne handle was introduced at the secondary amine position of ampicillin to perform click chemistry. 5-Hexynoic acid was converted into the acyl

chloride **66**. Ampicillin sodium salt was coupled to **66** to give the desired alkyne **68** (Scheme 5.1).

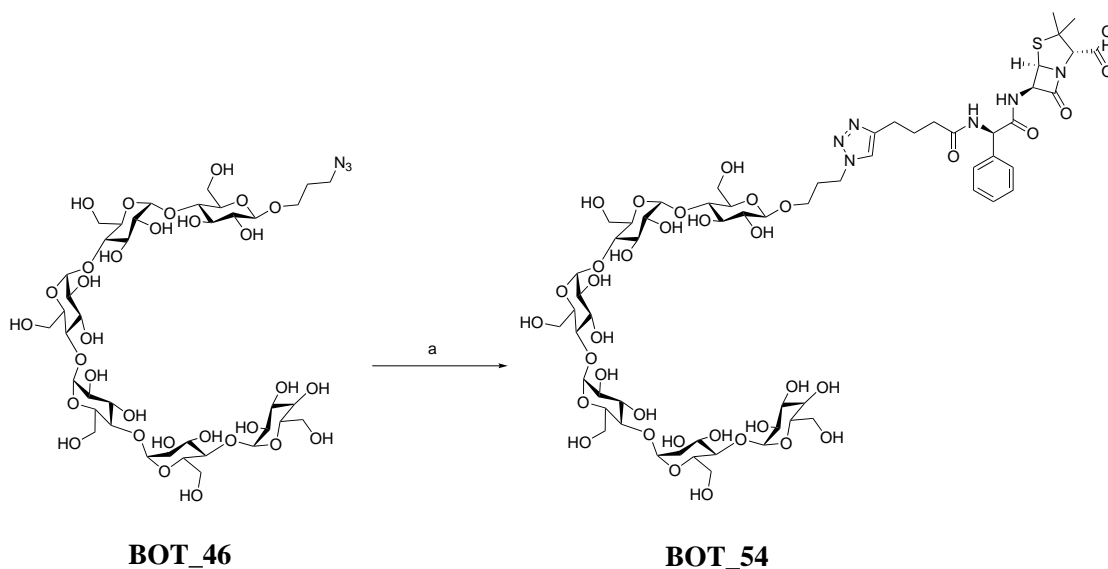


Scheme 5.1: **a.** Oxalyl chloride, THF, quant. **b.** 5-hexynoic acid, 78%.

Synthesis of ampicillin conjugates

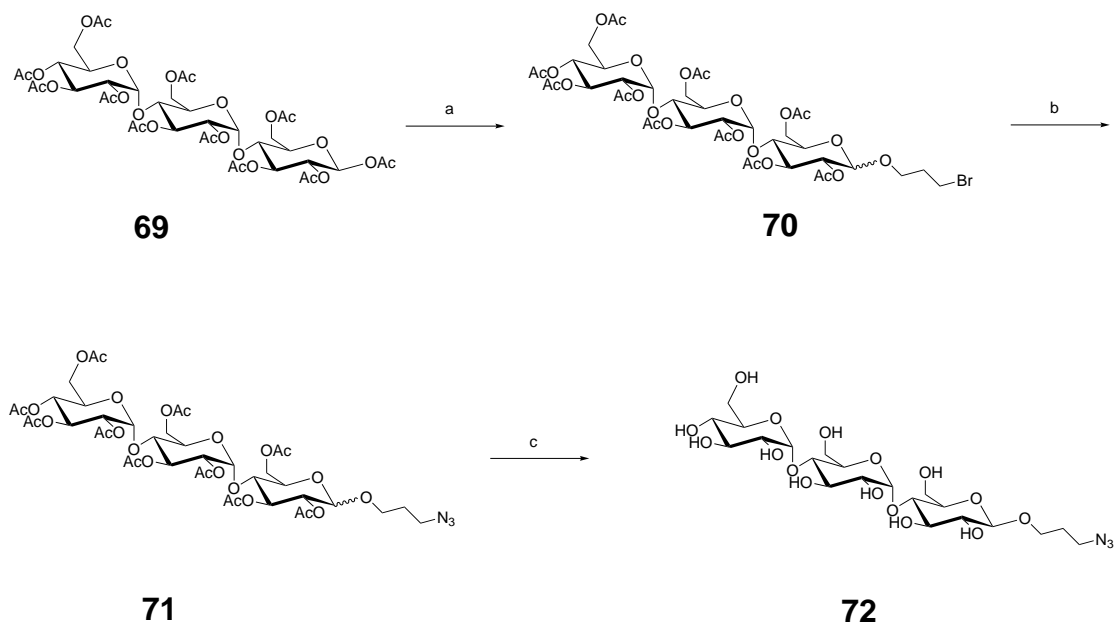
The β -lactam ring in ampicillin is a labile system. The standard click chemistry protocols resulted in high reaction time and the degradation of the β -lactam ring. Therefore, stoichiometric amounts of CuSO_4 and sodium ascorbate were employed to decrease the reaction time.

Ampicillin conjugate BOT_54 was synthesized by reacting azide intermediate BOT_46 and the ampicillin alkyne **68** in a CuAAC (Scheme 5.2).



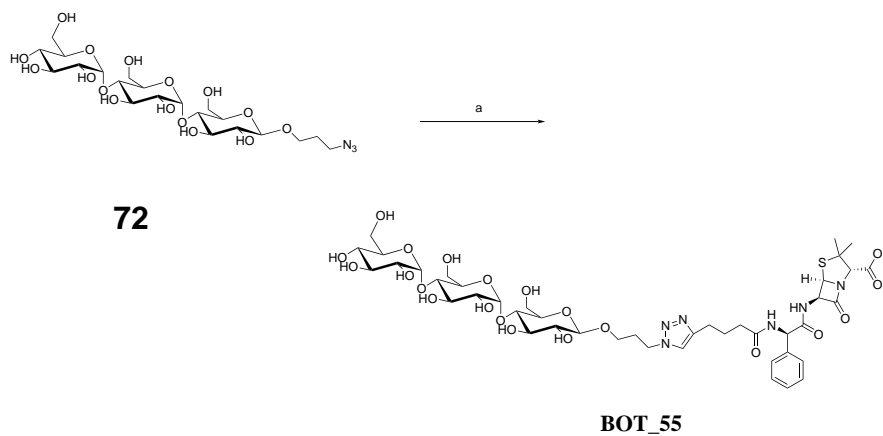
Scheme 5.2: **a.** **68**, CuSO₄, NaAsc, TBTA, DMSO/H₂O (4:1), rt, 50%

For the synthesis of BOT_55, **72** was synthesised in three steps starting from the peracetylated maltotriose as shown in Scheme 5.3. A Lewis acid promoted glycosylation of peracetylate maltotriose at the anomeric carbon was performed with 3-bromopropanol to yield the bromopropyl compound **70**.¹⁰⁴ The bromide was converted into an azide by a nucleophilic substitution. Zemplén deacetylation was carried out to give the desired intermediate **72**.



Scheme 5.3: **a.** 3-bromopropanol, $\text{BF}_3 \cdot \text{Et}_2\text{O}$, 0°C , CH_2Cl_2 , 24%, **b.** NaN_3 , DMF, 60°C , 78% **c.** NaOMe, MeOH, rt, 95%.

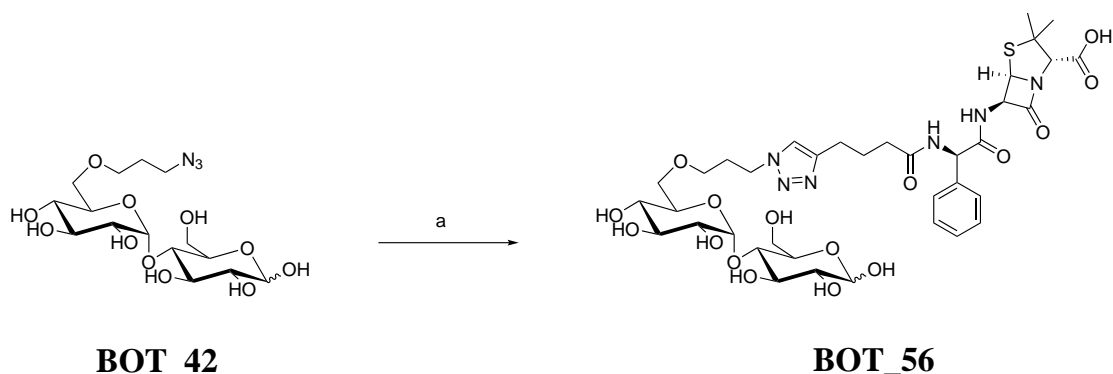
BOT_55 could be obtained from a CuAAC between azide intermediate **72** and ampicillin alkyne **68** (Scheme 5.4).



Scheme 5.4: **a.** **68**, CuSO_4 , NaAsc, TBTA, DMSO/ H_2O (4:1), rt, 28%.

Similarly, BOT_56 could be obtained from a CuAAC between azide intermediate

BOT_42 and ampicillin alkyne **68** (Scheme 5.5).



Scheme 5.5: **a.** **68**, CuSO₄, NaAsc, TBTA, DMSO/H₂O (4:1), rt, 12.2%.

5.4 The minimum inhibitory concentration (MIC) assay

MIC assays determine the quantitative measure of antimicrobial activity of a given compound. Since the maltodextrin probes were shown to be able to penetrate into *E. coli* and *K. oxytoca*, the compounds BOT_54, BOT_55, and BOT_56 were tested on the following bacterial strains: *E. coli* WT, *E. coli* Δ lamB, and *K. oxytoca*.

However, no antibacterial activity was observed for any of the compounds in the initial assay.

One reason for lack of antibacterial activity could be because the assay was performed in a sugar rich LB medium, which acts as a repressor of the maltodextrin transport pathway.

6 | Summary and outlook

The goal of the thesis was to investigate the possibility of synthesizing maltodextrin based conjugates modified at the non-reducing end with free reducing end.

A first aim of the thesis was to systematically investigate the preferred site of modification for an efficient uptake of conjugates. Six maltodextrins conjugates with a linker attached to the reducing or non-reducing end of the maltodextrin were synthesized. Growth recovery assays enabled the comparison of the uptake of the modified maltodextrins compared to the natural substrates of the maltodextrin transport system. BOT_41, a maltose conjugated to a small alkyl linker through an amide linkage at the non-reducing end was internalised by the *E. coli* and *K. oxytoca*. The major limitation of the growth recovery assay is that an absence of growth recovery does prove lack of uptake.

Secondly, a detailed investigation on the critical structural requirements for an efficient transport of the conjugates was performed. 12 novel fluorescent conjugates with modification at the non-reducing end of maltodextrins were successfully synthesized. A number of parameters including the type of linker, type of dye, position of modification and the choice of maltodextrin were modified in order to optimize and understand their effect on the uptake via the maltodextrin transport system.

Characterisation of uptake of these probes was performed by fluorescence microscopy and flow cytometry studies. Confocal microscopy showed that perylene conjugate BOT_47, Coumarin conjugate BOT_18 and NBD conjugate BOT_45 could label *E. coli* WT preferentially over Δ lamB *E. coli*. The NBD conjugate however appears to stick to the surface of the cells. The fluorescence intensity of the coumarin conjugate was much lower than that of the perylene and NBD conjugates. BODIPY conjugates appear to be toxic to the bacteria. On the linker front, short alkyl linkers proved to be

better suited for probe uptake compared to the PEG linker. Similar labelling was observed for BOT_47 with BOT_10, BOT_14, the literature reported perylene conjugates modified at reducing end. Therefore no clear conclusion on the effect of the attachment site could be made. The synthesis of the maltohexose conjugate BOT_51 was tedious due to poor yields. However, a microwave assisted synthesis of benzylidene acetal in maltohexose has been optimized to obtain enhanced yields. Only a weak labelling of *E. coli* was observed when incubated with BOT_51.

To get a quantitative understanding of the uptake FACS analysis was performed. The results showed significant labelling only for the perylene conjugates. However, 30% to 50% staining was observed for *E. coli* WT and Δ lamB *E. coli* indicating an uptake independent of lamB. However, this result could be due to the non specific binding to the surface of the cells.

To study the intracellular translocation of the probes two malachite green conjugates were synthesized. The uptake of the conjugates was studied in a FAP system. One of the probes BOT_52 showed efficient uptake.

Finally, three novel maltodextrin-ampicillin conjugates were synthesized and tested for antibiotic activity in *E. coli* and *K. oxytoca*. However, the MIC assay needs to be optimized, and the compounds should be re-tested for antibacterial activity.

In the future, the scope of the conjugates can be studied by testing them in medically important bacterial pathogens of the ESKAPE panel.

As maltotriose modified at the non-reducing end has been shown to have better serum stability compared to other maltodextrins,¹⁰⁷ novel maltotriose based conjugates could be synthesized for practical purposes.

Finally, the Trojan horse strategy using maltodextrins could be extended to antibiotics having cytoplasmic targets. Some of the antibiotic to be considered could be:

Linezolid

Linezolid is an oxazolidinone antibiotic that inhibits protein synthesis by preventing tRNA from binding to the ribosome. Linezolid is exclusively active against gram-positive bacterial making it an ideal candidate.

Rifampicin

Rifampin, inhibits the bacterial RNA polymerase by forming a stable drug-enzyme complex. It could be a suitable candidate for the trojan horse strategy as its activity against gram-positive bacteria is about 10^5 times more as compared to *E. coli*.

7 | Experimental

General

The solvents and reagents were purchased from commercial suppliers and used without further purification. All reactions were performed under nitrogen atmosphere unless otherwise mentioned. The reactions were monitored by Thin Layer Chromatography (TLC), LC-MS or by NMR. Purification was carried out by column chromatography, flash chromatography or HPLC.

For microwave assisted reaction, Biotage® Initiator+ was used.

Thin Layer Chromatography

Analytical thin-layer chromatography was performed on TLC Silica gel 60 F254 (Merck, Darmstadt) and visualized by UV and/or vanillin, CAM, DMP, bromocresol green or permanganate staining solution.

Purification

Flash chromatography was performed using Grace Reveleris® X2 flash chromatography system or via column chromatography using silica gel 60M MACHEREY-NAGEL (0.040-0.063 mm).

Preparative reversed phase high performance liquid chromatography was carried out with a Thermo Scientific Dionex (UltiMate 3000 HPLC system) with a Phenomenex 006-4252-P0 Luna C18 (250 mm * 21.2 mm, 5 μ) column with acetonitrile and water as eluent.

Nuclear Magnetic Resonance (NMR)

¹H-NMR spectra are measured on “Bruker WP-200 SY”, “Bruker AM-400” and

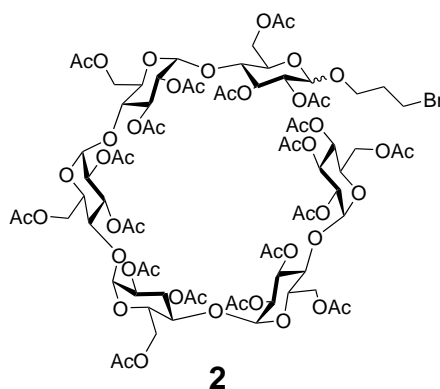
“Bruker AM-500” spectrometers. The chemical shifts are given in ppm on the δ -scale. The coupling constants are measured in hertz (Hz). The multiplets are labeled as: s = singlet, d = doublet, t = triplet, q = quartet, m = multiplet, dd = doublet of doublets, dt = doublet of triplets, br = broad.

High Resolution Mass spectrometry

High resolution mass spectrometry (HRMS) data were recorded using a Waters instrument equipped with a Waters Acquity detector and Waters QToF Premier mass detector with electrospray ionization (ESI).

Experimental procedure

β -D-glucopyranose,2,3,4,6-tetra-O-acetyl- α -D-glucopyranosyl-(1 \rightarrow 4)-O-2,3,6-tri-O-acetyl- α -D-glucopyranosyl-(1 \rightarrow 4)-O-2,3,6-tri-O-acetyl- α -D-glucopyranosyl-(1 \rightarrow 4)-O-2,3,6-tri-O-acetyl- α -D-glucopyranosyl-(1 \rightarrow 4)-O-2,3,6-tri-O-acetyl- α -D-glucopyranosyl-(1 \rightarrow 4)-2,3,6-triacetate 1-(3'-bromopropyl), **2**



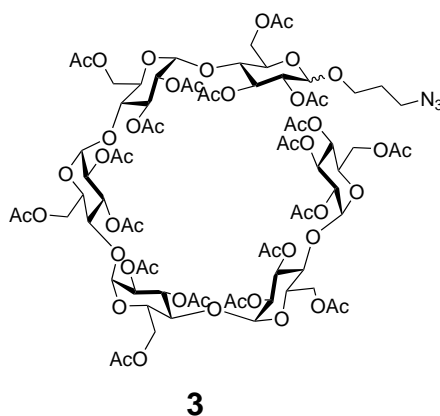
To a solution of maltohexose eicosaacetate **1** (500 mg, 0.27 mmol) in CH_2Cl_2 (10 mL) was added 3-bromopropanol (0.071 ml, 0.81 mmol). The solution was cooled to 0 °C and $\text{BF}_3 \cdot \text{OEt}_2$ (0.16 mL, 1.3 mmol) was added drop-wise. The RM was stirred ON. The reaction was quenched with saturated NaHCO_3 solution and extracted with CH_2Cl_2 . The combined organic extracts were washed with H_2O and brine, dried using Na_2SO_4 , and concentrated under reduced pressure. The crude material was purified by column chromatography on silica gel (PE/EtOAc: 40% to 60%) to afford **2** (128 mg, 24%) as a white solid.

$^1\text{H NMR}$ (400 MHz, CDCl_3) δ 5.43 – 5.21 (m, 11H, anomeric protons), 5.06 (t, J = 9.9 Hz, 1H, 4-H), 4.82 (dd, J = 9.9, 6.0 Hz, 1H, 2-H), 4.75 – 4.68 (m, 3H), 4.56 – 4.43 (m, 6H), 4.27 – 3.85 (m, 20H, skeletal protons), 3.75 – 3.65 (m, 1H, $-\text{OCH}_2$), 3.59 (m, 1H, $-\text{OCH}_2$), 3.34 (t, J = 4.0 Hz, 2H, $-\text{CH}_2\text{N}_3$), 2.29 – 1.90 (m, 59H, CH_3 , $-\text{OCH}_2\text{CH}_2\text{CH}_2\text{N}_3$).

^{13}C NMR (101 MHz, CDCl_3) δ 170.75, 170.70, 170.67, 170.58, 170.48, 170.46, 170.41, 170.40, 170.15, 169.79, 169.71, 169.66, 169.59, 169.57, 169.51, 169.49 ($19 \times \text{C}=\text{O}$), 100.26, 95.72, 95.62, 77.35, 77.04, 76.72, 75.31, 73.72, 73.42, 73.25, 72.28, 72.20, 72.15, 71.64, 70.50, 70.43, 70.05, 69.35, 68.95, 68.44, 67.91, 66.44, 62.84, 61.35 (skeletal carbons), 47.98 $-\text{CH}_2\text{N}_3$, 28.96 $-\text{OCH}_2\text{CH}_2\text{CH}_2\text{N}_3$, 23.83, 20.92, 20.89, 20.87, 20.82, 20.69, 20.61, 20.56, 17.49 ($19 \times \text{CH}_3$).

MS ESI m/z calculated for $\text{C}_{77}\text{H}_{105}\text{BrO}_{50}$ $[\text{M}+\text{Na}]^+$ 1931.4755, found 1931.5129.

β -D-glucopyranose,2,3,4,6-tetra-O-acetyl- α -D-glucopyranosyl-(1 \rightarrow 4)-O-2,3,6-tri-O-acetyl- α -D-glucopyranosyl-(1 \rightarrow 4)-O-2,3,6-tri-O-acetyl- α -D-glucopyranosyl-(1 \rightarrow 4)-O-2,3,6-tri-O-acetyl- α -D-glucopyranosyl-(1 \rightarrow 4)-O-2,3,6-tri-O-acetyl- α -D-glucopyranosyl-(1 \rightarrow 4)-2,3,6-triacetate 1-(3'-azidopropyl), **3**



The bromide **2** (125 mg, 65 μmol) was dissolved in DMF (1 mL) and sodium azide (6.3 mg, 98.2 μmol) was added to it. The solution was stirred ON at 60 $^\circ\text{C}$. The RM was cooled to 0 $^\circ\text{C}$, diluted with water, extracted with EtOAc. The residue was purified by flash column chromatography on silica gel ($\text{CH}_2\text{Cl}_2/\text{MeOH}$: 5%) to give **3** (65.8 mg, 92%) as a white solid.

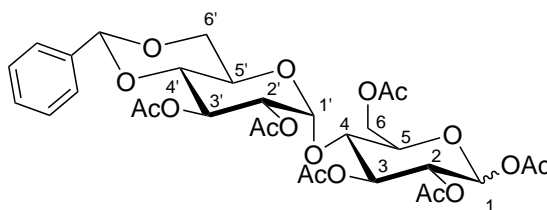
^1H NMR (400 MHz, CDCl_3) δ 5.42 – 5.18 (m, 11H, anomeric protons), 5.04 (t, J = 9.8 Hz, 1H, H-4), 4.80 (dd, J = 10.0, 5.9 Hz, 1H, H-2), 4.70 (m, J = 10.4, 3.4 Hz, 0H),

4.53 – 4.42 (m, 1H), 4.38 – 4.09 (m, 1H), 3.92 (dt, $J = 14.8, 5.6$ Hz, 1H), 3.77 – 3.63 (m, 0H), 3.62 – 3.53 (m, 0H), 3.49 (t, $J = 6.0$ Hz, 0H), 3.39 – 3.28 (m, 0H), 2.31 – 1.94 (m, 5H), 1.89 – 1.74 (m, 2H).

^{13}C NMR (101 MHz, CDCl_3) δ 20.7, 20.7, 20.7, 20.8, 20.9, 21.0, 21.0, 21.1 ($-\text{CH}_3$), 30.1, 32.4, 53.6, 61.5, 62.3, 62.4, 62.5, 62.6, 62.6, 63.0, 67.4, 68.0, 68.6, 69.1, 69.5, 70.2, 70.5, 70.6, 71.8, 71.9, 72.3, 72.3, 72.4, 73.3, 73.4, 73.9, 75.4, 95.7, 95.9, 100.6, 128.0, 128.3, 128.6, 128.6, 136.8, 136.8, 169.6, 169.6, 169.6, 169.7, 169.7, 169.9, 170.2, 170.5, 170.5, 170.6, 170.7, 170.8, 170.8, 170.8 ppm.

MS ESI m/z calculated for $\text{C}_{77}\text{H}_{105}\text{N}_3\text{O}_{50}$ $[\text{M}+\text{Na}]^+$ 1894.5664, found 1894.5942.

1,2,3,6,2',3'-hexa-O-acetyl-4',6'-O-benzylidene-4-O-(α -D-glucopyranosyl)- β -D-glucopyranose, **6**



6

Maltose (10.0 g, 29.2 mmol), benzaldehyde dimethylacetal (10.0 g, 65.7 mmol) and PTSA (500 mg, 2.63 mmol, 9.0 mol%) were dissolved in dry DMF (76 mL). The mixture was rotated for 6 hours on a rotary evaporator under reduced pressure (39 mbar) at 50 °C. The solution was neutralised with Et_3N (0.50 mL). Subsequently, the solvent was removed under reduced pressure to yield **5** as a viscous liquid. The crude product was used further without any purification. Pyridine (185 mL) was added to a solution of the **5** in Ac_2O (125 mL). The RM was allowed to stir overnight. The solvent was removed and the residue dissolved in EtOAc (100 mL). The solution was washed with

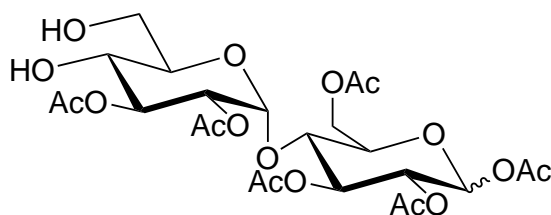
1 M Na₂CO₃ solution, 0.1 M HCl and brine. The organic phase was dried over Na₂SO₄ and the solvent evaporated to give the crude product. The crude product was then purified by column chromatography (PE/EtOAc: 60%) to give **6** (16.2 g, 81%) as a white solid.

¹ H NMR (400 MHz, CDCl₃) δ 7.42 (dd, J = 6.8, 2.9 Hz, 2H, Ar-CH), 7.39 – 7.31 (m, 2H, 3H, Ar-CH), 6.22 (d, J = 3.7 Hz, 0.05H, H-1 α), 5.74 (d, J = 8.2 Hz, 0.95 H, H-1 β), 5.51 – 5.40 (m, 2H, Bn-H, H-3'), 5.35 (d, J = 4.1 Hz, 1H, H-1'), 5.30 (t, J = 9.0 Hz, 1H, H-3), 4.97 (dd, J = 9.2, 8.3 Hz, 1H, H-2), 4.88 (dd, J = 10.2, 4.2 Hz, 1H, H-2'), 4.49 (dd, J = 12.3, 2.4 Hz, 1H, H-6a), 4.33 – 4.20 (m, 2H, H-6b, H-6a'), 4.04 (t, J = 9.2 Hz, 1H, H-4), 3.84 (ddd, J = 9.8, 7.0, 4.3 Hz, 2H, 5-H, H-5'), 3.72 (t, J = 10.2 Hz, 1H, H-6b'), 3.62 (t, J = 9.6 Hz, 1H, H-4'), 2.15 – 1.91 (m, 18H, –CH₃).

¹³C NMR (101 MHz, CDCl₃) δ 170.84, 170.25, 170.06, 169.72, 169.67, 168.80 (C=O), 136.67, 129.14, 128.23, 126.21 (Ar-CH), 101.65 (C-1 α), 96.62 (C-1 β), 91.25 (C-1'), 78.76, 77.35, 77.03, 76.71, 75.34, 73.04, 72.52, 71.01, 70.84, 68.43, 68.41, 63.78, 62.36, 20.90, 20.83, 20.77, 20.64, 20.58 (–CH₃).

HRMS (ESI) m/z calculated for C₃₁H₃₈O₁₇ [M+Na]⁺ 705.2007, found 705.2007.

1,2,3,6,2',3'-hexa-O-acetyl-4-O-(α-D-glucopyranosyl)-β-D-glucopyranose, **7**



7

To a solution of **6** (16.17 g, 23.7 mmol) in acetic acid (150 mL), water (100 mL) was

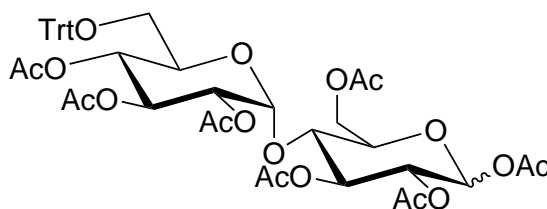
added in small portions. The RM was heated at 95 °C for 10 min. The RM was allowed to cool to room temperature (RT) and the solvent was removed under reduced pressure. Traces of water and acetic acid were removed by co-distillation with toluene. The product was purified by column chromatography (CH₂Cl₂/MeOH: 5%) to yield compound **7** (9.48 g, 67%) as colourless solid.

¹ H NMR (400 MHz, CDCl₃) δ 6.24 (d, J = 3.7 Hz, 0.3H, H-1 α), 5.74 (d, J = 8.2 Hz, 0.7H, H-1 β), 5.50 (dd, J = 10.1, 8.6 Hz, 1H, H-3), 5.36 (dd, J = 11.2, 4.0 Hz, 1H, H-1'), 5.32 – 5.14 (m, 1H, H-3'), 5.08 – 4.92 (m, 1H, H-2), 4.77 (dt, J = 10.5, 4.3 Hz, 1H, H-2'), 4.53 – 4.39 (m, 1H, H-6a), 4.29 – 4.16 (m, 1H, H-6b), 4.09 – 3.99 (m, 2H, H-5, H-4), 3.89 – 3.76 (m, 2H, H-6'a, H-6'b), 3.66 (t, J = 7.6 Hz, 2H, H-4', H-5'), 2.16 – 1.98 (m, 18H).

¹³C NMR (101 MHz, CDCl₃) δ 171.44, 171.37, 171.15, 171.13, 170.83, 170.79, 170.12, 169.99, 169.91, 169.67, 169.02, 168.87 (C=O), 95.93 (C-1' α), 95.82 (C-1' β), 91.28 (C-1 β), 88.88 (C-1 α), 77.35, 77.03, 76.71, 75.37, 73.16, 72.69, 72.38, 72.11, 71.99, 71.85, 70.94, 70.29, 70.20, 70.14, 69.89, 69.84, 69.70, 62.70, 62.62, 62.22, 60.42, 21.07, 21.04, 20.94, 20.91, 20.88, 20.83, 20.70, 20.66, 20.56, 20.46 (–CH₃).

HRMS (ESI) m/z calculated for C₂₄H₃₄O₁₇ [M+Na]⁺ 617.1694, found 617.1694.

1,2,3,6,2',3'-hexa-O-acetyl-6'-O-trityl-4-O-(α-D-glucopyranosyl)-β-D-glucopyranose, **8**



8

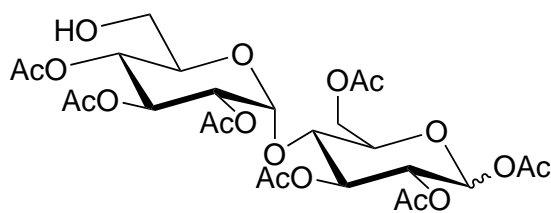
To a solution of compound **7** (9.48 g, 16.0 mmol) in dry pyridine (60 mL) was added trityl chloride (4.45 g, 16.0 mmol). The RM was stirred for 1.5 h at 80 °C after which the RM was cooled to 0 °C. Ac₂O (110 mL) was added and the RM was allowed to stir ON at RT, The RM was poured into ice cold water (500 mL) and stirred for 5 min. The precipitate was filtered to give the crude product as a yellow solid. The crude product was purified by column chromatography (PE/EtOAc: 30% to 50%) to give **8** (12.3, 86%) as white solid.

¹ H NMR (400 MHz, CDCl₃) δ 7.41 (dt, J = 8.2, 1.3 Hz, 5H, Ar-CH), 7.34 – 7.18 (m, 10H, Ar-CH), 6.23 (d, J = 3.7 Hz, 0.5H, H-1 α), 5.73 (d, J = 8.2 Hz, 0.5H, H-1 β), 5.58 – 5.42 (m, 1H, H-3'), 5.37 – 5.23 (m, 2H, H-3, H-1'), 5.08 – 4.86 (m, 2H, H-2, H-4'), 4.40 (m, 1H, H-6a), 4.22 – 4.14 (m, 1H, H-4), 4.13 – 4.04 (m, 2H, H-6b, H-6a'), 3.89 – 3.75 (m, 2H, H-5, H-5'), 3.25 (ddd, J = 10.6, 4.0, 1.9 Hz, 1H, H-6'b), 2.97 (dd, J = 10.6, 3.4 Hz, 1H, H-4'), 2.28 – 1.68 (m, 21H, –CH₃).

¹³C NMR (101 MHz, CDCl₃) δ 170.66, 170.31, 170.29, 170.19, 170.16, 170.11, 170.07, 169.95, 169.72, 168.98, 168.93, 168.88, 168.83 (C=O), 143.36, 129.69, 128.73, 127.94, 127.87, 127.73, 127.27, 127.10, 127.09 (Ar-CH), 95.99 (C-1' α), 95.86 (C-1' β), 91.33 (C-1 β), 88.95 (C-1 α), 86.51, 77.35, 77.03, 76.71, 75.22, 73.15, 72.22, 72.17, 72.10, 70.95, 70.46, 70.36, 70.28, 69.96, 69.92, 69.71, 68.09, 68.06, 62.37, 62.29, 60.78, 60.74 (skeletal protons), 21.03, 20.97, 20.83, 20.70, 20.67, 20.58, 20.57, 20.51, 20.48, 20.44 (CH₃).

HRMS (ESI) m/z calculated for C₄₅H₅₀O₁₈ [M+Na]⁺ 901.2895, found 901.2892.

1,2,3,6,2',3',4'-hepta-O-acetyl-4-O-(α -D-glucopyranosyl)- β -D-glucopyranose, **9**



9

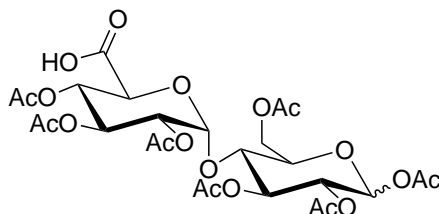
Tritylated compound **8** (12.3 g, 19.4 mmol) was dissolved in acetic acid (80%, 480 mL) heated at 100 °C for 1 h. The solvent was removed under reduced pressure. The residue was dissolved in a minimum amount of methanol and water was added until incipient turbidity was observed. The suspension was cooled to 0 °C and the precipitated trityl alcohol filtered. The filtrate was concentrated and traces of water were removed by co-distillation with toluene. The crude product was purified by column chromatography (PE/EtOAc: 50% to 70%) to yield **9** (6.7 g, 76%) was obtained as colourless solid .

¹H NMR (400 MHz, CDCl₃) δ 6.24 (d, J = 3.7 Hz, 0.3H, H-1 α), 5.74 (d J = 8.2 Hz, 0.7H, H-1 β), 5.52 – 5.16 (m, 3H, H-3, H-1', H-3'), 5.13 – 4.91 (m, 1H, H-2'), 4.91 – 4.72 (m, 1H, H-4'), 4.48 (dd, J = 17.2, 8.2 Hz, 1H, H-6a), 4.21 (m, 2H, H-6b, H-4), 4.05 – 3.89 (m, 1H, H-5), 3.89 – 3.45 (m, 3H, H-5', H-6a, H-6b), 2.18 – 1.90 (m, 21H, –CH₃).

¹³C NMR (101 MHz, CDCl₃) δ 171.42, 171.13, 170.77, 170.10, 169.65, 168.85 (C=O), 95.92 (C-1 α), 95.81 (C-1 β), 91.27 (C-1'), 88.87, 75.36, 73.15, 72.68, 72.37, 72.10, 71.98, 71.84, 70.93, 70.28, 70.19, 70.13, 69.88, 69.69, 62.69, 62.21, 60.42 (skeletal protons), 21.03, 20.90, 20.88, 20.83, 20.70, 20.66, 20.56, 20.45 (CH₃).

HRMS (ESI) m/z calculated for C₂₆H₃₆O₁₈ [M+Na]⁺ 659.1787, found 659.1792.

1,2,3,6,2',3',4'-hepta-O-acetyl-4-O-(α -D-glucopyranuronosyl)- β -D-glucopyranose, **10**

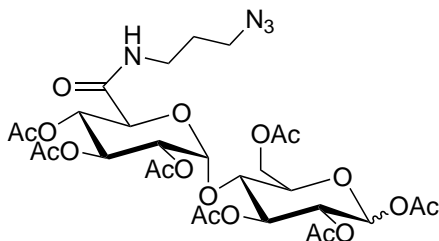


10

TEMPO (3.29 g, 21.0 mmol) and BAIB (6.78 g, 21.0 mmol) were added to a solution of alcohol **9** (6.7 g, 10.5 mmol) in $\text{CH}_2\text{Cl}_2/\text{H}_2\text{O}$ (1:1, 60 mL). The RM was ON at RT and quenched with saturated $\text{Na}_2\text{S}_2\text{O}_3$ (10 mL). The resulting solution was extracted with EtOAc. The combined organic extracts were washed with H_2O and brine, dried using Na_2SO_4 , and concentrated under reduced pressure. The crude product was purified by column chromatography ($\text{CH}_2\text{Cl}_2/\text{MeOH}$: 5% to 10%) to yield **10** (4.4 g, 64.7%) as a white solid.

HRMS (ESI) m/z calculated for $\text{C}_{26}\text{H}_{34}\text{O}_{19}$ $[\text{M}+\text{Na}]^+$ 673.1592, found 673.1592.

1,2,3,6,2',3',4'-hepta-O-acetyl-6'-O-((3-azidopropyl)carbamoyl)4-O-(α -D-glucopyranuronosyl)- β -D-glucopyranose, **12**



12

The carboxylic acid **10** (500mg, 0.769 mmol) and 3-azidopropan-1-amine (0.087 mL,

0.845 mmol) were dissolved in CH₂Cl₂ (0.461 mL). T3P (0.337 mL, 1.153 mmol) was added followed by Et₃N (1.07 mL, 7.69 mmol). The RM was allowed to stir ON. The RM was washed with saturated NaHCO₃ and extracted with CH₂Cl₂. The combined organic extracts were washed with H₂O and brine, dried using Na₂SO₄, and concentrated under reduced pressure. The crude product was purified by column chromatography (CH₂Cl₂/MeOH: 5%) to yield **12** (207 mg, 37%) as a white solid.

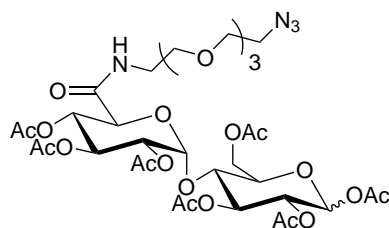
¹ H NMR (400 MHz, CDCl₃) δ 6.24 (d, J = 3.7 Hz, 0.6 H, H-1 α), 5.74 (d, J = 8.2 Hz, 0.3H, H-1 β), 5.58 – 5.23 (m, 3H, H-3, H-1', H-3'), 5.21 – 5.07 (m, 1H, H-4), 5.03 – 4.92 (m, 1H, H-2), 4.86 (ddd, J = 10.4, 6.1, 4.1 Hz, 1H, H-2'), 4.42 (dd, J = 12.2, 2.5 Hz, 1H, H-5'), 4.22 (dd, J = 12.2, 4.4 Hz, 1H, H-6a), 4.12 – 3.95 (m, 2H, H-4, H-4'), 3.90 – 3.79 (m, 1H, H-5), 3.56 (dd, J = 5.7, 3.7 Hz, 1H, H-6'a), 3.53 – 3.35 (m, 6H, –CH₂N₃, –NHCH₂–, H-6b, H-6'b), 2.04 (m, 21H, CH₃), 1.83 (m, 2H, CH₂CH₂CH₂N₃).

¹³C NMR (101 MHz, CDCl₃) δ 170.62, 170.59, 170.55, 170.47, 170.00, 169.88, 169.82, 169.70, 169.64, 169.60, 169.59, 168.86, 168.75, 166.69, 166.63 (C=O), 162.57 (C=N), 95.51 (C-1' α), 95.43 (C-1' β), 91.25 (C-1 β), 88.81 (C-1 α), 77.37, 77.05, 76.74, 74.82, 72.85, 72.33, 71.89, 70.90, 70.24, 70.12, 69.64, 69.46, 68.32, 68.26, 62.17, 62.04, 48.97 (–NHCH₂), 36.68 (–CH₂N₃), 28.44 (–CH₂CH₂CH₂N₃), 20.98, 20.92, 20.86, 20.77, 20.65, 20.63, 20.58, 20.53, 20.51, 20.40 (CH₃).

HRMS (ESI) m/z calculated for C₂₉H₄₀N₄O₁₈ [M+Na]⁺ 755.2236, found 755.2237.

1,2,3,6,2',3',4'-hepta-O-acetyl-6'-((2-(2-azidoethoxy)ethyl)carbamoyl)-4-O-(α-D-glucopyranuronosyl)-β-D-glucopyranose, **13**

To a solution of the carboxylic acid **10** (500mg, 0.769 mmol) in CH₂Cl₂ (0.5 mL) was added 1-azido-PEG₃-amine (0.168 mL, 0.845 mmol). T3P (0.337 mL, 1.153 mmol) was added to it, followed by triethylamine (1.07 mL, 7.69 mmol). The RM was allowed to stir ON. The RM was washed with saturated Na₂CO₃ and extracted with CH₂Cl₂.



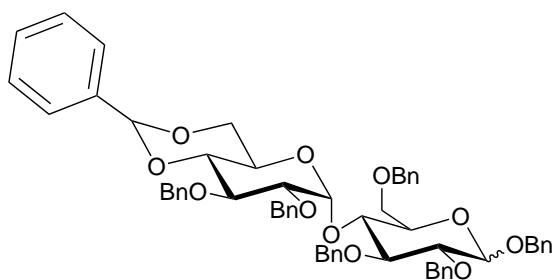
13

The combined organic extracts were washed with H₂O and brine, dried using Na₂SO₄, and concentrated under reduced pressure. The crude product was purified by column chromatography (CH₂Cl₂/MeOH: 5%) to yield **13** (405 mg, 62%) as a white solid.

¹H NMR (400 MHz, CDCl₃) δ 6.79 (t, J = 5.5 Hz, 1H, N-H), 6.23 (d, J = 3.8 Hz, 0.2H, H-1 α), 5.73 (d, J = 8.2 Hz, 0.8H, H-1 β), 5.52 (dd, J = 7.2, 3.9 Hz, 1H, H-3), 5.40 (t, J = 10.2 Hz, 1H, H-1'), 5.30 (t, J = 9.1 Hz, 1H, H-3'), 5.06 (t, J = 9.9 Hz, 1H, H-2), 5.01 – 4.92 (m, 1H, H-2'), 4.82 (dd, J = 10.5, 3.8 Hz, 1H, H-6a), 4.57 (dt, J = 12.7, 2.5 Hz, 1H, H-6b), 4.21 – 4.01 (m, 4H), 3.72 – 3.61 (m, 12H), 3.53 (tq, J = 10.2, 5.8, 4.5 Hz, 3H), 3.38 (dt, J = 10.6, 5.1 Hz, 3H), 2.13 – 1.96 (m, 21H).

HRMS (ESI) m/z calculated for C₃₄H₅₀N₄O₂₁ [M+Na]⁺ 873.2866, found 873.2866.

1,2,3,6,2',3'-hexa-O-benzyl-4',6'-O-benzylidene-4-O-(α-D-glucopyranosyl)-β-D-glucopyranose, **16**



16

A solution of **5** (12.5 g, 0.29 mmol) in dry DMF (120 mL) was stirred with NaH (14.4

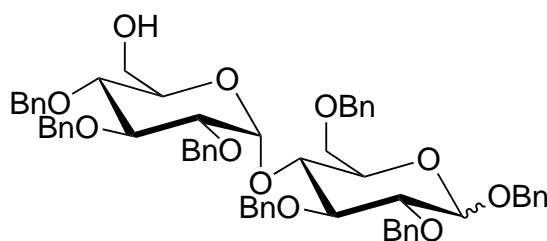
g, 0.354 mol) for 2 h at rt. The RM was cooled to 0 °C and benzyl bromide (43.8 mL, 0.368 mol) was added dropwise to the mixture and stirring was continued ON at RT. The mixture was cooled to 0 °C and excess NaH decomposed by dropwise addition of MeOH. The solution was concentrated and extracted with EtOAc. The combined organic layers were washed with water and brine, dried over Na₂SO₄, and concentrated. The residue was purified by column chromatography (n-pentane/Et₂O: 30%) to give **16** in (19.1 g, 67 %).

¹ H NMR (400 MHz, CDCl₃) δ 7.63 – 7.02 (m, 35H, Ar-CH), 5.76 (d, J = 3.8 Hz, 0.3H, H-1 α), 5.71 (d, J = 3.9 Hz, 0.7H, H-1 β), 5.52 (d, J = 4.1 Hz, 1H, Bn-CH), 5.02 – 4.44 (m, 14H, Bn-CH₂, H-1'), 4.17 – 3.40 (m, 12H, skeletal protons).

¹³ C NMR (101 MHz, CDCl₃) δ 138.64, 138.55, 138.11, 138.08, 138.00, 137.80, 137.30 (Bn-CH₂), 128.41, 128.35, 128.34, 128.32, 128.31, 128.26, 128.22, 128.17, 128.11, 127.97, 127.94, 127.92, 127.76, 127.73, 127.70, 127.69, 127.67, 127.65, 127.60, 127.57, 127.53, 127.50, 127.46, 127.44, 127.08, 126.82, 126.65, 126.53 (Ar-CH), 102.22 (C-1 α), 101.28 (C-1 β), 96.31 (C-1'), 84.73, 82.12, 81.66, 79.31, 77.46, 77.32, 77.00, 76.68, 75.40, 74.99, 74.58, 74.46, 73.81, 73.40, 73.19, 72.29, 71.66, 70.91, 68.56, 61.53 (skeletal carbons).

HRMS (ESI) m/z calculated for C₆₁H₆₄O₁₁ [M+Na]⁺ 993.4149, found 993.4182.

1,2,3,6,2',3',4'-hepta-O-benzyl-4-O-(α-D-glucopyranosyl)-β-D-glucopyranose, **17**



17

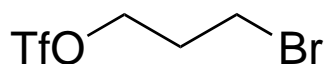
DiBAI-H (29.3 mL, 29.3 mmol) was added to the solution of the acetal **16** (19 g, 19.56 mmol) in toluene (98 mL) at -10 °C and the solution was stirred at room temperature. After 40 h the reaction was stopped at -10 °C with MeOH. The reaction mixture was washed with 10 % KOH solution and the aqueous layer extracted with Et₂O. The combined organic layers were dried over Na₂SO₄ and concentrated. The crude product was purified by column chromatography (n-pentane/Et₂O:30% to 50%) to yield **17** (9.3 g, 72 %) as a viscous liquid.

¹H NMR (400 MHz, CDCl₃) δ 7.50 – 7.05 (m, 35H, Ar-CH), 5.62 (d, J = 3.7 Hz, 1H, H-1), 5.00 – 4.41 (m, 15H, Bn-CH₂, H-1'), 4.20 – 3.36 (m, 1H, skeletal protons).

¹³C NMR (101 MHz, CDCl₃) δ 138.79, 138.69, 138.25, 138.24, 138.15, 137.95, 137.45 (Bn-CH₂), 128.53, 128.48, 128.47, 128.39, 128.35, 128.30, 128.23, 128.10, 128.05, 127.90, 127.85, 127.80, 127.78, 127.73, 127.69, 127.66, 127.62, 127.59, 127.20, 126.79, 126.67 (Bn-CH), 102.36 (C-1 α), 96.46 (C-1'), 84.86, 82.27, 81.80, 79.47, 77.62, 77.40, 77.08, 76.76, 75.53, 75.12, 74.71, 74.62, 73.93, 73.56, 73.32, 72.47, 71.78, 71.05, 68.72, 61.71, 53.47 (skeletal protons).

HRMS (ESI) m/z calculated for C₆₁H₆₂O₁₁ [M+Na]⁺ 995.4346, found 995.4346.

3-bromopropyl trifluoromethanesulfonate, **21**



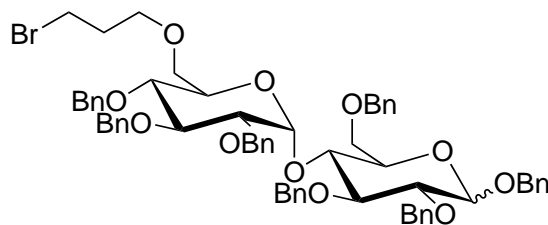
21

Pyridine (3.49 mL, 43.2 mmol) was added to a solution of 3-bromopropan-1-ol (3.25 ml, 36.0 mmol) in CH₂Cl₂ (55.4 mL) at -78 °C. Tf₂O (6.14 mL, 36.3 mmol) was added dropwise over 1 min, and stirring continued at -78 °C for 5 min. The solution was then warmed to 0 °C for 40 min. The RM was diluted with pentane (40 mL) and cold 1 M

aq.H₂SO₄. The layers were separated and organic layer dried over Na₂SO₄, filtered and concentrated. The colourless liquid was dried under high vacuum for 30 s to yield **21** (8.7 g, 89 %) as a colourless liquid.

¹H NMR (400 MHz, CDCl₃) δ 4.71 (t, J = 5.9 Hz, 2H), 3.58 - 3.47 (m, 3H), 2.36 (p, J = 6.0 Hz, 2H).

1,2,3,6,2',3',4'-hepta-O-benzyl-6'-O-(3-bromopropyl)-4-O-(α-D-glucopyranosyl)-β-D-glucopyranose, **19**



19

To a solution of **17** (9.30 g, 9.56 mmol) in CH₂Cl₂(47.8 mL), the triflate **19** (5.18 g, 19.11 mmol) was added followed by and DIPEA (1.83 g, 10.51 mmol). The RM was stirred ON. The solvent was evaporated and the crude product purified by column chromatography (PE/EtOAc: 20-40%) to yield **19** (1.80 g, 17.2 %) as a viscous colourless oil.

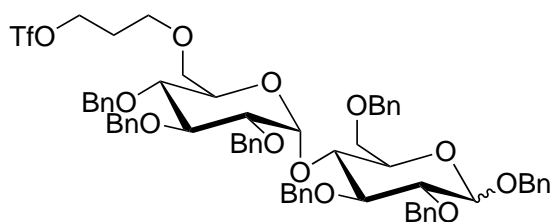
¹ H NMR (400 MHz, CDCl₃) δ 7.60 – 7.12 (m, 35H, Ar-H), 5.75 – 5.67 (m, 1H, H-1), 5.05 – 4.43 (m, 15H, Bn-CH₂, H-1'), 4.30 – 3.24 (m, 16H, skeletal protons, –CH₂O–, –CH₂Br), 2.31 – 1.82 (m, 2H, –CH₂CH₂CH₂Br).

¹³C NMR (101 MHz, CDCl₃) δ 139.09, 138.85, 138.79, 138.74, 138.66, 138.59, 138.43, 138.29, 138.25, 138.02, 138.00 (Bn-CH₂), 128.56, 128.49, 128.46, 128.45, 128.43, 128.42, 128.40, 128.36, 128.33, 128.31, 128.29, 128.27, 128.10, 128.07, 127.95, 127.92, 127.89, 127.86, 127.85, 127.79, 127.76, 127.72, 127.70, 127.63,

127.62, 127.60, 127.55, 127.48, 127.39, 127.15, 127.12, 126.76, 126.65 (Ar-CH), 102.42 (C-1 α), 96.75 (C-1 β), 96.66 (C-1'), 95.15, 84.86, 82.37, 82.03, 79.40, 77.76, 77.44, 77.12, 76.80, 75.64, 75.13, 74.74, 74.66, 73.98, 73.49, 73.31, 73.27, 72.67, 71.08, 71.04, 69.20, 69.16, 68.80 (skeletal protons, $-\text{OCH}_2$), 32.70 ($-\text{CH}_2\text{Br}$), 30.72 ($-\text{CH}_2\text{CH}_2\text{CH}_2\text{Br}$).

HRMS (ESI) m/z calculated for $\text{C}_{64}\text{H}_{69}\text{BrO}_{11}$ $[\text{M}+\text{Na}]^+$ 1115.3921, found 1115.3921.

1,2,3,6,2',3',4'-hepta-O-benzyl-6'-O-(3-trifluoromethylsulfonylpropyl)-4-O-(α -D-glucopyranosyl)- β -D-glucopyranose, **22**

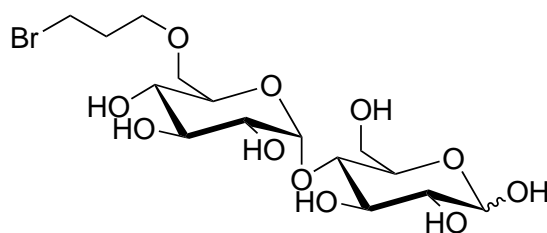


22

22 (250 mg, 3%) was obtained as a side product during the synthesis of **19**.

HRMS (ESI) m/z calculated for $\text{C}_{61}\text{H}_{62}\text{O}_{11}$ $[\text{M}+\text{Na}]^+$ 1185.4258, found 1185.4258.

6'-O-(3-bromopropyl)-4-O-(α -D-glucopyranosyl)- β -D-glucopyranose, **24**

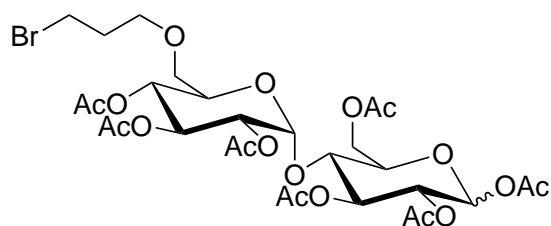


24

To a solution of the bromide **19** (1.7 g, 1.55 mmol) in EtOH/EtOAc (4:1, 50 mL) was added Pd(OH)₂/C (0.218 g, 0.155 mmol) and hydrogenated for 24 h under 10 bar. The RM was filtered over a pad of celite and concentrated to give the desired product **24** (684 mg, 84 % yield) as a colourless solid. The crude product was used further without any purification.

¹ H NMR (400 MHz, CDCl₃) δ 5.38 (d, J = 3.5 Hz, 0.8H, H-1_α), 5.22 (d, J = 3.6 Hz, 0.2H, H-1_β), 4.64 (d, J = 8.0 Hz, 1H, H-1'), 4.09 – 3.50 (m, 14H, skeletal protons, –OCH₂–), 3.50 – 3.19 (m, 2H, CH₂Br), 2.25 – 2.06 (m, 2H, –CH₂CH₂CH₂Br).

1,2,3,6,2',3',4'-hepta-O-acetyl-6'-O-(3-bromopropyl)-4-O-(α-D-glucopyranosyl)-β-D-glucopyranose, **15**



15

24, (684 mg, 1.476 mmol) was dissolved in Ac₂O(0.30 mL, 3.17 mmol) and sodium acetate (133 mg, 1.624 mmol) was added to the suspension. RM was heated to 100 °C for 2 h. The RM was poured onto ice-cold water (50 mL) with vigorous stirring to precipitate the expected product. The crude product was collected by filtration, and purified by column chromatography (CH₂Cl₂/MeOH: 5%) to yield **15** (873 mg, 78%) as a white solid.

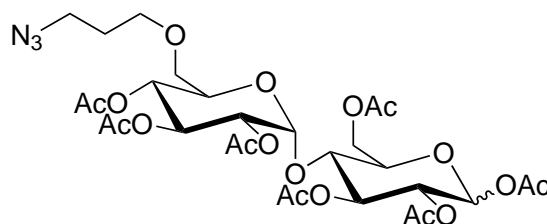
¹H NMR (400 MHz, CDCl₃) δ 6.23 (d, J = 3.7 Hz, 0.6H, H-1 α), 5.73 (d, J = 8.2 Hz, 0.3H, H-1 β), 5.54 – 5.23 (m, 3H, H-3, H-1', H-3'), 5.20 – 5.08 (m, 1H, H-4), 5.00 – 4.91 (m, 1H, H-2), 4.85 (m, 1H, H-2'), 4.42 (dt, J = 12.2, 2.3 Hz, 1H, H-5'), 4.21 (dd,

$J = 12.3, 3.8$ Hz, 1H, H-4), 4.16 – 3.97 (m, 2H, H-4', H-5), 3.88 – 3.78 (m, 1H, H-6a), 3.66 – 3.56 (m, 1H, H-6'a), 3.53 – 3.33 (m, 6H, –CH₂Br, –OCH₂, H-6b, H-6'a), 2.15 – 1.93 (m, 21H, CH₃, –CH₂CH₂CH₂Br).

¹³C NMR (101 MHz, CDCl₃) δ 170.56, 170.55, 170.48, 170.12, 170.09, 170.03, 169.98, 169.88, 169.63, 169.42, 169.38, 168.99, 168.83 (C=O), 95.82 (C-1 α), 95.75 (C-1 β), 91.28 (C-1' β), 88.86 (C-1' α), 77.37, 77.05, 76.73, 75.30, 73.01, 72.30, 72.12, 70.97, 70.13, 70.12, 70.07, 69.79, 69.74, 69.59, 69.54, 69.20, 68.80, 68.57, 68.20, 62.70, 62.58, 32.55, 30.67, 21.03, 20.93, 20.87, 20.85, 20.82, 20.68, 20.65, 20.63, 20.59, 20.55, 20.45.

HRMS (ESI) calculated for C₁₅H₂₅BrO₁₂ [M+Na]⁺ 779.1374, found 779.1371.

1,2,3,6,2',3',4'-hepta-O-acetyl-6'-O-(3-azidopropyl)-4-O-(α -D-glucopyranosyl)- β -D-glucopyranose, **14**



14

The bromide **14** (873 mg, 1.15 mmol) was dissolved in DMF (2 mL) and sodium azide (112 mg, 1.73 mmol) was added to it. The solution was stirred at 60 °C ON. The RM was cooled to 0 °C, diluted with water, extracted with EtOAc. The residue was purified by flash column chromatography on silica gel (CH₂Cl₂/ MeOH: 5%) to give **14** (788 mg, 95%) as a white solid.

¹H NMR (400 MHz, CDCl₃) δ 6.24 (d, $J = 3.7$ Hz, 0.6 H, H-1 α), 5.74 (d, $J = 8.2$ Hz, 0.3H, H-1 β), 5.58 – 5.23 (m, 3H, H-3, H-1', H-3'), 5.21 – 5.07 (m, 1H, H-4), 5.03 –

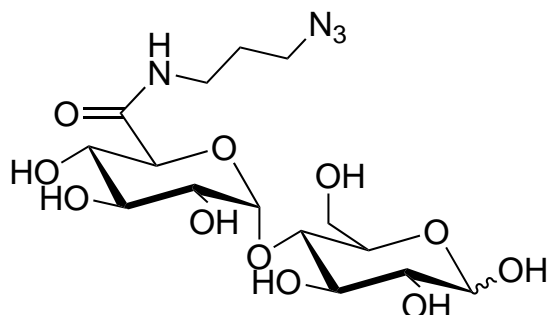
4.92 (m, 1H, H-2), 4.86 (ddd, J = 10.4, 6.1, 4.1 Hz, 1H, H-2'), 4.42 (dd, J = 12.2, 2.5 Hz, 1H, H-5'), 4.26 – 3.95 (m, 4H, H-4, H-4', H-5, H-6a), 3.51 – 3.16 (m, 6H, –CH₂N₃, –NCH₂, H-6b, H-6'), 2.04 (m, 21H, CH₃), 1.83 (m, 2H, –CH₂CH₂CH₂N₃).

¹³C NMR (101 MHz, CDCl₃) δ 170.56, 170.55, 170.47, 170.10, 170.09, 170.01, 169.97, 169.87, 169.62, 169.40, 169.36, 168.98, 168.83 (C=O), 95.81 (C-1 α), 95.74 (C-1 β), 91.27 (C-1' β), 88.84 (C-1' α), 77.37, 77.05, 76.74, 75.29, 73.00, 72.33, 72.29, 72.15, 70.96, 70.12, 70.10, 70.06, 69.78, 69.73, 69.53, 69.48, 68.71, 68.67, 68.46, 68.44, 68.21, 68.19, 62.72, 62.60, 48.14, 29.04, 21.02, 20.92, 20.86, 20.84, 20.83, 20.82, 20.66, 20.64, 20.63, 20.59, 20.55, 20.44 (CH₃).

HRMS (ESI) m/z calculated for C₂₉H₄₁N₃O₁₈ [M+Na]⁺ 742.2280, found 742.2283.

6'-O-((3-azidopropyl)carbamoyl)4-O-(α-D-glucopyranuronosyl)-β-D-glucopyranose,

BOT_41



BOT_41

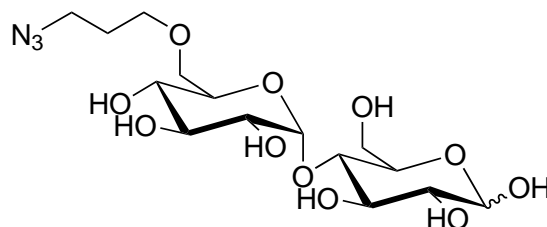
To a solution of **12** (150 mg, 0.204 mmol) in methanol (2 mL) was added catalytic amount of sodium methoxide (5 μL, 0.008 mmol). The RM was stirred ON at RT, acidified with Amberlyst IR-120 until pH 2 and filtered. The filtrate was concentrated to give the crude product. The crude product was purified by flash chromatography using an amino column (MeCN/H₂O: 95% to 70% over 30 min) to give **BOT_41** (35 mg, 36%) as a colourless liquid.

¹ H NMR (400 MHz, D₂O) δ 5.48 (d, J = 3.5 Hz, 1H, H-1_α), 5.22 (d, J = 3.7 Hz, 1H, H-1'), 4.24 – 3.50 (m, 10H, skeletal protons), 3.43 – 3.15 (m, 4H, –OCH₂, –CH₂N₃), 1.99 – 1.66 (m, 2H, C \underline{H}_2 CH₂N₃).

¹³C NMR (101 MHz, D₂O) δ 170.83 (C=O), 99.76 (C-1 α), 99.65 (C-1 β), 95.71 (C-1'), 76.78, 76.54, 76.11, 74.32, 73.95, 73.15, 72.44, 72.22, 71.26, 71.19, 69.74, 69.53, 68.57, 64.77, 60.49, 60.39 (skeletal carbons), 48.52 (–OCH₂), 36.53 (–CH₂N₃), 27.48 (C \underline{H}_2 CH₂N₃).

HRMS (ESI) m/z calculated for C₁₅H₂₅N₃O₁₂ [M+Na]⁺ 461.1489, found 461.1489.

6'-O-(3-azidopropyl)-4-O-(α -D-glucopyranosyl)- β -D-glucopyranose, **BOT_42**



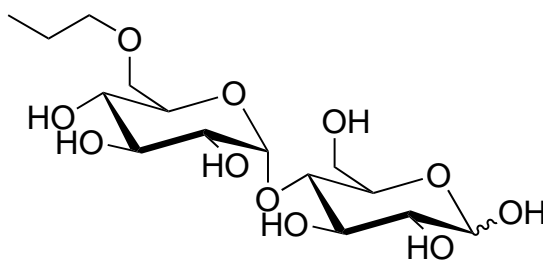
BOT_42

To a solution of **15** (300 mg, 0.416 mmol) in methanol (3 mL) was added catalytic amount of sodium methoxide (8 μ L, 0.016 mmol). The RM was stirred ON at RT, acidified with Amberlyst IR-120 until pH 2 and filtered. The filtrate was concentrated to give the crude product. The crude product was purified by flash chromatography using an amino column (MeCN/H₂O: 95% to 70% over 30 min) to give **BOT_42** (66.3 mg, 37.2%) as a colourless liquid.

¹ H NMR (400 MHz, CDCl₃) δ 5.40 (d, J = 3.9 Hz, 1H, H-1), 4.48 (d, J = 8.0 Hz, 1H, H-1'), 4.08 – 3.56 (m, 10H, skeletal protons), 3.56 – 3.22 (m, 4H, –OCH₂, –CH₂N₃), 1.92 (p, J = 6.5 Hz, 2H; C \underline{H}_2 CH₂N₃).

HRMS (ESI) m/z calculated for C₁₅H₂₇N₃O₁₁ [M+Na]⁺ 448.1543, found 448.1543.

6'-O-propyl-4-O-(α -D-glucopyranosyl)- β -D-glucopyranose, **BOT_43**



BOT_43

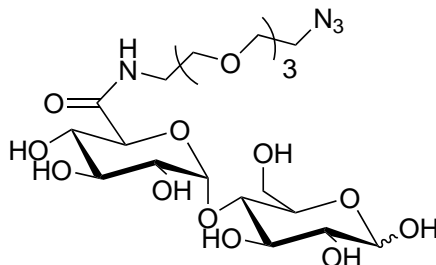
To a solution of the triflate **22** (250 mg, 0.214 mmol) in EtOH/EtOAc (4:1, 50 mL) was added Pd(OH)₂/C (0.218 g, 0.155 mmol) and hydrogenated for 24 h under 10 bar. The RM was filtered over a pad of celite and concentrated to give the desired product **BOT_43** (77.6 mg, 94 % yield) as a colourless solid.

¹ H NMR (400 MHz, D₂O) δ 5.28 (d, J = 3.9 Hz, 1H, H-1), 5.12 (d, J = 3.8 Hz, 0.5H, H-1'), 4.54 (d, J = 8.0 Hz, 0.5H, H-1 β), 3.98 – 3.12 (m, 14H, skeletal protons, –OCH₂CH₂), 1.50 (q, J = 7.2 Hz, 2H, –CH₂CH₃), 0.80 (t, J = 7.4 Hz, 3H, –CH₃).

¹³C NMR (101 MHz, CDCl₃) δ 99.50, 99.43, 95.71, 91.83, 76.95, 76.77, 76.14, 74.53, 73.94, 73.29, 73.15, 72.79, 71.66, 71.62, 71.53, 71.47, 71.23, 71.08, 69.91, 69.77, 69.53, 69.49, 69.08, 68.94, 66.76, 60.70, 60.56, 21.87, 9.65.

HRMS (ESI) m/z calculated for C₁₅H₂₈O₁₁ [M+Na]⁺ 407.1529, found 407.1529.

6'-((2-(2-azidoethoxy)ethyl)carbamoyl)-4-O-(α -D-glucopyranuronosyl)- β -D-glucopyranose, **BOT_49**



BOT_49

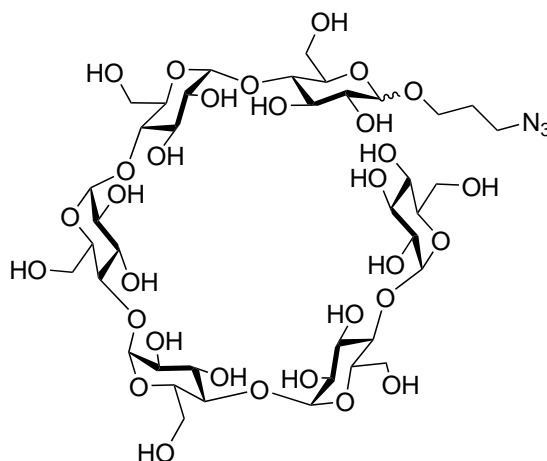
To a solution of **13** (158 mg, 0.186 mmol) in methanol (2ml) was added catalytic amount of sodium methoxide (4 μ L, 0.007 mmol). The RM was stirred ON at RT, acidified with Amberlyst IR-120 until pH 2 and filtered. The filtrate was concentrated to give the crude product. The crude product was purified by flash chromatography using an amino column (MeCN/H₂O: 95% to 70% over 30 min) to give **BOT_49** (66.3 mg, 64%) as a colourless liquid.

¹H NMR (400 MHz, D₂O) δ 5.46 (s, 0.6H, H-1 α), 5.20 (d, J = 3.7 Hz, 1H, H-1'), 4.63 (d, J = 7.9 Hz, 1H, H-1 β), 4.20 – 3.14 (m, 26H, skeletal protons, –OCH₂).

¹³C NMR (101 MHz, D₂O) δ 171.07 (C=O), 99.61 (C-1 α), 95.80 (C-1 β), 91.83 (C-1'), 76.82, 76.58, 76.11, 74.33, 73.97, 73.14, 72.39, 72.18, 71.31, 71.25, 69.75, 69.62, 69.54, 69.48, 69.17, 68.69, 65.68, 60.49, 60.39 (skeletal carbons, –OCH₂), 50.11 (-NHCH₂-), 38.85 (-CH₂N₃).

HRMS (ESI) m/z calculated for C₂₀H₃₆N₄O₁₄ [M+Na]⁺ 579.2126, found 579.2126.

β -D-glucopyranose,2,3,4,6-tetra-hydroxy- α -D-glucopyranosyl-(1 \rightarrow 4)-2,3,6-tri-hydroxy- α -D-glucopyranosyl-(1 \rightarrow 4)-2,3,6-tri-hydroxy- α -D-glucopyranosyl-(1 \rightarrow 4)-2,3,6-tri-hydroxy- α -D-glucopyranosyl-(1 \rightarrow 4)-2,3,6-tri-hydroxy- α -D-glucopyranosyl-(1 \rightarrow 4)-2,3,6-tri-hydroxy 1-(3'-azidopropyl), **BOT_46**



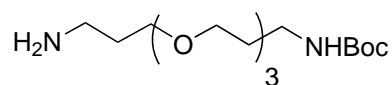
BOT_46

To a solution of **13** (158 mg, 0.186 mmol) in methanol (2ml) was added catalytic amount of sodium methoxide (4 μ L, 0.007 mmol). The RM was stirred ON at RT, acidified with Amberlyst IR-120 until pH 2 and filtered. The filtrate was concentrated to give the crude product. The crude product was purified by flash chromatography using an amino column (MeCN/H₂O: 95% to 70% over 30 min) to give **BOT_49** (66.3 mg, 72%) as a colourless liquid.

¹ H NMR (400 MHz, D₂O) δ 5.44 – 5.34 (m, 5H, H-1, H-1), 4.44 (d, J = 8.0 Hz, 1H, H-1'), 4.13 – 3.89 (m, 6H, skeletal protons), 3.88 – 3.70 (m, 19H, skeletal protons), 3.70 – 3.50 (m, 13H, skeletal protons), 3.47 – 3.35 (m, 3H, –OCH₂–, –CH₂N₃), 3.27 (dd, J = 9.5, 8.0 Hz, 1H, –CH₂N₃), 1.88 (q, J = 6.5 Hz, 2H, –CH₂CH₂N₃).

HRMS (ESI) m/z calculated for C₃₉H₆₇N₃O₃₁ [M+Na]⁺ 1096.3657, found 1096.3657.

tert-butyl (3-(3-aminopropoxy)propyl)carbamate, **28**



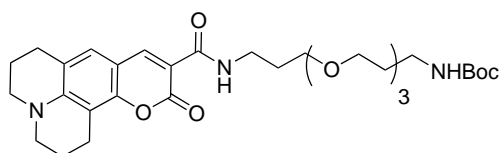
28

The diamine **33** (20.0 mL, 91.2 mmol, 10 eq.) was dissolved in anhydrous CH₂Cl₂ (65 mL) and cooled to 0 °C. Boc₂O (2.00 g, 9.12 mmol, 1.00 eq.) was dissolved in anhydrous CH₂Cl₂ (6.5 mL) and added dropwise over 45 min and stirred ON at RT. The reaction was quenched with H₂O and the aqueous layer extracted with CH₂Cl₂. The combined organic layers were dried over Na₂SO₄ and concentrated. The crude product was purified by column chromatography (CH₂Cl₂/MeOH/Et₃N- 1:0:0 to 9:0.5:0.5) to give the product **28** (1.40 g, 4.06 mmol, 48%).

¹ H NMR (400 MHz, CDCl₃) δ 5.11 (t, J = 5.9 Hz, 1H, -NHBoc), 3.58 (s, 12H, -OCH₂-), 3.21 (q, J = 6.4 Hz, 2H, -CH₂CH₂NH₂), 2.88 (t, J = 6.5 Hz, 2H, CH₂CH₂NHBoc), 1.77 (m, 4H, CH₂NH₂, CH₂NHBoc), 1.42 (s, 9H, Boc-CH₃).

¹³C NMR (101 MHz, CDCl₃) 156.09 (C=O), 70.62, 70.60, 70.25, 70.20, 69.50 (-OCH-2), 39.65 (CH₂NH₂), 33.28 (CH₂NHBoc), 29.63 (CH₂CH₂NHBoc), 28.46 (Boc-CH₃).

tert-butyl (3-(3-(11-oxo-2,3,6,7-tetrahydro-1H,5H,11H-pyrano[2,3-f]pyrido[3,2,1-*ij*]quinoline-10-carboxamido)propoxy)propyl)carbamate, **34**



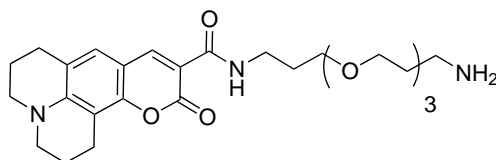
34

A solution of the linker **28** (203 mg, 0.69 mmol) in CH₂Cl₂ (5 mL) was added to a solution of coumarin 343 (200 mg, 0.63 mmol) in CH₂Cl₂ (16 mL). T3P (0.54 mL, 1.5 mmol, 50% w/w) was added to it followed by Et₃N (0.4 mL, 3.4 mmol). The bright yellow solution was stirred ON at RT. The reaction was quenched with NaHCO₃ (3 x 20 mL) and the aqueous layer extracted with CH₂Cl₂. The combined organic phases were dried over Na₂SO₄ and concentrated. The crude product was purified by column chromatography (CH₂Cl₂/MeOH/Et₃N- 98:1:1 to 96:3:1) to give the product **34** (290 mg, 0.49 mmol, 82%) as a yellow oil.

¹ H NMR (400 MHz, CDCl₃) δ 8.62 (s, 1H, Ar-CH), 7.01 (s, 1H, ArC-H), 3.77 – 3.47 (m, 12H, –OCH₂), 3.33 (dd, J = 11.1, 4.7 Hz, 4H, 2 × coumarin CH₂N), 3.22 (t, J = 6.5 Hz, 2H, CH₂NHCO), 2.77 (t, J = 6.2 Hz, 2H, CH₂NH₂), 2.04 – 1.70 (m, 8H, CH₂CH₂NH₂, CH₂CH₂NHCO, 2 × coumarin CH₂CH₂N), 1.43 (s, 9H, Boc-CH₃).

HRMS (ESI) m/z calculated for C₂₆H₃₈N₃O₆ [M+Na]⁺ 610.3104, found 610.3104.

N-(3-(2-(2-(3-aminopropoxy)ethoxy)ethoxy)propyl)-11-oxo-2,3,6,7-tetrahydro-1H,5H,11H-pyrano[2,3-f]pyrido[3,2,1-ij]quinoline-10-carboxamide, **31**



31

The Boc-protected amine **34** (75 mg, 0.12 mmol) was dissolved in TFA / CH₂Cl₂ (1:1, 2 mL) and stirred for 2 h at RT. The RM was partitioned between CH₂Cl₂ and NaHCO₃ solution and extracted with CH₂Cl₂ (3 x 10 mL). The combined organic phases were dried over Na₂SO₄ and concentrated. The crude product was purified by column chromatography (CH₂Cl₂/MeOH/Et₃N- 8.9:1.0:0.1) to give the desired amine **31** (48 mg, 56

%) as an orange oil.

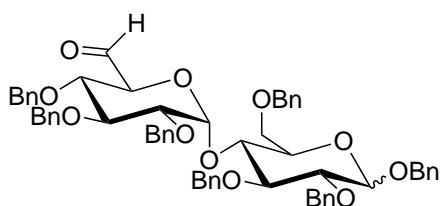
¹H NMR (400 MHz, CD₃OD) δ 8.45 (s, 1H, Ar-CH), 7.28 (s, 1H, Ar-CH), 3.66–3.54 (m, 12H, –OCH₂), 3.50 (t, J = 6.6 Hz, 2H, CH₂NHCO), 3.37–3.34 (m, 4H, 2 × coumarin CH₂N), 2.84–2.74 (m, 6H, CH₂NH, 2 × coumarin Bn-CH₂), 2.00–1.92 (m, 4H, 2 × coumarin CH₂CH₂N), 1.89–1.84 (m, 2H, PEG CH₂CH₂NHCO), 1.77–1.71 (m, 2H, PEG CH₂CH₂NH₂).

¹³C NMR (101 MHz, CD₃OD) δ 165.7, 164.2, 154.0, 150.1, 149.1, 128.4, 121.7, 109.3, 108.5, 106.5, 71.5, 71.5, 71.4, 71.2, 70.5, 70.2, 51.3, 50.8, 40.2, 38.3, 32.7, 30.5, 28.4, 22.2, 21.2, 21.0.

HRMS (ESI) m/z calculated for 26 H₃₇N₃O₆ [M+H]⁺ 488.2761, found 488.2760.

1,2,3,6,2',3',4'-hepta-O-acetyl-4-O-(α-D-1,5-glucohexodialdo)-β-D-glucofuranose,

36



36

2,2-dicholo acetic acid (121 mg, 0.935 mmol) and EDC (448 mg, 0.935 mmol) were added to a solution of the alcohol (455 mg, 0.468 mmol) in DMSO/toluene (1:1, 1.4 mL) and stirred ON at RT. The RM was fractionated between water and CH₂Cl₂. The organic layer was sequentially washed with water and with aq. NaHCO₃, dried with Na₂SO₄ and concentrated. The crude product was used in the next step without further purification.

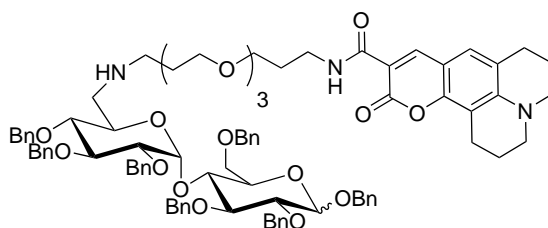
¹H NMR (400 MHz, CDCl₃) δ 9.45 (d, J = 28.8 Hz, 1H, CHO), 7.73 – 6.98 (m, 37H,

Ar-CH), 5.89 – 5.63 (m, 1H, H-1), 5.29 – 4.47 (m, 16H, Bn-CH₂), 4.41 – 3.26 (m, 12H, skeletal protons).

¹³C NMR (101 MHz, CDCl₃) δ 197.70 (CHO), 138.73, 138.43, 138.39, 138.19, 138.13, 137.98, 137.91, 137.72, 137.68, 137.44 (Bn-CH₂), 128.56, 128.51, 128.48, 128.45, 128.43, 128.41, 128.38, 128.36, 128.35, 128.27, 128.24, 128.22, 128.11, 128.08, 127.89, 127.86, 127.84, 127.77, 127.63, 127.60, 127.46, 127.23, 126.66, 126.59 (Bn-CH), 102.42 (C-1 α), 96.46 (C-1 β), 95.27 (C-1'), 84.67, 82.26, 81.83, 81.52, 80.24, 78.74, 78.66, 77.92, 77.45, 77.13, 76.81, 75.71, 75.10, 74.99, 74.74, 74.42, 73.93, 73.42, 73.32, 72.99, 72.74, 72.54, 71.06, 69.77, 69.36, 68.67.

HRMS (ESI) m/z calculated for C₆₄H₆₆O₁₁ [M+Na]⁺ 993.4190, found 993.4189.

Benzylated BOT_15, **35**



35

To a solution of aldehyde (181 mg, 0.08 mmol) in CH₂Cl₂ (2 mL), the amine **31** (181 mg, 0.310 mmol) was added, followed by NaBH(OAc)₃ (656 mg, 3.10 mmol). The RM was stirred ON at RT. The RM was fractionated between water and CH₂Cl₂. The organic layer was sequentially washed with water and with aq. NaHCO₃, dried with Na₂SO₄ and concentrated. The product was purified by column chromatography (CH₂Cl₂/MeOH- 5%) to give **35** (45 mg, 20%).

¹H NMR (400 MHz, CDCl₃) δ 8.94 (d, J = 5.5 Hz, 1H, coumarin O=CNH), 8.61 (s, 1H, coumarin Ar-CH), 7.54 – 7.09 (m, 35H, Bn-CH), 7.02 (s, 1H, coumarin Ar-CH),

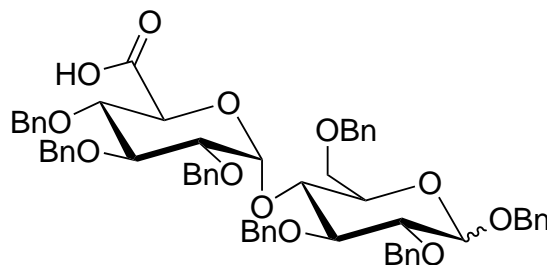
5.70 (dd, $J = 29.4, 3.3$ Hz, 1H, H-1), 5.21 – 4.43 (m, 14H, Bn-CH₂) 4.29 – 3.38 (m, 23H, skeletal protons, –OCH₂), 3.29 (dd, $J = 11.2, 5.6$ Hz, 4H, 2 × PEG –CH₂NH), 3.00 – 2.67 (m, 6H, coumarin CH₂N, 2 × coumarin Bn-CH₂), 2.14 – 1.59 (m, 8H, 2 × coumarin –CH₂CH₂N, 2 × PEG –CH₂CH₂NH).

¹³C NMR (101 MHz, CDCl₃) 163.64, 163.00 (C=O), 148.11, 148.10, 138.51, 138.46, 138.22, 138.18, 138.04, 137.82, 137.42 (Bn-CH₂), 128.53, 128.49, 128.46, 128.42, 128.36, 128.27, 128.17, 128.06, 128.03, 127.98, 127.92, 127.87, 127.85, 127.81, 127.71, 127.69, 127.67, 127.65, 127.63, 127.56, 127.40, 127.13, 127.00, 126.94 (Bn-CH), 119.62, 108.98, 108.30, 105.60, 102.43 (C-1), 96.19 (C-1), 84.69, 82.29, 81.55, 79.16, 78.65, 77.45, 77.34, 77.13, 76.81, 75.33, 74.90, 74.66, 74.61, 74.09, 73.57, 71.09, 70.47, 70.45, 70.31, 70.12, 69.63, 69.07, 50.22, 49.79, 47.38, 36.96, 29.59, 27.43, 21.14, 20.20, 20.12.

HRMS (ESI) m/z calculated for C₈₇H₉₉N₃O₁₆ [M+Na]⁺ 1442.7104, found 1442.7107.

1,2,3,6,2',3',4'-hepta-O-benzyl-4-O-(α -D-glucopyranuronosyl)- β -D-glucopyranose,

38



38

To a solution of the alcohol **17** (150 mg, 0.15 mmol) in CH₂Cl₂/H₂O (2:1, 1.5 mL), were added TEMPO (8 mg, 30 μ mol) and BAIB (145 mg, 0.45 mmol). The RM was stirred ON at RT. The RM was quenched with saturated Na₂S₂O₃ (2 mL), extracted with EtOAc, dried over Na₂SO₄ and concentrated. The crude product was purified by column

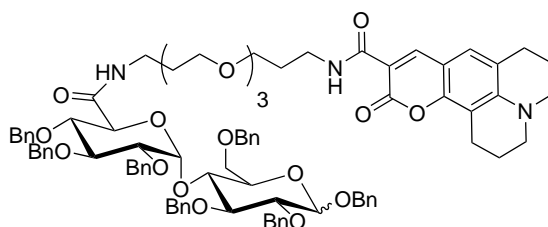
chromatography (CH₂Cl₂/MeOH- 2% to 5%) to give the desired acid **38** (126 mg, 85 %) as a viscous oil.

¹H NMR (400 MHz, CDCl₃) δ 7.58 – 6.99 (m, 35H, Ar-CH), 5.81 (dd, J = 7.4, 3.6 Hz, 1H, H-1), 5.17 – 4.47 (m, 15H, Bn-CH₂, H-1'), 4.43 – 3.44 (m, 11H, skeletal protons).

¹³C NMR (101 MHz, CDCl₃) δ 172.11 (C=O), 139.01, 138.72, 138.39, 138.36, 138.15, 137.89, 137.78, 137.77, 137.74, 137.72, 137.61, 137.51, 137.39, 137.12 (Bn-CH₂), 128.58, 128.53, 128.50, 128.46, 128.44, 128.41, 128.38, 128.37, 128.35, 128.34, 128.32, 128.31, 128.28, 128.26, 128.11, 128.07, 128.04, 127.98, 127.94, 127.88, 127.83, 127.80, 127.75, 127.71, 127.69, 127.64, 127.22, 126.57, 126.50 (Ar-CH), 102.45 (C-1 α), 97.49 (C-1 β), 95.22 (C-1'), 84.53, 82.27, 80.93, 80.23, 78.77, 78.39, 77.47, 77.15, 76.83, 75.51, 75.27, 74.76, 74.53, 74.23, 73.96, 73.74, 73.61, 73.50, 72.97, 71.22, 71.15, 70.05, 69.46, 68.15.

HRMS (ESI) m/z calculated for C₈₇H₉₇N₃O₁₇ [M+Na]⁺ 1478.6716, found 1478.6714.

Benzylated BOT_16, **37**



37

The acid **38** (60 mg, 60 μmol) and the amine **31** (35 mg, 60 μmol) were dissolved in dry CH₂Cl₂ (2.0 mL). T3P (50 % in DMF, 60 μL, 91 μmol) followed by Et₃N (85 μL, 0.6 mmol) were added to the RM. The RM was stirred at RT for 4 h. The RM was washed with saturated bicarbonate and extracted with CH₂Cl₂. The combined organic extracts were washed with H₂O and brine, dried using Na₂SO₄, and concentrated under reduced

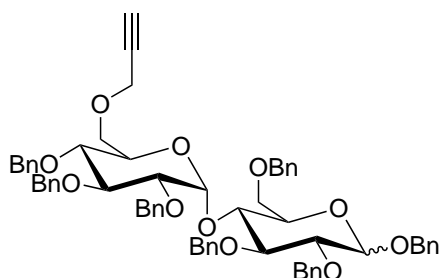
pressure. The crude product was purified by column chromatography (CH₂Cl₂/MeOH: 10%) to yield **37** (96 mg, 65%) as a white solid.

¹H NMR (400 MHz, CDCl₃) δ 8.93 (t, J = 5.6 Hz, 1H, amide-NH), 8.59 (s, 1H, coumarin Ar-CH), 7.54 – 7.13 (m, 35H, Bn-CH), 6.99 (s, 1H, coumarin Ar-CH), 6.64 (t, J = 5.9 Hz, 1H, NH), 5.77 (d, J = 3.6 Hz, 1H, H-1), 5.09 – 4.43 (m, 16H, Bn-CH₂, H-1'), 4.22 – 3.42 (m, 23H, skeletal protons, –OCH₂), 3.41 – 3.24 (m, 6H, coumarin CH₂N, 2 × coumarin Bn-CH₂), 3.16 – 2.66 (m, 4H, 2 × PEG –CH₂NH), 2.11 – 1.79 (m, 8H, 2 × coumarin –CH₂CH₂N, 2 × PEG –CH₂CH₂NH).

¹³C NMR (101 MHz, CDCl₃) δ 168.63, 163.58, 162.98 (C=O), 152.66, 148.04, 147.99, 138.67, 138.55, 138.41, 138.18, 137.98, 137.77, 137.40, 128.58, 128.52, 128.47, 128.35, 128.33, 128.31, 128.29, 128.21, 128.16, 127.97, 127.91, 127.90, 127.87, 127.75, 127.70, 127.64, 127.52, 127.26, 127.01, 126.68, 126.61, 119.56, 109.23, 108.28, 105.68, 102.55, 96.83, 84.92, 82.36, 81.30, 79.58, 78.64, 77.39, 77.27, 77.07, 76.75, 75.53, 75.17, 74.94, 74.78, 74.39, 74.02, 73.55, 72.11, 71.42, 71.14, 70.58, 70.56, 70.36, 70.11, 69.15, 68.97, 68.37, 50.23, 49.81, 36.95, 36.81, 29.62, 29.44, 27.47, 21.17, 20.24, 20.14.

HRMS (ESI) m/z calculated for C₈₇H₉₇N₃O₁₇ [M+Na]⁺ 1487.6716, found 1478.6716.

1,2,3,6,2',3'-hexa-O-benzyl-6'-O-propargyl-4-O-(α-D-glucopyranosyl)-β-D-glucopyranose, **39**



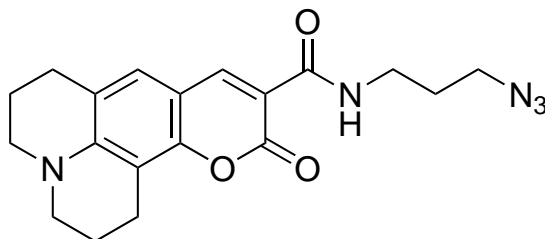
39

A solution of the alcohol **17** (500 mg, 0.50 mmol) and NaH (42 mg, 1.03 mmol) in THF (4.1 mL) was stirred for 20 min at RT. The RM was cooled to 0 °C, DMPU (1.4 mL) was added to the RM and allowed to stir for 10 min. Propargyl bromide (97 μ L, 1.03 mmol) was added and the RM was stirred ON at RT. The reaction was quenched with water (10 mL) and extracted with EtOAc. The combined organic layer was washed with brine and water, dried over Na₂SO₄ and concentrated. The crude product was purified by column chromatography (PE/EtOAc: 20%) to give the alkyne **39** (480 mg, 95 %) as a viscous oil.

¹H NMR (400 MHz, CDCl₃) δ 7.49 – 7.06 (m, 35H, Ar-CH), 5.68 (dd, J = 15.4, 3.7 Hz, 1H, H-1), 5.11 – 4.42 (m, 15H, Bn-CH₂, H-1'), 4.22 – 3.36 (m, 14H, skeletal protons, propargyl CH₂), 2.31 (dt, J = 10.8, 2.3 Hz, 1H, propargyl CH).

HRMS (ESI) m/z calculated for C₆₄H₆₆O₁₁ [M+Na]⁺ 1033.4503, found 1033.4501.

N-(3-azidopropyl)-11-oxo-2,3,6,7-tetrahydro-1H,5H,11H-pyrano[2,3-f]pyrido[3,2,1-ij]quinoline-10-carboxamide, **40**



40

Coumarin 343 (142 mg, 0.5 mmol) and 3-azido-1-propyl-amine (50 μ L, 0.5 mmol) were dissolved in dry CH₂Cl₂ (5.0 mL). T3P (50 % in DMF, 0.43 mL, 0.74 mmol) followed by Et₃N (0.7 mL, 4.9 mmol) were added to the RM. The RM was stirred at RT for 4 h. The RM was washed with saturated bicarbonate and extracted with CH₂Cl₂. The combined organic extracts were washed with H₂O and brine, dried using Na₂SO₄,

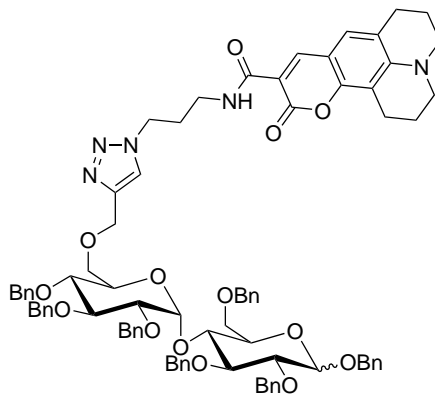
and concentrated under reduced pressure. The crude product was purified by column chromatography (CH₂Cl₂/MeOH: 10%) to yield **40** (137 mg, 74%) as a white solid.

¹ H NMR (400 MHz, CDCl₃) δ 8.95 (s, 1H, O=C-NH), 8.60 (s, 1H, Ar-CH), 7.01 (s, 1H, Ar-CH), 3.53 (q, J = 6.6 Hz, 2H, coumarin Bn-CH₂), 3.49 – 3.25 (m, 6H, coumarin Bn-CH₂, 2 × coumarin CH₂N), 2.89 (t, J = 6.4 Hz, 2H, -CH₂N₃), 2.77 (t, J = 6.2 Hz, 2H, -NHCH₂-), 2.09 – 1.77 (m, 6H, -CH₂CH₂N₃, 2 × coumarin NCH₂CH₂).

¹³C NMR (101 MHz, CDCl₃) δ 163.83 (ester C=O), 163.12 (amide C=O), 152.68, 148.18, 148.13, 127.04, 119.66, 108.82, 108.25, 105.68 (Ar-CH), 50.24, 49.83, 49.26, 36.84, 29.07, 27.47 (2 × coumarin Bn-CH₂, 2 × coumarin CH₂N), -NHCH₂-, -CH₂N₃), 21.14 (coumarin NCH₂CH₂), 20.20 (coumarin NCH₂CH₂), 20.12 (-CH₂CH₂N₃).

HRMS (ESI) m/z calculated for C₂₀H₃₆N₄O₁₄ [M+Na]⁺ 579.2126, found 579.2126.

Benzylated BOT_18, **41**



41

The alkyne **39** (100 mg, 0.1 mmol) and azide **40** (33 mg, 0.09 mmol) were dissolved in CH₂Cl₂/H₂O (1:1, 2 mL). Freshly prepared solution of CuSO₄ · H₂O (45 μL, 0.1 M) and NaAsc (134 μL, 0.1 M) were mixed until brown colour turns yellow. The mixed solution was added to the RM and the reaction allowed to stir ON. The RM was extracted

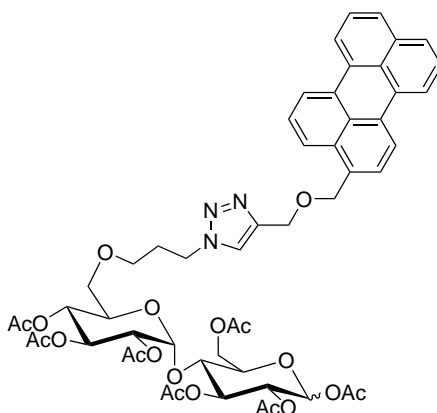
with CH₂Cl₂, organic layer dried over Na₂SO₄ and concentrated. The crude product was purified by column chromatography (CH₂Cl₂/MeOH: 2%) to yield the benzylated conjugate **41** (100 mg, 73.5%) as an orange oil.

¹ H NMR (400 MHz, CDCl₃) δ 8.96 (t, J = 5.9 Hz, 1H, O=C-NH), 8.58 (s, 1H, Coumarin Ar-CH), 7.59 (s, 1H, Pyrazole C-H), 7.48 – 7.09 (m, 35H, Benzyl Ar-CH), 6.98 (s, 1H, Coumarin Ar-CH), 5.68 (dd, J = 18.2, 3.5 Hz, 1H, H-1), 5.03 – 4.41 (m, 18H, 7 × Bn-CH₂, 2 × coumarin Bn-CH₂), 4.30 – 3.22 (m, 18H, 13 × skeletal protons, 2 × coumarin CH₂N, propargyl –OCH₂), 2.89 (t, J = 6.3 Hz, 2H, –NHCH₂–), 2.76 (t, J = 6.0 Hz, 2H, –CH₂N₃), 2.12-1.98 (m, 6H, –CH₂CH₂N₃, 2 × coumarin NCH₂CH₂).

¹³C NMR (101 MHz, CDCl₃) δ 164.13 (O=C-O), 163.10 (O=C-NH), 152.75, 148.31, 148.18 (coumarin Ar-CH), 144.64, 138.81, 138.46, 138.37, 138.27, 138.02, 137.49 (maltose Bn-CH₂), 128.51, 128.43, 128.39, 128.36, 128.33, 128.31, 128.30, 128.26, 128.23, 128.20, 128.02, 127.83, 127.78, 127.75, 127.70, 127.62, 127.52, 127.45, 127.11, 126.74, 126.65, 123.11 (maltose Bn-CH), 119.73, 108.57, 108.25, 105.70 (coumarin Ar-CH), 102.36 (maltose C-1), 96.84 (maltose C-1'), 84.80, 82.32, 81.98, 79.33, 77.39, 77.08, 76.76, 74.67, 73.40, 73.25, 72.93, 71.00, 64.81 (maltose skeletal protons), 50.27, 49.85, 47.87, 36.37, 30.64, 27.47 (2 × coumarin Bn-CH₂, 2 × coumarin CH₂N, –NHCH₂–, –CH₂N₃), 21.13 (coumarin NCH₂CH₂), 20.19 (coumarin NCH₂CH₂), 20.12 (–CH₂CH₂N₃).

HRMS (ESI) m/z calculated for C₈₃H₈₉N₅O₁₄ [M+Na]⁺ 1402.6304, found 1402.6299.

Acetylated BOT_47, **44**



39

The azide **14** (39.9 mg, 0.054 mmol) and Perylene-azide **43c** (15.6 mg, 0.049 mmol) were dissolved in DMF (0.6 ml). Freshly prepared solution of $\text{CuSO}_4 \cdot \text{H}_2\text{O}$ (27 μL , 0.1 M) and NaAsc (325 μL , 0.1 M) were mixed until brown colour turns yellow. The mixed solution was added to the RM and the reaction allowed to stir ON. TBTA (271 μL , 20 mM) was added to the above mixture. The mixed solution was added to the RM and the reaction allowed to stir ON. The RM was directly injected into HPLC and purified (MeCN/ H_2O : 20% to 95% over 90 min) to yield **44** (28 mg, 49%) as a yellow solid.

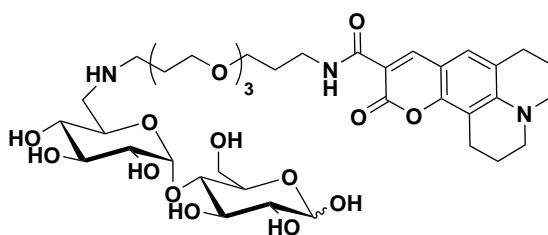
$^1\text{H NMR}$ (400 MHz, CDCl_3) δ 8.38 – 8.07 (m, 4H, perylene C-H), 7.94 (d, $J = 8.1$ Hz, 1H), 7.68 (t, $J = 7.7$ Hz, 3H, perylene C-H), 7.61 – 7.44 (m, 4H, perylene C-H), 7.37 (d, $J = 4.5$ Hz, 1H, pyrazole CH), 6.23 (d, $J = 3.6$ Hz, 0.7H, H-1 α), 5.73 (d, $J = 8.2$ Hz, 0.3H, H-1 β), 5.59 – 5.13 (m, 4H, H-1', H-3', H-4, H-2), 5.13 – 4.76 (m, 6H, H-2', H-5', 2 \times –OCH₂), 4.65 – 4.35 (m, 3H, H-4, H-4', H-5), 4.21 (dd, $J = 12.1, 3.3$ Hz, 1H, H-6a), 4.15 – 3.96 (m, 2H, H-6b, H-6'a), 3.83 (d, $J = 9.8$ Hz, 1H, H-6'b), 3.41 (dd, $J = 46.5, 39.0$ Hz, 4H, –CH₂N₃, –NCH₂), 2.38 – 1.76 (m, 23H, CH₃), –CH₂CH₂CH₂N₃.

$^{13}\text{C NMR}$ (101 MHz, CDCl_3) δ 170.56, 170.50, 170.09, 169.97, 169.62, 168.84 (C=O), 144.98, 134.62, 133.05, 133.01, 131.59, 131.22, 131.05, 129.18, 129.01, 128.46,

128.10, 127.95, 127.90, 127.58, 126.82, 126.59, 123.89, 123.22, 120.39, 120.35, 120.31, 119.61 (perylene Ar-CH), 95.86 (C-1 α), 91.28 (C-1 β), 88.85 (C-1'), 77.37, 77.05, 76.74, 75.28, 72.99, 72.50, 72.30, 71.00, 70.06, 69.68, 69.55, 68.59, 68.04, 67.80, 63.75, 62.75, 60.41, 46.99, 30.31, 21.06, 20.87, 20.85, 20.81, 20.71, 20.63, 20.61, 20.56 (CH₃).

HRMS (ESI) m/z calculated for C₅₃H₅₇N₃O₁₉ [M+Na]⁺ 1062.3484 found 1062.3485.

Maltose-PEG-Coumarin 343 conjugate, **BOT_15**



BOT_15

Benzylated conjugate (20 mg, 13.8 μ mol) and pentamethylbenzene (43 mg, 0.290 mmol) were dissolved in 2 mL of anhydrous CH₂Cl₂. The solution was cooled to -78 °C and BCl₃ (0.58 mL, 0.58 mmol) was added slowly along the flask wall. After the solution was stirred for 1.5 h, DIPEA (0.11 mL, 0.67 mmol) was added to the flask, followed by MeOH (2 mL) to quench the reaction. The reaction was then warmed to RT, and the solvents were removed under reduced pressure. The resulting solid was dissolved in 5:3 MeOH/1,4-dioxane and purified by preparative HPLC (MeCN/H₂O: 20% to 95% over 90 min) yielding the desired conjugate **BOT_15** (4 mg, 36%).

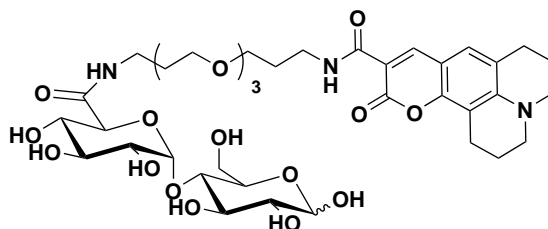
¹H NMR (500 MHz, MeOD) δ 8.56 (s, 1H, coumarin Ar-CH), 7.17 (s, 1H, coumarin Ar-CH), 5.52 (dd, J = 12.2, 3.9 Hz, 1H, H-1), 5.12 (d, J = 3.8 Hz, 1H, H-1'), 4.51 (d, J = 7.8 Hz, 1H,), 4.04 – 3.38 (m, 27H, skeletal protons, -OCH₂, coumarin CH₂N), 3.28 – 3.11 (m, 6H, coumarin CH₂N, 2 \times coumarin Bn-CH₂), 2.85 (dt, J = 31.5, 6.2 Hz,

4H, 2 × PEG –CH₂NH), 2.10 – 1.80 (m, 6H, 2 × coumarin –CH₂CH₂N, 2 × PEG –CH₂CH₂NH).

¹³C NMR (101 MHz, MeOD) δ 164.39, 162.99 (C=O), 152.67, 148.80, 147.87, 127.62, 127.09, 126.11, 120.40, 107.99, 107.02, 105.15, 99.33, 99.22 (C-1 α), 96.83 (C-1 β), 92.49 (C-1'), 76.77, 75.96, 75.01, 74.62, 73.64, 73.14, 72.54, 72.19, 72.07, 72.04, 70.08, 69.89, 69.84, 69.82, 69.69, 68.71, 68.50, 68.41, 60.61, 36.82, 29.07, 27.03, 20.77, 19.82, 19.63.

HRMS (ESI) m/z calculated for C₃₈H₅₇N₃O₁₆ [M+Na]⁺ 834.3637 found 834.3637.

Maltose PEG coumarin 343 conjugate, **BOT_16**



BOT_16

Benzylated conjugate (65 mg, 0.04 mmol) and pentamethylbenzene (285 mg, 1.2 mmol) were dissolved in 6 mL of anhydrous CH₂Cl₂ to give a light yellow solution. This solution was cooled to -78 °C and BCl₃ (0.94 mL, 0.84 mmol) was added slowly along the flask wall. After the solution was stirred for 1.5 h, DIPEA (0.357 mL, 2.04 mmol) was added to the flask, followed by MeOH (2 mL) to quench the reaction. The reaction was then warmed to RT, and the solvents were removed under reduced pressure. The resulting solid was dissolved in 5:3 MeOH/1,4-dioxane and purified by preparative HPLC (MeCN/H₂O: 20% to 95% over 90 min) yielding the desired conjugate **BOT_16** (16 mg, 45%) as an orange solid.

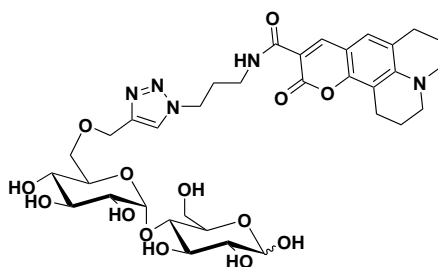
¹H NMR (500 MHz, D₂O) δ 8.20 (s, 1H, NH), 7.84 (s, 1H, coumarin Ar-CH), 6.95 (s,

1H, coumarin Ar-CH), 5.38 (d, J = 2.5 Hz, 1H, H-1), 5.11 (d, J = 3.8 Hz, 1H, H-1'), 4.52 (d, J = 8.0 Hz, 1H, H-5'), 3.96 – 2.95 (m, 24H, skeletal protons, –OCH₂, coumarin CH₂N), 2.78 – 2.46 (m, 6H, coumarin CH₂N, 2 × coumarin Bn-CH₂), 1.83 (dd, J = 12.5, 6.3 Hz, 4H, 2 × PEG –CH₂NH), 1.27 - 1.09 (m, 8H, 2 × coumarin –CH₂CH₂N, 2 × PEG –CH₂CH₂NH).

¹³C NMR (101 MHz, D₂O) δ 170.68, 164.81, 164.80, 163.33 (4 × C=O), 151.60, 148.90, 148.88, 127.02, 120.62, 107.53, 104.44, 104.38, 99.87, 95.78 (C-1), 91.85 (C-1), 77.24, 77.01, 76.09, 74.39, 74.38, 73.95, 73.93, 73.14, 72.49, 72.15, 71.27, 69.85, 69.67, 69.65, 69.61, 69.59, 69.54, 69.38, 69.01, 68.98, 68.19, 68.17 (skeletal protons, -OCH₂), 60.54, 49.90, 49.33, 37.08, 36.19, 28.50, 28.17, 26.66, 20.08, 19.03.

HRMS (ESI) m/z calculated for C₃₈H₅₅N₃O₁₇ [M+Na]⁺ 848.3429, found 848.3429.

Maltose triazole coumarin conjugate, **BOT_18**



BOT_18

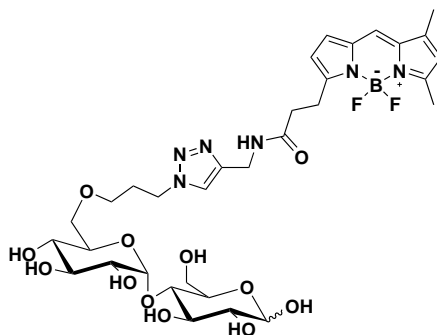
Benzylated conjugate (22.0 mg, 15.9 μmol) and pentamethylbenzene (66.2 mg, 0.45 mmol) were dissolved in 2 mL of anhydrous CH₂Cl₂ to give a light yellow solution. This solution was cooled to -78 °C and BCl₃ (0.45 mL, 0.45 mmol) was added slowly along the flask wall. After the solution was stirred for 1.5 h, DIPEA (0.11 mL, 0.34 mmol) was added to the flask, followed by MeOH (2 mL) to quench the reaction. The reaction was then warmed to RT, and the solvents were removed under reduced pressure. The resulting solid was dissolved in 5:3 MeOH/1,4-dioxane and purified by preparative

HPLC (MeCN/H₂O: 20% to 95% over 90 min) yielding the desired conjugate **BOT_18** (3.3 mg, 28%) as a orange solid.

¹ H NMR (400 MHz, D₂O) δ 8.38 (br, 1H, NH), 8.03 (s, 1H, pyrazole-CH), 7.84 (s, 1H, couamrin Ar-CH), 6.64 (s, 1H, coumarin Ar-CH), 5.19 (br, 1H, maltose H-1), 4.67 – 4.48 (m, 4H, –OCH₂C–, –NCH₂–), 4.06 – 3.12 (m, 19H, maltose skeletal protons, 2 × coumarin –NCH₂–, linker –NCH₂–), 2.44 (d, J = 38.3 Hz, 4H, 2 × Bn-CH₂), 2.33 – 2.13 (m, 2H, linker –NCH₂CH₂–), 1.78 (s, 4H, 2 × coumarin –NCH₂CH₂–).

HRMS (ESI) m/z calculated for C₃₄H₄₅N₅O₁₄ [M+Na]⁺ 770.2861, found 770.2861.

Maltose triazole BODIPY conjugate, **BOT_44**



BOT_44

The azide **BOT_42** (10.0 mg, 0.024 mmol) and BODIPY-alkyne **43a** (6.96 mg, 0.021 mmol) were dissolved in DMF/H₂O (1:4, 2 mL). Freshly prepared solution of CuSO₄ · H₂O (100 mM, 11.8 μL) and NaAsc (100 mM, 141 μL) were mixed until brown colour turns yellow. TBTA (100 mM, 47.0 μL) was added to mixture. The resulting mixture was added to the RM and allowed to stir ON at RT. The RM was directly injected into HPLC and purified (MeCN/H₂O: 20% to 95% over 90 min) to yield **BOT_44** (15 mg, 85%) as an yellow solid.

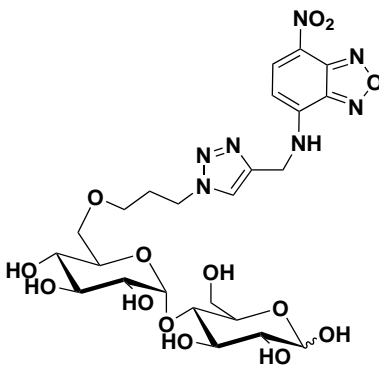
¹ H NMR (400 MHz, D₂O) δ 7.62 (s, 1H, pyrazole C-H), 7.03 (s, 1H, BODIPY Ar-CH),

6.72 (s, 1H, BODIPY Ar-CH), 6.13 (s, 1H, BODIPY Ar-CH), 5.92 (s, 1H, BODIPY Ar-CH), 5.33 – 5.06 (m, 1H, maltose H-1), 4.60 (d, J = 7.7 Hz, 1H, maltose H-1'), 4.32 (d, J = 22.6 Hz, 4H, linker –CH₂N–, BODIPY –NHCH₂–), 4.10 – 3.44 (m, 12H, skeletal protons, linker –OH₂–), 3.30 (dd, J = 36.1, 8.0 Hz, 4H, skeletal protons), 3.15 (d, J = 60.2 Hz, 2H, BODIPY –COCH₂–), 2.59 (s, 2H, BODIPY –CH₂CH₂C–), 2.28 (s, 3H, BODIPY–CH₃), 1.94 (s, 5H, BODIPY-CH₃, maltose –OCH₂CH₂–).

¹³C NMR (101 MHz, CDCl₃) δ 174.06 (C=O), 160.51, 160.40, 155.99, 145.27, 144.59, 134.95, 133.00, 128.57, 124.28, 123.66, 101.88, 100.41, 99.90, 98.24, 98.23 (maltose C-1), 95.81 (maltose C-1'), 91.90, 91.86, 78.39, 77.82, 77.64, 76.07, 74.60, 74.58, 73.93, 73.89, 73.12, 72.91, 71.76, 71.68, 71.55, 71.26, 70.06, 70.01, 69.55, 69.47, 69.35, 67.57, 66.78, 60.72, 53.86, 47.17, 34.35, 29.32, 29.27, 24.14, 14.15 (BODIPY–CH₃), 10.42 (BODIPY –CH₃).

HRMS (ESI) m/z calculated for C₃₂H₄₅BF₂N₆O₁₂ [M+Na]⁺ 777.3055, found 777.3054.

Maltose triazole NBD conjugate, **BOT_45**



BOT_45

The azide **BOT_42** (20.0 mg, 0.047 mmol) and NBD-alkyne **43b** (9.23 mg, 0.042 mmol) were dissolved in DMF/H₂O (1:4, 1.2 mL). Freshly prepared solution of

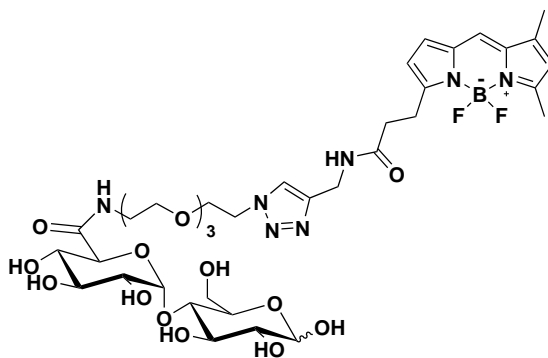
CuSO₄ · H₂O (100 mM, 23.5 μL) and NaAsc (100 mM, 282 μL) were mixed until brown colour turns yellow. TBTA (100 mM, 47.0 μL) was added to mixture. The mixed solution was added to the RM and the reaction allowed to stir ON. The RM was directly injected into HPLC and purified (MeCN/H₂O: 20% to 95% over 90 min) to yield **BOT_45** (22 mg, 72.7%) as a red solid.

¹H NMR (400 MHz, CDCl₃) δ 8.01 (s, 2H, NBD-CH, pyrazole C-H), 6.10 (s, 1H, NBD-CH), 5.16 (dd, J = 29.1, 3.9 Hz, 1H, H-1), 3.97 – 2.99 (m, 20H, skeletal protons, –OCH₂–, –CH₂N, –NHCH₂), 2.09 (d, J = 5.3 Hz, 2H, –OCH₂CH₂CH₂N).

¹³C NMR (101 MHz, CDCl₃) δ 144.06, 142.53, 138.29, 137.78, 124.66, 101.86, 100.35, 99.71, 98.21, 95.75, 94.27, 91.84, 77.38, 76.07, 74.54, 74.07, 73.91, 73.08, 72.81, 71.69, 71.58, 71.45, 71.23, 71.08, 69.92, 69.68, 69.43, 69.38, 69.08, 67.87, 67.64, 66.77, 60.74, 47.49, 38.69, 29.11.

HRMS (ESI) m/z calculated for C₂₄H₃₃N₇O₁₄ [M+Na]⁺ 666.1983, found 666.1983.

Maltose PEG BODIPY conjugate, **BOT_48**



BOT_48

The azide **BOT_42** (25.0 mg, 0.045 mmol) and BODIPY-alkyne **43a** (13.3 mg, 0.040 mmol) were dissolved in DMF/H₂O (1:4, 1.2 mL). Freshly prepared solution of CuSO₄ · H₂O (100 mM, 22.46 μL) and NaAsc (100 mM, 270 μL) were mixed until

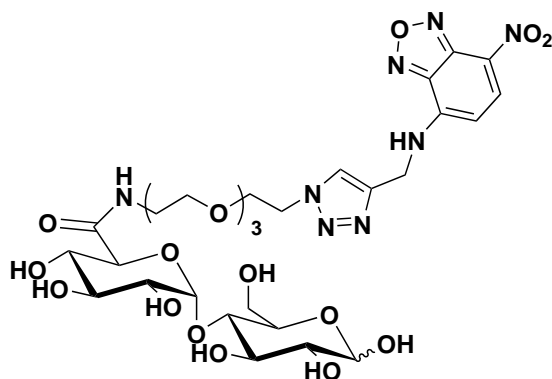
brown colour turns yellow. TBTA (100 mM, 47.0 μ L) was added to the above mixture. The mixed solution was added to the RM and the reaction allowed to stir ON. The RM was directly injected into HPLC and purified (MeCN/H₂O: 20% to 95% over 90 min) to yield **BOT_48** (6.6 mg, 17%) as an red solid.

¹ **H NMR (400 MHz, D₂O)** δ 7.59 (d, J = 15.0 Hz, 1H, BODIPY-CH), 7.25 (d, J = 6.2 Hz, 1H, BODIPY-CH), 6.83 (s, 1H, pyrazole-CH), 6.32 (d, J = 14.6 Hz, 1H, BODIPY-CH), 6.14 (d, J = 4.1 Hz, 1H, BODIPY-CH), 5.32 (s, 1H, maltose H-1), 5.09 (s, 1H, maltose H-1'), 4.61 – 4.44 (m, 1H, maltose H-3), 4.43 – 4.22 (m, 4H, maltose skeletal protons), 4.19 – 3.10 (m, 27H, maltose skeletal protons, –OCH₂), 2.98 (dd, J = 14.3, 7.1 Hz, 2H, BODIPY-COCH₂), 2.59 (dd, J = 11.0, 6.8 Hz, 2H, BODIPY-CH₂C), 2.35 (d, J = 20.2 Hz, 3H, CH₃), 2.15 (d, J = 40.8 Hz, 3H, CH₃).

¹³ **C NMR (101 MHz, D₂O)** δ 174.64 (C=O), 174.20 (C=O), 170.96, 163.27, 163.04, 162.80, 162.57, 159.91, 150.66, 144.34, 132.94, 127.94, 125.68, 124.56, 124.21, 124.11, 119.28, 119.19, 117.26, 115.32, 113.39, 99.83, 99.79, 99.75, 99.67, 95.76 (BODIPY Ar-CH) (maltose C-1), 91.87 (maltose C-1'), 76.99, 76.88, 76.78, 76.60, 76.12, 74.36, 74.01, 73.99, 73.15, 72.45, 72.41, 72.16, 71.35, 71.29, 71.24, 69.79, 69.63, 69.61, 69.55, 69.51, 69.41, 69.35, 68.64, 68.61, 60.52, 60.43, 50.12, 49.93, 38.82, 34.20, 34.15, 34.05, 24.16, 24.00, 14.12 BODIPY-COCH₂, 13.87 (BODIPY-CH₂C), 11.26 (-CH₃), 10.48 (-CH₃), 10.45 (-CH₃).

HRMS (ESI) m/z calculated for C₃₇H₅₄BF₂N₇O₁₅ [M+Na]⁺ 908.3625, found 908.3621.

Maltose PEG NBD conjugate, **BOT_50**



BOT_50

The azide **BOT_49** (25 mg, 0.045 mmol) and NBD-alkyne **43b** (8.82 mg, 0.040 mmol) were dissolved in DMF/H₂O (1:4, 2 mL). Freshly prepared solution of CuSO₄ · H₂O (100 mM, 22.46 μL) and NaAsc (100 mM, 270 μL) were mixed until brown colour turns yellow. TBTA (100 mM, 47.0 μL) was added to the above mixture. The mixed solution was added to the RM and the reaction allowed to stir ON. The RM was directly injected into HPLC and purified (MeCN/H₂O: 20% to 95% over 90 min) to yield **BOT_50** (5 mg, 15%) as an yellow solid.

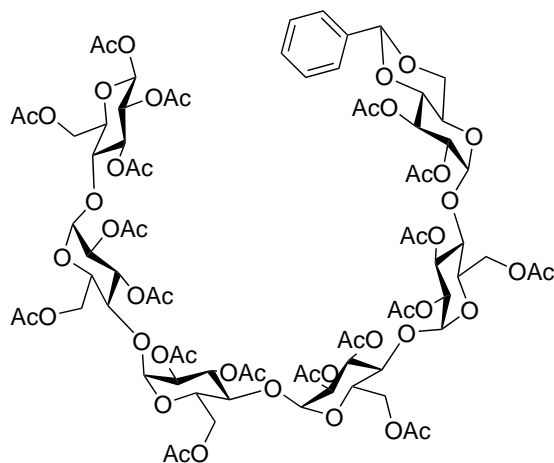
¹H NMR (400 MHz, CDCl₃) δ 8.49 (d, J = 8.9 Hz, 1H, NBD-CH), 8.03 (s, 1H, pyrazole-CH), 6.39 (d, J = 9.0 Hz, 1H, NBD-CH), 5.38 (d, J = 3.8 Hz, 1H, H-1), 5.12 (d, J = 3.8 Hz, 1H, H-1'), 4.64 – 4.45 (m, 2H, –NHCH₂–), 4.26 – 3.04 (m, 27H, skeletal protons, –OCH₂).

¹³C NMR (101 MHz, CDCl₃) δ 170.96 (C=O), 144.61, 144.09, 138.90, 124.77, 99.78, 99.66 (NBD-CH), 95.75 (maltose C-1), 91.86 (maltose C-1'), 76.86, 76.60, 76.13, 74.37, 74.00, 73.15, 72.44, 72.40, 72.14, 71.34, 71.28, 71.23, 69.78, 69.59, 69.50, 69.42, 69.34, 68.71, 68.64, 60.54 (skeletal protons, –OCH₂), 60.44 ((–CH₂N–)), 50.14

NBD ($-\text{NHCH}_2-$), 38.80 PEG ($-\text{NHCH}_2-$).

HRMS (ESI) m/z calculated for $\text{C}_{29}\text{H}_{42}\text{N}_8\text{O}_{17}$ $[\text{M}+\text{Na}]^+$ 797.2566, found 797.2562.

Acetylated maltohexose benzylidene acetal, **50**



50

Maltohexose (500 mg, 0.505 mmol), benzaldehyde dimethylacetal (738 μL , 5.05 mmol) and PTSA (28.8 mg, 0.151 mmol) were dissolved in dry DMF (76 mL). The mixture was rotated for 6 hours on a rotary evaporator under reduced pressure (39 mbar) at 50 $^{\circ}\text{C}$. The solution was neutralised with Et_3N (0.50 mL). The solvent was removed under reduced pressure to yield **54** as a viscous liquid. The crude product was used further without any purification. The crude product was dissolved in acetic anhydride (1 mL) and the reaction heated to reflux. Sodium acetate (78 mg, 0.918 mmol) was added portion-wise to the refluxing reaction. The RM was stirred for 1.5 h under reflux then poured onto ice-cold water (500 mL) with vigorous stirring to precipitate the expected product. The crude product was collected by vacuum filtration and purified by column chromatography (PE/EtOAc: 60%) to give **50** (197 mg, 53%) as a white solid.

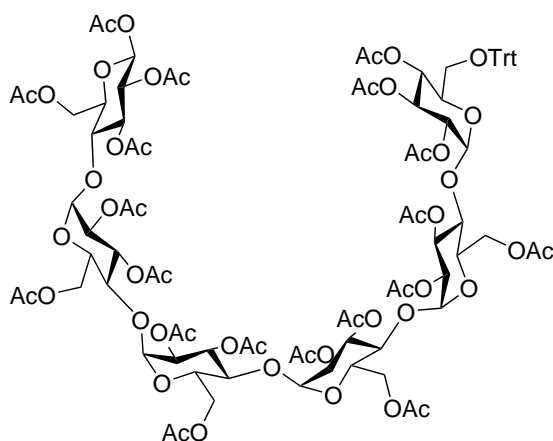
$^1\text{H NMR}$ (400 MHz, CDCl_3) δ 7.56 – 7.16 (m, 6H, Ar-CH), 5.70 (d, $J = 8.0$ Hz, 1H, H-1), 5.59 – 5.13 (m, 10H, skeletal protons), 5.05 – 3.49 (m, 31H, skeletal protons),

2.41 – 1.66 (m, 54H, 18 × CH₃).

¹³C NMR (101 MHz, CDCl₃) δ 170.96, 170.68, 170.41, 170.25, 169.60, 168.83 (C=O), 136.64, 129.12, 128.20, 126.21 (Bn-CH), 101.64 (C-1), 96.30, 95.64, 91.25 (Anomeric C), 78.78, 77.43, 77.11, 76.79, 75.19, 72.95, 71.90, 70.80, 70.46, 68.97, 68.38, 63.69, 61.97, 40.87, 33.80 (skeletal C), 28.42, 23.86, 20.84, 20.81, 20.76, 20.73, 20.54, 17.48, 17.26 (CH₃).

MS (ESI) m/z calculated for C₇₉H₁₀₂O₄₉ [M+H]⁺ 1834.54, found 1834.40.

maltohexose tritylated , **52**



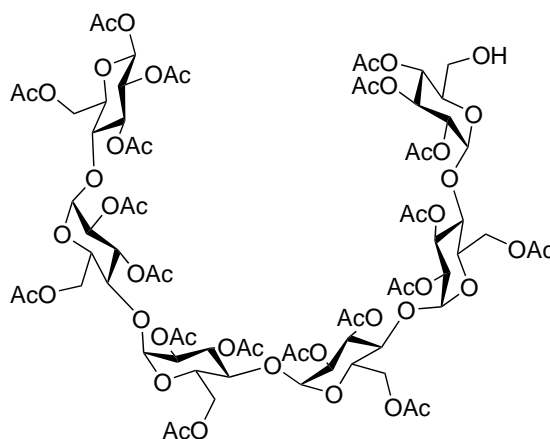
49

To a solution of **50** (197 mg, 23.7 mmol) in acetic acid (2 mL), water (1.6 mL) was added in small portions. The RM was heated at 95 °C for 10 min. The RM was allowed to cool to room temperature (RT) and the solvent was removed under reduced pressure. Traces of water and acetic acid were removed by co-distillation with toluene. The product was purified by column chromatography (CH₂Cl₂/MeOH: 5%) to yield compound **52** (9.48 g, 67%) as colourless solid. To a solution of compound **52** (188 mg, 0.108 mmol) in dry pyridine (6 mL) was added trityl chloride (45 mg, 0.161 mmol). The RM was stirred for 1.5 h at 80 °C after which the RM was cooled to 0 °C. Ac₂O (11 mL) was added and

the RM was allowed to stir ON at RT, The RM was poured into ice cold water (50 mL) and stirred for 5 min. The precipitate was filtered to give the crude product as a yellow solid. The crude product was purified by column chromatography (PE/EtOAc: 30% to 50%) to give **49** (180 mg, 81%) as white solid.

MS (ESI) m/z calculated for C₉₃H₁₁₄O₅₀ [M+H]⁺ 2030.63, found 2030.65.

Maltohexose 6'OH , **48**

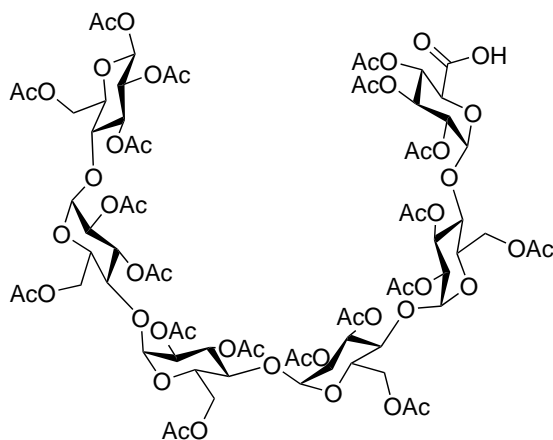


48

Tritylated compound **49** (300 mg, 0.148 mmol) was dissolved in acetic acid (80%, 5 mL) heated at 100 °C for 1 h. The solvent was removed under reduced pressure. The residue was dissolved in a minimum amount of methanol and water was added until incipient turbidity was observed. The suspension was cooled to 0 °C and the precipitated trityl alcohol filtered. The filtrate was concentrated and traces of water were removed by co-distillation with toluene. The crude product was purified by column chromatography (PE/EtOAc: 50% to 70%) to yield **48** (150 mg, 56.8%) was obtained as colourless solid .

MS (ESI) m/z calculated for C₇₄H₁₀₀O₅₀ [M+H]⁺ 1788.52, found 1788.64.

Maltohexose 6' glucuronic acid, **47**



47

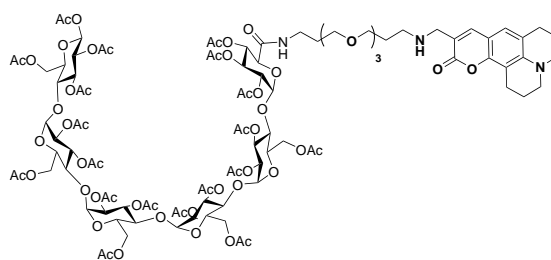
TEMPO (11.79 g, 0.075 mmol) and BAIB (81 mg, 0.251 mmol) were added to a solution of alcohol **48** (150 mg, 10.5 mmol) in $\text{CH}_2\text{Cl}_2/\text{H}_2\text{O}$ (1:1, 300 μL). The RM was ON at RT and quenched with saturated $\text{Na}_2\text{S}_2\text{O}_3$ (2 mL). The resulting solution was extracted with EtOAc. The combined organic extracts were washed with H_2O and brine, dried using Na_2SO_4 , and concentrated under reduced pressure. The crude product was purified by column chromatography ($\text{CH}_2\text{Cl}_2/\text{MeOH}$: 5% to 10%) to yield **47** (75 g, 50%) as a white solid.

$^1\text{H NMR}$ (400 MHz, CDCl_3) δ 10.02 (s, 1H, COOH), 5.75 (d, $J = 8.1$ Hz, 1H, H-1), 5.57 – 5.18 (m, 10H, skeletal protons), 5.17 – 3.52 (m, 31H, skeletal protons), 2.35 – 1.85 (m, 54H, $18 \times \text{CH}_3$).

$^{13}\text{C NMR}$ (101 MHz, CDCl_3) δ 170.69, 170.69, 170.40, 170.40, 170.24, 169.67, 169.67, 169.59, 169.59, 168.84, 168.84 (C=O), 101.67 (C-1), 96.32, 95.66, 95.66, 91.27 (anomeric C), 77.35, 77.35, 77.04, 77.04, 76.72, 76.72, 75.22, 72.98, 72.98, 71.77, 70.46, 70.46, 68.98, 68.98 (skeletal C), 20.87, 20.87, 20.80, 20.80, 20.58, 20.58 (CH_3).

MS (ESI) m/z calculated for $\text{C}_{74}\text{H}_{98}\text{O}_{51}$ $[\text{M}+\text{H}]^+$ 1803,5153, found 1803,5153.

Acetylated maltohexose-coumarin conjugate, **45**

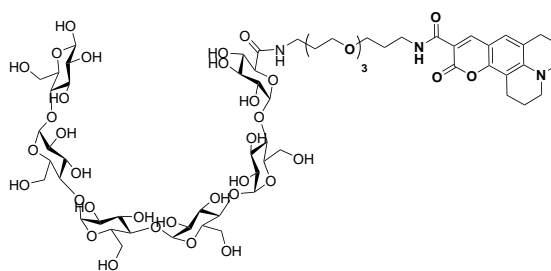


45

The acid **47** (14.0 mg, 7.76 μmol) and the amine **31** (4.49 mg, 8.59 μmol) were dissolved in dry CH_2Cl_2 (51.7 μL). T3P (50 % in DMF, 6.51 μL , 0.012 μmol) followed by Et_3N (10.91 μL , 0.078 mmol) were added to the RM. The RM was stirred at RT for 4 h. The RM was washed with saturated bicarbonate and extracted with CH_2Cl_2 . The combined organic extracts were washed with H_2O and brine, dried using Na_2SO_4 , and concentrated under reduced pressure. The crude product was purified by column chromatography ($\text{CH}_2\text{Cl}_2/\text{MeOH}$: 10%) to yield **45** (10 mg, 56%) as a white solid.

ESI m/z calculated for $\text{C}_{100}\text{H}_{135}\text{N}_3\text{O}_{55}$ $[\text{M}+\text{H}]^+$ 2258,79, found 2258,82.

Maltohexose coumarin conjugate, **BOT_51**



BOT_51

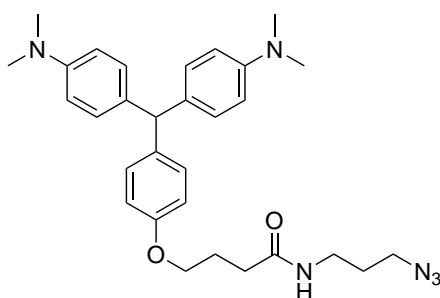
To a solution of **45** (10 mg, 5.28 μmol) in methanol (2 ml) was added catalytic amount of sodium methoxide (4 μL , mmol). The RM was stirred ON at RT, acidified with Amberlyst IR-120 until pH 2 and filtered. The filtrate was concentrated to give the

crude product. The crude product was purified by flash chromatography using HPLC (MeCN/H₂O: 20% to 95% over 90 min) to give **BOT_51** (0.7 mg, 10.4%) as a colourless liquid.

MS (ESI) m/z calculated for C₆₂H₉₇N₃O₃₆ [M+H]⁺ 1482.5751, found 1482.5751.

N-(3-azidopropyl)-4-(4-(bis(4-(dimethylamino)phenyl)methyl)phenoxy)butanamide,

56



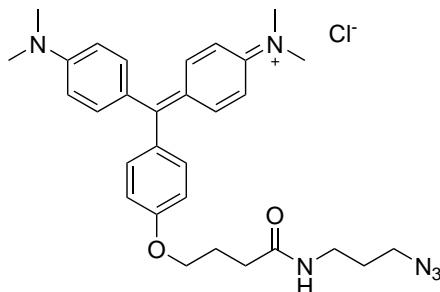
56

The acid **55** (225 mg, 0.520 mmol) was dissolved in CH₂Cl₂ (1 mL) and 3-azidopropylamine (56.2 μL, 0.572 mmol) was added to it. T3P (0.456 mL, 0.780 mmol) followed by Et₃N (0.725 mL, 5.20 mmol) was added to the RM. The RM was stirred ON at RT. RM was diluted with DCM (2 mL), extracted with Bicarbonate (2 mL), followed by water (2 × 3 mL). The OL was dried with Na₂SO₄ and concentrated to give **58** (100 mg, 37%).

¹ **H NMR (400 MHz, MeOD)** δ 7.36 (dt, J = 9.6, 5.7 Hz, 6H, Ar-CH), 7.27 – 7.20 (m, 2H, Ar-CH), 7.20 – 7.10 (m, 4H, Ar-CH), 5.71 (s, 1H, CH), 4.39 (t, J = 6.1 Hz, 2H, –OCH₂), 3.77 – 3.63 (m, 4H, –NHCH₂, –CH₂N₃), 3.31 (s, 12H, NCH₃), 2.88 – 2.74 (m, 2H, –CH₂CO), 2.58 – 2.40 (m, 2H, –OCH₂CH₂–), 2.17 (dp, J = 20.2, 6.7 Hz, 2H, CH₂CH₂CH₂N₃).

HRMS (ESI) m/z calculated for C₃₀H₃₈N₆O₂ [M+Na]⁺ 537.2954, found 537.2954.

N-(4-((4-(4-((3-azidopropyl)amino)-4-oxobutoxy)phenyl)(4-(dimethylamino)phenyl)methylene)cyclohexa-2,5-dien-1-ylidene)-N-methylmethanaminium, **57**

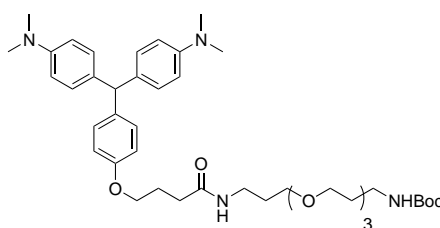


57

To a light blue solution of **56** (100 mg, 0.194 mmol) in EtOAc (1.0 mL) was added p-chloranil (71.7 mg, 0.291 mmol). The reaction mixture was refluxed for 1 h, filtered and concentrated to yield dark blue oil. The crude material was dissolved in EtOH/HCl (1:1, 1 mL) and stirred for 2 h at 25 °C. The resulting red solution was purified by HPLC to yield **57** (30 mg, 30%) as a dark blue solid.

HRMS (ESI) m/z calculated for $C_{30}H_{37}N_6O_2^+$ [M+H]⁺ 513.2973, found 513.2973.

tert-butyl (3-(3-(4-(4-(bis(4-(dimethylamino)phenyl)methyl) phenoxy)butanamido)propoxy)propyl)carbamate, **58**



58

The acid **55** (84.0 mg, 0.274 mmol) was dissolved in CH₂Cl₂ (0.548 mL) and the PEG linker **28** (0.130 g, 0.302 mmol) was added to it. T3P (0.120 mL, 0.411 mmol) followed by Et₃N (0.382 mL, 2.74 mmol) was added to the RM. The RM was stirred ON at RT.

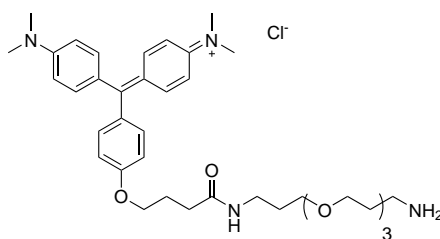
RM was diluted with DCM (2 mL), extracted with Bicarbonate (2 mL), followed by water (2 × 3 mL). The OL was dried with Na₂SO₄ and concentrated to give **58** (75.0 mg, 51%).

¹ H NMR (400 MHz, CDCl₃) δ 6.99 (dd, J = 21.3, 8.6 Hz, 6H, Ar-CH), 6.77 (d, J = 8.6 Hz, 2H, Ar-CH), 6.66 (d, J = 8.7 Hz, 4H, Ar-CH), 5.31 (s, 1H, CH), 3.96 (t, J = 5.9 Hz, 2H, -OCH₂), 3.56 (ddt, J = 20.0, 11.9, 4.9 Hz, 12H, PEG -OCH₂), 3.37 (dd, J = 12.0, 6.0 Hz, 2H, -CH₂NH), 3.20 (d, J = 5.9 Hz, 2H, -NHCH₂), 2.90 (s, 12H, -NCH₃), 2.35 (t, J = 7.3 Hz, 2H, O=CCH₂), 2.10 (dd, J = 13.4, 6.3 Hz, 2H, -OCH₂CH₂-), 1.86 - 1.62 (m, 4H, PEG -NHCH₂CH₂), 1.43 (s, 9H, Boc-CH₃).

¹³C NMR (101 MHz, CDCl₃) δ 172.31 (C=O), 156.99, 148.91, 133.20, 130.22, 129.85, 114.01, 112.54 (Ar-C-H), 77.38, 77.34, 77.06, 77.02, 76.75, 76.70, 70.52, 70.22, 70.13, 66.95 (-OCH₂), 54.16, 40.77 (-NCH₃), 33.07, 28.47 (Boc-CH₃), 25.36 .

HRMS (ESI) m/z calculated for C₃₇H₆₂N₄O₇ [M+Na]⁺ 757.4516, found 757.4517.

N-(4-((4-(4-((3-azidopropyl)amino)-4-oxobutoxy)phenyl)(4-(dimethylamino)phenyl)methylene)cyclohexa-2,5-dien-1-ylidene)-N-methylmethanaminium chloride, **59**



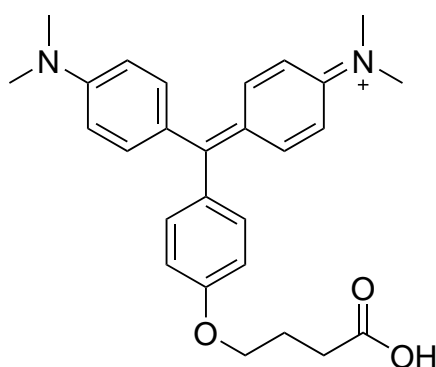
To a light blue solution of **58** (26.5 mg, 0.036 mmol) in EtOAc (1.0 mL) was added p-chloranil (19.5 mg, 0.079 mmol). The reaction mixture was refluxed for 1 h, filtered and concentrated to yield dark blue oil. The crude material was dissolved in EtOH/HCl (1:1, 1 mL) and stirred for 2 h at 25 °C. The resulting red solution was diluted in water

(30 mL) and washed with EtOAc (3 × 20 mL). The aqueous layer was lyophilized to yield a blue solid. The crude material was purified by HPLC to yield **59** (9.5 mg, 43%) as a dark blue solid.

¹H NMR (400 MHz, CDCl₃) δ 7.39 (d, J = 9.4 Hz, 4H, Ar-CH), 7.36 – 7.22 (m, 2H, Ar-CH), 7.12 (d, J = 8.2 Hz, 2H, Ar-CH), 6.88 (d, J = 9.0 Hz, 4H, Ar-CH), 4.20 (d, J = 6.4 Hz, 2H, MG –OCH₂), 3.83 – 3.40 (m, 12H, PEG –OCH₂), 3.27 (d, J = 33.0 Hz, 12H, –NCH₂), 2.47 (s, 2H, PEG–NHCH₂CH₂), 2.18 (s, 2H, PEG–CH₂CH₂NH), 1.81 (d, J = 20.1 Hz, 2H, O=NHCH₂), 1.25 (s, 2H, –CH₂CH₂O).

HRMS (ESI) m/z calculated for C₃₇H₅₄N₄O₅⁺ [M+Na]⁺ 633.4106, found 633.4106.

N-(4-((4-(3-carboxypropoxy)phenyl)(4-(dimethylamino)phenyl)methylene) cyclohexa-2,5-dien-1-ylidene)-N-methylmethanaminium, **60**



60

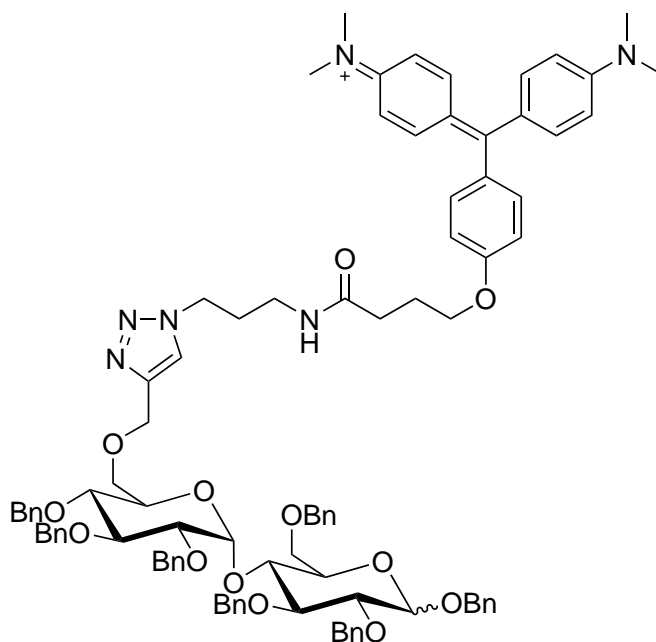
To a light blue solution of compound 42 (200 mg , 462 μmol) in CH₂Cl₂ (5 mL) was added *p*-chloranil (100 mg , 691 μmol). The RM was stirred at RT for 2 h , filtered and concentrated to yield a dark blue coloured solid . The crude material was dissolved in MeOH and purified by HPLC (MeCN/H₂O: 20% to 95% over 90 min). The fractions were lyophilized to yield **60** (85 mg, 43%) as a dark blue colored solid.

¹ H NMR (400 MHz, DMSO) δ 7.21 (dd, J = 24.7, 8.9 Hz, 6H, Ar-CH), 7.00 (d, J = 8.7 Hz, 3H, Ar-CH), 6.87 (d, J = 9.2 Hz, 3H, Ar-CH), 4.04 (s, 2H, -OCH₂), 3.15 (s, 12H, NCH₃), 2.32 (d, J = 7.2 Hz, 2H, -CH₂COOH), 2.05 – 1.90 (m, 2H, -CH₂CH₂COOH).

¹³C NMR (101 MHz, CDCl₃) δ 177.42 (C=O), 163.50 (C=N), 156.14, 139.65, 136.69, 130.97, 126.06, 113.79, 112.23 (Ar-CH), 38.66 (-NCH₃).

HRMS (ESI) m/z calculated for C₂₇H₃₁N₂O₃⁺ [M+H]⁺ 431.2329, found 431.2329.

Benzylated BOT_17, **61**



61

The alkyne **39** (58.5 mg, 0.058 mmol) and azide **40** (27 mg, 0.053 mmol) were dissolved in CH₂Cl₂/H₂O (1:1, 2 mL). Freshly prepared solution of CuSO₄ · H₂O (473 μ L, 0.1 M) and NaAsc (526 μ L, 0.1 M) were mixed until brown colour turns yellow. The mixed solution was added to the RM and the reaction allowed to stir ON. The RM was extracted with CH₂Cl₂, organic layer dried over Na₂SO₄ and concentrated. The crude product was purified by column chromatography (CH₂Cl₂/MeOH: 2%) to yield the benzylated

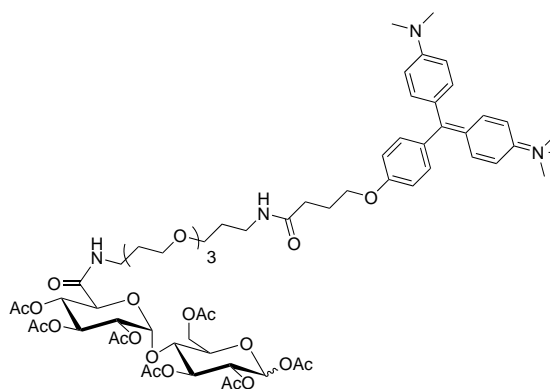
conjugate **61** (76 mg, 95%) as an green oil.

¹ H NMR (400 MHz, CDCl₃) δ 7.44 (s, 1H, pyrazole-CH), 7.40 – 7.05 (m, 35H, Bn-CH), 7.07 – 6.87 (m, 6H, MG-CH), 6.78 (dd, J = 8.9, 2.7 Hz, 3H, MG-CH), 6.68 (m, 3H, MG-CH), 5.79 – 5.67 (m, 1H, H-1), 5.31 (d, J = 9.4 Hz, 1H, H-1'), 5.02 – 4.35 (m, 16H, Bn-CH₂, –OCH₂C–), 4.26 – 3.28 (m, 17H, skeletal protons, –CH₂O–, –CH₂NH–), 3.22 – 3.02 (m, 2H, –CH₂NH–), 2.98 – 2.85 (m, 12H, N-CH₃), 2.36 (dt, J = 18.1, 7.3 Hz, 2H, O=C-CH₂), 2.08 (dd, J = 13.9, 6.5 Hz, 2H, CH₂CH₂CH₂O⁻), 2.02 – 1.85 (m, 2H, CH₂CH₂CH₂NH⁻).

¹³C NMR (101 MHz, CDCl₃) δ 172.77 (C=O), 156.96, 145.18, 138.74, 138.70, 138.44, 138.31, 138.18, 137.93, 137.40 Bn-CH₂), 130.28, 129.91, 128.51, 128.45, 128.41, 128.38, 128.35, 128.34, 128.32, 128.29, 128.25, 128.20, 128.04, 128.02, 127.84, 127.79, 127.73, 127.68, 127.62, 127.57, 127.55, 127.40, 127.15, 126.74, 126.64, 122.77, 114.03 (Bn-CH, MG-CH), 102.37 (C-1), 96.66 (C-2), 84.83, 82.35, 81.97, 79.29, 77.59, 77.36, 77.05, 76.73, 75.54, 74.95, 74.68, 74.49, 73.94, 73.39, 73.26, 71.05 (skeletal protons), 66.77, 64.89, 54.20, 47.43, 36.28, 32.97, 30.03, 25.23 (CH₂, CH₃).

HRMS (ESI) m/z calculated for C₉₄H₁₀₃N₆O₁₃ [M+H]⁺ 1524.7661, found 1524.7660.

Acetylated BOT_52, **62**

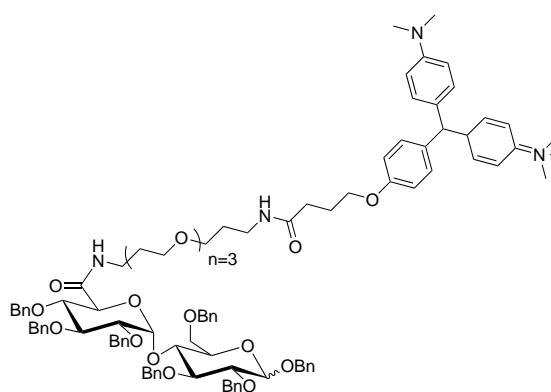


62

The acid **10** (20.4 mg, 0.032 mmol) was dissolved in CH₂Cl₂ (0.548 mL) and the amine **28** (20.0 mg, 0.302 mmol) was added to it. T3P (13.9 μL, 0.047 mmol) followed by Et₃N (27.5 μL, 0.159 mmol) was added to the RM. The RM was stirred ON at RT. RM was diluted with DCM (2 mL), extracted with Bicarbonate (2 mL), followed by water (2 × 3 mL). The OL was dried with Na₂SO₄ and concentrated to give **62** (20 mg, 50%).

HRMS (ESI) m/z calculated for C₆₃H₈₅N₄O₂₃⁺ [M+H]⁺ 1265.5599, found 1265.5599.

Benzylated BOT_52, **64**



64

The acid **38** (14.7 mg, 0.015 mmol) was dissolved in CH₂Cl₂ (0.548 mL) and the amine **28** (9.50 mg, 0.015 mmol) was added to it. T3P (6.55 μL, 0.022 mmol) followed by Et₃N (13.1 μL, 0.075 mmol) was added to the RM. The RM was stirred ON at RT. RM was diluted with DCM (2 mL), extracted with Bicarbonate (2 mL), followed by water (2 × 3 mL). The OL was dried with Na₂SO₄ and concentrated to give **64** (9.6 mg, 40%) as a dark blue solid.

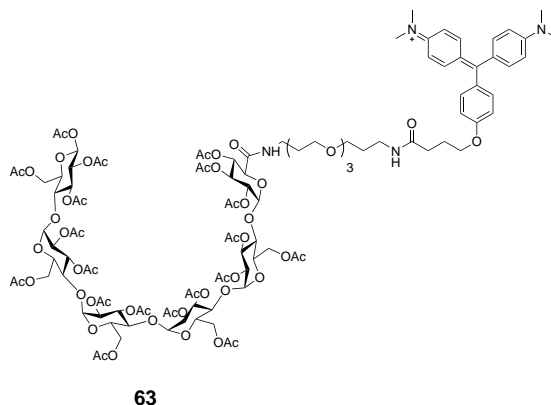
¹H NMR (400 MHz, CDCl₃) δ 8.04 (d, J = 7.4 Hz, 1H, N-H), 7.48 – 6.99 (m, 44H, Bn-CH, MG-CH), 6.88 (d, J = 9.2 Hz, 4H, MG-CH), 5.75 (d, J = 3.4 Hz, 1H, malose H-1), 5.06 – 4.39 (m, 16H, Bn-CH₂, H-1'), 4.29 – 3.40 (m, 28H, skeletal protons, –OCH₂), 3.31 (d, J = 15.3 Hz, 12H, –NCH₃), 2.88 (s, 2H, PEG–CH₂NH–), 2.43 (m,

2H, PEG–NHCH₂–), 2.18 – 2.09 (m, 3H, PEG–NHCH₂CH₂), 1.82 – 1.73 (m, 2H, PEG–CH₂CH₂NH), 1.53 – 1.42 (m, 2H, O=NHCH₂), 1.22 (s, 2H, –CH₂CH₂O).

¹³C NMR (101 MHz, CDCl₃) δ 156.62 (C=O), 140.84 (C=N), 138.76, 138.58, 138.48, 138.36, 138.18, 138.03, 138.00, 137.93, 137.68, 137.51, 137.41, 137.39, 137.32 (Bn-CH₂), 128.58, 128.46, 128.34, 128.32, 128.27, 128.17, 128.08, 127.94, 127.90, 127.69, 127.09, 126.60 (Bn-CH), 115.29, 113.28 (MG-CH), 102.51 (maltose C-1), 96.91 (maltose C-1'), 85.10, 84.05, 82.71, 81.59, 80.02, 78.45, 77.35, 77.03, 76.71, 75.54, 74.04, 73.59, 70.48, 70.04, 68.88, 68.20, 40.90, 39.51, 38.74, 37.95, 36.37, 32.18, 29.49, 29.11, 27.77, 25.08 (N-CH₃).

HRMS (ESI) m/z calculated for C₉₈H₁₁₃N₄O₁₆⁺ [M+H]⁺ 1601.8152, found 1601.8146.

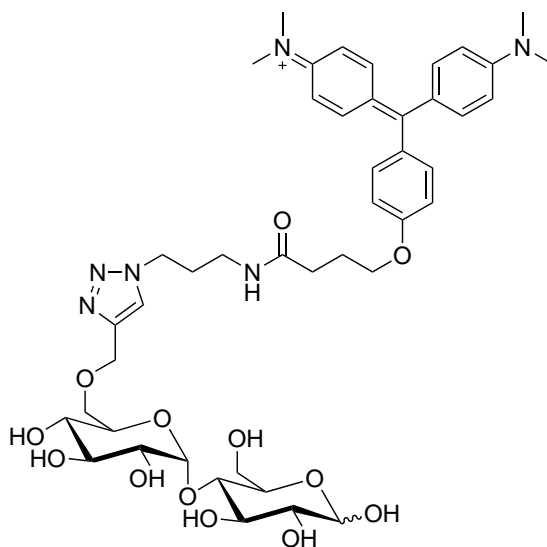
Acetylated maltohexose-MG conjugate, **63**



The acid **63** (14 mg, 7.76 μmol) was dissolved in CH₂Cl₂ (0.548 mL) and the amine **28** (7.38 mg, 0.012 mmol) was added to it. T3P (4.67 μL, 8.00 mmol) followed by Et₃N (10.8 μL, 0.078 mmol) was added to the RM. The RM was stirred ON at RT. RM was diluted with DCM (2 mL), extracted with Bicarbonate (2 mL), followed by water (2 × 3 mL). The OL was dried with Na₂SO₄ and concentrated to give **63** (8 mg, 43%).

MS (ESI) m/z calculated for C₁₁₁H₁₄₉N₄O₅₅⁺ [M+Na]⁺ 2417.90, found 2417.85.

Maltose triazole MG conjugate, **BOT_17**



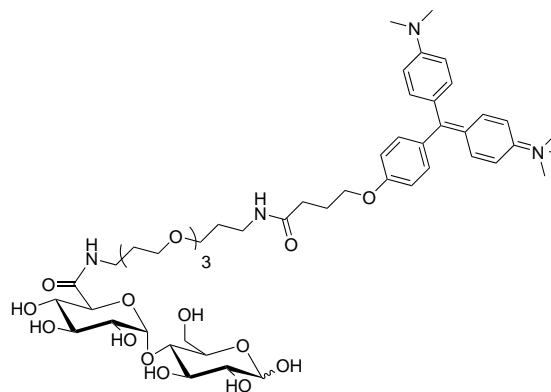
BOT_17

Benzylated conjugate (22.0 mg, 15.9 μmol) and pentamethylbenzene (66.2 mg, 0.45 mmol) were dissolved in 2 mL of anhydrous CH_2Cl_2 to give a light yellow solution. This solution was cooled to $-78\text{ }^\circ\text{C}$ and BCl_3 (0.45 mL, 0.45 mmol) was added slowly along the flask wall. After the solution was stirred for 1.5 h, DIPEA (0.11 mL, 0.34 mmol) was added to the flask, followed by MeOH (2 mL) to quench the reaction. The reaction was then warmed to RT, and the solvents were removed under reduced pressure. The resulting solid was dissolved in 5:3 MeOH/1,4-dioxane and purified by preparative HPLC (MeCN/ H_2O : 20% to 95% over 90 min) yielding the desired conjugate **BOT_18** (3.3 mg, 28%) as a orange solid.

HRMS (ESI) m/z calculated for $\text{C}_{45}\text{H}_{61}\text{N}_6\text{O}_{13}^+$ $[\text{M}+\text{H}]^+$ 893.4301, found 893.4299.

Maltose PEG MG conjugate, **BOT_52**

To a solution of **62** (20 mg, 0.016 mmol) in MeOH (1 mL), was added NaOMe (7 μL , 0.013 mmol). The RM was stirred ON at RT, acidified with Amberlyst IR-120 until pH 2 and filtered. The filtrate was concentrated to give the crude product. The crude



BOT_52

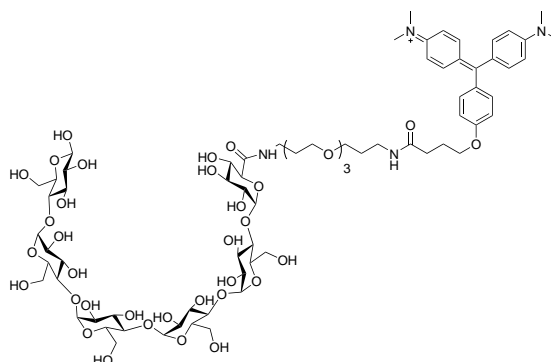
product was purified by HPLC (MeCN/H₂O/0.005% TFA: 20% to 95% over 90 min) to give **BOT_52** (1.2 mg, 20%) as a colourless liquid.

¹ **H NMR (600 MHz, D₂O)** δ 7.19 (dd, *J* = 36.6, 8.8 Hz, 6H, MG-CH), 6.98 (d, *J* = 8.7 Hz, 2H, MG-CH), 6.83 (d, *J* = 9.1 Hz, 4H, MG-CH), 5.33 (d, *J* = 3.8 Hz, 1H, maltose H-1), 5.11 (d, *J* = 3.8 Hz, 1H, maltose H-1'), 4.53 (d, *J* = 8.0 Hz, 1H), 4.08 (t, *J* = 5.8 Hz, 2H, MG--OCH₂), 4.05 – 3.26 (m, 24H, maltose skeletal protons, PEG –OCH₂), 3.26 – 3.05 (m, 14H, –CH₃N, NHCH₂), 2.36 (t, *J* = 6.9 Hz, 2H, NHCH₂), 2.10 – 2.02 (m, 2H, CH₂CO), 1.69 – 1.57 (m, 4H, –NHCH₂CH₂–), 1.26 (dd, *J* = 6.5, 2.0 Hz, 2H, –CH₂CH₂CO–).

¹³ **C NMR (101 MHz, CDCl₃)** δ 176.53 (C=O), 175.69 (C=O), 170.66, 163.12, 156.48, 140.47, 137.57, 131.84, 129.81, 126.58, 120.07, 114.60, 113.14, 99.89, 99.78 (MG Ar-CH), 95.75 (maltose C-1), 91.86 (maltose C-1'), 77.08, 76.82, 76.10, 74.39, 73.98, 73.13, 72.49, 72.46, 72.12, 71.36, 71.29, 69.81, 69.52, 69.33, 68.46, 68.13, 67.73, 60.55, 60.45, 46.28 (skeletal carbons, PEG –OCH₂), 40.04 (–NCH₃), 38.69 (–NCH₃), 36.43 (NHCH₂), 36.16 (NHCH₂), 32.59 (CH₂CO), 28.19 –NHCH₂CH₂–, 28.15 –NHCH₂CH₂–, 24.65 (–CH₂CH₂CO).

HRMS (ESI) *m/z* calculated for C₄₉H₇₀N₃O₁₇+ [M+Na]⁺ 973.4561, found 973.4561.

Maltohexose-MG conjugate, **BOT_53**

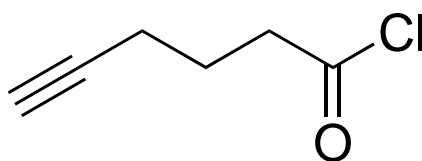


BOT_53

To a solution of **63** (8 mg, 3.3 μmol) in methanol (66 μl) was added catalytic amount of sodium methoxide (4 μL , 0.007 mmol). The RM was stirred ON at RT, acidified with Amberlyst IR-120 until pH 2 and filtered. The filtrate was concentrated to give the crude product. The crude product was purified by flash chromatography using HPLC (MeCN/H₂O: 20% to 95% over 90 min) to give **BOT_51** (0.5 mg, 9%) as a colourless liquid.

HRMS (ESI) m/z calculated for C₇₃H₁₁₁N₄O₃₆⁺ [M+Na]⁺ 1619,69, found 1619,73.

hex-5-ynoyl chloride, **66**



66

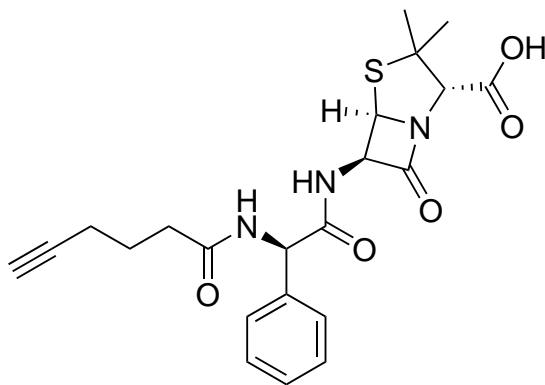
hex-5-ynoic acid **65** (0.5 g, 4.46 mmol) and oxalyl chloride (0.585 ml, 6.69 mmol) were dissolved in THF (5.14 mL) to give a colorless solution. A few drops of DMF were

added, resulting in formation of HCl gas. The solution turned yellow and finally to purple in a few minutes. The RM was stirred at RT for 2h. The solvent was removed under reduced pressure and the crude material was distilled by vacuum distillation at 63 °C and 22 mbar pressure to afford **66** (44mg, 7.56%) as a pale yellow oil.

¹H NMR (400 MHz, CDCl₃) δ 3.06 (t, J = 7.2 Hz, 2H, 2 × H-5), 2.29 (td, J = 6.8, 2.7 Hz, 2H, 2 × H-4), 2.01 (t, J = 2.7 Hz, 1H, H-6), 1.90 (p, J = 7.1 Hz, 2H, 2 × H-3).

¹³C NMR (101 MHz, CDCl₃) δ 173.46 (C=O), 82.16 (C-1), 70.01 (C-6), 45.58 (C-5), 23.63 (C-4), 17.22 (C-3).

Ampicillin alkyne, **68**



68

Hex-5-ynoyl chloride **66** (262 mg, 2.003 mmol) was dissolved in acetone (1 mL). Ampicillin sodium salt **67** (372mg, 1.002 mmol) was dissolved in a solution of sodium hydrogen carbonate (421 mg, 5.01 mmol) in Water/Acetone (4:1, 2.5 mL) and cooled on ice. The acyl chloride was added slowly to the above mixture with continuous stirring. The reaction was subsequently warmed to RT and stirred for 1 h. Water (3 mL) was added to the reaction, and the aqueous phase was washed with EtOAc (2 × 10 mL), acidified to pH 2 by addition of HCl, and extracted with EtOAc (20 mL). The resulting

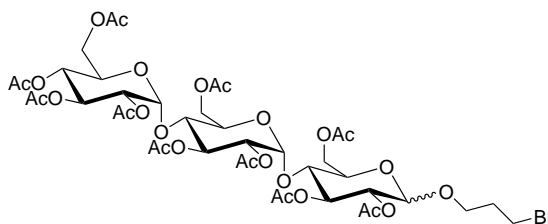
organic phase was washed with cold water (2×5 mL), dried over Na_2SO_4 , and concentrated under reduced pressure. The crude reaction was triturated with hexanes, to yield **68** (345 mg, 78%). The crude product was used in the following steps without further purification.

^1H NMR (400 MHz, DMSO) δ 9.11 (d, $J = 8.0$ Hz, 1H, O=C-NH), 8.57 (d, $J = 8.0$ Hz, 1H, O=C-NH), 7.25 - 7.43 (m, 5H, Ar-CH), 5.70 (d, $J = 8.0$ Hz, 1H, Bn-CH), 5.52 (dd, $J = 4.0, 8.0$ Hz, 1H, lactam O=C-CH-), 5.39 (d, $J = 4.0$ Hz, 1H, -CH-COOH), 4.20 (s, 1H, lactam -SCH-), 2.77 - 2.78 (m, 1H, alkyne C-H), 2.29 - 2.32 (m, 2H, ampicillin - CCH_2CH_2 -), 2.13 - 2.16 (m, 2H, sugar - $\text{CH}_2\text{CH}_2\text{CH}_2$ -), 1.64 - 1.69 (m, 2H, ampicillin - $\text{CH}_2\text{CH}_2\text{CH}_2$ -), 1.55 (s, 3H, CH_3), 1.41 (s, 3H, CH_3).

^{13}C NMR (101 MHz, DMSO) δ 174.43, 171.89, 170.81, 170.67, 169.38 (C=O), 138.61, 128.65, 128.00, 127.64 (Ar-CH), 84.27 (Bn-CH), 72.08 (lactam O=C-CH-), 70.76 (-CH-COOH), 67.69 (lactam -SCH-), 64.17, 60.23, 55.95, 34.24, 32.85, 30.82, 27.07, 23.95, 21.23 (CH_3), 17.60 (CH_3).

HRMS (ESI) m/z calculated for $\text{C}_{22}\text{H}_{25}\text{N}_3\text{O}_5\text{S}$ $[\text{M}+\text{H}]^+$ 444.1595, found 444.1593.

β -D-glucopyranose,2,3,4,6-tetra-O-acetyl- α -D-glucopyranosyl-(1 \rightarrow 4)-O-2,3,6-tri-O-acetyl- α -D-glucopyranosyl-(1 \rightarrow 4)-2,3,6-triacetate 1-(3'-bromopropyl), **70**



70

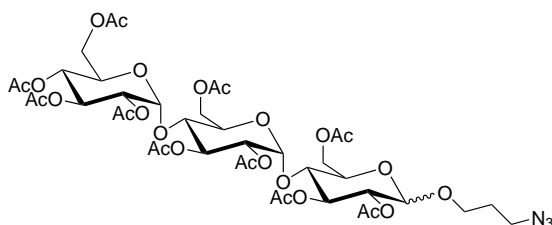
To a solution of maltotriose peracetate **69** (3 g, 0.3 mmol) in CH_2Cl_2 (10 mL) was added 3-bromopropanol (0.071 mL, 0.9 mmol). The solution was cooled to 0°C and $\text{BF}_3 \cdot \text{OEt}_2$ (0.16 mL, 1.5 mmol) was added drop-wise. The RM was stirred ON. The

reaction was quenched with saturated NaHCO₃ solution and extracted with CH₂Cl₂. The combined organic extracts were washed with H₂O and brine, dried using Na₂SO₄, and concentrated under reduced pressure. The crude material was purified by column chromatography on silica gel (PE/EtOAc: 40% to 60%) to afford **2** (770 mg, 24%) as a white solid.

¹ H NMR (400 MHz, CDCl₃) δ 5.50 – 5.20 (m, 5H, skeletal protons), 5.07 (t, J = 9.9 Hz, 1H, skeletal protons), 4.93 – 4.68 (m, 3H, skeletal protons), 4.57 – 4.39 (m, 3H, skeletal protons), 4.33 – 4.12 (m, 6H, skeletal protons), 4.11 – 3.85 (m, 1H, skeletal protons), 3.71 (ddd, J = 9.6, 4.0, 3.2 Hz, 1H, –OCH₂CH₂–), 3.60 (ddd, J = 9.9, 7.6, 5.0 Hz, 1H, –OCH₂CH₂–), 3.44 – 3.23 (m, 2H, CH₂N₃), 2.26 – 1.96 (m, 30H, CH₃), 1.93 – 1.75 (m, 2H, CH₂CH₂Br).

HRMS (ESI) m/z calculated for C₄₁H₅₇BrO₂₆ [M+Na]⁺ 1067.2219, found 1067.2219.

β-D-glucopyranose,2,3,4,6-tetra-O-acetyl-*α*-D-glucopyranosyl-(1→4)-O-2,3,6-tri-O-acetyl-*α*-D-glucopyranosyl-(1→4)-2,3,6-triacetate 1-(3'-azidopropyl), **71**



71

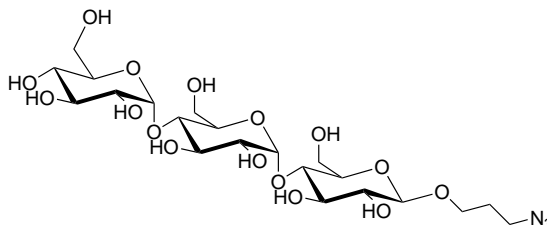
To a solution of **70** (500 mg, 0.564 mmol) in DMF (1 mL) was added NaN₃ (55.0 mg, 0.847 mmol) and stirred ON at 60 °C. The solvent was evaporated. The resulting residue was dissolved in DCM (5 mL) and washed with cold water (3 × 10 mL). The OL was dried with Na₂SO₄ and concentrated. The crude product was purified by column chromatography **71** (375 mg, 78%).

¹ H NMR (400 MHz, CDCl₃) δ 5.50 – 5.20 (m, 5H, skeletal protons), 5.07 (t, J = 9.9 Hz, 1H, skeletal protons), 4.93 – 4.68 (m, 3H, skeletal protons), 4.57 – 4.39 (m, 3H, skeletal protons), 4.33 – 4.12 (m, 6H, skeletal protons), 4.11 – 3.85 (m, 1H, skeletal protons), 3.71 (ddd, J = 9.6, 4.0, 3.2 Hz, 1H, –OCH₂CH₂–), 3.60 (ddd, J = 9.9, 7.6, 5.0 Hz, 1H, –OCH₂CH₂–), 3.44 – 3.23 (m, 2H, CH₂N₃), 2.26 – 1.96 (m, 30H, CH₃), 1.93 – 1.75 (m, 2H, CH₂CH₂N₃).

¹³C NMR (101 MHz, CDCl₃) δ 170.64, 170.60, 170.54, 170.49, 170.37, 170.12, 169.85, 169.72, 169.70, 169.45 (C=O), 100.26 (C-1), 95.75 (C-1), 95.68 (), 75.27, 73.81, 72.51, 72.18, 72.13, 71.76, 70.46, 70.08, 69.38, 68.93, 68.52, 67.90, 66.47, 62.91, 62.34, 61.38 (skeletal protons, –OCH₂CH₂–), 47.98 (CH₂N₃), 28.97 (CH₂CH₂N₃), 20.89, 20.60, 20.59 (CH₃).

HRMS (ESI) m/z calculated for C₄₁H₅₇BrO₂₆ [M+Na]⁺ 1030.3128, found 1030.3128.

β-D-glucopyranose-*α*-D-glucopyranosyl-(1→4)-*α*-D-glucopyranosyl-(1→4)1-(3'-azidopropyl), **72**



72

To a solution of **70** (379 mg, 0.447 mmol) in MeOH (1 mL) was added sodium methoxide (24.15 mg, 0.447 mmol). The RM was stirred ON at RT. The RM was stirred ON at RT, acidified with Amberlyst IR-120 until pH 2 and filtered. The filtrate was concentrated to give the crude product. The crude product was purified by flash chromatography using an amino column (MeCN/H₂O: 95% to 70% over 30 min) to give **72** (250

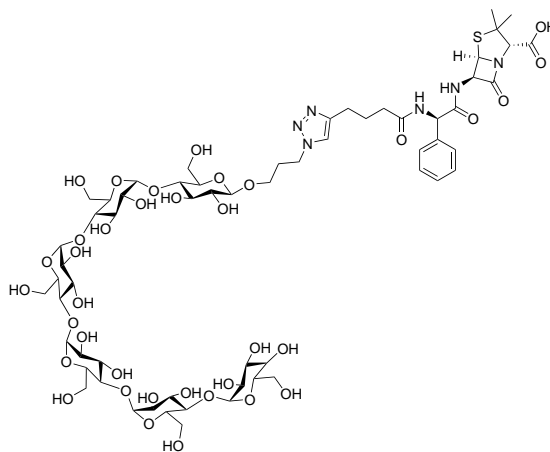
mg, 95 %) as a viscous oil.

$^1\text{H NMR}$ (400 MHz, D_2O) δ 5.40 (d, $J = 3.2$ Hz, 2H, H-1', H-1''), 4.48 (d, $J = 8.0$ Hz, 1H, H-1), 4.05 – 3.57 (m, 19H, skeletal protons), 3.53 – 3.24 (m, 4H, $-\text{OCH}_2\text{CH}_2-$, CH_2N_3), 1.92 (p, $J = 6.5$ Hz, 2H, $\text{CH}_2\text{CH}_2\text{N}_3$).

$^{13}\text{C NMR}$ (101 MHz, CDCl_3) δ 102.10, 99.72, 99.44, 76.96, 76.72, 76.13, 74.49, 73.27, 72.94, 72.83, 72.67, 71.70, 71.43, 71.16, 69.28, 67.30, 60.63, 60.43, 48.84 ($-\text{OCH}_2\text{CH}_2-$), 47.85 (CH_2N_3), 28.21 ($\text{CH}_2\text{CH}_2\text{N}_3$).

HRMS (ESI) m/z calculated for $\text{C}_{21}\text{H}_{37}\text{N}_3\text{O}_{16}$ $[\text{M}+\text{Na}]^+$ 610.2072, found 610.2072.

Maltohexose-ampicillin conjugate, **BOT_54**



BOT_54

The azide **BOT_42** (7.0 mg, 6.6 μmol) and alkyne **66** (8.49 mg, 19.1 μmol) were dissolved in 0.3 mL DMSO. copper sulfate (2.84 mg, 17.8 μmol) in 100 μL H_2O and TBTA (2.84 mg, 17.8 μmol) in 100 μL DMSO were mixed together to give a dark blue solution. To this solution was added NaAsc (14.3 mg, 71.9 μmol) in 100 μL H_2O . The RM was stirred for 1h. The RM was diluted with $\text{H}_2\text{O}/\text{MeCN}$ (1:1) to make the volume three fold. The resulting solution was centrifuged at 4 $^\circ\text{C}$ for 10 min. The supernatant was purified by HPLC ($\text{MeCN}/\text{H}_2\text{O}/0.005\%$ TFA: 20% to 95% over 60 min) to give

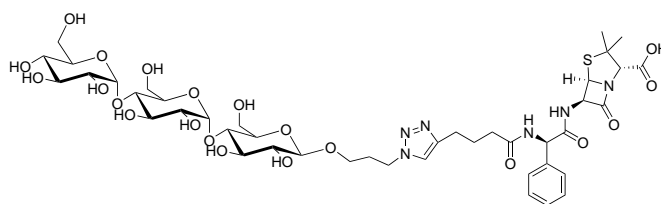
as **BOT_54** (5 mg, 50%) a white powder.

¹H NMR (400 MHz, DMSO) δ 9.11 (d, J = 7.6 Hz, 1H, O=C-OH), 8.55 (d, J = 8.2 Hz, 1H, O=C-NH), 7.87 (s, 1H, pyrazole CH), 7.53 – 7.19 (m, 5H, Ar-CH), 5.73 (d, J = 8.3 Hz, 1H, Bn-CH), 5.60 – 5.46 (m, 1H, lactam O=C-CH-), 5.40 (d, J = 3.8 Hz, 1H, -CHCOOH), 5.03 (s, 6H, anomeric protons), 4.40 (s, 3H, skeletal protons), 4.20 (s, 1H, lactam -SCH-), 4.18 – 2.99 (m, 45H, skeletal protons, -OH), 2.61 (dd, J = 23.7, 16.3 Hz, 2H, ampicillin, -CCH₂-), 2.27 (d, J = 7.1 Hz, 2H, ampicillin COCH₂), 2.05 (s, 2H, maltohexose -CH₂CH₂CH₂-), 1.82 (d, J = 7.8 Hz, 2H, ampicillin -CH₂CH₂CH₂-), 1.55 (s, 3H, CH₃), 1.41 (s, 3H, CH₃).

¹³C NMR (101 MHz, CDCl₃) δ 173.89, 172.21, 170.71, 169.38 (C=O), 146.85, 138.66, 128.66, 128.52, 128.00, 127.86, 127.61, 122.53, 103.13, 101.25, 100.99, 80.20, 79.91, 76.64, 75.55, 73.94, 73.78, 73.59, 73.46, 73.00, 72.52, 72.18, 70.75, 70.38, 67.68, 65.98, 64.18, 61.26, 60.73, 58.58, 55.89, 46.80, 40.56, 40.47, 40.40, 40.30, 40.23, 40.14, 40.06, 39.97, 39.89, 39.80, 39.64, 39.47, 34.88, 30.80, 30.56, 27.07, 25.73, 25.12.

HRMS (ESI) m/z calculated for C₆₁H₉₂N₆O₃₆S [M+H]⁺ 1517.5350, found 1517.5352.

Maltose ampicillin conjugate, **BOT_55**



BOT_55

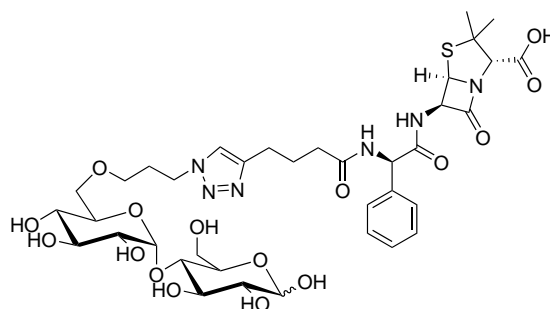
The azide **71** (22 mg, 37 μ mol) and alkyne **66** (25 mg, 56 μ mol) were dissolved in 0.5 mL DMSO. copper sulfate (16 mg, 0.100 mmol) in 173 μ L H₂O and TBTA (60 mg, 0.113 mmol) in 173 μ L DMSO were mixed together to give a dark blue solution. To

this solution was added NaAsc (74 mg, 0.375 mmol) in 174 μL H_2O . The RM was stirred for 1h. The RM was diluted with $\text{H}_2\text{O}/\text{MeCN}$ (1:1) to make the volume three fold. The resulting solution was centrifuged at 4 $^\circ\text{C}$ for 10 min. The supernatant was purified by HPLC ($\text{MeCN}/\text{H}_2\text{O}/0.005\%$ TFA: 20% to 95% over 60 min) to give as **BOT_55** (10 mg, 28%) a white powder.

$^1\text{H NMR}$ (400 MHz, D_2O) δ 7.82 (s, 1H, pyrazole-CH), 7.34 (m, 5H, ampicillin Ar-CH), 5.35 (m, 6H, anomeric H, lactam $\text{O}=\text{C}-\text{CH}-$, $-\text{CHCOOH}$, Bn-CH), 4.44 (t, $J = 6.8$ Hz, 2H, $-\text{OCH}_2$), 4.40 – 4.25 (m, 2H, $-\text{NCH}_2-$), 3.97 – 3.08 (m, 22H, skeletal protons), 2.68 (t, $J = 7.6$ Hz, 2H, ampicillin, $-\text{CCH}_2-$), 2.28 (d, $J = 6.0$ Hz, 2H, ampicillin COCH_2), 2.18 – 2.00 (m, 2H, maltotriose $-\text{CH}_2\text{CH}_2\text{CH}_2-$), 2.00 – 1.78 (m, 2H, ampicillin $-\text{CH}_2\text{CH}_2\text{CH}_2-$), 1.35 (d, $J = 9.7$ Hz, 6H, $2 \times \text{CH}_3$).

HRMS (ESI) m/z calculated for $\text{C}_{43}\text{H}_{62}\text{N}_6\text{O}_{21}\text{S}$ $[\text{M}+\text{Na}]^+$ 1053.3587, found 1053.3587.

Maltose ampicillin conjugate, **BOT_56**



BOT_56

BOT_42 (121 mg, 0.273 mmol) and alkyne **66** (25 mg, 56 μmol) were dissolved in 0.5 mL DMSO. copper sulfate (63.4 mg, 0.254 mmol) in 173 μL H_2O and TBTA (150 mg, 0.282 mmol) in 173 μL DMSO were mixed together to give a dark blue solution. To this solution was added NaAsc (186 mg, 0.940 mmol) in 174 μL H_2O . The RM was stirred for 1h. The RM was diluted with $\text{H}_2\text{O}/\text{MeCN}$ (1:1) to make the volume three fold. The

resulting solution was centrifuged at 4 °C for 10 min. The supernatant was purified by HPLC (MeCN/H₂O/0.005% TFA: 20% to 95% over 60 min) to give as **BOT_56** (5 mg, 12.2%) a white powder.

¹ **H NMR (400 MHz, D₂O)** δ 7.77 (br, 1H, pyrazole-CH), 7.38 (d, J = 14.8 Hz, 5H, ampicillin Ar-CH), 5.48 – 5.19 (m, 3H, maltose H-1, lactam O=C-CH-, -CHCOOH, Bn-CH), 4.40 (d, J = 6.0 Hz, 2H, -NCH₂-), 4.01 – 3.05 (m, 17H, skeletal protons), 2.67 (s, 2H, ampicillin, -CCH₂-), 2.28 (s, 1H, ampicillin COCH₂), 2.07 (s, 2H, maltose -CH₂CH₂CH₂-), 1.89 (s, 2H, ampicillin -CH₂CH₂CH₂-), 1.51 (s, 1H, CH₃), 1.35 (d, J = 11.5 Hz, 3H, CH₃), 1.26 (s, 2H, CH₃).

HRMS (ESI) m/z calculated for C₃₇H₅₂N₆O₁₆S [M+H]⁺ 869.3239, found 869.3239.

Bibliography

- [1] WEF, *Global Risks 2020 — Fifteenth Edition*, 2020, http://www3.weforum.org/docs/WEF_Global_Risk_Report_2020.pdf.
- [2] GBD, *Lancet*, 2020, **396**, 1160–1203.
- [3] R. S. Schwartz, *New England Journal of Medicine*, 2004, **350**, 1079–1080.
- [4] Sneader and Walter, *History of Sulfonamides*, Wiley, 2001.
- [5] A. Fleming, *British journal of experimental pathology*, 1929, 226–236.
- [6] E. Sidebottom, *Nobel Prizes that Changed Medicine*, Imperial College, London, UK, 2012.
- [7] H. C. Reilly, A. Schatz and S. A. Waksman, *Journal of bacteriology*, 1945, **49**, 585–594.
- [8] B. M. Duggar, *Annals of the New York Academy of Sciences*, 1948, **51**, 177–181.
- [9] J. Mcguire, R. L. Bunch, R. C. Anderson, H. E. Boaz, E. H. Flynn, H. M. Powell and J. W. Smith, *Antimicrobial agents and Chemotherapy*, 1952, 281–283.
- [10] J. E. Geraci, F. R. Heilman, D. R. Nicholas, E. W. Wellman and G. T. Ross, *Antibiotics Annual*, 1956, 90–106.
- [11] J. Mcguire, R. N. Wolfe and D. W. Ziegler, *Antibiotics Annual*, 1956, 612–618.
- [12] A. D. Russell, *Journal of Antimicrobial Chemotherapy*, 1975, **1**, 97–101.
- [13] V. T. Andriole, *Infectious Diseases in Clinical Practice*, 1994, **3**, S211.
- [14] K. L. Leach, S. J. Brickner, M. C. Noe and P. F. Miller, *Annals of the New York Academy of Sciences*, 2011, **1222**, 49–54.

-
- [15] G. Kapoor, S. Saigal and A. Elongavan, *Journal of Anaesthesiology Clinical Pharmacology*, 2017, **33**, 300–305.
- [16] Created by Biorender.com.
- [17] WEF, *Global Risks 2019 — Fourteenth Edition*, 2019, http://www3.weforum.org/docs/WEF_Global_Risks_Report_2019.pdf.
- [18] CDC, *2019 Antibiotic resistance threats reports, United States.*, 2019, http://www3.weforum.org/docs/WEF_Global_Risks_Report_2019.pdf.
- [19] CDC, *The bacterial challenge: time to react*, 2019, <https://www.cdc.gov/drugresistance/pdf/threats-report/2019-ar-threats-report-508.pdf>.
- [20] J. G. Bartlett, D. N. Gilbert and B. Spellberg, *Clinical Infectious Diseases*, 2013, **56**, 1445–1450.
- [21] I. Alav, J. M. Sutton and K. Rahman, *The Journal of antimicrobial chemotherapy*, 2018, **73**, 2003–2020.
- [22] L. DM, *Clinical Microbiology and Infection*, 2004, **10**, 1–9.
- [23] L. S. Munoz-Price, L. Poirel, R. A. Bonomo, M. J. Schwaber, G. L. Daikos, M. Cormican, G. Cornaglia, J. Garau, M. Gniadkowski, M. K. Hayden, K. Kumarasamy, D. M. Livermore, J. J. Maya, P. Nordmann, J. B. Patel, D. L. Paterson, J. Pitout, M. V. Villegas, H. Wang, N. Woodford and J. P. Quinn, *The Lancet Infectious diseases*, 2013, **13**, 785–796.
- [24] WHO, *2019 Antibacterial agents in clinical development*, 2019, <https://apps.who.int/iris/bitstream/handle/10665/>

258965/WHO-EMP-IAU-2017.11-eng.pdf;jsessionid=CD7EF4892B2FFA93B7BC72964C703EC5?sequence=1.

- [25] *Tracking the Global Pipeline of Antibiotics in Development*, April 2020, 2020, <https://www.pewtrusts.org/en/research-and-analysis/issue-briefs/2020/04/tracking-the-global-pipeline-of-antibiotics-in-development>.
- [26] *Priority pathogen list*, 2017, https://www.who.int/medicines/publications/WHO-PPL-Short_Summary_25Feb-ET_NM_WHO.pdf.
- [27] L. J. van Doorn, Y. Henskens, N. Nouhan, A. Verschuuren, R. Vreede, P. Herbink, G. Ponjee, K. van Krimpen, R. Blankenburg, J. Scherpenisse and W. Quint, *Journal of clinical microbiology*, 2000, **38**, 13–17.
- [28] M. L. James and S. S. Gambhir, *Physiological Reviews*, 2012, **92**, 897–965.
- [29] S. Vaidyanathan, C. N. Patel, A. F. Scarsbrook and F. U. Chowdhury, *Clinical Radiology*, 2015, **70**, 787–800.
- [30] S. K. Jain, *Molecular Imaging and Biology*, 2017, **19**, 341–347.
- [31] X. Ning, W. Seo, S. Lee, K. Takemiya, M. Rafi, X. Feng, D. Weiss, X. Wang, L. Williams, V. M. Camp, M. Eugene, W. R. Taylor, M. Goodman and N. Murthy, *Angewandte Chemie (International ed. in English)*, 2014, **53**, 14096–14101.
- [32] K. L. Peterson, W. C. Reid, A. F. Freeman, S. M. Holland, R. I. Pettigrew, A. M. Gharib and D. A. Hammoud, *Nuclear medicine and biology*, 2013, **40**, 638–642.
- [33] P. H. Nibbering, M. M. Welling, A. Paulusma-Annema, P. Brouwer, A. Lupetti and K. Pauwels, *Journal of Nuclear Medicine*, 2004, **45**, 321–326.
- [34] K. E. Britton, D. W. Wareham, S. S. Das, K. K. Solanki, H. Amaral, A. Bhatnagar,

-
- A. H. S. Katamihardja, J. Malamitsi, H. M. Moustafa, V. E. Soroa, F. X. Sundram and A. K. Padhy, *Journal of clinical pathology*, 2002, **55**, 817–823.
- [35] E. M. Sletten and C. R. Bertozzi, *Angewandte Chemie (International ed. in English)*, 2009, **48**, 6974–6998.
- [36] V. Martynov, A. Pakhomov, N. Popova, I. Deyev and A. Petrenko, *Acta naturae*, 2016, **8**, 33–46.
- [37] H. Chen, C. Liu, D. Chen, K. Madrid, S. Peng, X. Dong, M. Zhang and Y. Gu, *Molecular Pharmaceutics*, 2015, **12**, 2505–2516.
- [38] M. van Oosten, T. Schäfer, J. A. C. Gazendam, K. Ohlsen, E. Tsompanidou, M. C. de Goffau, H. J. M. Harmsen, L. M. A. Crane, E. Lim, K. P. Francis, L. Cheung, M. Olive, V. Ntziachristos, J. M. van Dijl and G. M. van Dam, *Nature Communications*, 2013, **4**, 2584.
- [39] K. Ferreira, H. Y. Hu, V. Fetz, H. Prochnow, B. Rais, P. P. Muller and M. Brönstrup, *Angewandte Chemie (International ed. in English)*, 2017, **129**, 8384–8389.
- [40] C. Szent-Gyorgyi, B. F. Schmidt, Y. Creeger, G. W. Fisher, K. L. Zakel, S. Adler, J. A. J. Fitzpatrick, C. A. Woolford, Q. Yan, K. V. Vasilev, P. B. Berget, M. P. Bruchez, J. W. Jarvik and A. Waggoner, *Nature Biotechnology*, 2008, **26**, 235–240.
- [41] H. Nikaido and M. Vaara, *Microbiology and Molecular Biology Reviews*, 1985, **49**, 1–32.
- [42] T. Schirmer, *Journal of Structural Biology*, 1998, **121**, 101–109.
- [43] Z. H. I., *Future Microbiology*, 2009, **4**, 919–932.
- [44] B. Loh, C. Grant and R. E. Hancock, *Antimicrobial Agents and Chemotherapy*, 1984, **26**, 546–551.

-
- [45] I. J. Sud and D. S. Feingold, *Antimicrobial Agents and Chemotherapy*, 1975, **8**, 34–37.
- [46] D. R. Storm, K. S. Rosenthal and P. E. Swanson, *Annual Review of Biochemistry*, 1977, **46**, 723–763.
- [47] D. R. S. Kenneth S. Rosenthal, *The Journal of Antibiotics*, 1977, **30**, 1087–1092.
- [48] S. Chihara, A. Ito, M. Yahata, T. Tobita and Y. Koyama, *Agricultural and Biological Chemistry*, 1974, **38**, 521–529.
- [49] M. Vaara and T. Vaara, *Nature*, 1983, **303**, 526–528.
- [50] M. Vaara and T. Vaara, *Antimicrobial agents and chemotherapy*, 1983, **24**, 114–122.
- [51] M. Vaara and T. Vaara, *Antimicrobial agents and chemotherapy*, 1983, **24**, 107–113.
- [52] M. Vaara, *Journal of Chromatography A*, 1988, **441**, 423–430.
- [53] V. Petri, M. Hisami, K. Yukio and M. Vaara, *The Journal of Antibiotics*, 1991, **44**, 517–523.
- [54] K. Yukio, M. Hisami and M. Vaara, *The Journal of Antibiotics*, 1992, **45**, 742–749.
- [55] G. M. Hogg, J. G. Barr and C. H. Webb, *Journal of Antimicrobial Chemotherapy*, 1998, **41**, 494–495.
- [56] A. Giacometti, O. Cirioni, F. Barchiesi, M. Fortuna and G. Scalise, *Journal of Antimicrobial Chemotherapy*, 1999, **44**, 641–645.
- [57] A. Giacometti, O. Cirioni, M. S. Del Prete, F. Barchiesi, M. Fortuna, D. Drenaggi and G. Scalise, *Antimicrobial agents and chemotherapy*, 2000, **44**, 1716–1719.

-
- [58] M. Vaara and M. Porro, *Antimicrobial agents and chemotherapy*, 1996, **40**, 1801–1805.
- [59] J. G. Sawyer, N. L. Martin and R. E. Hancock, *Infection and Immunity*, 1988, **56**, 693–698.
- [60] H. Lee, S. I. Lim, S.-H. Shin, Y. Lim, J. W. Koh and S. Yang, *ACS omega*, 2019, **4**, 15694–15701.
- [61] K. Kikuchi, E. M. Bernard, A. Sadownik, S. L. Regen and D. Armstrong, *Antimicrobial agents and chemotherapy*, 1997, **41**, 1433–1438.
- [62] B. Ding, Q. Guan, J. P. Walsh, J. S. Boswell, T. W. Winter, E. S. Winter, S. S. Boyd, C. Li and P. B. Savage, *Journal of Medicinal Chemistry*, 2002, **45**, 663–669.
- [63] C. Li, M. R. Lewis, A. B. Gilbert, M. D. Noel, D. H. Scoville, G. W. Allman and P. B. Savage, *Antimicrobial agents and chemotherapy*, 1999, **43**, 1347–1349.
- [64] D. Nicolosi, S. Cupri, C. Genovese, G. Tempera, R. Mattina and R. Pignatello, *International Journal of Antimicrobial Agents*, 2015, **45**, 622 – 626.
- [65] M. Chen, S. Xie, J. Wei, X. Song, Z. Ding and X. Li, *ACS Applied Materials & Interfaces*, 2018, **10**, 36814–36823.
- [66] P. Kumar, R. A. Shenoi, B. F. L. Lai, M. Nguyen, J. N. Kizhakkedathu and S. K. Straus, *Biomacromolecules*, 2015, **16**, 913–923.
- [67] X.-Y. Xue, X.-G. Mao, Z. Li, Z. Chen, Y. Zhou, Z. Hou, M.-K. Li, J.-R. Meng and X.-X. Luo, *Nanomedicine: Nanotechnology, Biology and Medicine*, 2015, **11**, 329 – 339.
- [68] A. M. Fayaz, M. Girilal, S. A. Mahdy, S. Somsundar, R. Venkatesan and P. Kalaichelvan, *Process Biochemistry*, 2011, **46**, 636–641.
-

-
- [69] P. J. Weldrick, S. Iveson, M. J. Hardman and V. N. Paunov, *Nanoscale*, 2019, **11**, 10472–10485.
- [70] R. Pignatello, D. Nicolosi and V. Nicolosi, *Science against microbial pathogens: communicating current research and technological advances*, 2011, 52–60.
- [71] R. C. Hider and X. Kong, *Natural Product Reports*, 2010, **27**, 637–657.
- [72] V. Braun and K. Hantke, *Current Opinion in Chemical Biology*, 2011, **15**, 328 – 334.
- [73] Y.-M. Lin, M. Ghosh, P. A. Miller, U. Möllmann and M. J. Miller, *BioMetals*, 2019, **32**, 425–451.
- [74] A. Pandey, C. Savino, S. H. Ahn, Z. Yang, S. G. Van Lanen and E. Boros, *Journal of Medicinal Chemistry*, 2019, **62**, 9947–9960.
- [75] M. Ghosh, P. A. Miller, U. Möllmann, W. D. Claypool, V. A. Schroeder, W. R. Wolter, M. Suckow, H. Yu, S. Li, W. Huang, J. Zajicek and M. J. Miller, *Journal of Medicinal Chemistry*, 2017, **60**, 4577–4583.
- [76] A. Paulen, V. Gasser, F. Hoegy, Q. Perraud, B. Pesset, I. J. Schalk and G. L. A. Mislin, *Organic and Biomolecular Chemistry*, 2015, **13**, 11567–11579.
- [77] T. Zheng and E. M. Nolan, *Journal of the American Chemical Society*, 2014, **136**, 9677–9691.
- [78] I. Schalk, *Clinical Microbiology and Infection*, 2018, **24**, 801 – 802.
- [79] G. G. Zhanel, A. R. Golden, S. Zelenitsky, K. Wiebe, C. K. Lawrence, H. J. Adam, T. Idowu, R. Domalaon, F. Schweizer, M. A. Zhanel, P. R. S. Lagacé-Wiens, A. J. Walkty, A. Noreddin, J. P. Lynch III and J. A. Karlowisky, *Drugs*, 2019, **79**, 271–289.

-
- [80] M. J. Miller, A. J. Walz, H. Zhu, C. Wu, G. Moraski, U. Möllmann, E. M. Tristani, A. L. Crumbliss, M. T. Ferdig, L. Checkley, R. L. Edwards and H. I. Boshoff, *Journal of the American Chemical Society*, 2011, **133**, 2076–2079.
- [81] A. Kim, A. Kutschke, D. E. Ehmann, S. A. Patey, J. L. Crandon, E. Gorseth, A. A. Miller, R. E. McLaughlin, C. M. Blinn, A. Chen, A. S. Nayar, B. Dangel, A. S. Tsai, M. T. Rooney, K. E. Murphy-Benenato, A. E. Eakin and D. P. Nicolau, *Antimicrobial agents and chemotherapy*, 2015, **59**, 7743–7752.
- [82] E. Goldsmith, S. Sprang and R. Fletterick, *Journal of Molecular Biology*, 1982, **156**, 411 – 427.
- [83] T. Schirmer and S. W. Cowan, *Protein science : a publication of the Protein Society*, 1993, **2**, 1361–1363.
- [84] T. Schirmer, T. Keller, Y. Wang and J. Rosenbusch, *Science*, 1995, **267**, 512–514.
- [85] J. C. Spurlino, G. Y. Lu and F. A. Quioco, *Journal of Biological Chemistry*, 1991, **266**, 5202–5219.
- [86] J. C. Spurlino, L. E. Rodseth and F. A. Quioco, *Structure*, 1997, **5**, 997–1015.
- [87] X. Duan, J. A. Hall, H. Nikaido and F. A. Quioco, *Journal of Molecular Biology*, 2001, **306**, 1115 – 1126.
- [88] A. J. Sharff, L. E. Rodseth and F. A. Quioco, *Biochemistry*, 1993, **32**, 10553–10559.
- [89] A. J. Sharff, L. E. Rodseth, J. C. Spurlino and F. A. Quioco, *Biochemistry*, 1992, **31**, 10657–10663.
- [90] D. Khare, M. L. Oldham, C. Orelle, A. L. Davidson and J. Chen, *Molecular cell*, 2009, **33**, 528–536.

-
- [91] D. Boyd, C. Manoil and J. Beckwith, *Proceedings of the National Academy of Sciences*, 1987, **84**, 8525–8529.
- [92] M. Ehrmann, D. Boyd and J. Beckwith, *Proceedings of the National Academy of Sciences*, 1990, **87**, 7574–7578.
- [93] S. Froshauer, G. Green, D. B. K. McGovern and J. Beckwith, *Journal of Molecular Biology*, 1988, **200**, 501 – 511.
- [94] D. Boyd, B. Traxler and J. Beckwith, *Journal of Bacteriology*, 1993, **175**, 553–556.
- [95] E. Dassa and S. Muir, *Molecular Microbiology*, 1993, **7**, 29–38.
- [96] J. E. Walker, M. Saraste, M. J. Runswick and N. J. Gay, *The EMBO journal*, 1982, **1**, 945–951.
- [97] T. Ferenci, *Journal of Bacteriology*, 1980, **144**, 7–11.
- [98] M. Luckey and H. Nikaido, *Proceedings of the National Academy of Sciences of the United States of America*, 1980, **77**, 167–171.
- [99] M. Reyes, N. A. Treptow and H. A. Shuman, *Journal of Bacteriology*, 1986, **165**, 918–922.
- [100] T. Ferenci, M. Muir, K.-S. Lee and D. Maris, *Biochimica et Biophysica Acta (BBA) - Biomembranes*, 1986, **860**, 44 – 50.
- [101] R. Thieme, H. Lay, A. Oser, J. Lehman, S. Wrissenberg and W. Boos, *European Journal of Biochemistry*, 1986, **160**, 83–91.
- [102] R. Dutzler, Y.-F. Wang, P. Rizkallah, J. Rosenbusch and T. Schirmer, *Structure*, 1996, **4**, 127 – 134.

-
- [103] M. L. Oldham, S. Chen and J. Chen, *Proceedings of the National Academy of Sciences*, 2013, **110**, 18132–18137.
- [104] X. Ning, S. Lee, Z. Wang, D. Kim, B. Stubblefield, E. Gilbert and N. Murthy, *Nature Materials*, 2011, **10**, 602–607.
- [105] L. B. Josefsen and R. W. Boyle, *Theranostics*, 2012, **2**, 916–966.
- [106] A. Galstyan, D. Block, S. Niemann, M. C. Grüner, S. Abbruzzetti, M. Oneto, C. G. Daniliuc, S. Hermann, C. Viappiani, M. Schäfers, B. Löffler, C. A. Strassert and A. Faust, *Chemistry – A European Journal*, 2016, **22**, 5243–5252.
- [107] A. Axer, S. Hermann, G. Kehr, D. Clases, U. Karst, L. Fischer-Riepe, J. Roth, M. Fobker, M. Schäfers, R. Gilmour and A. Faust, *ChemMedchem*, 2018, **13**, 241–250.
- [108] E. Dumont, J. Vergalli, J. Pajovic, S. P. Bhamidimarri, K. Morante, J. Wang, D. Lubriks, E. Suna, R. A. Stavenger, M. Winterhalter, M. Réfrégiers and J.-M. Pagès, *Life Science Alliance*, 2019, **2**, e201800242.
- [109] X. Wang, C. A. Borges, X. Ning, M. Rafi, J. Zhang, B. Park, K. Takemiya, C. L. Sterzo, W. R. Taylor, L. Riley and N. Murthy, *Bioconjugate Chemistry*, 2018, **29**, 3935–3935.
- [110] C. Brunkhorst, C. Andersen and E. Schneider, *Journal of Bacteriology*, 1999, **181**, 2612–2619.
- [111] P. L. Haddix, S. Jones, P. Patel, S. Burnham, K. Knights, J. N. Powell and A. LaForm, *Journal of Bacteriology*, 2008, **190**, 7453–7463.
- [112] J. A. Thomas, *Chemical Society Reviews*, 2015, **44**, 4494–4500.
- [113] M. U. Roslund, O. Aitio, J. Wärnå, H. Maaheimo, D. Y. Murzin and R. Leino, *Journal of the American Chemical Society*, 2008, **130**, 8769–8772.

-
- [114] D. W. Kim, C. E. Song and D. Y. Chi, *The Journal of Organic Chemistry*, 2003, **68**, 4281–4285.
- [115] Y. Ju, D. Kumar and R. S. Varma, *The Journal of Organic Chemistry*, 2006, **71**, 6697–6700.
- [116] M. H. Park, R. Takeda and K. Nakanishi, *Tetrahedron Letters*, 1987, **28**, 3823 – 3824.
- [117] P. K. Mandal and J. S. McMurray, *The Journal of Organic Chemistry*, 2007, **72**, 6599–6601.
- [118] A. Williamson, *The London, Edinburgh, and Dublin Philosophical Magazine and Journal of Science*, 1850, **37**, 350–356.
- [119] S. Renggli, W. Keck, U. Jenal and D. Ritz, *Journal of bacteriology*, 2013, **195**, 4067–4073.
- [120] J. Holleran, D. Brown, M. H. Fuhrman, S. A. Adler, G. W. Fisher and J. W. Jarvik, *Cytometry Part A*, 2010, **77A**, 776–782.
- [121] L. Philippe and R. Ethan, *Expert Opinion on Drug Safety*, 2012, **11**, 381–399.
- [122] A. Brochu, N. Brochu, T. I. Nicas, T. R. Parr, A. A. Minnick, E. K. Dolence, J. A. McKee, M. J. Miller, M. C. Lavoie and F. Malouin, *Antimicrobial Agents and Chemotherapy*, 1992, **36**, 2166–2175.
- [123] K. H. Negash, J. K. Norris and J. T. Hodgkinson, *Molecules*, 2019, **24**, 3314.
- [124] Y. Fan, A. Pauer, Gonzales, A.A. and H. Fenniri, *International Journal of Nanomedicine*, 2019, **14**, 7281–7289.
- [125] H. Kishida, S. Unzai, D. I. Roper, A. Lloyd, S.-Y. Park and J. R. H. Tame, *Biochemistry*, 2006, **45**, 783–792.

Steffi Kruba Stephen

Date of Birth- 27 May, 1991

Curriculum Vitae

Education

- 2015 – present **PhD student in Chemical Biology**, *Leibniz University Hannover, Germany*, PhD thesis titled "Oligo-saccharides based antibacterial drug conjugates."
- 2010 – 2015 **Integrated M.Sc in Chemistry**, *Cumulative Grade Point Average – 8.51/10*, National Institute of Science Education and Research, Bhubaneswar, India.
An **INSPIRE** (Innovation in Science Pursuit for Inspired Research) fellow (2010-2015). INSPIRE fellowship is awarded by DST (Department of Science and Technology), Govt. of India to reward meritorious students in science.
- 2008 – 2009 **All India Senior School Certificate Examination, AISSCE**, *Central Board of Secondary Education*, Kendriya Vidyalaya Sec-VIII, R K Puram, New Delhi, India, Percentage-84.5%.
Awarded **Post Matric Scholarship** by Ministry of minority affairs, Government of India.

Research Experience

- September 2015 – Present **Oligosaccharides based antibacterial drug conjugates**, *Leibniz University Hannover, Germany*, Supervisor– Prof. Dr. Mark Brönstrup.
- PhD Thesis
- Familiar with carbohydrate chemistry, MIC assays, fluorescence microscopy and imaging, and growth recovery experiments.
 - Active collaboration and communication with people from diverse backgrounds (pharmacology, microbiology, spectroscopy, etc.).
 - Supervision of 9 students from different disciplines (Chemistry, Life sciences) on multiple projects in English and German.
 - Responsible for 1 preparative HPLC Dionex Ultimate 3000, hydrogenation apparatus, IR-spectrometer and inventory keeping.
 - Involved in conducting exercises for two M.Sc courses: Chemical Biology and Hetero-cyclic Chemistry.
- May 2014 – Apr 2015 **Catalysis by Ruthenium complexes**, *National Institute of Science Education and Research, Bhubaneswar, India*, Project Instructor- Dr. C. Gunanathan.
- Master Thesis
- Novel Ruthenium catalysed synthesis of Aziridines and transamidation reactions were devised. Extensive reaction condition optimisation and substrate scope studied in both projects.
 - Experienced in air and moisture sensitive chemistry using Schlenk-line technique and glove-box.
 - Regular updates in the form of reports and oral presentations to the faculty under strict deadlines.
 - Supervising and training a summer research intern for two months.

May – Jul 2013 **Dipeptide ligand based asymmetric catalysis**, *Indian Institute of Science, Bangalore, India*, Project Instructor-Prof. A.G. Samuelson.

Summer Project

- Using the strategy of protection, coupling and deprotection a chiral dipeptide ligand was synthesised in partial fulfilment of the project.
- Analysis of complex molecules using ^1H , ^{13}C and 2D NMR spectroscopy.
- Introduced to online databases like Scifinder, Web of Knowledge, Reaxys etc for literature and citation search.

Jun – Jul 2012 **Polymers and cooperative catalysis**, *National Institute of Science Education and Research, Bhubaneswar, India*, Project Instructor– Dr. V Krishnan.

Summer Project

- Synthesis of Iron complexes with salen ligand was carried out.
- Gained hands on experience in IR-spectroscopy, NMR spectroscopy, Mass spectrometry and Cyclic Voltametry.
- Maintaining the regulatory protocols and documentation.

Conferences and Presentations

- o Poster presentation titled "Oligosaccharide-based antibacterial drug conjugates" at the EFMC-ASMC'17 symposium.
- o Poster presentation titled "Oligosaccharide-based cellular delivery of antibiotics" at the 19th European Carbohydrate Symposium (EUROCARB 2017).
- o Poster presentation titled "Maltodextrin based antibacterial conjugates" at the Leibniz symposium 2016, Hannover.
- o Participated in the "Drug Innovation in Academia" conference, 2016, at the German Cancer Research Center (DKFZ), Heidelberg.